IL
NUOVO CIMENTO
ORGANO DELLA SOCIETÀ ITALIANA DI FISICA
SOTTO GLI AUSPICI DEL CONSIGLIO NAZIONALE DELLE RICERCHE

VOL. XIV, N. 4 *Serie decima* 16 Novembre 1959

Coincidence Counting with Scintillation Counters.

H. S. MURDOCH and K. W. OGILVIE

The F.B.S. Falkiner Nuclear Research and Adolph Basser Computing Laboratories, School of Physics (*), *The University of Sydney - Sydney, N.S.W.*

(ricevuto il 10 Ottobre 1958)

Summary. — An examination is made of the factors affecting the coincidence technique when scintillation counters are used. Approximate expressions for the distribution of random time delays due to the photomultipliers are employed to derive the dependence of the so called « prompt » and « delayed » counting rates upon the inserted delay especially when this is small. Comparison with experiment shows that these expressions are applicable in many cases. The choice of optimum resolving time is treated, and the characteristics of coincidence circuits discussed.

1. – Introduction.

In a delayed coincidence counting experiment performed for instance to measure the life time of an excited state, the counting rate for a delay t_d is given by the expression

$$F(\lambda, t_d) = \int_0^\infty \lambda \exp[-\lambda t] P(t_d - t)\mathrm{d}t \,, \tag{1}$$

(*) Also supported by the Nuclear Research Foundation within the University of Sydney.

where λ is the disintegration constant of the state and $P(t_d)$ is the probability of recording a truly coincident pair of radiations when a delay t_d is introduced in the prompt channel (*).

$P(t_d)$ depends on the time distribution of pulses at the input to the coincidence circuit, and on the response of the coincidence circuit to the input pulses, the latter depending in general both on the properties of the circuit and on the shape of the pulses.

In the case of Geiger counters, the delay distribution of pulses arriving at the coincidence circuit may adequately be regarded as gaussian [1]. The coincidence counting rate has been discussed for this case by several authors [2-4], all of whom assume a coincidence circuit which responds to rectangular pulses. This treatment cannot be applied to experiments with scintillation counters, where the fluctuations in the delays may be as large as the delays themselves and where the coincidence circuit may itself have an important influence. A gaussian distribution cannot be correct under these circumstances as it would predict an appreciable number of negative delays. We shall develop an approximate treatment of the more general situation, and compare our results with experiments.

2. – The prompt resolution curve.

In using scintillation counters, the chief sources of delay are

i) the time which elapses until sufficient photoelectrons are ejected from the photo cathode to give an effective output pulse;

ii) transit time in the photo-multiplier;

iii) delays in any electronic circuits prior to the coincidence circuit.

Only relative delays are of course important so that if two identical photo-multipliers having the same mean transit time are used, only fluctuations in transit time need be considered. Unintentional circuit delays can be eliminated with good design and the collection time of the photo-electrons can be reduced by a high cathode-dynode voltage. In the ideal case the ejection of one photo-

(*) We restrict ourselves to the case where each channel responds only to the appropriate radiation.

(1) H. BRADT and P. SCHERRER: *Helv. Phys. Acta*, **16**, 259 (1943).

(2) D. E. BUNYAN, A. LUNDBY and D. WALKER: *Proc. Phys. Soc. Lond.*, A **62**, 253 (1949).

(3) B. D. NAG, S. SEN and S. CHATTERGEE: *Ind. Journ. Phys.*, **24**, 261 (1950).

(4) H. S. MURDOCH: *Proc. Phys. Soc. London*, A **66**, 944 (1953).

3536

electron is sufficient to give an effective pulse and the time before the emission of the first photo-electron is the only relevant delay (*).

BELL, GRAHAM and PETCH (5) who used IP21 photomultipliers consider they closely approximated these ideal conditions.

With many photomultipliers, however, the transit time spread is greater than the delays in the phosphor. Under these circumstances, there is an optimum value of n/R which minimizes the variance of the total delay distribution where R is the total number of photoelectrons emitted and n is the number required for an output pulse. This situation has been discussed by several workers and is well summarized by DE WAARD (6).

We will consider the case where only the first source of delay is relevant. This case will be of increasing interest as photomultipliers with more uniform transit time become available. If n electrons are required for an effective pulse, then the delay distribution $\varphi(t)\,\mathrm{d}t$, defined as the probability that the n-th electron is emitted between times t and $t+\mathrm{d}t$, is given by POST and SCHIFF (7),

$$\varphi(t)\,\mathrm{d}t = [f(t)]^{n-1}\frac{\exp[-f(t)]}{(n-1)!}\frac{\mathrm{d}f}{\mathrm{d}t}\,\mathrm{d}t\,, \tag{2}$$

where $f(t)$ is the expected number of photo-electrons emitted between 0 and t. We may obtain a good approximation to this function by considering an exponentially decaying scintillator, so that

$$f(t) = R(1-\exp[-\beta t])\,,$$

where β is the decay constant of the light flash. This expression when fed into (2) is somewhat intractable, but, for large R, a good approximation, especially when n is small, is

$$f(t) = rt\,,$$

where $r = R\beta$. We shall consider this situation in detail. With this approximation, the delay distribution becomes

and

$$\begin{cases} \varphi_1 = r\exp[-rt] & \text{for} \quad n=1 \\ \varphi_2 = r^2 t\exp[-rt] & \text{for} \quad n=2\,. \end{cases}$$

(*) The time between the absorption of the photons by the cathode and the ejection of the electron has been shown to be negligible.

(5) R. E. BELL, R. L. GRAHAM and M. E. PETCH: *Can. Journ. Phys.*, **30**, 35 (1952).

(6) H. DE WAARD: *Nucl. Instr.*, **2**, 73 (1958).

(7) R. F. POST and L. I. SCHIFF: *Phys. Rev.*, **80**, 1113 (1950).

3567

We note that φ_1 has a maximum at the origin while φ_2 rises rather rapidly to a maximum at $t = 1/r$ and then decays relatively slowly. We might expect, at least quantitatively, that φ_2 would also approximate to the case where one photo-electron is adequate but other possible sources of delay such as transit time spread are not entirely negligible. With this interpretation of φ_2, r becomes an arbitrary parameter and loses its strict significance as $R\beta$.

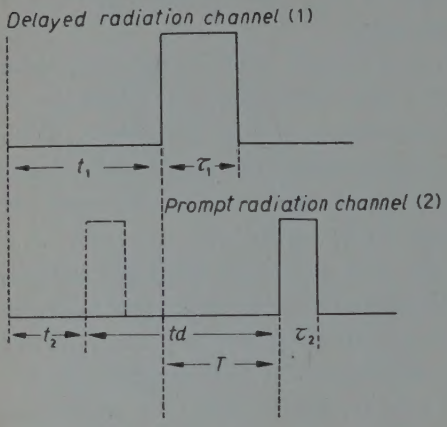

Fig. 1.

The general expression for $P(t_d)$ is

$$(4) \qquad P(t_d) = \int_0^\infty dt_1 \int_0^\infty dt_2 \varphi(t_1)\varphi(t_2)\, e(T) \ ,$$

where T is the separation time between the two pulses at the input to the coincidence circuit (see Fig. 1) and $e(T)$ is the probability of an output pulse from the coincidence circuit for a separation time T. This may be rewritten as

$$P(t_d) = \int_{t_d}^\infty dT\, e(T) \int_0^\infty dt_1 \varphi(t_1)\varphi(t_1 + T - t_d) + \int_{-\infty}^{t_d} dT\, e(T) \int_{t_d - T}^\infty dt_1 \varphi(t_1)\varphi(t_1 + T - t_d) \ .$$

We will assume here that $e(T) = 1$ for $-\tau_2 \leqslant T \leqslant \tau_1$ corresponding to a perfect coincidence circuit accepting rectangular pulses of widths τ_1 and τ_2 at the delayed and prompt inputs respectively, and we shall discuss in Section 6 the effect of coincidence circuits which do not have this idealized behaviour.

For the two cases $n = 1$ and $n = 2$ we obtain respectively for $-\tau_2 \leqslant t_d \leqslant \tau_1$

$$P_1(t_d) = \tfrac{1}{2}[2 - \exp[r(t_d - \tau_1)] - \exp[-r(t_d + \tau_2)]] \ ,$$

$$P_2(t_d) = \tfrac{1}{4}[4 + \exp[r(t_d - \tau_1)]\{r(t_d - \tau_1) - 2\} - \exp[r(t_d + \tau_2)]\{r(t_d + \tau_2) + 2\}]$$

and for $t_d \geqslant \tau_1$

$$P_1(t_d) = \frac{\exp[-rt_d]}{2}\,[\exp[r\tau_1] - \exp[-r\tau_2]] \ ,$$

$$P_2(t_d) = \frac{\exp[-rt_d]}{4}\,[\exp[r\tau_1]\{2 + r(t_d - \tau_1)\} - \exp[-r\tau_2]\{2 + r(t_d + \tau_2)\}] \ .$$

5568

If we put $\tau_1 = \tau_2 = \tau/2$, a common situation, $P(t_d)$ is symmetrical and is plotted in Fig. 2 as a function of $m = t_d/\tau$ with $r\tau$ as a parameter.

The coincidence efficiency is sometimes defined as the probability of recording a coincidence with zero delay. This is given for the two cases by

$$(6) \qquad \begin{cases} P_1(0) = 1 - \exp[-r\tau/2], \\ P_2(0) = 1 - (1 + r\tau/4)\exp[-r\tau/2]. \end{cases}$$

BELL, GRAHAM and PETCH estimate that for a pulses width 3 times the mean delay, the coincidence efficiency is 90%. This corresponds to $r\tau = 6$ and we see from (6) that the efficiency defined in this way is 95% where P_1 applies and 88% where P_2 applies.

It is also interesting to note that

$$(7) \qquad \begin{cases} P_1(\tau_1) = \tfrac{1}{2}[1 - \exp[-r\tau]], \\ P_2(\tau_2) = \tfrac{1}{2}[1 - (1 + r\tau/2)\exp[-r\tau]]. \end{cases}$$

In both cases for $r\tau$ large, $P(\tau_1) = \tfrac{1}{2}P(0)$. When the pulse widths are equal this occurs at $t_d = \tau/2$. Beyond τ_1, P_1 decays exponentially for all $r\tau$ while P_2 decays approximately exponentially.

If $\tau_1 \ll \tau_2$, then as delay is inserted, exponential decay of the counting rate occurs almost at once. Any asymmetry in the pulse widths reduces $P(0)$ and in the limit where $\tau_1 \to 0$ and $\tau_2 \to \tau$, $P(0)$ is given by (7) but this does not represent a real drop in efficiency as we shall show in Section **4**.

BELL, GRAHAM and PETCH give an experimentally determined prompt resolution curve for the case $\tau_1 = \tau_2 = 10^{-9}$ s in which they claim that one photo-electron was sufficient for an effective pulse and the delays other than those arising from the trans-stilbene phosphor were negligible. One half of the curve repre-

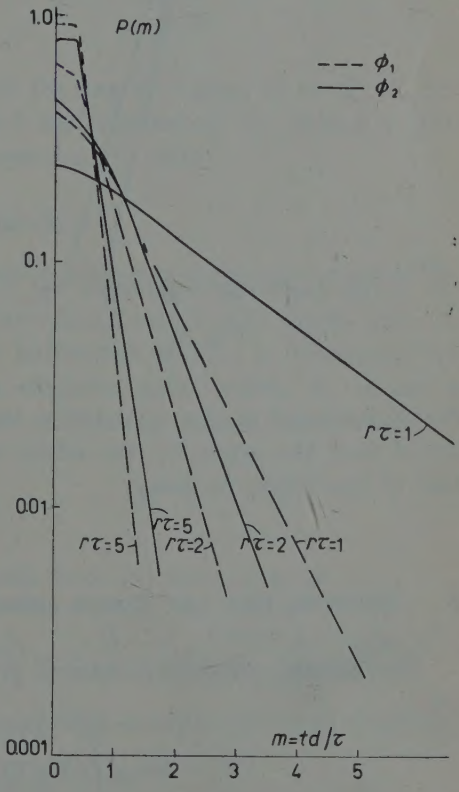

Fig. 2.

sents pulses due to a constant energy loss of 100 keV by hard β-rays passing through the phosphor, and from figures given by them for β and R in this case, we obtain $r\tau = 6.25$. In Fig. 3 their curve is plotted along with P_1 for this value of $r\tau$. Their curve falls somewhat more steeply and has a slope at large delays equal to that of P_1 for $r\tau = 8.7$. This sets a minimum value for $r\tau$ as any other sources of delay would increase the slope; hence their estimate of $r(= R\beta)$ is somewhat low. It will be noted that the Bell curve does not fall exponentially from $t_d/\tau = 0.5$ indicating that P_1 is not strictly applicable. However, as the departure from this condition is slight and the curve does not fall greatly short of the expected curve at small delays, their claim that one photo-electron was sufficient for a pulse and that delays other than in the phosphor are small is substantiated. P_2 has also been plotted in Fig. 3 for $r\tau = 10$ (considered here as an arbitrary parameter) and it will be seen that this is a fairly good fit for large delays but does not fully correct for the effect of transit time delays near the origin. It should be noted in this connection that the ordinate of the Bell curve is reduced near the origin by the effect of the part of the curve on the other side of the origin of delay.

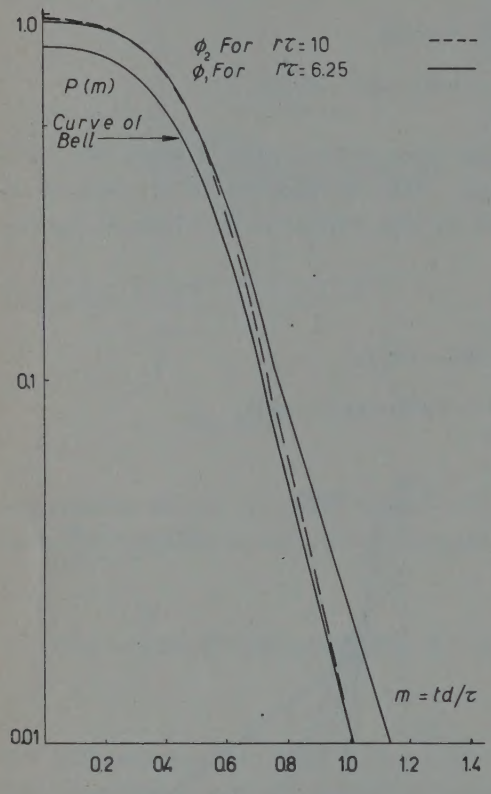

Fig. 3.

3. – Resolving time and chance coincidences.

The chance coincidence rate is given by

$$N_c = N^2 e_1 e_2 \int_{-\infty}^{\infty} \mathrm{d}T\, e(T) \int_{t_d - T}^{\infty} \mathrm{d}t_1\, \varphi(t_1)\varphi(t_1 + T - t_d)\,,$$

3570

where e_1 and e_2 are the net efficiencies of the counters and N is the source strength in disintegrations per second. Assuming the same form for $e(T)$ as in the previous section leads for both φ_1 and φ_2 to

$$N_c = N^2 e_1 e_2 \tau \, .$$

In this approximation for $e(T)$, the resolving time as measured by chance coincidences is determined entirely by the pulse widths τ_1 and τ_2 and not by the delay distribution (*).

A commonly used measure of resolving time is the full width of the prompt resolution curve at half-height which we designate T_e. T_e may be determined from Fig. 2 and in Table I, T_e/τ is plotted for various values of $r\tau$.

TABLE I.

$r\tau$	T_e/τ from φ_2	T_e/τ from φ_1
1	3.0	1.86
2	1.9	1.26
5	1.08	1.02

For $r\tau \gg 1$, T_e and τ are identical but for smaller values of $r\tau$, T_e is considerably greater and should not be used for calculating the chance coincidence rate. It can also be seen from equation (7) that

$$T_e = \tau \qquad \text{for} \quad r\tau \gg 1 \, .$$

For small values of $r\tau$, the half-width of the prompt resolution curve is influenced by the delay distribution but the chance rate is still unaffected. In general we might say that whenever the half-width of $P(t_d)$ is determined by the delay distribution rather than the effective pulse width, T_e is not a suitable value of resolving time to use for calculating chance coincidences.

4. – Delayed coincidence rate.

The delayed coincidence rate calculated from (1) for $t_d \geqslant \tau_1$ is

$$F_1(\lambda, t_d) = \exp\left[-\lambda(t_d - \tau_1)\right]\left[(1 - \exp\left[-\lambda\tau\right])\left(1 - \frac{\lambda}{2(\lambda - r)}\right) + \frac{\lambda \exp\left[(t_d - \tau_1)(\lambda - r)\right]}{2(\lambda - r)} \cdot \right.$$
$$\left. \cdot \left(1 - \exp\left[-(\lambda - r)(t_d - \tau_1)\right] - \exp\left[r\tau\right](1 - \exp\left[-(\lambda - r)(t_d + \tau_2)\right])\right)\right] ,$$

(*) This is also pointed out by BAY *et al.* [8].

[8] Z. BAY, V. P. HENRI and H. KANNER: *Phys. Rev.*, **100**, 1197 (1955).

$$F_2(\lambda, t_d) = \frac{\exp[-\lambda(t_d-\tau_1)]}{4(\lambda-r)^2}\left[\frac{4r^4}{(\lambda+r)^2}(1-\exp[-\lambda\tau]) + \right.$$
$$+\lambda(r-(\lambda-r)(r\tau+2))(\exp[-r\tau]-\exp[-2r\tau_1]) +$$
$$+\lambda\exp[(\lambda-r)t_d-\lambda\tau_1](\exp[r\tau_1]((2-r\tau_1+rt_d)(\lambda-r)-r)-$$
$$\left.-\exp[-r\tau_1]((2+r\tau_2+rt_d)(\lambda-r)-r)\right].$$

Here subscripts 1 and 2 again correspond to φ_1 and φ_2. For $r \gg \lambda$, *i.e.* for phosphor and phototube delays negligible in comparison to the lifetime being measured, we obtain in both cases

$$F(\lambda, t_d) = \exp[-\lambda(t_d-\tau_1)](1-\exp[\lambda\tau]).$$

This agrees with the expression for no delays and rectangular input pulses ([4]). The value of $F(\lambda, t_d)$ at $t_d = \tau_1$ is $(1-\exp[-\lambda\tau])$ and this is independent of τ_1/τ_2 for a given τ. Beyond this, F decays as $\exp[-\lambda t_d]$. It is therefore an advantage to keep τ_1 small as the exponential decay then starts at a smaller value of t_d. There is no loss in efficiency as the counting rate at which exponential decay sets in is unaltered.

In general, $F(\lambda, t_d)$ decays exponentially for $t_d - \tau_1$ sufficiently large that $P(t_d)$ is small. Progress towards the measurements of shorter γ lifetimes requires first the reduction of transit time spread in photomultipliers and ultimately faster phosphors. Circuits presently available do not limit the technique.

The lower limit to the lifetimes which can be measured by following the exponential decay depends only on the ratio of λ to r, and not at all on τ. Somewhat shorter lifetimes can of course be measured by the centroid method but the exponential method is simpler and is much more generally applicable than would appear if one considers only the relation of λ to τ or T_e as do BAY *et al.* ([8]).

JOHANSSON ([9]) using a resolving time of 30 ns (determined primarily by pulse width), was able to measure a half life of 1.1 ns by following the exponential decay beyond $t_d = \tau/2$. As we shall show presently, there is considerable advantage in using a large resolving time but it introduces a rectangular centre section into the prompt resolution curve. This is of no consequence except that larger delays are required to measure the desired lifetime. A method of removing it using a so-called differential coincidence circuit is discussed by MINTON ([10]). This system uses two fast and one slow coinci-

([9]) B. JOHANSSEN: *Nucl. Instr.*, **2**, 61 (1958).
([10]) G. H. MINTON: *Journ. Res. Nat. Bur. Stand.*, **57**, 119 (1956).

2572

dence circuits in order to remove the centre section and preserve symmetry. A less complicated solution is to remove only the positive delay side of the centre section by making τ_1 small. As already pointed out, exponential decay then begins almost immediately.

On the other hand it is an advantage to make $\tau_2 \gg 1/\lambda$, as may be seen by means of Fig. 4. One achieves a higher counting rate by measuring, for each value of t_d, the disintegration rate integrated from t_d to infinity, and if a multichannel time-analyser is used ([9]) many values of t_d can be measured simultaneously.

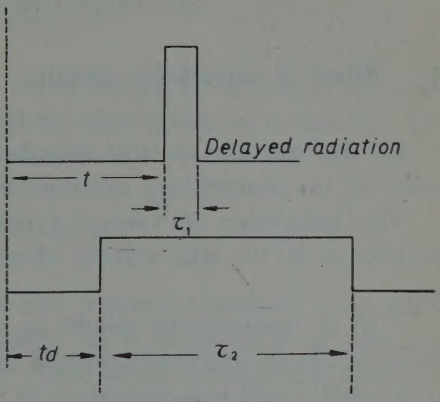

Fig. 4.

5. – The optimum resolving time.

The use of a large τ_2, while increasing the genuine coincidence rate, also increases the chance rate. Where chance coincidences are at all significant, it is necessary to seek a compromise.

We shall find now the optimum value of τ defined as that value which for a given genuine coincidence rate, leads to a minimum chance rate. This is expressed by the condition

$$F \frac{\partial N_c}{\partial \tau} - 2N_c \frac{\partial F}{\partial \tau} = 0 .$$

The resulting expressions are somewhat involved but for $r \gg \lambda$, they reduce to the expression obtained by MURDOCH ([4]) for the case of no delays,

$$\exp[\lambda\tau] = 1 + 2\lambda\tau ,$$

which has the solution $\lambda\tau = 1.26$. This determines the optimum value of τ which should consist mainly of τ_2, τ_1 being made as small as practicable.

For the often used case $\tau_1 = \tau_2 = \tau/2$, as in Fig. 2, the general expressions reduce, for φ_1 and φ_2 respectively to

$$2\lambda\tau + 1 = \exp[\lambda\tau] + \frac{\lambda \exp[-r\tau]}{\lambda - 2r}(1 + 2\lambda\tau - \exp[\lambda\tau]) -$$

$$- \frac{\lambda}{\lambda - 2r}(1 + 2r\tau - \exp[r\tau]) \exp[\lambda(t_d + \tau) - r(t_d + 2\tau)] ,$$

$$2\lambda\tau + 1 = \exp[\lambda\tau]\left[1 + \frac{\lambda\tau}{2r}(\lambda - r(r\tau + 1)) \exp[-r\tau]\right] .$$

3573

These expressions assume $r > \lambda$ and the second one neglects certain small terms, and assumes $\tau_1 = \tau_2 = \tau/2$.

4. – Effect of coincidence circuit.

In this Section we will consider the effect of the coincidence circuit on some of the simplifying assumptions we have used in the previous section.

The behaviour of various types of coincidence circuit are discussed by HUIJER *et al.* [11] who classify them as follows:

1) A regenerative circuit in which an output is obtained whenever a pulse of above a given threshold appears at both inputs. The output pulse rises rapidly and is independent of the input pulses once they are both above the threshold at the same instant.

2) A circuit where there is an output pulse whenever one or both pulses exceed a given threshold, being much larger in the latter case. The rise time of the output pulse is here slower than that of the input pulses and a discriminator is used to eliminate single pulses. HUIJER *et al.* show that if σ is the time for which the input pulse is above the threshold and $\sigma_{\min}$ is the minimum such time to allow an output pulse to rise above the discriminator bias, the effective pulse width τ_1 or τ_2 (separation time in their terminology) is given by $\sigma - \sigma_{\min}$. The Rossi circuit is of this type.

3) The rise time of the output is of the same order as the rise time of the input and the height of the output pulse at any moment depends on the height of the input pulses at that moment. The Bell circuit is of this type. HUIJER *et al.* show that the input pulses may be regarded as having a definite effective width which depends on their height and on the discriminator bias.

For all types of circuit, if pulses of fixed height and rise-time are used, there are definite effective pulse widths τ_1 and τ_2. Non-rectangular pulses of varying height can cause a variation of effective pulse width in the latter two types of circuit, but this can be overcome as in the Bell circuit by clipping all pulses to a fixed height, or by use of pulse height discriminator [5].

If the variation in effective pulse width is appreciable, one should average $P(t_d)$ over the distributions in τ_1 and τ_2. Thus if $P^1(t_d)$ is the true prompt

---

[11] P. HUIJER, E. F. DE HAAN and C. C. JONKER: *Physica*, **21**, 571 (1955).

3574

resolution curve we have

$$P^1(t_d) = \iint P(t_d, \tau_1, \tau_2) f_1(\tau_1) f_2(\tau_2) \, d\tau_1 \, d\tau_2 ,$$

where $f_1(\tau_1)$ and $f_2(\tau_2)$ are the probability distributions of the effective pulse widths and the integration is taken over all possible values of τ_1 and τ_2. For most purposes a sufficient approximation should be

$$P^1(t_d) = P(t_d, \bar{\tau}_1, \bar{\tau}_2) .$$

The time for the input pulses to reach the required threshold is an additional delay which if constant, has no effect. (If it is different for the two inputs, it merely alters the introduced delay t_d and shifts the zero of the prompt resolution curve). Any variation of pulse rise time modifies the delay distribution in a similar manner to transit time spread in the photo-multiplier.

If variation in pulse rise time is small, and if variation of effective pulse width is reduced by one of the methods indicated, the analysis given in earlier sections in terms of rectangular pulses τ_1 and τ_2 is valid provided these are interpreted as the effective pulse widths.

The influence of the discriminator on effective widths may be seen in the prompt resolution curves of DE BENEDETTI and RICHINGS ([12]) where increasing the discriminator bias reduced the half width and $P(0)$ as would be expected for a decrease in τ, but the slope of the curve for large delays was unchanged indicating that the delay distribution remained the same.

Using $P_1(0)$ as the efficiency, the value of r obtained from the slope at large delays is much higher than the measured values. This indicates that several electrons were required to give an effective pulse in this apparatus. The gaussian slope of their prompt resolution curve lends support to this conclusion.

We have deduced expressions for the prompt resolution curves in two interesting cases, and have shown that these curves agree with experiment when we have reason to expect that the original assumptions are fulfilled. The delayed coincidence counting rates are calculated and allow us to deduce a criterion giving the optimum value of resolving time. It is shown that it is often better to use unequal pulse widths to provide a given resolving time. Attention is focussed on the need to reduce the time delay spread of pulses in order to be able to measure smaller half lives in the interesting region of 10^{-10} to 10^{-12} s.

([12]) S. DE BENEDETTI and M. J. RICHINGS: *Rev. Sci. Instr.*, **23**, 37 (1952).

* * *

The authors wish to thank Professor MESSEL for the laboratory and computational facilities.

RIASSUNTO (*)

Si prendono in esame i fattori che, nell'uso dei contatori a scintillazione, influenzano la tecnica delle coincidenze. Per derivare la dipendenza della velocità di conteggio cosiddetto « rapido » e « ritardato » dal ritardo inserito, specialmente quando il tempo è breve, si impiegano espressioni approssimate della distribuzione dei ritardi casuali di tempo dovuti ai fotomoltiplicatori. Il raffronto con l'esperienza dimostra che tali espressioni sono applicabili in molti casi. Si tratta della scelta di un tempo risolvente « optimum », e si discutono le caratteristiche dei circuiti in coincidenza.

(*) *Traduzione a cura della Redazione.*

3570

IL NUOVO CIMENTO Vol. XIV, N. 4 16 Novembre 1959

About the Concept of Particle in Quantum Field Theory.

P. G. O. Freund

Chair of Physics of the Facultatea de Matematică și Fizică - Timișoara

(ricevuto il 3 Giugno 1959)

Summary. — Since the infinite vacuum fluctuations of the quantized fields are due to the fact that the particle number operators don't commute with the field operators, in order to eliminate such actually infinite fluctuations, non commutativity of particle number operators corresponding to particles of different sorts is admitted and thus automatically states with determined numbers of particles of various sorts are physically impossible. This leads to a non canonical quantization which is investigated. It is shown that in the case of non-canonical quantization the elementary oscillators of the field are not independent but coupled and that a cut-off automatically appears in the Green function which thus appears entirely regular. It also results that the concept of particle has no physical meaning.

1. – Introduction.

The higher order quantum effects are, as it is well known, due to the vacuum fluctuations of the interacting quantized fields. Let us consider *e.g.* the quantized electromagnetic field. In this case these fluctuations are a consequence of the fact that the particle number operators $N^{(\lambda)}(\boldsymbol{k})$ of the electromagnetic field don't commute with the field operators $F_{\mu\nu}$. Since the vacuum is an eigenstate of all $N^{(\lambda)}(\boldsymbol{k})$ according to the uncertainty relations $F_{\mu\nu}$ may have infinite fluctuations. Yet such infinite fluctuations should not be actually admitted as possible physical phenomena. The possibility of such infinite fluctuations also leads to divergencies in the theory. It is therefore necessary to eliminate the possibility of such infinite fluctuations in *physically possible* states. Since such fluctuations appear in any state in which the numbers $n^{(\lambda)}(\boldsymbol{k})$ of particles of any possible sort $(\lambda, \boldsymbol{k})$ are known (*), we simply must

(*) In particular the vacuum is such a state: $n^{(\lambda)}(\boldsymbol{k})=0$ for all λ and $\boldsymbol{k}$.

eliminate such states from the category of physical states. Thus, there should not exist common eigenstates to all the particle number operators $N^{(\lambda)}(\boldsymbol{k})$. This is the case only if we admit that the $N^{(\lambda)}(\boldsymbol{k})$ operators don't commute among them:

$$[N^{(\lambda_i)}(\boldsymbol{k}_i), N^{(\lambda_j)}(\boldsymbol{k}_j)] = f(\lambda_i, \lambda_j, \boldsymbol{k}_i, \boldsymbol{k}_j) \neq 0 \,. \tag{1}$$

For not complicating too much the notation let us mark an operator $X^{(\lambda_i)}(\boldsymbol{k}_i)$ referring to a state $(\lambda_i, \boldsymbol{k}_i)$ simply by X_i. With this convention relation (1.1) may be rewritten:

$$[N_i, N_j] = f_{ij} \neq 0 \,. \tag{1.1a}$$

Since

$$N_i = a_i^* a_i \qquad (i = 1, 2) \tag{1.2}$$

where a_i^*, a_i are the creation and annihilation operators, (1.1a) yields:

$$a_i^* a_i a_j^* a_j - a_j^* a_j a_i^* a_i = f_{ij} \,. \tag{1.3}$$

Such a relation cannot be actually satisfied by the operators a_i, a_i^* if the cannonical commutation rules for these operators hold. We are thus led to the necessity of a modification of the canonical commutation rules. In order that by an adequate limiting procedure the new commutation rules should lead to the canonical rules, we state them in the following way:

$$\begin{cases} [a_i, a_j^*] = m_{ij} \,, \\ [a_i, a_j] = [a_i^*, a_j^*] = 0 \,, \end{cases} \tag{1.4}$$

for $\lambda_i \neq \lambda_j$, $\boldsymbol{k}_i \neq \boldsymbol{k}_j$ as well as for $\lambda_i = \lambda_j$, $\boldsymbol{k}_i = \boldsymbol{k}_j$. Here:

$$m_{ij} = m(\lambda_i, \lambda_j, \boldsymbol{k}_i, \boldsymbol{k}_j) \neq \delta_{\lambda_i \lambda_j} \delta_{\boldsymbol{k}_i \boldsymbol{k}_j} \,. \tag{1.5}$$

From (1.4) there follows immediately the very useful relation:

$$m_{ij} = m_{ji}^* \,. \tag{1.6}$$

From (1.3), (1.4) and (1.6) the relation between m_{ij} and f_{ij} is easily found to be:

$$f_{ij} = m_{ij} a_i^* a_j - m_{ij}^* a_j^* a_i \,. \tag{1.7}$$

In order that this relation should be satisfied we have to admit m_{ij} to be a *c-number*, f_{ij} a *q-number*. Moreover (1.7) implies f_{ij} to be an antihermitic operator:

$$f_{ij} = -f_{ji}^* . \tag{1.8}$$

2. – The Hamilton operator.

Since the form:

$$H = \tfrac{1}{2} \sum_{k_i, \lambda_i} \omega_i \{a_i^*, a_i\} \tag{2.1}$$

for the Hamilton operator is independent of the commutation rules [1] it holds also with the new commutation rules (1.4). Let us restrict our considerations to the case of transversally polarized photons $\lambda = 1$. Considering the operators:

$$\begin{cases} q_i = \dfrac{1}{\sqrt{2\omega_i}} (a_i + a_i^*) , \\ p_i = -i \sqrt{\dfrac{\omega_i}{2}} (a_i - a_i^*) , \end{cases} \tag{2.2}$$

in this case the Hamilton operator can be written:

$$H = \tfrac{1}{2} \sum_{k_i, \lambda_i = 1} (p_i^2 + \omega_i^2 q_i^2) . \tag{2.3}$$

The commutation rules for q_i, p_i can be immediately obtained from (12). and (1.4), (1.6):

$$\begin{cases} [q_i, q_j] = \dfrac{1}{\omega_i \omega_j} [p_i, p_j] = \dfrac{m_{ij} - m_{ij}^*}{2\sqrt{\omega_i \omega_j}} = \alpha_{ij} , \\ [q_i, p_j] = \dfrac{i}{2} \sqrt{\dfrac{\omega_j}{\omega_i}} (m_{ij} + m_{ij}^*) = \beta_{ij} . \end{cases} \tag{2.4}$$

The canonical equations are:

$$\begin{cases} \dot{q}_i = i[H, q_i] , \\ \dot{p}_i = i[H, p_i] . \end{cases} \tag{2.5}$$

---

[1] G. KÄLLÉN: *Quantenelektrodynamik in the Encyclopedia of Physics*, edited by S. FLÜGGE, vol. 5, part I (Berlin, 1958).

The computation of the commutators on the right hand side yields:

$$\text{(2.6)} \qquad \begin{cases} i\dot{q}_i = \sum\limits_{k_j} (\beta_{ij} p_j + \alpha_{ij} \omega_j^2 q_j) , \\ i\dot{p}_i = \sum\limits_{k_j} (\alpha_{ij} \omega_i \omega_j p_j - \beta_{ij} \omega_i \omega_j q_j) . \end{cases}$$

Since α_{ij}, β_{ij} depend upon k_j, in order that the infinite system of differential eqs. (2.6) should be soluble one has to admit either α_{ij} or β_{ij} to vanish (otherwise neither the p variables nor the q variables could be separated within a finite number of differentiations of the eqs. (2.6)). Since by an adequate limiting procedure (*) (2.4) ought to pass into the usual commutation rules for the q_i, p_i we have to put:

$$\text{(2.7)} \qquad \alpha_{ij} = 0 .$$

Relation (2.4) then yields:

$$\text{(2.8)} \qquad m_{ij} - m_{ij}^* = 0$$

and thus

$$\text{(2.9)} \qquad \mathrm{Im}\,(m_{ij}) = 0 .$$

Thus m_{ij} is purely real and by (2.4) the commutator $[q_i, p_j]$ purely immaginary as it ought to be.

With (2.7), (2.4) the canonical eqs. (2.6) become:

$$\text{(2.10)} \qquad \begin{cases} \dot{q}_i = \sum\limits_{k_j} \sqrt{\frac{\omega_j}{\omega_i}}\, m_{ij} p_j , \\ \dot{p}_i = -\sum\limits_{k_j} \sqrt{\omega_i \omega_j}\, \omega_j m_{ij} q_j . \end{cases}$$

These equations prove that our new commutation rules (1.4) imply a coupling of the elementary oscillators. Opposite to what happens when the usual canonical quantization is undertaken and when the field appears as a sum of uncoupled harmonic oscillators, with our new commutation rules (1.4) *a coupling of the elementary oscillators* is introduced. Elimination of the p variables from (2.10) yields:

$$\text{(2.11)} \qquad \ddot{q}_i = -\sum_{k_j} \sqrt{\frac{\omega_j}{\omega_i}}\, m_{ij} \sum_{k_l} \sqrt{\omega_j \omega_l}\, \omega_l m_{jl} q_l .$$

(*) Here as well as in stating the new commutation rules the existence of such a limiting procedure is assured by the general correspondence principle.

3580

Let us consider the stationary states for which the matrix elements $(q_i)_{st}$ (which we shall simply mark q_{ist}) are harmonic functions of the time with the pulsation ω_{ist}. Taking the st matrix element of (2.11) one obtains the infinite system of linear homogeneous equations:

$$\sum_{k_l} q_{lst} \left\{ \sum_{k_j} \omega_j \omega_l \sqrt{\frac{\omega_l}{\omega_i}} m_{ij} m_{jl} - \delta_{k_j k_l} \omega_{ist}^2 \right\} = 0 . \tag{2.12}$$

With the notation:

$$A_{k_i k_l} = \sum_{k_j} \omega_j \omega_l \sqrt{\frac{\omega_l}{\omega_i}} m_{ij} m_{jl} - \delta_{k_i k_l} \omega_{ist}^2 , \tag{2.13}$$

the compatibility of the linear system (2.12) is expressed by the condition:

$$|A_{k_i k_l}| = 0 . \tag{2.14}$$

Since the m_{ij} are small as they correspond to higher effects (in the canonical approximation they vanish except for $i = j$) we may approximate the determinant (2.14) with the product of its diagonal elements. Eq. (2.14) then yields:

$$\omega_{ist} = \pm \sqrt{\omega_i} (\sqrt{\sum_{k_j} m_{ij}^2 \omega_j}) . \tag{2.15}$$

In the canonical approximation ($m_{ij} = \delta_{ij}$) (2.15) gives the well known result $\omega_{ist} = \pm \omega_i$. In the general case the root factor characterizes the coupling of the oscillators. Since only two values for ω_{ist} are possible (in our approximation), as usually one may put

$$\omega_{it\,t+1\,t} = - \omega_{it\,t-1\,t} = + \sqrt{\omega_i} \sqrt{\sum_{k_j} m_{ij}^2 \omega_j} . \tag{2.16}$$

Taking the diagonal matrix element of the commutator $[q_i, p_i]$ and making use of (2.10) and the harmonic time-dependence of the q_i and p_i matrix elements one finds the following recurrent equation for the matrix elements:

$$\sum_{k_l} \frac{\sqrt{\omega_i \omega_l} \omega_l m_{jl}}{\omega_{jt+1\,t}} [q_{it+1\,t} q_{ltt+1} - q_{itt-1} q_{lt-1\,t}] + \\ + [q_{itt+1} q_{lt+1\,t} - q_{it-1\,t} q_{ltt-1}] = m_{ij} . \tag{2.17}$$

Like in the cannonical case only the two neighbour paralleles to the main diagonal of the q_i (and p_i) matrix are non vanishing. Thus the Hamilton ope-

rator in this representation is diagonal but its eigenvalues are not anymore the different sums of the energies of all sorts of photons multiplied by the respective number of particles, since by the new commutation rules the elementary oscillators of the field are coupled and *the concept of particle has no physical meaning.*

3. – The Green function.

Since in the canonical theory the divergencies are raised by the singular character of the Green functions (for the electromagnetic field the D functions) let us find the Green function of the electromagnetic field quantized by our new commutation rules (1.4). Making use of the plane wave decomposition of the electromagnetic potentials:

$$A_\mu(x) = \frac{1}{\sqrt{V}} \sum_{k,\lambda} \frac{e_\mu^{(\lambda)}}{\sqrt{2\omega}} \left(a^{(\lambda)}(\boldsymbol{k}) \exp\left[ikx\right] + a^{*(\lambda)}(\boldsymbol{k}) \exp\left[-ikx\right]\right) . \tag{3.1}$$

and of the new commutation rules (1.4), one finds for the commutator of the field operators taken at two arbitrary moments:

$$\left[A_\mu(x), A_\nu(x')\right] = -\widetilde{D}_{\mu\nu}(x', x) , \tag{3.2}$$

where

$$\widetilde{D}_{\mu\nu}(x', x) = \frac{1}{(2\pi)^3} \int \frac{\mathrm{d}^3 k}{\sqrt{\omega}} \sum_{k',\lambda,\lambda'} \frac{e_\mu^{(\lambda)} e_\nu^{(\lambda')}}{\sqrt{\omega'}} m(\boldsymbol{k}, \boldsymbol{k}', \lambda, \lambda') \sin\left(k'x' - kx\right) . \tag{3.3}$$

Since in the cannonical quantization the divergencies arise because of the momentum integration and not because of the summation over all polarizations, it is of interest to consider:

$$m(\boldsymbol{k}, \boldsymbol{k}', \lambda, \lambda') = \delta_{\lambda\lambda'} m(\boldsymbol{k}, \boldsymbol{k}') . \tag{3.4}$$

Since:

$$\sum_\lambda e_\mu^{(\lambda)} e_\nu^{(\lambda)} = \delta_{\mu\nu} , \tag{3.5}$$

from (3.3), (3.4) one obtains in this case:

$$\widetilde{D}_{\mu\nu}(x', x) = \delta_{\mu\nu} \widetilde{D}(x', x) , \tag{3.6}$$

where

$$\widetilde{D}(x', x) = \frac{1}{(2\pi)^3} \int \frac{\mathrm{d}^3 k}{\sqrt{\omega}} \sum_{k'} \frac{m(\boldsymbol{k}, \boldsymbol{k}')}{\sqrt{\omega'}} \sin\left(k'x' - kx\right) . \tag{3.7}$$

3682

Thus it is clearly to be seen that the new quantization leads to a cut-off ($m(\boldsymbol{k}, \boldsymbol{k}')$ as was already pointed out takes small values) in the Green function which thus becomes *regular* and the usual divergencies (due to the singular Green functions) will not appear.

4. – Conclusions.

A) The physical necessity of non-canonical quantization led us to three important physical consequences: *a*) *the concept of particle has no physical meaning*; *b*) *the elementary oscillators of the field are not independent but coupled*; *c*) *the Green functions are not anymore singular but are entirely regular because of the cut-off that automatically appeared.*

B) Our considerations developed on the case of the electromagnetic field are valid for any other quantized field.

With the electromagnetic field canonical quantization led to satisfactory results when by means of perturbation theory the interaction of electromagnetic and electronic fields was investigated. Non-canonical quantization ought to lead to observable effects at very high energy processes. The energy threshold corresponding to observable effects of non-canonical quantization ought to be much lower with pion-nucleon interaction where the application of non-canonical quantization could be used in order to determine the real form of the m_{ij} function, since this function appears as a cut-off in the Green function which itself appears at the computation of observables. Because of the regular character of the Green function observable results will not diverge.

C) Since in physical states no infinite fluctuations of the electromagnetic field ($F_{\mu\nu}$) are possible, there must exist a maximal value for the $F_{\mu\nu}$. In this respect the non-canonical quantization realizes the features of a non-linear theory.

D) The presence of an invariant cut-off is incompatible with both: the usual field equations and the canonical commutation rules. Starting from the necessity of a cut-off FEYNMAN [2] suggested a modification of the field equations. By our method it appears clearly that non-canonical quantization is able to furnish an invariant cut-off. Moreover this method doesn't lack of physical justification.

E) Since PAULI's [3] proof of the correspondence theorem between spin and quantization rules (commutative or anticommutative) is independent of

---

([2]) R. P. FEYNMAN: *Phys. Rev.*, **74**, 939, 1430 (1948).
([3]) W. PAULI: *Phys. Rev.*, **58**, 716 (1940).

3588

the actual value of the commutator or anticommutator it is clear that the non-canonical commutation rules are consistent with the Lorentz invariance and the positive definiteness of the energy if only, as usually commutators (anticommutators) are, used with fields corresponding to particles with integer (half integer) spin. Since in any physically possible state the number of particles of different sorts is not determined, the problem of statistics itself ought to be essentially modified whenever we deal with non-canonical quantization.

* * *

I wish to express my thanks to Prof. C. I. SĂLCEANU for the hospitality extended to me at the Chair of Physics of the Facultatea de Matematică şi Fizică, Timişoara during the performance of this work and to Lecturer M. ZĂGĂNESCU for valuable discussions.

RIASSUNTO (*)

Poichè le infinite fluttuazioni del vuoto dei campi quantizzati sono dovute al fatto che gli operatori del numero di particelle non commutano con gli operatori del campo, allo scopo di eliminare tali fluttuazioni effettivamente infinite, si ammette la non commutatività degli operatori del numero di particelle corrispondenti a particelle di differenti specie; segue allora automaticamente che sono fisicamente impossibili gli stati con numero determinato di particelle di varie specie. Ciò conduce ad una quantizzazione non canonica che si prende in esame. Si dimostra che, nel caso della quantizzazione non canonica, gli oscillatori elementari del campo non sono indipendenti bensì accoppiati, e che compare automaticamente un taglio nella funzione di Green che in tal caso è completamente regolare. Risulta altresì che il concetto di particella non ha significato fisico.

(*) *Traduzione a cura della Redazione.*

2584

IL NUOVO CIMENTO Vol. XIV, N. 4 16 Novembre 1959

The β-Decay of ^{234}Pa (UZ) (*).

P. W. De Lange, H. Schneider (**) and J. W. L. De Villiers

C.S.I.R. - Pretoria

(ricevuto il 15 Giugno 1959)

Summary. — The β- and γ-ray spectra observed in the decay of UZ (6.66 hours) have been investigated. Results of β-γ-coincidence measurements are given. γ-γ-coincidences obtained with selected γ-photopeaks in a scintillation unit are discussed. A decay scheme involving 6 β-transitions and 39 γ-transitions is presented. It is proved that UZ is the ground state of ^{234}Pa with UX2 (22 ± 12) keV above it. A spin of 6^- for UZ is explained in terms of Nilsson states.

1. – Introduction.

It has been known since 1921 (1) that the β-decay of ^{234}Th(UX1) with a halflife of 24.1 days leads to two daughters in ^{234}Pa. The two daughters are called UX2 (1.175 min) and UZ (6.66 hours). These two states of ^{234}Pa emit β- and γ-radiation in their decay to ^{234}U, which is α-radioactive ($2.48 \cdot 10^5$ y). The radiation from this UX-complex has been studied extensively (2-7).

(*) This work forms part of a D.Sc. thesis submitted to the University of Pretoria by P. W. de Lange, November, 1958. This investigation was partially sponsored by the South African Atomic Energy Board.

(**) Present address: Physikinstitut der Universität Fribourg.

(1) O. Hahn: *Naturwiss.*, **9**, 84 (1921); *Ber. dtsch. chem. Ges.*, B **54**, I, 1131 (1921).

(2) H. Bradt, H. G. Heine and P. Scherrer: *Helv. Phys. Acta*, **16**, 455 (1943).

(3) M. Heerschap: *Thesis*, Vrije Universteit, Amsterdam (1951).

(4) P. H. Stoker, M. Heerschap and O. P. Hok: *Physica*, **19**, 433 (1953).

(5) S. A. E. Johansson: *Phys. Rev.*, **96**, 1075 (1954).

(6) E. F. De Haan, G. J. Sizoo and P. Kramer: *Physica*, **21**, 803 (1955).

(7) O. P. Hok, J. Th. Verschoor and P. Born: *Physica*, **22**, 465 (1956).

3565

It was previously pointed out ([8]) that with the available data three problems remained unsolved:

1) Spin and parity assignment of UX2 exhibited a serious inconsistency with the log *ft* value of the β-transition to the ground state of ^{234}U.

2) The knowledge of the excited states of ^{234}U was rather vague.

3) The relative position of the two states of ^{234}Pa was not yet definite. In the earlier works BRADT, HEINE and SCHERRER ([2]) regarded UZ to be the ground state. After doing certain coincidence experiments JOHANSSON ([5]) concluded that UZ should have an energy slightly higher than UX2.

The decay of UX2 has been discussed by the present authors ([8]), solving the first problem and a part of the second.

The purpose of this paper is to present the results of the measurements that have been carried out and to describe the procedure that has been followed in the construction of a decay scheme for UZ. The two decay schemes of UZ and UX2 are compared and a conclusion is reached regarding the ground-state of ^{234}Pa.

2. – Experiments.

2·1. *The source.* – The preparation of UZ sources from 60 kg U_3O_8 (86 % purity) has been described elsewhere ([8,10]).

2·2. *The β-spectrum of* UZ. – An intermediate image β-spectrometer (LKB 3024 Siegbahn-Slätis) was used. The original model was altered to permit the use of different Geiger tubes or scintillation units to register the β-rays. A scintillation unit (2 in. × 1¾ in. diameter NaI crystal; 2 cm light guide; EMI 6260 photomultiplier) was fitted behind the source holder so that β-γ- and e^--γ-coincidence measurements could be made.

The β-spectrum of UZ above 1000 G·cm (Fig. 1) was obtained using a halogen G.M. counter (100 NB - Amperex Electronics Corporation: 3.5 mg/cm² mica window; inherent time delay 0.60 μs). The β spectrometer was set at 2.5 % resolution.

([8]) H. SCHNEIDER, P. W. DE LANGE and J. W. L. DE VILLIERS: *Nuovo Cimento*, **14**, 11 (1959).

([9]) W. L. ZIJP, SJ. TOM and G. J. SIZOO: *Physica*, **20**, 727 (1954).

([10]) J. v. R. SMIT, M. PEISACH and F. W. E. STRELOW: *Second Intern. Conf. on the Peaceful Uses of Atomic Energy*, A/Conf. 15/P/1119 (1958).

3586

For the low energy region the halogen tube was replaced with a thin window tube. The thin window was an ethyl acetate film of 0.03 mg/cm². The film

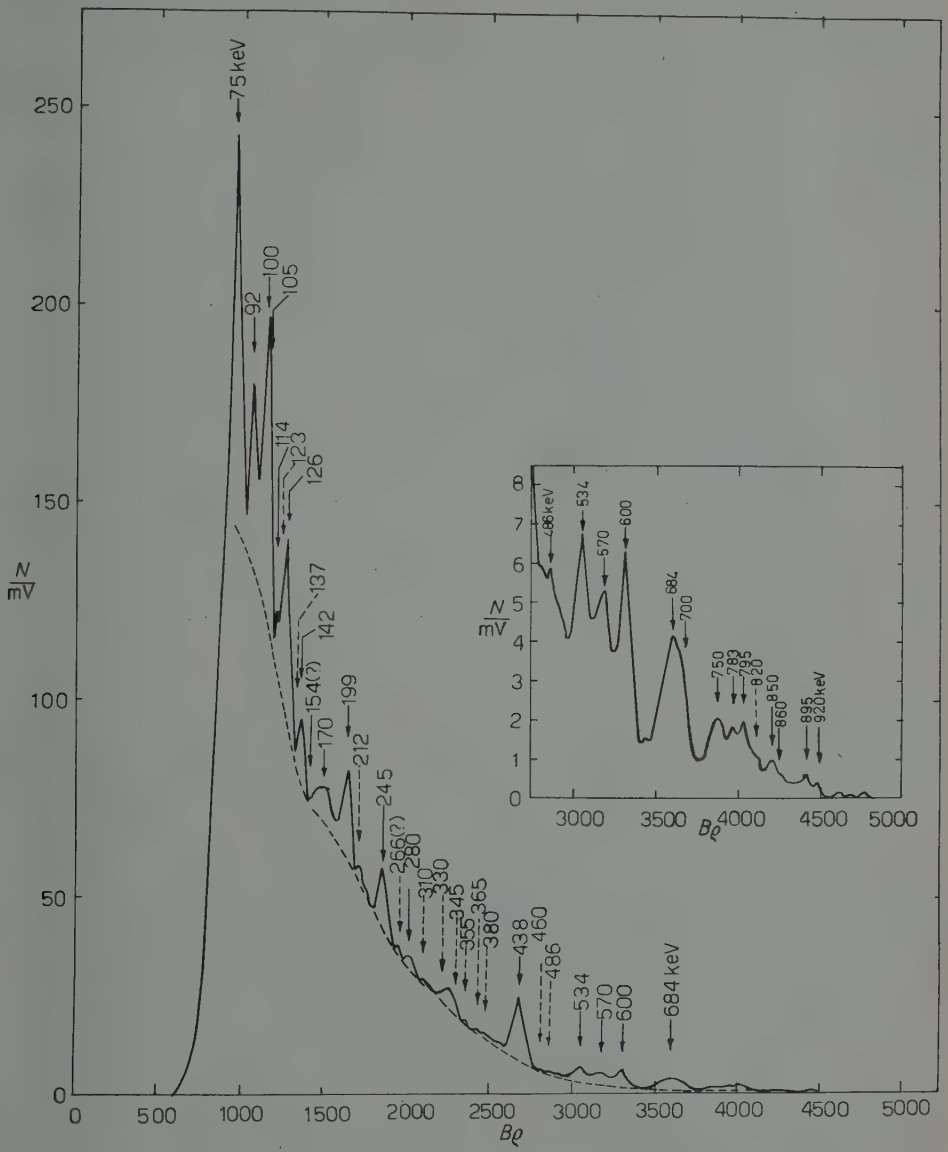

Fig. 1. – β-spectrum of ^{234}Pa(UZ): high energy part.

was obtained by dropping one drop of a 2 % solution of ethyl acetate in acetone on water. This Geiger tube performed quite well with ethyl alcohol vapour at

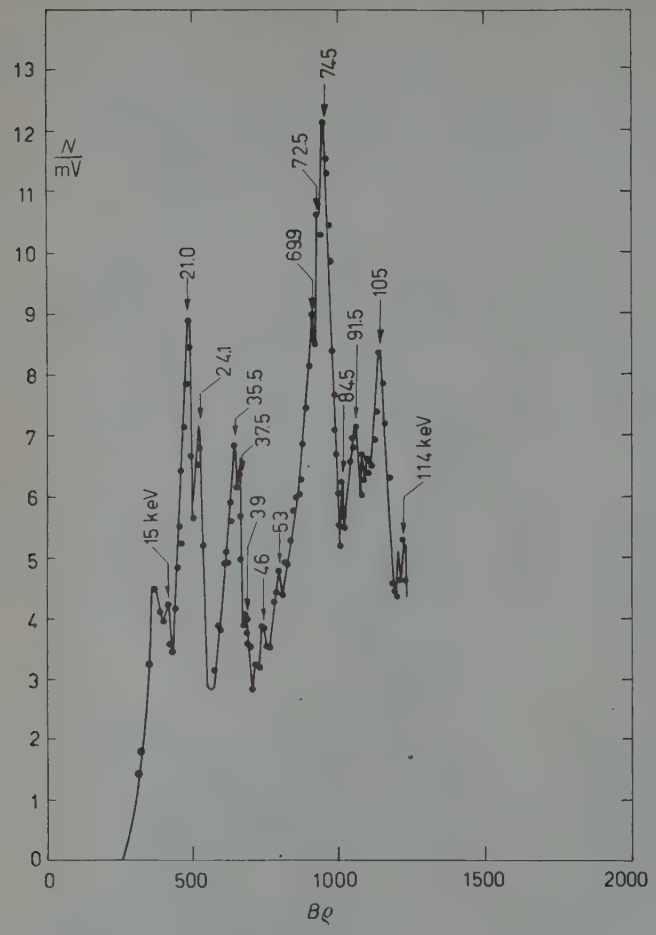

a pressure of 2 cm Hg. To compensate for alcohol vapour diffusion through the thin film and to maintain a constant pressure, a flask of alcohol connected to the Geiger tube was kept at a temperature of about 11 °C. Plateau curves (60 V) as well as time delay settings were checked every four hours. The inherent delay of this Geiger tube is about 0.20 μs.

Subsequently the low energy β-spectrum of UZ (Fig. 2) was measured between 300 and 1500 G·cm. The

Fig. 2. – β-spectrum of ^{234}Pa(UZ): low energy part.

TABLE I. – *Results of* F-K *analysis of the* β*-spectrum of* UZ. *Calibration of the* β*-spectrometer is based on the conversion lines of* ^{137}Cs *and the different lines in* Th(B+C+C″) (13).

No.	E_0 in keV	Relative intensity (%)	log *ft*.
1	1042 ± 20	3.6	8.21
2	576 ± 10	13.2	6.80
3	477 ± 10	16.0	6.47
4	363 ± 10	10.3	6.31
5	275 ± 10	21.4	5.57
6	141 ± 10	35.5	4.51

3588

TABLE II. – *Assignment of conversion lines in the decay of* UZ.

No.	E_{e^-} in keV (*)	Intensity %	Assignment of e⁻-line in keV		No.	E_{e^-} in keV (*)	Intensity %	Assignment of e⁻-line in keV	
			Fig. 1, 2	HOK(7)				Fig. 1, 2	HOK(7)
1	920	—	L 935	—	28	142	0.50	K257	M_{II}152
2	895	—	L 915	—				L 165	—
3	850	—	L 870	—	29	138	0.05	M143	L_{III}153
4	820	—	K935	K924	30	126	2.7	L_{III}143	—
5	795	—	K915	—		123		L_{II}143	—
6	783	?	L 805	L 801	31	114	0.05	K229	—
7	750	0.12	K870	—	32	105	4.0	L 125	—
8	700	0.46	L 715	—				M110	—
9	684		K805	K801	33	100		K215±5	K226
10	600	0.40	K715	K731	34	92	1.34	K205	—
11	570	0.05	K685	—				L_{III}110	—
12	534	0.22	L 553	L 565	35	88		M95	—
13	486	?	K600	K603?				L_{II}110	—
14	460	—	L 480	—	36	84.5		M90?	M_{II}99
15	442	1.28	K560?	K567				L_{III}99	—
			L 470	—	37	78		L_I99	—
	438		K553	—				L_{III}95	L_{II}99
16	422	—	L 445	—		74.5	9.6	L_{II}95	—
17	355	?	K480	—		73		L_I 95	—
18	365	0.23	K470	—	38	69.9		M75	—
19	345	0.34	L 360	L 368	39	53±4		K172	—
	330		K445	—				L 75	—
20	310	—	L 327	L 331	40	46		K161	—
21	280	0.20	L 295	L 292	41	39	?	L_{III}57	—
22	266	?	K380	—	42	37.5	4.0	L_{II} 57	M_{II}43
23	245	1.0	K360	K369	43	35.5		L_I57	K153
	204		L 257	—				M41.5	—
24	212	0.12	K327	K334	44	24	6.4	M_I28	—
			L 229	—				K143	—
25	199	2.0	L 220	L 225				L_{III}41	—
26	170±15	0.96	K295	K294	45	20.7		L_{II}41	—
			L 205	—	46	15–17		Auger	—
27	154	?	L 175	N_{II}153					

(*) The error in the energy values is about 1 % except where a larger error is indicated

3589

TABLE III. – *Summary of results obtained with various methods of investigation of transitions in* UZ *decay.*

I	II	III	IV	V	VI											
No.	E_γ keV	E_γ keV	± keV	Int. ratio	1670 keV		1380 keV		910 keV		710 keV		560 keV		230 keV	
					a	*b*	*a*	*b*	*a*	*b*	*a*	*b*	*a*	*b*	*a*	*b*
1	1680	1670	20	1		—		—		—		—		—		—
2	1430	1385	30	2.6		—		—		—		—		—		—
3	—	1400	—			—		—		—		—		—		—
4	1240	1200	20	0.54		—		—		—		—		—		—
5 (*)	—	1140	20	0.18		—		—		—		—		—		—
6	924	935	15	13.8		—		—		w		—		w		—
7	—	915	15			—		—	w	w	w			—		—
8	877	870	15			—		—	N	?		—	w			—
9 (*)	—	(815)	15	?		—		—		—		—		—		—
10	803	805	10	N		—		—	?		w		?		w	
11	732	715	10	13.1		—		—	w	m	w	w	w		w	
12	—	685	10			—		—	w	?		w		—	w	
13 (*)	(603)	600?	10	N		—		—		—	w		w	w	N	
14	566	560	10	13.8		—		—		m		m		w		—
15	—	553	10			—	w		m		m		m		m	
16	—	480	10	—		—	m		w	w	?	w	w	w		—
17	—	470	10	w		—	N		w		w				w	
18	—	445	10	w		—	w		w	?	N	w	N		N	
19 (*)	—	380	5	w		—		—	N		w			—	w	
20	268	360	5	w		w	w	w	w	w	?	w	w		m	
21	333	327	5	?	—		w	w	m		m		w		s	

3591

26	226	220	5		w		?		s	N	s	s	m	w	s					
27	—	215	5	m		—		—		—		—		—		—				
28	—	205	5		w	w	m	m	?	m	w	w	w	w	w					
29 (*)	—	175	5	—		—		—		—		—		—		—				
30	—	165	3	?	N		w		s	m	w	m	w		w					
31	153	143	3	s	w	w	w	?	s	I ?	w	?	s			—				
32	125	125	3			?		?	s	I		N	w				s			
33	—	110	3	N		—	w		m		w		s			—				
34	99.2	100	2	≡	s	≡	w	s	w	s	s	s	s	s	s					
35	—	95	3		s						s		s		s					
36	—	76	3	w	w	w	w	w	m		w	w	w	w	w					
37	—	66	3																	
38	—	57	3	?	w						not measured									
39	43	43	3	N	s	N					not measured									
40	—	33	5	?		—		—		—		—		—		—				
41	—	17	—	X-rays		—		—		—		—		—		—				

(*) These weak γ transitions have not been allocated in the decay scheme.

Column: I number;
II γ-transitions Hok *et al.* (7);
III γ-transitions found in this investigation;
IV estimated error in the energy values;
V intensity ratio with respect to the intensity of the 1670 keV γ-transition in single γ-spectrum;
VI γ-transitions that are in coincidence with different photo-peak energies. The ranges covered by the window of the discriminator are as follows: (1670 ± 100) keV; (1380 ± 100) keV; (910 ± 100) keV; (710 ± 70) keV; (560 ± 60) keV; (230 ± 45) keV.

Columns *a* and *b* represent e^--γ- and γ-γ-coincidence measurements respectively.

Estimation of Intensity: w weak;
m reasonable;
s strong;
N not detected.

Fermi-Kurie analysis ([11,12]) of the β-spectrum of UZ gave the results shown in Table I ([13]).

These results are in some disagreement with the latest results of HOK, VERSCHOOR and BORN ([7]), who found 4 transitions whereas our analysis exhibits 6. However, it seems reasonable that the partial spectra of lower intensity are undetectable with weak sources although their presence in the spectrum has an influence on the E_0 of the other partners in the F-K analysis.

2·3. *Conversion line spectrum of* UZ. – The energies of the γ-transitions which are responsible for the different conversion lines in Figs. 1 and 2 are tabulated in Table II. The intensities of the conversion lines, single or complex, are given in relation to the total area of the β-spectrum.

No effort has been made to determine the conversion coefficients of the various γ-transitions. The β-spectrometer with its high transmission power is suitable for coincidence analysis but not for measurements where high resolution is necessary. Coincidence measurements formed the major part of this investigation.

Because the transition energies from conversion lines are about a factor of 10 more accurate than those measured with scintillation counters, some attempt has been made to correct the γ-energies below 1000 keV where possible. However the coincidence experiments described in later paragraphs involve in almost all cases complex photo-peaks. It was therefore decided to take the errors in the energy values of γ-transitions from the scintillation counter measurements and these are quoted in Table III.

2·4. *γ-spectrum.* – The γ-spectrum was measured with a single channel scintillation unit.

In general (Fig. 3) it is in good agreement with that of HOK *et al.* ([7,14]). Slightly better resolution of the photo-peaks was possible. The lower energy spectrum taken with another source and 4× increased amplification, is shown in Fig. 4. The photo-peak at 230 keV consists of at least three different peaks, a conclusion which could only be reached from the results of the coincidence measu-

---

([11]) S. A. MOSZKOWSKI: *Phys. Rev.*, **82**, 35 (1951).

([12]) D. STROMINGER, J. M. HOLLANDER and G. T. SEABORG: *Rev. Mod. Phys.*, **30**, 585 (1958).

([13]) K. SIEGBAHN: Chapter III in *Beta and Gamma Ray Spectroscopy* (Amsterdam, 1955).

([14]) O. P. HOK and G. J. SIZOO: *Physica*, **19**, 1205 (1953).

3592

rements. It is this complex peak which caused some controversy among previous investigators ([4,6,7]).

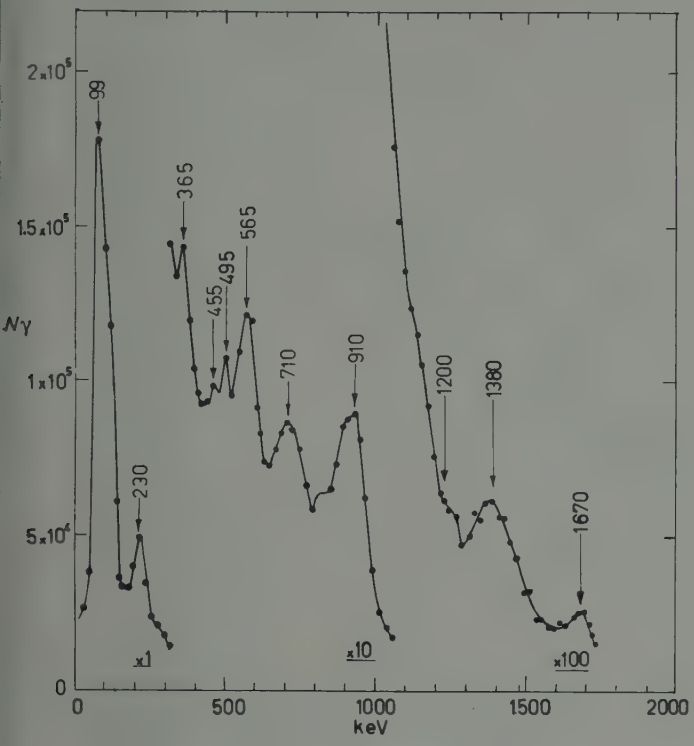

Fig. 3. – γ-spectrum of ^{234}Pa(UZ).

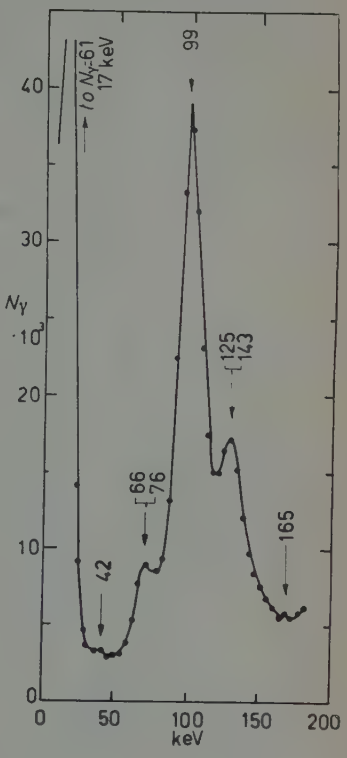

Fig. 4. – γ-spectrum of ^{234}Pa(UZ): low energy part.

The intensities of the γ transitions in the single γ-spectrum (Table III) are given with respect to the intensity of the 1670 keV transition. The relative intensities were determined with the method of Berger and Doggett ([15]). A detailed discussion of the motivations for the existence of all the different γ-rays is given elsewhere ([16]).

2·5. β-γ- and e⁻-γ-*coincidence measurements.* – Some of the important measurements that were made are the β-γ- and e⁻-γ-coincidences with the photo-

([15]) M. J. Berger and J. Doggett: *Journ. Res. Natl. Bur. Stand.*, **56**, 355 (1956).
([16]) P. W. De Lange: *D.Sc. Thesis*, University of Pretoria, Nov. 1958.

3563

peak of the 1670 keV γ-transition. It was assumed that this photo-peak is quite pure and ideally suited to coincidence studies. However, the number of coincidence counts that can be expected is rather low with a crystal to source distance of 3.2 cm. Only 0.8% of the activity emitted by the source at this energy will be registered in the photo-electric peak at 1670 keV.

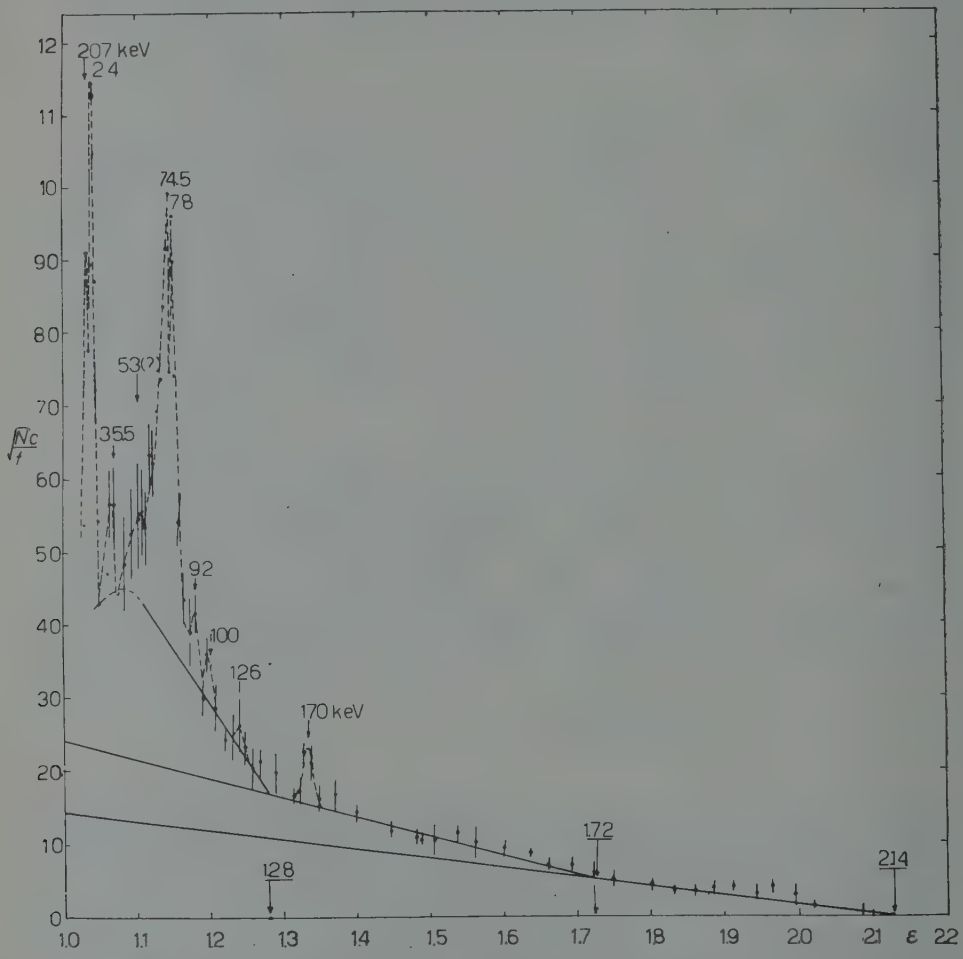

Fig. 5. – Complete F-K plot of β-γ_{1670}-coincidences. Measurements on 20 different UZ sources have been combined. Coincidence peaks can be seen with the conversion line at 20.7, 24, 35.5, 74.5, 78, 92, 100, 126 and 170 keV.

Twenty UZ sources have been used to obtain the β-γ- and e^--γ-coincidence measurements. The counting time for each point ranged between 30 and 120 minutes. Each run with a particular source took twelve to eighteen hours. The

3594

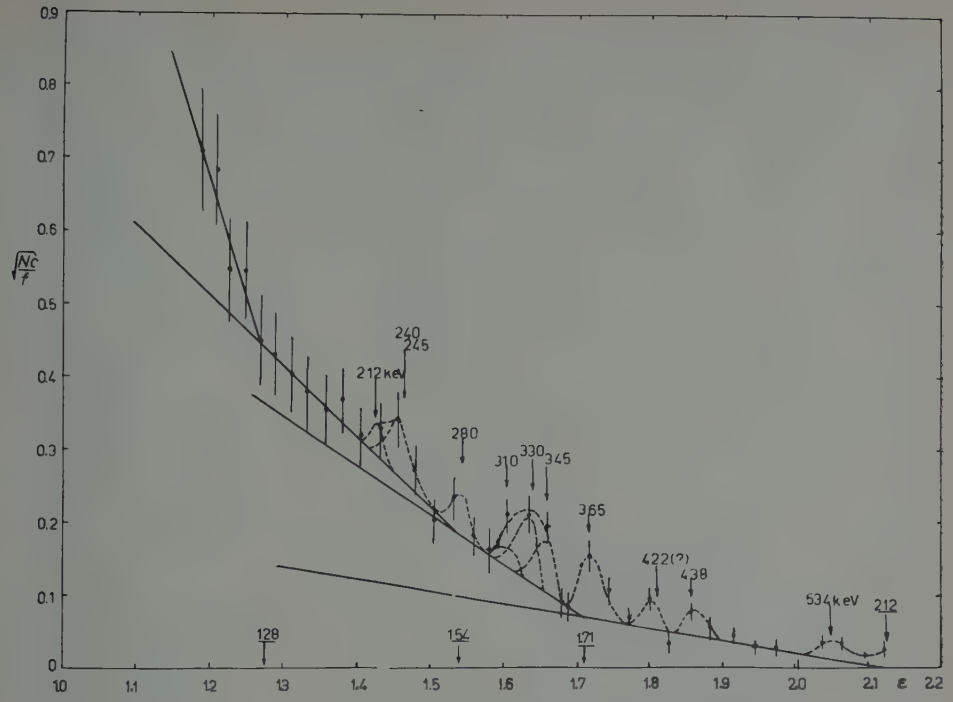

Fig. 6. – Complete F-K plot of β-γ_{1380}-coincidences.

transmission of the β-spectrometer was 5% with the intermediate slit fully open giving a resolving power of 5% with sources of 2-3 mm in diameter. A combined F-K plot is given in Fig. 5.

TABLE IV. – *Coincidences between β-spectra and different γ-lines.*

Column I			Column II					
No.	E_0 in keV	E_0 in mc^2-units	1 670 keV	1 380 keV	910 keV	710 keV	560 keV	230 keV
1	1 042	3.04	—	—	1	1	1	1
2	576	2.13	1	1	2	—	—	—
3	477	1.93	—	—	—	19	33	12
4	363	1.71	0.5	7.6	11	?	—	—
5	275	1.54	—	3.9	—	23	30	8.9
6	141	1.28	1.8	12	23	86	74	51

Column I: Number and maximum energy of β-transitions in UZ decay.
Column II: Ratio of different β-transitions which are coincident with specific γ-photo-peaks, single or complex. In each sub-column the intensity of the most energetic β-transition present is chosen as unity.

3595

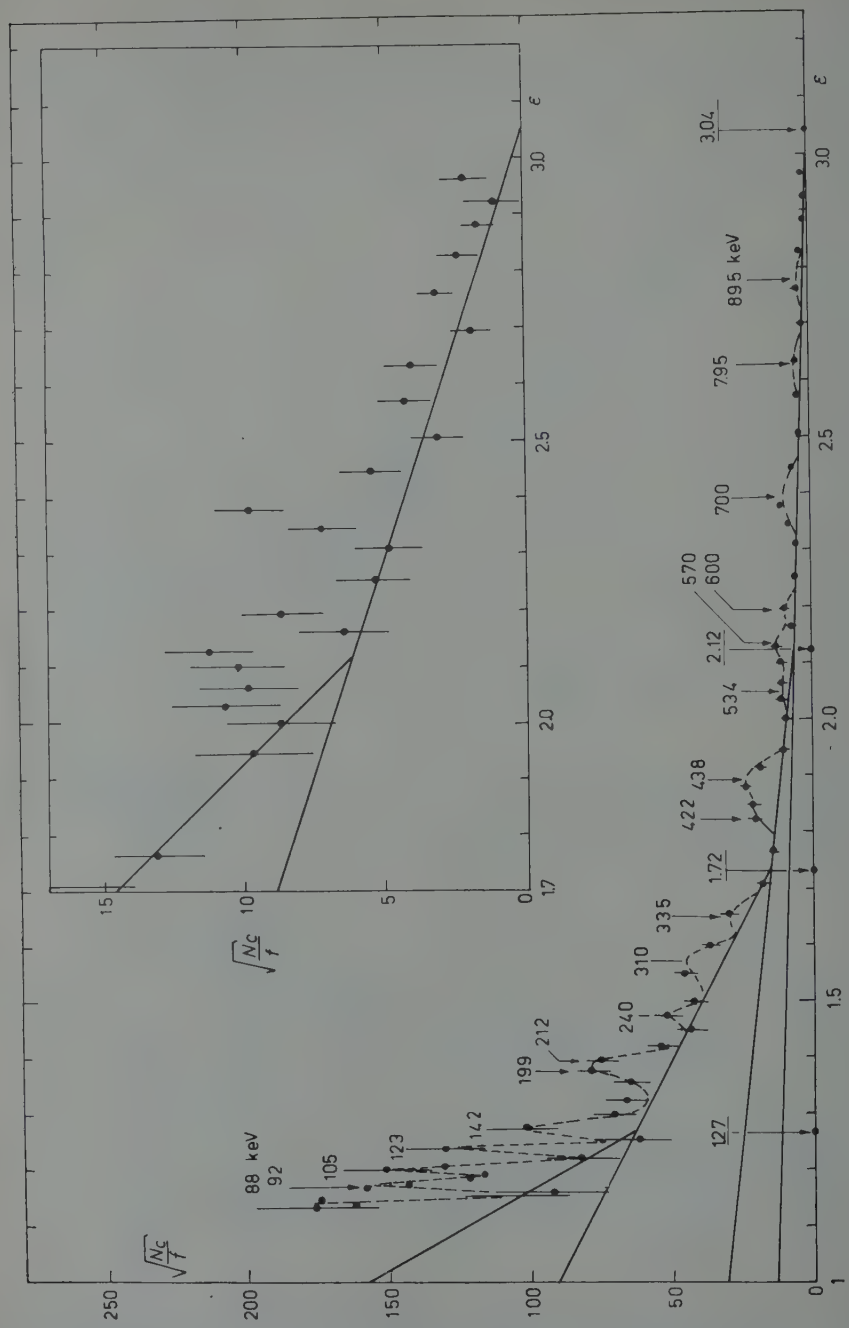

Fig. 7. – Complete F-K plot of β-γ_{810}-coincidences.

The F-K plots of the β-γ-coincidences with the photo-peaks at 1380, 910, 710 and 560 keV respectively, are given in Figs. 6, 7, 8 and 9. Two to three sources were used in obtaining each of these F-K plots. The F-K plot of the β-γ-coincidence measurements with the 230 keV complex photo-peak has also been obtained and is similar to that of Figs. 8 and 9.

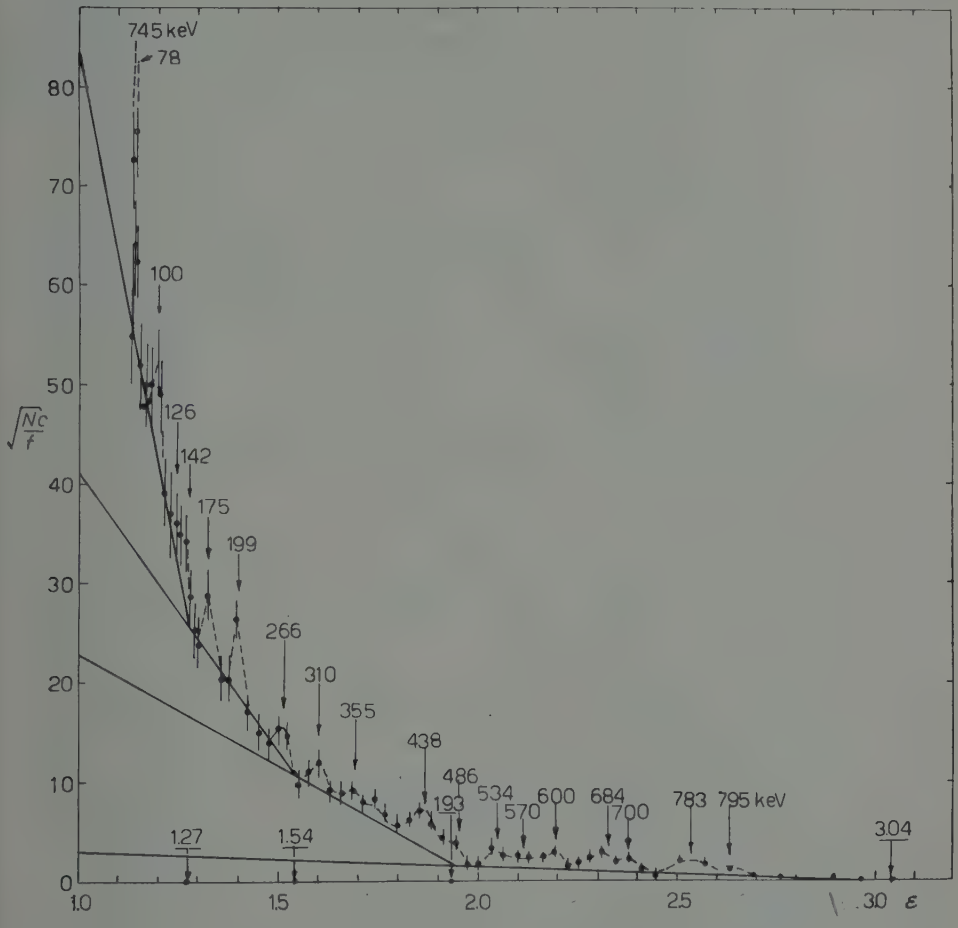

Fig. 8. – Complete F-K plot of β-γ_{710}-coincidences.

The analysis of the F-K plots of the various β-γ-measurements gave the intensity ratios (Table IV) for the different β-transitions coincident with each γ-photo-peak, single or complex. Qualitative values for the intensities of e^--γ-coincidences obtained with the different photo-peaks are tabulated in Table III.

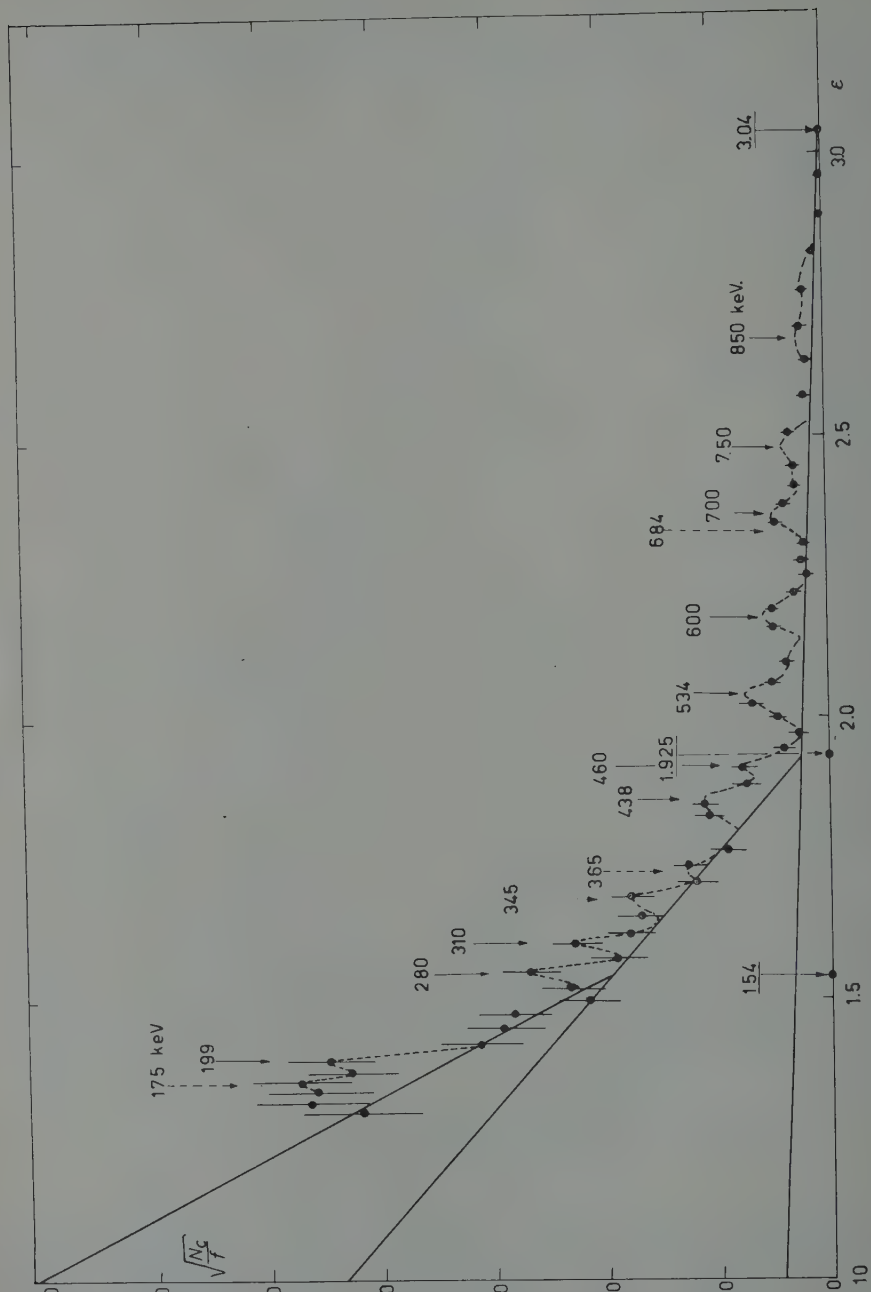

Fig. 9. – Part of the F-K plot of β-γ_{560}-coincidences.

2·6. *γ-γ-measurements.* – The window of one of the channels of a two channel scintillation spectrometer was kept fixed across a selected photo-peak and the other channel automatically scanned the γ-spectrum registering γ-γ-coincidence counts.

Such measurements were performed on all six photo-peaks from 1670 to 230 keV. The results are tabulated in the *b*-columns of Table III. Examples

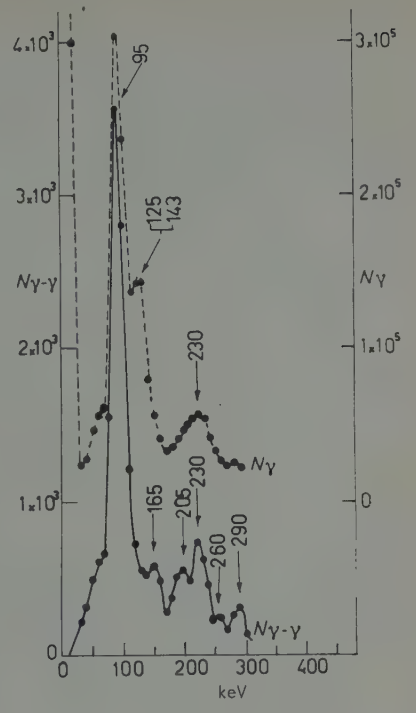

Fig. 10. – γ-γ-coincidences (below 300 keV) with 910 keV complex. N_γ: single counts $N_{\gamma-\gamma}$: coincidence counts. →

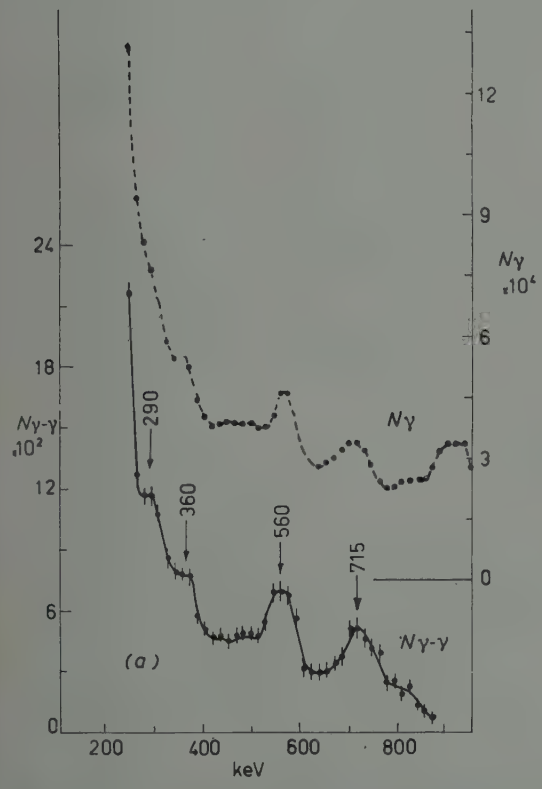

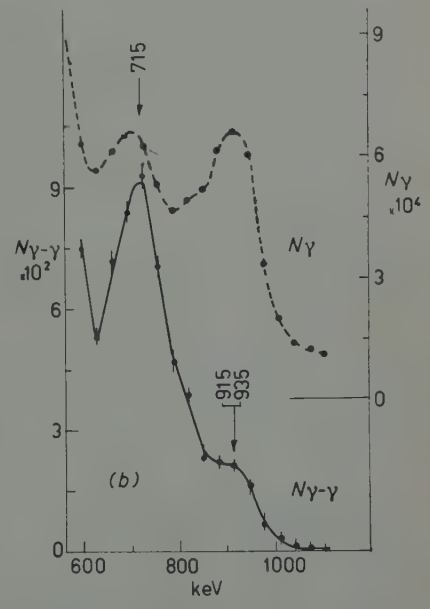

Fig. 11. – γ-γ-coincidences (above 280 keV) with 910 keV complex using different sources and amplification settings: *a*) energy range: 280 to 880 keV; *b*) energy range: 600 to 1100 keV. N_γ single counts; $N_{\gamma-\gamma}$: coincidence counts.

3599

of some of the results obtained are shown in Figs. 10, 11 and 12 which represent the γ-γ-measurements with the photo-peaks at 910 keV (low energy and high energy) and 710 keV respectively. From these coincidence measurements, obtained with separate sources, it is clear that the 710 keV complex is strongly in coincidence with a (215 ± 5) keV γ-ray which is not coincident with the γ's giving rise to the 910 keV photo-peak.

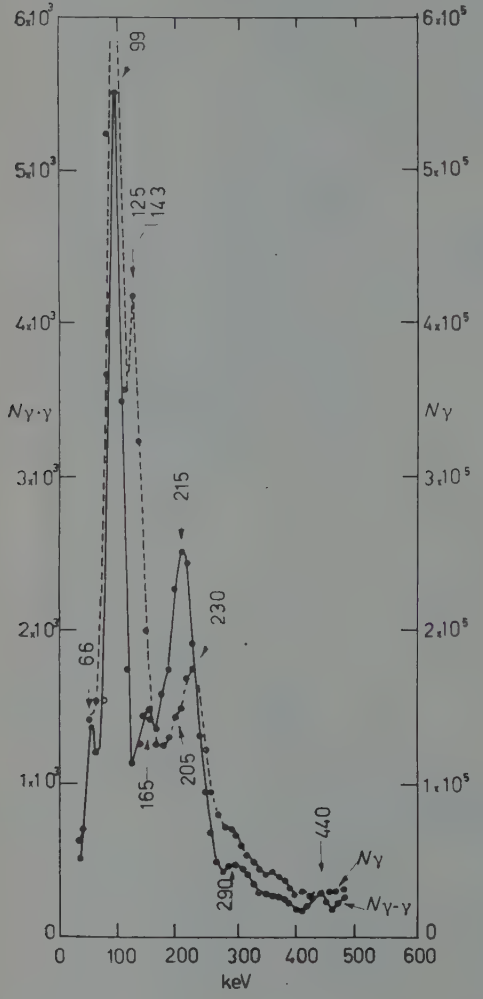

From Fig. 11(*a*) (γ-γ_{910}-coincidences) it is clear that the 715 keV and the 560 keV photo-peaks are in coincidence with the 910 keV complex. Furthermore, a weak indication is obtained in Fig. 11(*b*) that the 910 keV complex is in coincidence with itself. The two γ-rays, 935 and 910 keV, however, differ considerably in intensity, with the 910 keV being the much stronger transition.

It is remarkable that the grouping of photo-peaks below 300 keV appears to be similar to that in the γ-γ-coincidence spectra of UX2 ([8]), but it can be shown that *e.g.* the 205 and $(225 \div 230)$ keV transitions are not the same in the decay of UX2 and UZ. This point will be clarified in the discussion of the coincidence measurements.

Fig. 12. – γ-γ-coincidences with 710 keV complex. N_γ: single counts; $N_{\gamma-\gamma}$: coincidence counts.

3. – Decay scheme of UZ.

A decay scheme of UZ (Fig. 13) is proposed following a compilation of the knowledge obtained from the β-transitions; the photo-peaks in the γ-spectrum;

the conversion lines in the β-spectrum; and the β-γ-, e⁻-γ-, and γ-γ-coincidence measurements.

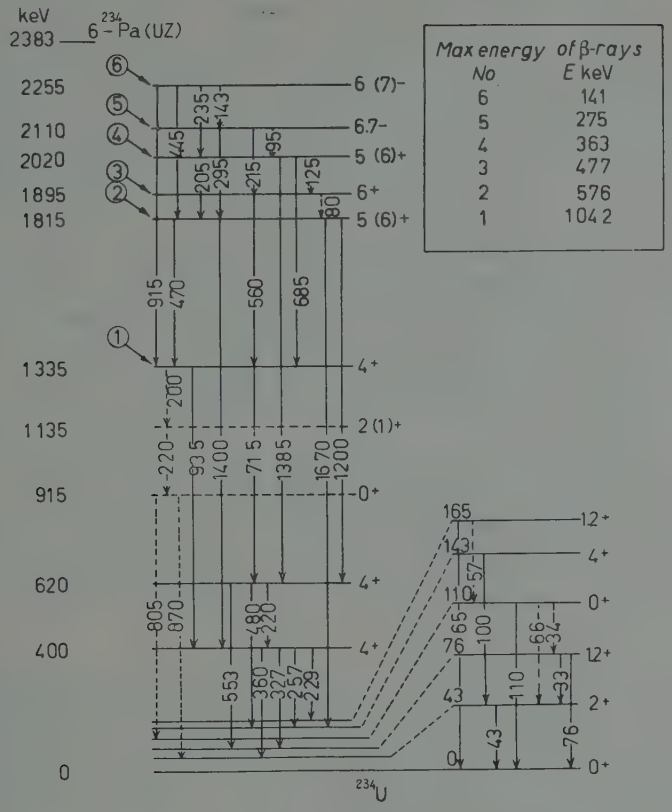

Fig. 13. – Decay scheme of ^{234}Pa(UZ).

3·1. *Discussion of β-γ-coincidence measurements.* – The relative intensities of the β-transitions (Table IV) obtained in the β-γ-coincidence measurements are extremely useful.

1) The 576 keV β-transition directly feeds the 1815 keV level which in turn is de-excited by the 1670 keV γ-transition. Apart from energy addition possibilities, this photo-peak is taken to be pure because the pattern of the ratios of the β-transitions involved is 1 : 0.5 : 1.8, and is similar to that of the same β-transitions in the single β-spectrum, *i.e.* 1 : 0.78 : 2.65. Of course it cannot be expected that these ratios should be exactly the same if some activity from the upper levels bypasses the 1815 keV level. In fact, from the discrepancy between these two ratio patterns the amount of cross-over activity can be estimated. Unfortunately this requires a much better knowledge of

the γ-transitions in general. Nevertheless the deviation must be in the right sense and order of magnitude and therefore offers additional information. If on the other hand the ratio of the partial spectra in the coincidence experiment is greater than that found in the β-spectrum (Table I) and the effect of Compton tails can be excluded, the respective γ-line must be complex and the deviation of the ratios is a measure of the respective intensities of mixing lines.

The interpretations of the ratios given in Table IV seem to indicate in some cases that there are still more components in the respective γ-lines. *E.g.* the high ratio of coincidences between the 910 complex and the β-transition no. 4 can only be understood if another γ-line with $\sim$ 900 keV is emitted in the decay of the 2020 keV level. This is quite possible and could lead to one of the dotted levels (Fig. 13) or in particular to a non-zero spin level lying close to the 1135 keV level. This would be a further explanation for the coincidence peak being weak at 910 keV in the γ-γ_{910}-coincidence measurements (Fig. 11(*b*)). This will be a postulate in parallel with the present one, *viz.* that the 900 and 1135 keV levels present in UX2 decay are weakly excited in the decay of UZ. Similar additional cascades might be present in other cases. However, none of these possibilities are indicated in Fig. 13, because the subtraction of coincidences due to Compton tails in the γ-spectrum and the unknown branching ratios represent appreciable uncertainty in the calculation,

2) A γ transition of (1380 $\pm$ 100) keV is weak, but definitely preceded by the 576 β-transition. Compton effects of the 1670 keV transition can be ignored. The ratios of the coincidence β-spectra show that there is still another γ-ray in this energy range, *e.g.* (1385 $\pm$ 20) keV which immediately follows the 363 keV β-transition. Coincidences with the sum peak of (685 + 715) keV will also add to the β-γ-coincidence count.

3) The 910 keV γ-complex was found to be in weak coincidence with β-transitions no. 1 and no. 2, and in strong coincidence with β-transitions no. 4 and no. 6. From coincidence measurements we know that the 910 keV peak is complex in agreement with HOK, VERSCHOOR and BORN ([7]). So at least two of these components must be in coincidence. The 915 keV transition fits within the experimental error between the 2255 keV and the 1335 keV levels. A weak 935 keV γ-ray is emitted in the decay of the 1335 keV level, giving rise to coincidences with the β-ray no. 1 directly and with no. 2 via the 470 keV transition. The 870 and 805 keV transitions present in the decay of UX2 are also detected in the decay of UZ ([7]), but they are weak. (Broken lines Fig. 13). The 770 and 1025 keV γ-transitions in the UX2 decay might be present, but then they are completely masked due to their low intensity. Contamination of the source with ^{234}Th activity (24 days) was checked by re-measuring the β- and the γ-spectra of UZ sources after four days' decay.

3603

Over the entire energy range the observed counts lay within the statistical variation of the background, proving the absence of any long half-life contamination.

4) The 710 keV γ-complex is strongly fed by the 477 keV β-transition via the 560 keV γ-transition, and by the 275 keV β-transition via the (215÷560) keV γ-cascade. The 685 keV γ-transition is weak so that the β-γ_{710} coincidences with the 363 keV β-transition are not measurable in the presence of the other stronger β-γ-coincidences.

5) In the β-γ_{560}-coincidences the ratios (Table IV) have changed even further in favour of the 477 keV β-transition beyond the change already noted in the β-γ_{710}-coincidences. The coincidences with the 1042 keV β-transition may be due to β-γ_{553}-coincidences. Alternatively, this may be due to Compton electrons of the 710 keV γ-transition, but this effect is small.

6) The high coincidence rate found between the pronounced 230 keV peak and the low energy β-transition also strongly suggests that this peak is complex and that a fairly intense component follows directly on the β-transition no. 6. The rest of these coincidences registered are indistinguishable from Compton electrons and scattering effects.

3·2. *Discussion of the* e^--γ- *and* γ-γ-*coincidence measurements.* – It can be expected that the first few excited states of ^{234}U involved in the decay of UX2 ([3]) should also play some part in the decay of UZ.

The 1670 keV γ-transition is assigned to be in cascade with the 100 and 43 keV γ-transitions between the first two rotational states. This follows from the observed β-γ- and e^--γ-coincidences. This is not in agreement with Hoк *et al.* ([7]) who assigned a 1690 keV γ-transition to lead onto the 43 keV level in parallel with the 100 keV transition. This assignment of Hoк *et al.* is in contradiction with the results in Table III.

Most of the γ-transitions below 300 keV are in coincidence with the 1670 keV γ-transition in agreement with Johansson ([5]). Apart from the 100 keV and the 43 keV transitions such transitions are taking place between the high energy levels of ^{234}U and this is to some extent in contradiction with Johansson who assigned a strong 250 keV γ-transition leading to the ground state of ^{234}U. No correspondence can be found with the latest decay scheme of Hoк ([7]).

The e^--γ- and γ-γ-coincidence results, except with 1670 keV show that together with the first two rotational levels the other lower energy excited states of ^{234}U also take part in the decay of UZ. Therefore γ-transitions such as 553, 480, 327, 257 and 220 keV appear ([16]). Using the results of the various coincidences measurements, conclusions are drawn regarding possible energy levels in ^{234}U which are not directly excited by measurable β-transitions. This

implies that β-transitions to such levels should be twice or more times forbidden.

3·3. *Decay scheme.*

1) 43 keV level. The first excited state in ^{234}U has already been found in the decay of UX2. The 43 keV γ-transition to the ground state is also present in UZ decay.

2) 76 keV level: This energy level is identical with that in UX2 decay. A 76 keV γ-transition to the ground state has been detected. A 33 keV γ-transition is assigned from this level to the 43 keV level, but the intensity of this transition is much weaker than in the case of UX2 decay where this level is directly excited by a 13% β-transition.

3) 110 keV level: No γ photo-peak of 110 keV is found in the scintillation spectrum, but conversion lines of such a transition are obtained in the β-spectrum. This transition is probably a 0-0 transition, as was also found in the UX2 decay.

4) 143 keV level. This is the second rotational level identified in UX2 decay.

5) 165 keV level. A (57 ± 3) keV γ-transition is possible from this level to the 110 keV level. A weak indication of such a line is found. Similar to UX2 decay a weak transition of 165 keV is found leading to the ground state.

6) 1815 keV level. The most energetic γ-transition measured is that of 1670 keV. It is coincident with the 576 keV β-transition, and in strong coincidence with γ-transitions of 100 and 43 keV which are in cascade.

7) 400 keV level. The 935 keV γ-transition is in coincidence with the 1042 keV β-transition, and this cascade feeds the postulated 400 keV level in ^{234}U. This is apparent from the γ-transitions below 500 keV which are not in coincidence with the 1670 keV γ-transition. It is not the same energy level (370 keV) which was postulated in the decay scheme of UX2.

8) 1335 keV level. A 715 keV γ-transition is in coincidence with a 220 keV γ-transition according to γ-γ-measurements. This cascade is in parallel with the 935 keV γ-transition, leading to the 400 keV level. It is assumed that the 1042 keV β-transition is directly in weak coincidence with the 935 keV γ-transition and is therefore partly responsible for the excitation of the 1335 keV level.

9) 620 keV level. The order of the $(715 \div 220)$ keV γ-cascade is born out by the 553 keV γ-transition which leads to the 76 keV level from this 620 keV level. This level is also excided by the (1385 ± 20) keV γ following the 363 keV β-transition.

3604

10) 1895 keV level. According to β-γ-measurements the 560 keV γ-transition is coincident with the 477 keV β-transition, and leads to the 1335 keV level.

11) 2255 keV level. The 445 keV γ-transition is not in coincidence with the 560 keV γ-transition and the 230 keV complex. The only place where this transition fits in is between a 2255 keV level, excited by the 141 keV β-transition, and the 1815 keV level.

12) 2020 keV level. The 205 keV γ-transition is in weak coincidence with the 560 keV γ-ray (the 553 keV) but also coincident with the 235, 710, 910 and 1380 keV complex photo-peaks. The 235 keV γ-transition therefore precedes the 205 keV transition to the 1815 keV level, establishing a level of 2020 keV above the ground state. This arrangement is in good agreement with the energy differences between the 2-nd, 4-th and 6-th β-transitions (Table I).

13) 2110 keV level. A 215 keV γ-transition is reasonably in coincidence with the 560 keV γ-complex, and weakly with the 1670 keV γ-ray. This determines the assignment of this 215 keV transition. It is expected that the two γ-transitions of (220 ± 5) keV have different multipolarity. This level is excited by the 275 keV β-transition in good agreement with the β-ray spectra.

14) 915 and 1135 keV levels. These are some of the energy levels of ^{234}U that occur in the decay of UX2. The excitation of these levels in UZ decay is rather weak. It is not possible to fit in any measured γ-transition to lead to the third rotational state at 296 keV ([7]). This level should have a spin of 6+ and it can be expected that it should be excited in the decay of UZ.

4. – Conclusions.

4·1. *The ground state of* ^{234}Pa. – The difference between the UZ and the ^{234}U levels is obtained from the sums of the maximum energy of each β-transition and the respective energy level in ^{234}U which they excite. The mean energy difference between the UZ and the ^{234}U levels is therefore

$$(2383 \pm 9) \text{ keV} .$$

The UX2 level is (2405 ± 3) keV above the ground state of ^{234}U ([8]).

Therefore the difference between UX2 and UZ is (22 ± 12) keV with UZ as the ground state of ^{234}Pa.

4·2. *The spin of* UZ. – It is known that the spin of UX2 is 1 — ([7,8]). Spin values for UZ of 5 and less causes difficulty in explaining the absence of β-transitions to the lower states in ^{234}U (Section 4.3). The lowest possible spin value for UZ is 6 with parity not fixed.

The odd neutron can be in the $\frac{7}{2}$ — (743 ↑) orbit (ground state of ^{235}U $N = 143$) or alternatively in the $\frac{1}{2}$ + (631 ↓) orbit (26 min state in ^{237}U). The states are labelled, following NILSSON and MOSZKOWSKI ([17,18]), as $\Omega\pi$ (N, n_z, Λ, ↑ or ↓). The symbols are defined in reference ([18]). The ↓ or ↑ appearing under the parenthesis are in accordance with $\Omega = \Lambda + \frac{1}{2}$ or $\Omega = \Lambda - \frac{1}{2}$.

The odd proton can either be in the $\frac{3}{2}$ — (521 ↑) state (ground state of ^{231}Pa, $Z = 91$) or in the first excited particle state of ^{234}Pa with spin $\frac{5}{2}$ — (642 ↑) ([17,19]). According to STEPHENS, ASARO and PERLMAN ([20]) the ground states of ^{231}Pa and ^{233}Pa are in the $\frac{1}{2}$ — (530 ↑) orbit. These possibilities for highly deformed nuclei can be seen in the Nilsson energy level diagram ([18]). The levels originating from the $j\ \frac{15}{2}$ orbit in the spherical limit have later been calculated by NILSSON and published by HOLLANDER ([21]).

Following MOSZKOWSKI's ([17,22]) extension of the Nordheim rule for odd-odd nuclei ([23]) an assignment of the possible spin and parity value of UZ can be obtained.

Out of the various coupling possibilities a spin of 6 is only obtained by assuming that the proton is in the $\frac{5}{2}$ + orbit (642 ↑) and the neutron in the $\frac{7}{2}$ — (743 ↑) orbit ($\Omega_n + \Omega_p$ is obtained because $\Omega_n = \Lambda_n + \frac{1}{2}$, $\Omega_p = \Lambda_p + \frac{1}{2}$).

This implies that the parity of the UZ level is odd.

4·3. *The spins and parities of levels of* ^{234}U *encountered in the decay of* UZ. – The spins of the lower excited states of ^{234}U (Fig. 13) *viz.* of the 165 keV level and lower levels, follow from the decay scheme of UX2.

The spin of the 400 keV level which is not present in the decay of UX2 must be higher than that of the 370 keV level which is 3 —. It is assumed to be a 4 + level. Other values will cause difficulties in explaining the absence of β-transitions to this state. Possible γ-transitions in UX2 to this state with a spin value of 4 + should have, except in one case, multipolarities of $M3$, $E4$ or higher. Such transitions would be very weak. The high energy states of ^{234}U that take part in the decay of UX2 have spins of 0, 1, 2 and negative

---

([17]) S. A. MOSZKOWSKI: Private communication.
([18]) S. G. NILSSON: *Kgl. Dan. Mat. Fys. Medd.*, **29**, No. 16 (1955).
([19]) F. H. BAKKE: *Nuclear Physics*, **9**, 4, 670 (1958-59).
([20]) F. S. STEPHENS, F. ASARO and I. PERLMAN: *Phys. Rev.*, **113**, 1, 212 (1959).
([21]) J. M. HOLLANDER: *Phys. Rev.*, **105**, 1518 (1957).
([22]) C. J. GALLAGHER Jr. and S. A. MOSZKOWSKI: *Phys. Rev.*, **111**, 1282 (1958).
([23]) L. W. NORDHEIM: *Rev. Mod. Phys.*, **23**, 322 (1951).

3605

parity. Only in one case can it possibly be 1 or 2+. For the 620 keV level a spin value of 4+ is likewise the most probable.

It is assumed that the 1042 keV β-transition is unique first forbidden ($\Delta I = 2$, yes), because with a second forbidden transition the parity of this state would be negative (4 or 8 —). HOK *et al.* ([7]) obtained a log *ft* value of 7.7 for this β-transition, which is on the edge of the first forbidden range. A log *ft* value of 8.1 was obtained by JOHANSSON ([5]). A $\Delta I = 2$, no, transition will present the same difficulties discussed above in explaining the absence of the 1335 keV level in UX2 decay. The spin of this state is thus assumed to be 4+.

For the 1815, 1895 and 2020 keV levels the parity is + and the spin 5, 6 or 7. Speculations can be made regarding the amount of conversion taking place for various γ-transitions. The ranges of possible spin values are given in the decay scheme. Similar speculations ([16]) can also be made for the 2255 and 2110 keV levels having negative parity.

It is most unfortunate that it was not possible to obtain reliable conversion coefficients of the different γ-transitions. A resolving power better than 0.3% is desired for the e^--spectrum analysis which has been proved to be very complex.

* * *

The authors wish to thank Dr. S. J. DU TOIT for suggesting the problem and stimulating discussions with Dr. H. R. LEMMER and Dr. W. FRAHN are much appreciated. We are greatly indebted to Dr. S. A. MOSZKOWSKI for his suggestions regarding the application of the shell model. One of us (J. W. L. DE VILLIERS) is indebted to the South African Atomic Energy Board for a research fellowship.

RIASSUNTO (*)

Sono stati investigati gli spettri dei raggi β e γ osservati nel decadimento UZ (6.66 ore). Si riportano i risultati di misure coincidenza β-γ. Si discutono le coincidenze γ-γ con fotopicchi γ selezionati rilevate in un apparecchio a scintillazione. Si propone uno schema di decadimento che comporta 6 transizioni β e 39 transizioni γ. Si prova che l'UZ è lo stato fondamentale del ^{234}Pa con sovrapposto l'UX2 di (22±12) keV. Uno spin 6^-, per lo stato fondamentale dell'UZ si spiega in funzione degli stati di Nilsson.

(*) *Traduzione a cura della Redazione.*

IL NUOVO CIMENTO Vol. XIV, N. 4 16 Novembre 1959

Negative Pion Interactions at 1.3 GeV/c (*).

M. Blau, C. F. Carter and A. Perlmutter

University of Miami - Coral Gables, Fla.

(ricevuto il 18 Luglio 1959)

Summary. — A total of 340 m of track of negative pions of momentum 1.3 GeV/c have been followed in emulsion, and pion interactions have been recorded. Special emphasis is placed on inelastic scattering on free protons (single meson production). The resulting angular and momentum distributions of the emitted particles are investigated and compared with previous experiments at similar energies. An attempt is made to explain these results on the basis of an isobar decaying into a nucleon and the slower pion. In the case of reaction $\pi^- + p \to \pi^- + \pi^0 + p$, it appears that there exists an anisotropy in the isobar frame of reference, in which the slower pion is emitted predominantly backward, with respect to the isobar direction. The results are compared with the π-π coupling model. Angular and energy distributions of mesons emitted in nuclear interactions are investigated and compared with other results and Monte Carlo calculations. The meson multiplicity and energy degradation in these collisions are also discussed. Strange particles found during the investigation are analysed.

1. – Introduction.

The problem of fast pion interactions with nucleons is far from being theoretically understood, and not even the experimental data thus far accumulated are in complete agreement. Therefore, we felt that the additional data coming from the study of even a small stack might make a modest contribution to

(*) This research was supported in part by the United States Air Force through the Air Force Office of Scientific Research of the Air Research and Development Command, under contract no. AF 49(638)-97. Reproduction in whole or in part is permitted for any purpose of the United States Government.

this problem. At a time when neither of the high energy accelerators was in operation, Dr. G. ZORN kindly provided us with a small stack exposed to fast negative pions at the Cosmotron at an earlier date.

The emphasis of the study is on inelastic interactions with protons, the results of which are compared with existing theories. A concomitant feature of the work is data on nuclear interactions of the pions and the production of strange particles.

2. – Experimental procedure.

The stack consists of 30 — 3 in. × 2 in. × 100 μm Ilford G-5 emulsions. Because the energy of the incident pions was not precisely known, considerable attention was given to a direct measurement of the momentum by multiple scattering technique. The value of the momentum was found in this way to be (1.3 ± 0.1) GeV/c, which was borne out by kinematic considerations of elastic scattering on protons.

The plates were scanned by following the incident pions from the lead edge. The track length scanned was 381 meters and the number of interactions found was 811. After correcting for scanning efficiency and for the contamination of the incident beam by muons and electrons, the corrected track length was 340 m, giving a total cross-section in agreement, within statistical limits, with the results obtained by other investigators.

Scattering measurements were made on all outgoing tracks of interest with dip angles less than 15°, and in some cases up to 20°, before development. The original emulsion thickness was checked by measurements of μ-meson ranges from π-μ decays. Wherever possible, grain counts and blob and gap measurements with a semi-automatic ionization meter were made as a function of residual range.

Every effort was made to determine the characteristics of tracks emitted in apparent fundamental events, which naturally required extensive calibration measurements. In the course of this investigation, several K-mesons produced in nuclei and on single nucleons were found.

Momentum and energy conservation were applied to all events which appeared to be fundamental. By applying these kinematic considerations, we tried to conscientiously separate interactions with free protons from those with protons found in nuclei [1]. A fundamental event, or one requiring the addition of Fermi momentum to the target nucleon, was not accepted as such if there was a visible recoil or electrons, or if the emitted nucleon had an energy less than 25 MeV.

---

[1] W. D. WALKER and J. CRUSSARD: *Phys. Rev.*, **98**, 1416 (1955).

3. – Experimental results on nucleon interactions.

3·1. *Summary of results.* – Table I is a summary of all interactions with free or edge nucleons, according to the above criteria for such events. The numbers without parentheses refer to collisions with free protons, in so far as they satisfied the kinematic requirements of the interactions after all the visible tracks could be measured. The numbers in parentheses refer to collisions with edge nucleons, in which the kinematic requirements can be met with the addition of Fermi momentum to the target nucleon. The numbers in curly braces refer to events which appear to be clean, but where for experimental reasons (steep tracks, edge of plate, etc.) or because of the possibility of two neutral particles, the events could not be completely analyzed.

TABLE I. – *Summary of fundamental events.*

		a) Proton collisions			
I)	(p —)	10	(7)		
II)	(p — 0)	11	(15)		
III)	(n + —)	5	(1)		
IV)	(p — 0) or (p — 00)			{5}	
V)	(n + —) or (n + — 0)			{9}	
VI)	0 prong (n0) or (n00)			{24}	(2 with electron pairs)
VII)	Strange particles		(3)		
		b) Neutron collisions			
VIII)	(n —)		(8)		
IX)	(n —) or (n—0) or (n—00)			{29}	(1 with electron pair)
X)	(p — —)		(1)		
XI)	(p — —) or (p — — 0)			{2}	
XII)	(n — — +)		(1)	{1}	
XIII)	Strange particles		(1)		

A comparison of the total number of events and those in individual categories in Table I with those of WALKER and CRUSSARD [1], at a somewhat higher energy, does not indicate any disagreement which could not be explained by statistical considerations. The low ratio of events in category III to those in II could be explained in this way.

It is of interest, in view of the results to be presented later, to substantiate the claim that the events in I, II and III, without parentheses, represent free proton interactions; this supposition can be verified in part by calculating the total free proton cross-section. However, in order to do so, one needs to know the relative contributions of multiple pion production and events of type VI to the total free proton cross-section. Although these contributions

cannot be found directly from our data, they could be estimated from the hydrogen cloud chamber data of EISBERG *et al.* (2) and from the recent curves derived from bubble chamber experiments of the Wisconsin group (3). Both groups find a total cross-section of 34 mb.

The cloud chamber results (2) seem to indicate that one should expect the double production events to amount to about 25% of those in categories II and III, and that the number of zero prong stars should be about 15% of all visible proton events, including double production. Applying these corrections to our data, we obtained a mean free path for free proton collisions of 9.7 m (30 mb). The contribution of zero prong stars could also be estimated from the bubble chamber data (3), yielding a charge exchange cross-section (elastic and inelastic) at 1.2 GeV of 30% of the visible proton interactions. This leads to a mean free path of 8.7 m (34 mb) for our emulsion data.

Two of the events included among endings (category VI) are actually endings with electron pairs, signifying the emission of a π^0-meson. One of these pairs has a very small opening angle, and is quite energetic (about 600 MeV). Considering the number of endings, the existence of two Dalitz pairs seems rather high.

The above results support our contention that we probably have not included collisions with edge protons in the events without parentheses in categories I, II, III, and furthermore supports Walker's assertion (1) that about half of his tabulated proton events are actually interactions with edge protons. This can also be seen from the ratio of bracketed to non-bracketed numbers in Table I.

Part *b* of Table I lists all of the observed neutron interactions, the total number being about equal to the number of proton events less the number of free proton collisions. Of the 37 observed cases in categories VIII and IX which represent all scattered π^- with deflections greater than 10°, the energy of the scattered pions was determined in 25 events of which 8 could be fitted to elastic scatterings. The others probably involved the production of additional π^0's, and the fact that they might even be nuclear interactions without visible recoils or heavy prongs cannot be completely excluded. The table also shows one fairly definite case of 3 emitted charged mesons. In category IX, the existence of a pair suggests the production of a π^0 upon interaction with a neutron; this lends support to the possibility that the excess of single meson scatterings over the 8 elastic events probably indicates production of single π^0's.

The 10 events in Table I corresponding to elastic scattering on free protons

---

(2) L. M. EISBERG, W. B. FOWLER, R. M. LEA, W. D. SHEPHARD, R. P. SHUTT, A. M. THORNDIKE and W. L. WHITTEMORE: *Phys. Rev.*, **97**, 797 (1955).

(3) R. R. CRITTENDEN, J. H. SCANDRETT, W. D. SHEPHARD, W. D. WALKER and J. BALLAM: *Phys. Rev. Lett.*, **2**, 121 (1959).

3611

show a pronounced forward angular peak of the scattered mesons, in agreement with previous results, but will not be discussed here because it has been done with much larger samples by other workers ([1,2,4]).

2·2. *Inelastic scattering.* – In the discussion that follows it should be borne in mind that the size of the sample is small. Nevertheless, some of the features of the results, when combined with cloud chamber data ([2]), seem to suggest a regularity which warrants further investigations of these questions on much larger samples than are available in the present experiment.

Of all the available published data, the Brookhaven cloud chamber data ([2]) were chosen for comparison because of a marked general similarity in the angular and momentum distributions of the outgoing particles in the single production cases. Furthermore, the energy is not too different from that in the present case. We can again emphasize the similarity between our results and those from hydrogen-filled cloud chambers in presenting the following data ([5]).

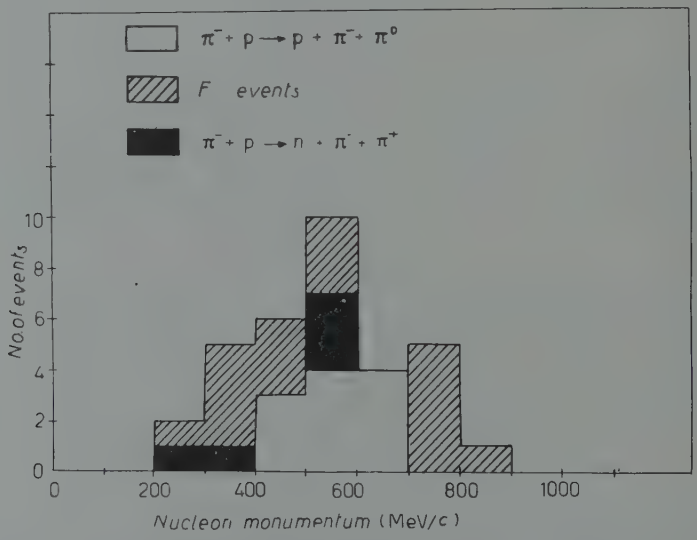

Fig. 1*a*. – The momentum distribution in the c.m. system of nucleons emitted from $\pi^- + p$ collisions in which a single π^+ or π^0 meson is produced (see II and III in Table I). The dashed areas represent the cases in which Fermi momentum must be added to the target proton in order to satisfy the kinematic requirements for collision with a single proton.

([4]) M. Chretien, J. Leitner, N. Samios, M. Schwartz and J. Steinberger: *Phys. Rev.*, **108**, 383 (1957).

([5]) V. P. Kenney (*Phys. Rev.*, **104**, 784 (1956)), with his deuterium cloud chamber, finds that the distribution of angles between emitted pions is more similar to emulsion data than to hydrogen cloud chamber data.

The momentum and angular distributions of the emitted nucleons in reactions II and III, in the c.m.s., are given in Figs. 1(*a*) and 1(*b*). The white areas correspond to reactions II, the black areas to reaction III and the shaded areas to Fermi events of both kinds. It may be observed, in Fig. 1(*a*), that the momentum distribution in free proton collisions shows qualitative agreement with both the statistical (6) and isobar (7) models of pion production. Fig. 1(*b*)

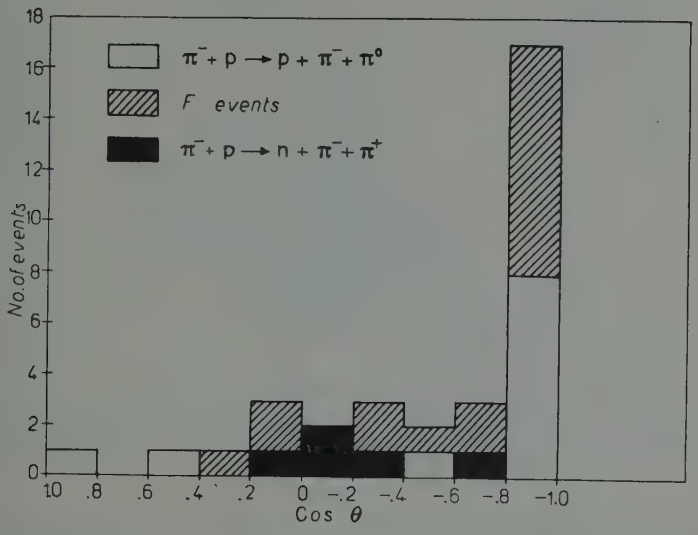

Fig. 1*b*. – The angular distribution of the nucleons from Fig. 1*a* in the c.m. system.

shows that the angular distribution of nucleons is sharply peaked in the backward direction, also in agreement with the isobar model (8). In both cases it is evident that the Fermi events cause an apparent broadening of the distributions.

Figs. 2(*a*) and 2(*b*) give the momentum and angular distributions of the protons from events of type II, combined with the corresponding data of EISBERG *et al.* (2), while 3(*a*) and 3(*b*) refer to the neutrons from events of type III (9). The angular distributions in Figs. 2(*b*) and 3(*b*) seem to differ markedly from each other because of the absence of the strong backward

(6) E. FERMI: *Prog. Theor. Phys.* (*Japan*), **5**, 570 (1950); *Phys. Rev.*, **92**, 452 (1953); **93**, 1735 (1954).

(7) R. M. STERNHEIMER and S. J. LINDENBAUM: *Phys. Rev.*, **109**, 1723 (1958).

(8) J. E. CREW, R. D. HILL and L. S. LAVATELLI: *Phys. Rev.*, **106**, 1051 (1957).

(9) The cloud chamber data which were taken for inclusion in these figures are only the probable events in the case of reaction II and the definite and probable events in the case of reaction III.

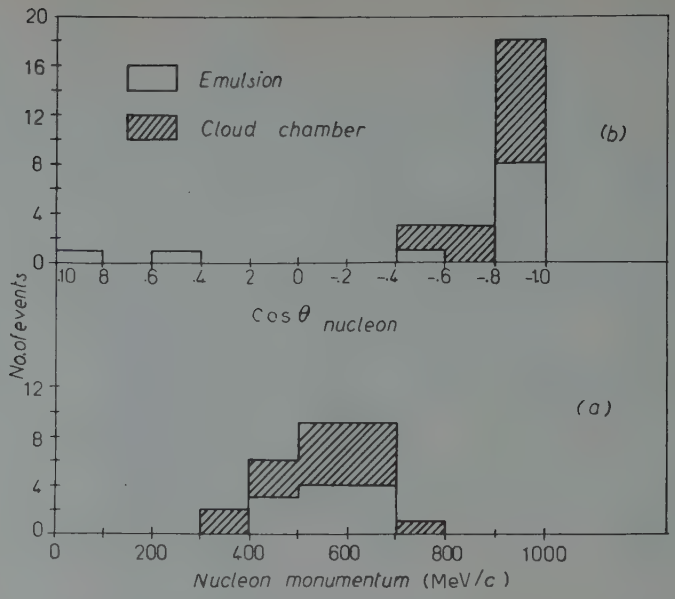

Fig. 2. – (*a*) The momentum distribution in the c.m. system of protons from reaction II in Table I for the present experiment (clear areas) plus similar data from the cloud chamber experiment ([2]) (shaded areas). (*b*) The angular distribution of the same protons in the c.m. system.

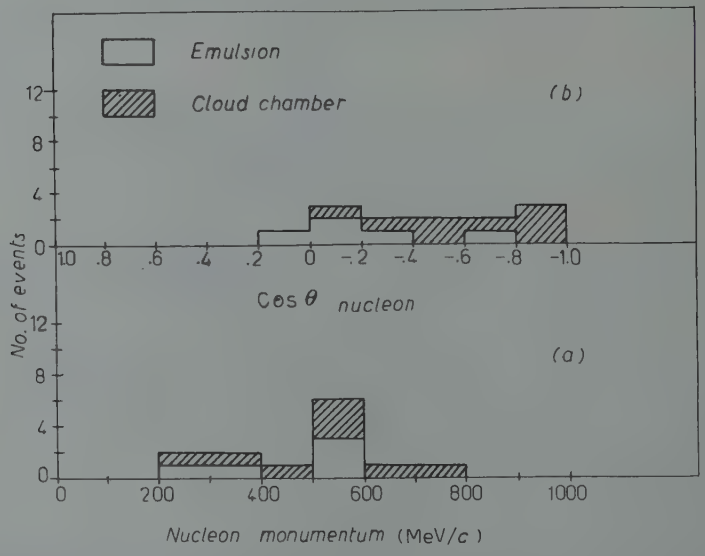

Fig. 3. – (*a*) The momentum distribution in the c.m. system of neutrons from reaction III in Table I for the present experiment (clear areas) plus similar data from the cloud chamber experiment ([2]) (shaded areas). (*b*) The angular distributions of the same neutrons in the c.m. system.

3614

peak in the latter. Also, the neutron momentum distribution, Fig. 3(*a*), seems to be different from that for the emitted protons, Fig. 2(*a*).

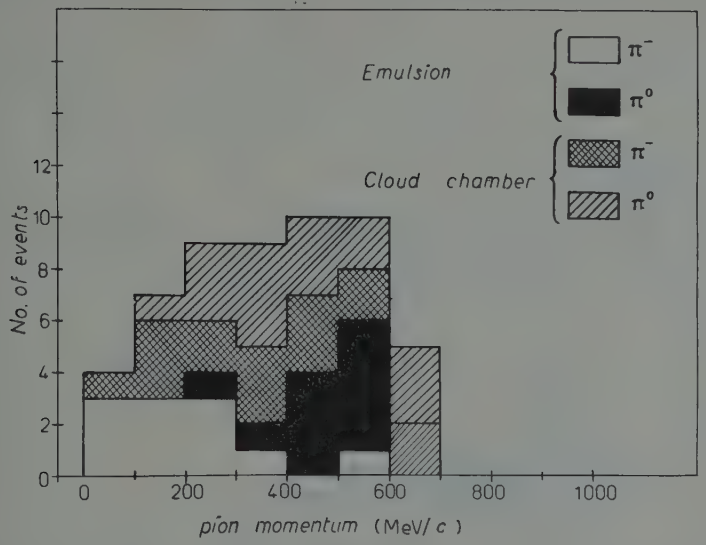

Fig. 4*a*. – The momentum distribution in the c.m. system of both emergent pions in reaction II of Table I for the present experiment and the cloud chamber experiment ([2]) as shown.

Figs. 4(*a*) and 4(*b*) give the momentum and angular distributions of both pions emitted in reaction II together with the cloud chamber data, while Figs 5(*a*) and 5(*b*) give analogous information for reaction III. The π^0 mesons in Fig. 4(*a*) appear to be the faster ones, especially so for the present data, while all of the emitted pions contributed strongly to a pronounced forward peak in the angular distribution (Fig. 4(*b*)). The c.m. system angular distribution of pions

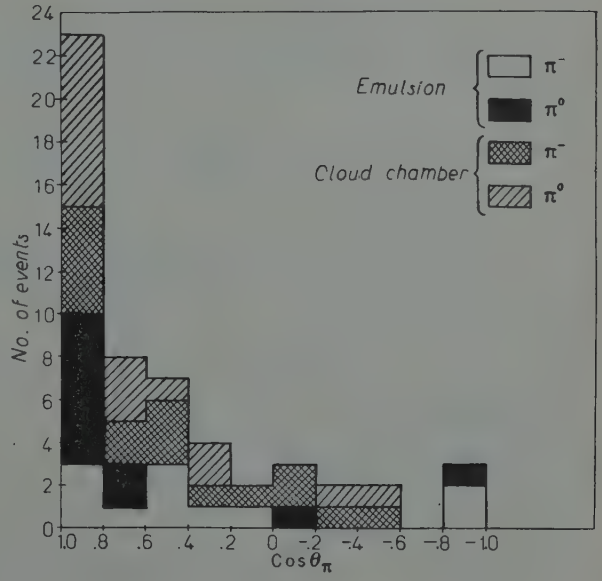

Fig. 4*b*. – The angular distribution of the pions from Fig. 4*a* in the c.m. system.

from reaction III (Fig. 5(*a*)) appears more isotropic, although the cloud chamber data suggest a somewhat forward peak.

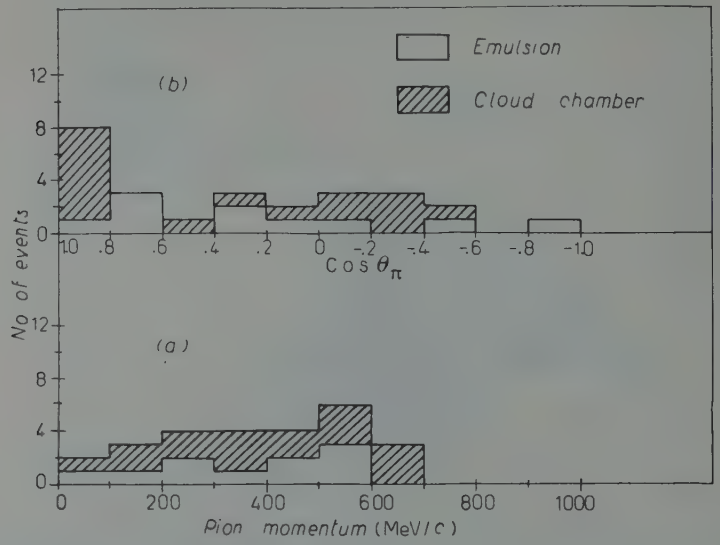

Fig. 5. – (*a*) The momentum distribution in the c.m. system of both emergent pions in reaction III of Table I for the present experiment and the cloud chamber data (²). (*b*) The angular distribution of the same pions in the c.m. system.

Figs. 6(*a*) and 6(*b*) show the angular distributions in the c.m. system between the slower pion and proton, and between two pions, respectively, in the case of reaction II. The analogous data for reaction III are not included because, as has been pointed out, the results appear to be different from those of reaction II, and are not given separately because of the still smaller available sample. The angle between the fast pion and proton is not shown, but is greater than 143° in all cases. The angle between the slow pion and proton is also generally large (cf. Fig. 6(*b*)), suggesting that the slow pion does not always follow the nucleon, and hence that the angle between pions need not be large (cf. Fig. 6(*a*)), where in 7 out of 11 cases, it is less than 90°). This result is in contrast with the emulsion data (¹), but seems to be in agreement with cloud chamber data (²); this latter agreement follows from the similarity between the results of the present experiment and the cloud chamber experiment which is apparent in Figs. 2(*a*)-5(*b*) (a tendency for predominantly backward nucleons and forward pions).

The laboratory angles between pions emitted in reaction II, together with cloud chamber data (which include the cases that are not definitely (p — 0)) are

3616

shown in Table II. Also included in the table are the results of a scalar theory calculation by KOVACS ([10]) for 1 GeV mesons on the effect expected from strong

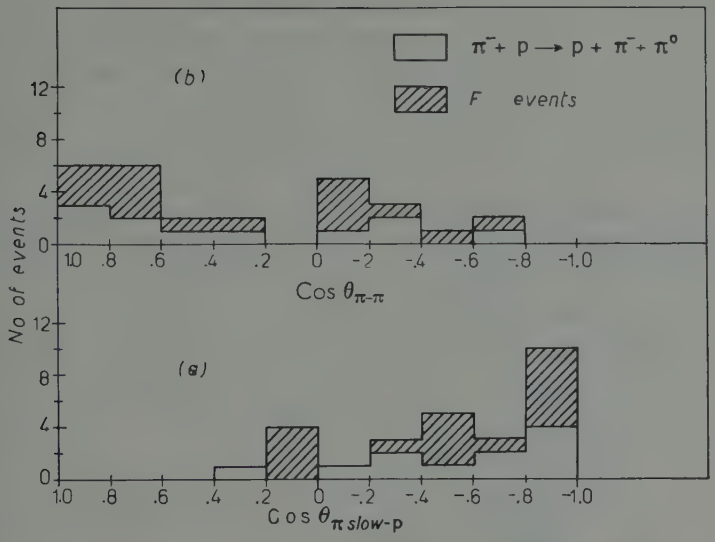

Fig. 6. – (*a*) Histogram showing the distribution of angles between the slow pion and proton in the c.m. system for reaction II in Table I. The shaded areas represent those cases in which Fermi momentum must be added to the target proton in order to satisfy the kinematic requirements for collision with a single proton. (*b*) Histogram showing the distribution of angles between both pions emitted in reaction II.

π-π coupling and strong π-nucleon coupling models. The present data are not in disagreement with the calculated values for π-π interactions in so far as the latter are valid.

TABLE II. – *Laboratory angles between pions for reaction* II.

Angle	Present work	Cloud chamber experiment	Kovacs' calculation	
			π-π coupling	π-nucleon coupling
0° ÷ 60°	8	5.5	7.1	3.9
60° ÷ 90°	1	4.5	3.1	2.9
90° ÷ 120°	0	1.0	0.6	2.2
120° ÷ 180°	2	0.0	0.2	2.0

([10]) J. S. KOVACS: *Phys. Rev.*, **93**, 252 (1954).

The cloud chamber results for reaction III show a less forward-peaked distribution, as it appears also from our few events. A difference between these two reactions is not unexpected inasmuch as in reaction II the pions would interact in a $T=1$ state and in reaction III in a $T=0$ state.

The Q-values of the π-π isobar range from 0 to more than 400 MeV. The distribution of all pion angles with respect to the isobar direction in the isobar rest frame is more or less isotropic, although a slight preference for the forward and backward directions is not completely excluded.

2·3. *Nucleon isobar.* – The question of the existence of a nucleon isobaric state was examined in the case of the (p — 0) reaction. The excited isobar was assumed to decay into the proton and the slower of the two pions, the momentum of the isobar being equal and opposite to that of the recoil pion in the c.m. system. The Q-value of this decay in the rest frame of the isobar is shown in Fig. 7, where the few events of reaction III are included. Un-

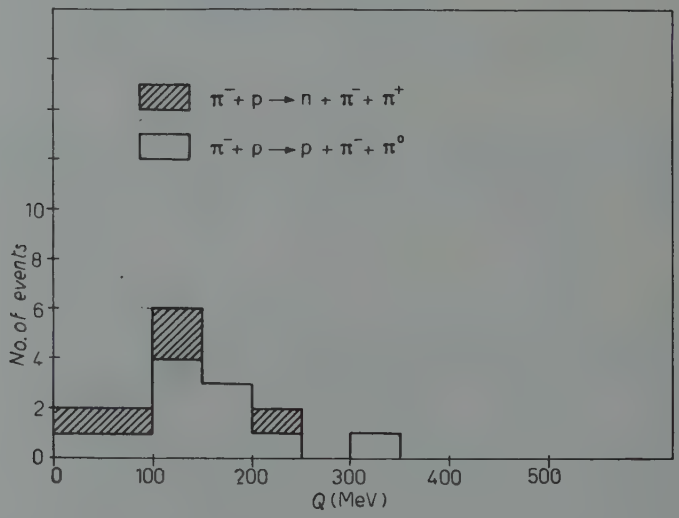

Fig. 7. – Histogram of the Q values for reactions II and III in Table I, the isobar decaying into the nucleon and slow pion.

fortunately, the sample is quite small, but there does seem to be some bunching of the events near 150 MeV, suggesting the existence of a discrete Q-value near the meson mass.

Assuming that this Q-value distribution implies the existence of a real state, we then found the angle between the slower pion in the isobar frame of reference and the isobar, as shown in Fig. 8. The cases of reactions II and III must be considered separately, because of the fact that in reaction III

there can exist a $\frac{3}{2}$ isotopic spin state, although this would be impossible to detect here, as the π^+ and π^- could not be distinguished in so small a stack. The strong backward peaking in the isobar system of the slow pion in reaction III, showing that only 1 out of 11 cases is in the forward direction, is

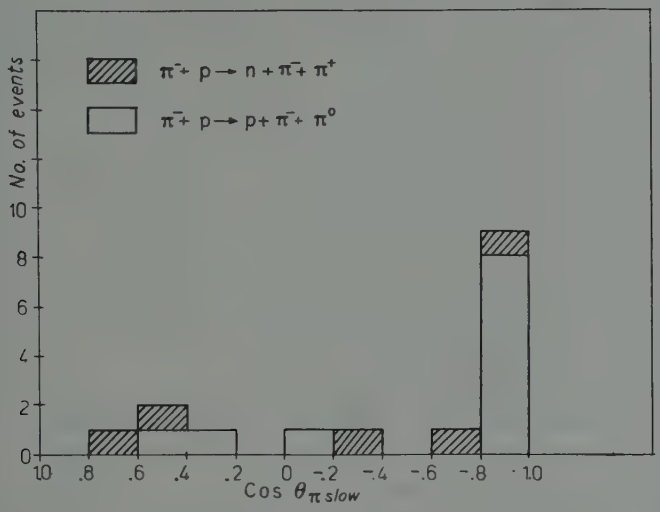

Fig. 8. – Histogram of the distribution of angles between the directions of the slow pion in the isobar frame of reference and the isobar itself for reactions II and III in Table I.

rather striking. From the fact that this is a two body system, the proton is, of course, emitted at a small angle with respect to the isobar. This effect is a kinematic consequence of the backward emission of the proton, its relatively large momentum, the large angle between fast pion and proton, and the relatively small angle between the two pions, all in the center of mass system. The similarity of the cloud chamber data in reaction II to the present data leads us to believe that an analogous effect exists there also ([2]). In order to substantiate this supposition, we attempted to fit all three particles in reaction II of the cloud chamber results from the scatter diagrams (which should be possible in principle, since the momentum and c.m.s. direction of each particle are given) in such a way that momentum is conserved and that the total energy in the c.m.s. is equal to the theoretical value for the incident pion energy. In two separate attempts, we arrived at the conclusion that, at most, in four cases out of fourteen, the slow pion would move in the forward hemisphere with respect to the isobar.

Combining the cloud chamber and emulsion data (25 events), one finds, from simple probability considerations, that the confidence level for a non-isotropic distribution is 99.4%. If only the 11 emulsion events are taken into

account (10 backward and 1 forward) then we are still at the 98.8% confidence level. Furthermore, the detailed angular distribution (Fig. 8), with the marked backward peak, enhances still further the contention that the distribution is non-isotropic.

For the case of reaction III, from our data, which are also shown in Fig. 8, and from the evidence given by the angular and momentum distributions in reference ([2]), it seems that the angular distribution in the isobar system tends far more to an isotropic distribution. Whether the apparent differences in angular and momentum distributions between reactions II and III, which should be investigated further, are due to the existence of a $T = \frac{3}{2}$ state in reaction III, comprising a neutron and a π^-, is not clear, inasmuch as some authors find the π^+ to be the slower of the two mesons.

Referring again to reaction II, it must be pointed out than in 9 of the 11 cases, the π^0 is the faster meson; this preference may be due to our small sample, although other authors generally support this view ([1,2]). On the other hand, the anisotropy in Fig. 8 may in part be due to an apparent change in roles between π^- and π^0.

A practical consequence of the calculated angular distribution in the isobar frame is that in calculations one should not assume an isotropic distribution of the decay particles in the isobar frame ([7,8]) without further proof.

Finally, we mention here that, following a suggestion of MORPURGO ([11]), we investigated the problem of parity conservation in single pion production, and found no « up-down » asymmetry of the decay particles with respect to the production plane of the isobar.

4. – Nuclear interactions.

The pion interactions with nuclei were investigated with regard to emitted mesons and strange particle production.

A total of 725 interactions with nuclei were found, *i.e.*, all events which are not classified as free proton collisions. Among these events, 39 are endings, including the 19 interactions without any visible prongs (cf. Section 3), while the remainder have associated Auger electrons or recoils. Adding these to the 263 stars without emitted charged mesons, we find that in 41% of all events no mesons are emitted. The number of 1 meson:2 meson:3 meson stars is 317:94:14. Hill's data ([12]) give analogously 50% and ratios of 169:57:8, for 1.5 GeV pions, not in disagreement with the present results

([11]) G. MORPURGO: *Nuovo Cimento*, **9**, 564 (1958).
([12]) J. E. CREW and R. D. HILL: *Phys. Rev.*, **110**, 177 (1958).

3620

if one takes into account the fact that the latter are derived from along-the-track scanning (yielding therefore a number of events with only light tracks which correspond to edge collisions).

Fig. 9 gives the laboratory angular distribution of all mesons smaller, and greater, than 150 MeV, where curves (*a*) include mesons from collisions with edge nucleons and curves (*b*) refer only to mesons from stars with evaporation prongs. The dividing point of 150 MeV is based on a grain count criterion.

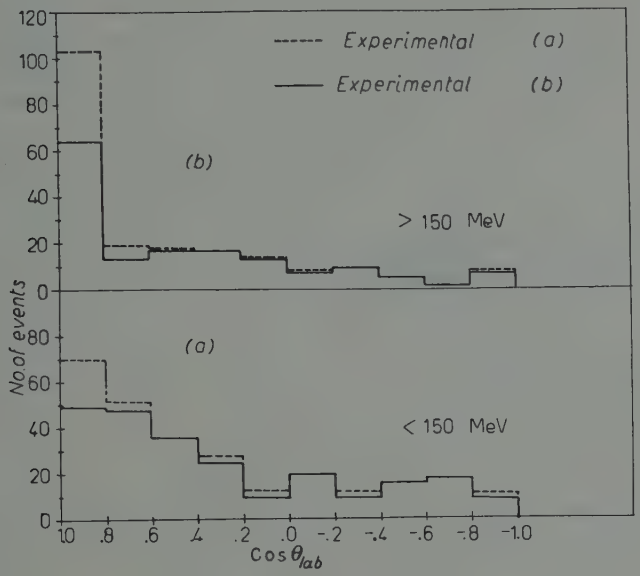

Fig. 9. – Histogram of the angular distribution in the laboratory system of mesons emitted from interactions with nuclei with kinetic energies (*a*) less than 150 MeV and (*b*) greater than 150 MeV. Curves (*b*) refer to mesons emitted from stars with evaporation prongs, while curves (*a*) include those mesons coming from interactions with edge nucleons (cfr. Table I).

Both sets of curves show a marked forward peak in the angular distribution, which is more pronounced for the higher energy mesons, as expected. The angular characteristics of the low energy mesons agree with an assumption of secondary interactions of these mesons before they emerge from the nucleus. These results again seem to agree qualitatively with the data of CREW and HILL ([12]).

In Figs. 10 and 11, only those mesons (213) whose energies were uniquely determined by grain count and multiple scattering are shown, (*a*) and (*b*) having meanings analogous to those in Fig. 9. Fig. 10 gives the angular distribution of these mesons and compares it with the result of the Monte Carlo

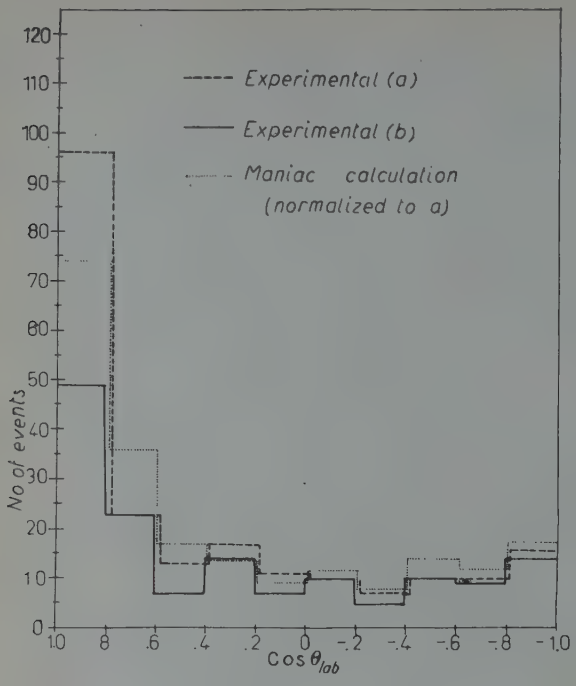

calculation ([13]), as quoted by CREW and HILL ([12]). The result of the calculation is normalized to curve (*a*) for an equal number of mesons, while curves (*a*) and (*b*) give

Fig. 10. – Angular distribution in the laboratory system of mesons emitted from nuclear interactions. The energies of these mesons were uniquely determined by grain density and multiple scattering measurements. Curves (*a*) and (*b*) are defined as in Fig. 9. The Maniac distribution has been normalized to curve (*a*), while the ordinate refers to the actual numbers of events in curves (*a*) and (*b*)

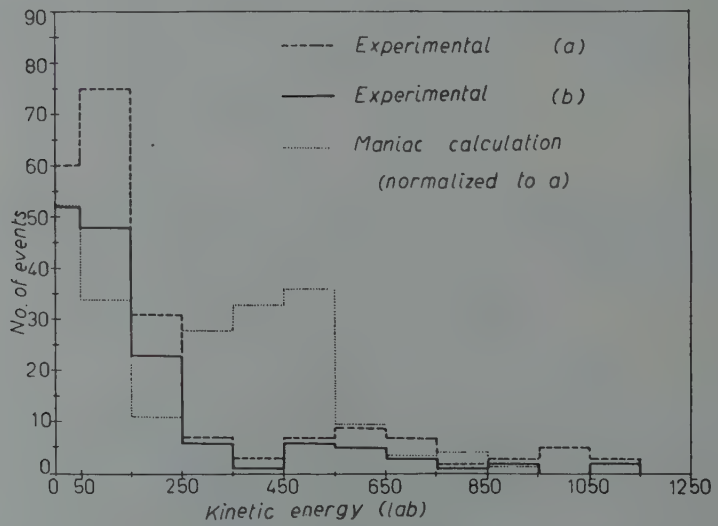

Fig. 11. – Energy spectrum, in the laboratory system of mesons emitted from nuclear interactions. Curves (*a*) and (*b*) are defined as in Fig. 9. The Maniac distribution has been normalized to curve *a*, while the ordinate refers to the actual numbers of events in curves (*a*) and (*b*).

([13]) N. METROPOLIS, R. BIVINS, M. STORM, J. M. MILLERR, G. FRIEDLANDER and A. TURKEVICH: *Phys. Rev.*, **110**, 204 (1958).

3622

the actual numbers of events found. In both cases, the experimental distributions show more forward scattering than the Maniac calculations.

A comparison of the energy spectrum, as shown in Fig. 11, is more difficult, as the experimental sample is possibly biased as a consequence of large dip angles and limited emulsion volume. However, the ratio of mesons with energies < 150 MeV to those with energies > 150 MeV is the same for mesons whose energies were uniquely determined as for the sample comprising all mesons, *i.e.*, including those which could be classified on the basis of the grain count criterion alone. It cannot be excluded that the detailed energy distribution in the higher region may not represent the true one. But the peak in the Maniac calculation in the interval $(250 \div 550)$ MeV could not be reproduced even if all the mesons with energies > 150 MeV whose energies were not determined would be uniformly distributed in this interval. Furthermore, the experimental results show more mesons in the $(50 \div 150)$ MeV interval than does the calculation, and possibly in the $(0 \div 50)$ MeV interval as well. The present data show more mesons in the lowest energy interval than in the experimental results of Crew and Hill, thereby masking the 150 MeV peak seen by these authors.

The percentage of stars without mesons as well as the observed spectrum of the emitted mesons is not unexpected, as the following argument can show. For this estimate, we assume 1.2 neutrons per proton, that the cross-sections of mesons on protons and neutrons are equal, and that the collisions of mesons with nucleons inside the nucleus follow the same behavior as collisions with free or edge nucleons. Considering only the first nucleon collision, we obtain the following frequencies for the various reactions. In 100 stars, one would expect: I) 23.4 elastic scatterings, II) 6.6 charge exchange events, III) 58.4 single meson production events, IV) 11.7 double meson production events. If only charged mesons are considered, one finds that one should get from I) 23.4 fast mesons, from III) 65 mesons of medium energy, and from IV) 23.6 mesons of low energy, or in all 112 meson from 100 stars (including the 7% charge exchange). By noting that the elastic scatterings on nucleons generally yield only very fast mesons (greater than 800 MeV) we assume that these mesons will not be completely degraded in energy even after other collisions in the nucleus. Mesons from category III) should leave with energies from 150 to 600 MeV while in category IV) from 30 to 200 MeV. In cases III) and IV) an appreciable number should be completely absorbed; this estimate can be obtained from absorption coefficients for various energies found in the literature. Taking for category III) an absorption of 62% for 500 MeV mesons ([14]), and for IV) an absorption of 75% for 100 MeV mesons ([15]). and

([14]) M. Blau and M. Caulton: *Phys. Rev.*, **96**, 150 (1954).

([15]) Md. Shafi and D. J. Prowse: *Proc. of the Padua-Venice Conference on Mesons and Recently Discovered Particles* (September 1957), p. x-2.

3623

assuming that a meson produced in the nucleus has to penetrate only about $\frac{1}{2}$ of the nucleus, one arrives at a frequency of 86 mesons per 100 stars, while the observed frequency is $547/725 = .76$ meson per star. Considering the approximate treatment, these numbers are in good agreement. Furthermore, the large number of low energy mesons (cf. Fig. 11) represents the energy-degraded mesons from categories III) and IV). Further details will be given later in connection with antiproton and K^- interactions in emulsions.

There were no definite cases of strange particle production on free protons; however, 3 events could be interpreted as production on bound protons and one on a neutron. All these events are summarized in Table III, with their

TABLE III. – *Strange particle events.*

a) Nucleon events	Production (c.m.s.)						Decay (c.m.s.)
	$\bar{T}_K$ (MeV)	$\bar{\varphi}_K$	$\bar{T}_Y$ (MeV)	$\bar{\varphi}_Y$	$\bar{T}_\pi$ (MeV)	$\bar{\varphi}_\pi$	
1. $(\pi^- p) \rightarrow (\pi^- K^+ \Lambda^0)$	49	70°	11	150°	123	90°	
2. $\rightarrow (\pi^- K^+ \Lambda^0)$	29	64°	43	80°	121	133°	
3. $\rightarrow (\pi^\pm \Sigma^\pm K^0)$	63	20°	40	157°	8	86°	$\Sigma \rightarrow \pi + n \quad \bar{\varphi}_\pi = 59°$
4. $(\pi^- n) \rightarrow (\Sigma^- K^0)$	88	19°	43	161°	—	—	$\Sigma \rightarrow \pi + n \quad \bar{\varphi}_\pi = 146°$

b) Nuclear events	T (MeV)	Production (lab.)	Decay (c.m.s.)	Other tracks
5. K^+	420	14°	—	200 MeV proton 2 short α's
6. K^+	100	8°	—	9 gray or black
7. K^+	400	6°	—	1 pion, 3 gray or black
8. Σ^+	4.5	49°	$\Sigma^+ \rightarrow p + \pi^0 \quad \bar{\varphi}_p = 65°$	5 gray or black

9. Non-mesic hyperfragment-decays into two heavy tracks which may be 2α's, one Li and one α, or 2 Li isotopes.
10. Non-mesic hyperfragment-decays into 2 short heavy tracks + 1 recoil. Cannot be analyzed.

c.m.s. characteristics. The above events met the kinematic requirements for collisions on bound nucleons within the limits allowed by Fermi momentum. Also shown in Table III are the laboratory angles and energies of the strange particles emitted in nuclear interactions (stars).

3624

* * *

We wish to thank Dr. G. ZORN for the use of his plates, Dr. C. S. RAINWATER for his assistance on part of the project, and to L. GIANOS, D. HANER, T. KLEINMAN, M. KOVEN, V. MELUS, and D. RICE for their help in scanning and making measurements on the plates.

RIASSUNTO (*)

Si è seguita in emulsione una lunghezza totale di 340 m di traccia di pioni negativi di quantità di moto 1.3 GeV/c, e si sono rilevate le interazioni pioniche. Si pone in particolare rilievo lo scattering anelastico su protoni liberi (produzione di mesoni singoli). Si investigano le distribuzioni angolari risultanti e le distribuzioni della quantità di moto delle particelle emesse confrontandole poi con esperimenti precedenti effettuati ad energie analoghe. Si cerca di spiegare questi risultati in base ad un decadimento isobarico in un nucleone e nel pione più lento. Nel caso della reazione $\pi^- + p \rightarrow \rightarrow \pi^- + \pi^0 + p$ sembra che esista, nella struttura isobarica di riferimento, un'anisotropia nella quale il pione più lento è emesso in modo predominante a ritroso rispetto alla direzione isobarica. Si confrontano i risultati con il modello di accoppiamento π-π. Si esaminano le distribuzioni angolari ed energetiche dei mesoni emessi nelle interazioni nucleari e si confrontano con altri risultati e con calcoli tipo Montecarlo. Si discutono altresì la molteplicità mesonica e la degradazione dell'energia in queste collisioni. Si analizzano le particelle strane trovate durante tale ricerca.

(*) *Traduzione a cura della Redazione.*

IL NUOVO CIMENTO Vol. XIV, N. 4 16 Novembre 1959

K^+-Deuterium Inelastic and Exchange Scattering. - II (*).

M. Gourdin

Ecole Normale Supérieure - Paris
Faculté de Sciences - Bordeaux

A. Martin

Ecole Normale Supérieure - Paris
C.E.R.N - Genève

(ricevuto il 22 Luglio 1959)

Résumé. — L'importance de la diffusion K^+-deuterium dans l'étude de l'interaction K^+-nucléon nous a conduit à améliorer un calcul précédent. Ici nous tenons compte de l'interaction des nucléons dans l'état final lorsque le deuterium est dissocié dans la collision. Les autres approximations faites précédemment — approximation d'impulsion, constance des amplitudes de diffusion élémentaires — sont maintenues. Les sections efficaces totales sont relativement peu modifiées. Les sections efficaces différentielles sont au contraire très sensibles à l'interaction dans l'état final. Les calculs numériques ont été effectués sur machine électronique IBM 704. Nous donnons les distributions angulaires et les sections efficaces totales de diffusion. Ces dernières apparaissent, ainsi que le rapport de la diffusion avec échange à la diffusion sans échange de charge, comme le moyen le plus simple d'obtenir des renseignements sur l'amplitude de diffusion dans l'état de spin isotopique $I = 0$ du système méson K^+-nucléon.

1. – Introduction.

In a preceding paper designated here by I ([1]), we have studied the K^+-deuterium scattering—elastic, inelastic and possibly charge exchange—using impulse approximation and neglecting the final state interaction of the nucleons. The elementary scattering amplitudes were assumed to be constant in angle

(*) Supported in part by theUnited States Air Force through the European Office, Air Research and Development Command.

([1]) M. Gourdin and A. Martin: *Nuovo Cimento*, **11**, 670 (1959).

and in energy. A similar independent calculation has been made by E. M. FERREIRA (2).

The impulse approximation seems to be more or less legitimate in this problem because the K^+-nucleon is weak. More precisely if we describe the K^+-proton interaction for instance by a repulsive core of radius $0.24\,\hbar/\mu c$ (3) we see that the ratio of the radius of this hard core to the averaged inter nucleon distance is very small so that one could expect that even at relatively low energies the impulse approximation—which is equivalent, when the amplitude is energy independent and angle independent, to the use of a δ-function pseudo-potential—is still justified to some extent.

The assumption of a scattering amplitude constant in energy and angle is certainly not justified in the case of the $I=0$ isotopic spin part of the K^+-nucleon interaction (4), since the experimental results show that the $I=0$ amplitude is small at low energies (3) and above 500 MeV of the same order of magnitude as the $I=1$ amplitude (5). On the other hand, the latest experimental results seem to confirm that the $I=1$ amplitude is fairly constant in angle and energy (5). In spite of this result in the $I=0$ state we maintain this simplicity assumption especially because nothing is known on the four p wave phase shifts. Following the spirit of the impulse approximation one can get the angular distribution corresponding to non-isotropic elementary amplitude by multiplying our results by a function $A(k)+B(k)\cos\theta$ (6). However the high mass of the K-meson (one half the nucleon mass) makes this procedure dubious because there is here no well defined method to go from the center of mass system of the elementary collision to the laboratory system.

The neglect of the final state interaction of this two nucleon system, in the case of inelastic collisions, is certainly a very poor approximation when one is interested in detailed information on the process such as direct inelastic, exchange inelastic differential cross-section. It is instructive to compare with a problem which has some similarities with the one under consideration: in the photodisintegration of the deuteron the cross-section computed with the exact final state is much larger than the cross-section computed with plane waves.

---

(2) E. M. FERREIRA: *Notas de Fisica*, IV, **20**, to be published in the *Phys. Rev.*

(3) J. E. LANNUTTI, S. GOLDHABER, G. GOLDHABER, W. CHUPP, S. GIAMBUZZI, C. MARCHI, G. QUARENI and A. WATAGHIN: *Phys. Rev.*, **109**, 2121 (1958).

(4) It is implicitly assumed here as in I that K^+K^0 is an isotopic spin doublet with even relative parity.

(5) H. C. BURROWES, D. O. CALDWELL, H. L. FRISCH, D. M. RITSON and R. SCHLUTER: *Phys. Rev. Lett.*, **2** 117 (1959).

(6) This procedure is justified only if the elementary scattering process cannot flip the spin of the nucleon, *i.e.* if the phase shifts do not depend on the total angular momentum.

3627

However the present situation is different because we have here three particles in the final state and one should expect to find that the total cross-section is approximately equal to the « inelastic total cross-section » computed with plane waves in the final state (7); this approximate sum rule is a consequence of an exact sum rule for fixed momentum transfer of the K-meson in the collision; this point was not clearly understood in I.

Consequently we felt that it was necessary to improve the computation made in I by taking into account the final state interaction of the nucleons, all the other assumptions being maintained. In the present case, only triplet states will occur. Results on deuteron photodisintegration (8) show us that it is sufficient to retain, in the final state wave function, the plane wave and the asymptotic form of the scattered wave in which the centrifugal effects are incorporated, with appropriate damping at short distance; it is also clear that the results are not sensitive to the precise choice of the nucleon-nucleon potential. The Coulomb interaction of the proton-proton system in the case of exchange scattering has been neglected, mainly because it is extremely difficult to treat it exactly; we give some arguments to show that this error is not too serious. We neglect also the D state in the deuteron; the error commited here mainly comes (9) from the matrix elements connecting the initial ^3D state of the deuteron to the final ^3S state of the nucleon-nucleon system; so that the exchange cross-section in which the final S state is a singlet state is unaffected; here one should expect a completely negligible change in the total cross-section, but the change in the inelastic cross-section may be as large as $\sqrt{p_D}$, *i.e.*; about 20% (p_D is the proportion on ^3D state in the deuteron ground state) for sufficiently large momentum transfers of the K-meson. We have also neglected the K^0-K^+ mass difference; this affects only the low energy region (up to 40 MeV). Another improvement with respect to I is that we treat in a relativistic way the kinematics of the K-meson. This turns out to be necessary for energies larger than 100 keV for the incident K^+-meson.

2. – The final state interaction.

Keeping the same notations as in I:

$\boldsymbol{q} = \boldsymbol{k}' - \boldsymbol{k}$	momentum transfer of the K-meson
$\boldsymbol{p} = \boldsymbol{k}'_p - \boldsymbol{k}'_n$ (or $\boldsymbol{k}'_{P_1} - \boldsymbol{k}'_{P_2}$)	difference between the final momenta of the nucleons

(7) Y. YAMAGUCHI: Private communication.
(8) R. E. MARSHAK and J. J. DE SWART: *Phys. Rev.*, **111**, 272 (1958).
(9) This question was raised by Dr. D. GEFFEN.

3628

we can write the matrix elements for the *inelastic* scattering as proportional to

$$(1) \qquad A_p \int \psi^*_{f(p/2)}(\boldsymbol{r}) \exp\left[-i\frac{\boldsymbol{q}\cdot\boldsymbol{r}}{2}\right] \psi_D(\boldsymbol{r})\,\mathrm{d}_3\boldsymbol{r} + A_{q\bar{q}} \int \psi^*_{f(p/2)}(\boldsymbol{r}) \exp\left[i\frac{\boldsymbol{q}\cdot\boldsymbol{r}}{2}\right] \psi_D(\boldsymbol{r})\,\mathrm{d}_3\boldsymbol{r}\,,$$

with

$$A_p = A_1 + f_a\,, \qquad A_{q\bar{q}} = \frac{A_1 + A_0}{2}\,,$$

and where $\psi_{f(p/2)}(\boldsymbol{r})$ is now an exact eigenstate of the two nucleon system with c.m. momentum $\boldsymbol{p}/2$, the asymptotic behaviour being a plane wave plus an outgoing wave. The approximation made in I consisted in replacing ψ_f by a pure plane wave $\exp[i(\boldsymbol{p}\cdot\boldsymbol{r}/2)]$.

The first term of equation (1) corresponds to scattering on the proton and the second to scattering on the neutron. As already indicated in I, it is legitimate to neglect multiple scattering.

The matrix element for exchange scattering is proportional to

$$(2) \qquad A_e \int \frac{1}{\sqrt{2}}\left[\psi^*_{f(p/2)}(\boldsymbol{r}) - \psi^*_{f(p/2)}(-\boldsymbol{r})\right] \exp\left[i\frac{\boldsymbol{q}\cdot\boldsymbol{r}}{2}\right] \psi_D(\boldsymbol{r})\,\mathrm{d}_3\boldsymbol{r}\,,$$

with

$$A_e = \frac{A_1 - A_0}{2}\,.$$

The final state wave function is antisymmetrical in space because the assumption made on the elementary amplitude forbids any spin flip collision, so that the final nucleon-nucleon state is a triplet state.

From the formulae written above it is already clear that the plane wave approximation is very poor for small momentum transfers because ψ_f and ψ_D are orthogonal so that the true matrix element is very small while the approximate one is large. For large momentum transfers it is also clear that a small shift in the oscillations of the final wave function will be felt rather strongly.

In principle, one should solve the Schrödinger equation with a convenient potential for each value of p and insert its solution in the matrix elements. This leads to an enormous computational problem because for a given incident energy and a given angle of scattering one has a one parameter family of coupled values $|\boldsymbol{p}|$ and $|\boldsymbol{q}|$. Fortunately the calculations made on a similar problem, the deuteron photodisintegration [8] show that in the computation of the matrix element:

$$\int \psi^*_{f(p/2)}(\boldsymbol{r}) r \psi_D(\boldsymbol{r})\,\mathrm{d}_3\boldsymbol{r}\,,$$

one can replace the final wave function by a plane wave plus the asymptotic form of the outgoing wave, the centrifugal effects being taken into account, with a cut-off inside the nuclear potential. This is permissible because the extension of the deuteron is much larger than the extension of the nuclear potential; it is important to suppress the scattered wave inside the interaction region in order to avoid a spurious divergence of the wave function at the origin. We feel that this approximation is still permissible in our problem, provided the factor $\exp[i(\boldsymbol{q}\cdot\boldsymbol{r}/2)]$ does not oscillate inside the potential. The condition $qr_0/2 < \pi$ gives, with $r_0 \simeq 1/\mu$, $k < 5\mu$ when the maximum possible transfer q is taken for a momentum k of the incident K^+-meson. The maximum incident momentum we consider is $k = 3.5\mu$.

Rather than using a straight cut-off, it is both more satisfactory and more convenient to introduce a damping factor $(1 - \exp[-Zr])^{L+1}$. For instance in the simple case $L = J$ (coupling coming from tensor force disappears here) the radial wave function is proportional to:

$$j_J\left(\frac{pr}{2}\right) + (1 - \exp[-Zr])^{J+1} \operatorname{tg} \delta_{JJ} n_J\left(\frac{pr}{2}\right). \tag{3}$$

The wave function in $L \neq 0$ states would be better simulated by using $(1 - \exp[-Zr])^{2L+1}$, but the error near the origin is completely negligible because this is multiplied by the L-th term of the decomposition of $\exp[i(q\cdot r/2)]$ in spherical harmonics, *i.e.*, $j_L(pr/2)$. The special choice made for the damping factor makes an analytic evaluation of the integrals feasible when the deuteron is described by a Hulthén wave function.

The choice of the interaction or equivalently of the phase shifts is not very important as shown by MARSHAK and DE SWART ([8]). We take the S, P, D, F, GAMEL and THALER phase shifts ([10]). For the higher angular momenta we only keep the truncated plane wave. This limitation is justified by a preliminary study of the distribution of c.m. energy of the final nucleon-nucleon system versus the scattering angle of the K-meson (here the final state interaction is neglected); it turns out that with $k \ll 3.5\,\mu$ the nucleon-nucleon energy expressed in laboratory energy for the nucleon-nucleon scattering does not appreciably exceed 200 MeV which is half the maximum permitted by kinematic values (see Fig. 1).

Another problem is the Coulomb interaction in the final proton-proton system for the exchange scattering. For high energies of the p-p system it can clearly be neglected because the long distance distortion of the wave function by Coulomb effects is outside the effective volume of integration.

([10]) J. L. GAMEL and R. M. THALER: *Phys. Rev.*, **107**, 291, 1337 (1957).

3630

At low energies the wave function is also modified at short distance but this can be described to some extent by a penetration factor C given by

$$|C(p)|^2 = \frac{2\varepsilon\pi}{\exp[2\varepsilon\pi]-1},$$

where $\varepsilon = \alpha M/p$, α is the fine structure constant, and M the nucleon mass.

This factor can be much less than unity for small values of p. Fortunately these momenta are strongly inhibited by the Pauli principle so that we can neglect a correction which makes smaller something which is already small. For instance, $p = \mu/4$, corresponds to $|C|^2 \simeq 0.5$ and to a c.m. energy of the p-p system around 0.3 MeV, for which the reduced P wave function is very well represented by $(pr/2)j_1(pr/2) \simeq (pr/2)^2/3$. At the deuteron radius this is of the order of 1/20. Of course we are aware of the fact that these arguments fail when the maximum possible c.m. energy of the p-p system is too low. For an incident momentum $k = \mu$, the maximum possible value of p for any scattering angle of the K-meson is larger than 0.5μ. All the exchange scattering will take place through final states in which $0.5\mu < p < 1.4\mu$, so that the true exchange cross-section lies between 80% and 100% of the calculated one.

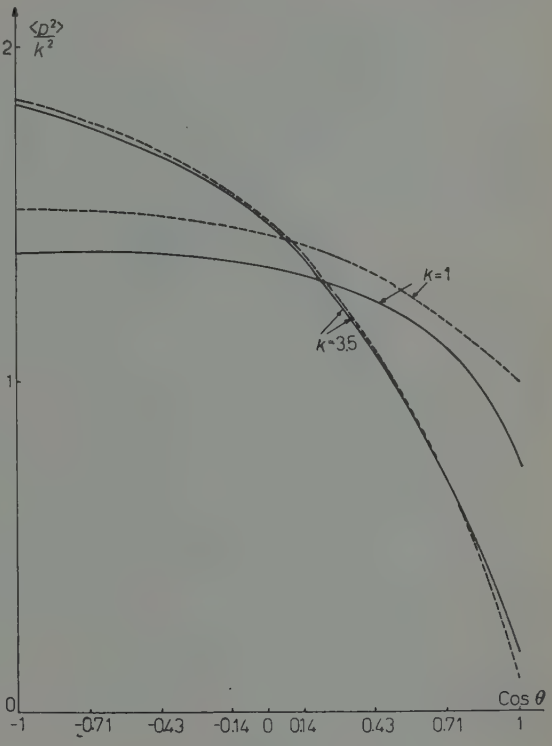

Fig. 1.

From the matrix elements written above (equations (1) and (2)) we obtain in the laboratory system the differential inelastic cross-section:

$$(3) \qquad d\sigma(k, k', \cos\theta) = \frac{\alpha\beta(\alpha+\beta)}{(\alpha-\beta)^2}\,\frac{M}{2M_r}\{[|A_p|^2 + |A_{q\pi}|^2]F(p,q) + [A_p^* A_{q\pi} + A_p A_{q\pi}^*]G(p,q)\}\cdot\frac{p}{k}\,k'^2\,dk'\,d\cos\theta,$$

and the exchange cross-section

$$(4) \quad d\sigma(k, k', \cos\theta) = \frac{\alpha\beta(\alpha+\beta)}{(\alpha-\beta)^2} \frac{M}{2M_r} \{|A_e|^2[F(p, q) - G(p, q)]\} \cdot \frac{p}{k} k'^2 dk' d\cos\theta ;$$

α and β are the two parameters of the Hulthén wave function and the form factors $F(p, q)$ and $G(p, q)$ are functions of the nuclear phase shifts, explicitly given in the Appendix.

3. – Numerical results.

We have computed the differential and total cross-sections for a $I = 1$ scattering length of $0.338 \cdot 10^{-13}$ cm ([3]) and various values of a $I = 0$ scattering length: 0, -0.013 and $-0.019 \cdot 10^{-13}$ cm. At high energy the elementary amplitude A_1 cannot be real because of the optical theorem:

$$\frac{I_m A_1}{|A_1|} = k_{cM} |A_1| = \sin \Phi_1 ,$$

where k_{cM} is the energy of the K^+-nucleon system in their center of mass system. A similar relation holds for A_0 but since we know from complex nuclei experiments that it is much smaller than A_1, its imaginary part is negligible. At the maximum energy we have considered ($k = 3.5\mu$ in the lab. system) we find $\Phi_1 = 33°$, while A_0 can be taken as real. When Coulomb effects are neglected, it is possible to replace the complex amplitudes A_1 and A_0 by the real numbers $|A_1|$ and $A_0' = A_0 \cos\Phi_1$; then the Coulomb interference is slightly overestimated; but this is unimportant at such energies.

The damping parameter Z entering in the factor multiplying the scattered wave has been taken equal to 2μ. We have also tried $Z = \mu$ (stronger damping); it turns out that the results are a little smaller but without significant difference.

3·1. *Exchange differential cross-section* (Fig. 2). – The general behaviour is the same as in the case of free antisymmetrical final state. We find the same maximum at some angle in the forward hemisphere, but we notice that in the backward direction the cross-section is much smaller than in I and almost energy independent. We think that is due to the relatively large energies of the final nucleons for the backward direction (see Fig. 1). This phenomenon does not seem to have any connection with the Pauli principle and will also appear in the direct inelastic process.

The dependence of the exchange cross-section on the elementary amplitude is just given by the multiplying factor $[|A_1| - A_0 \cos\Phi_1]^2$. We have plotted the angular distribution for two values of A_0 (Fig. 3).

3632

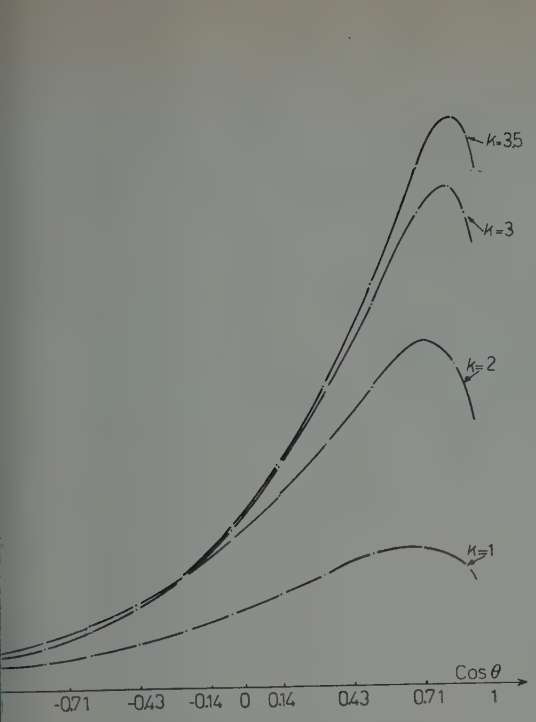

Fig. 2.

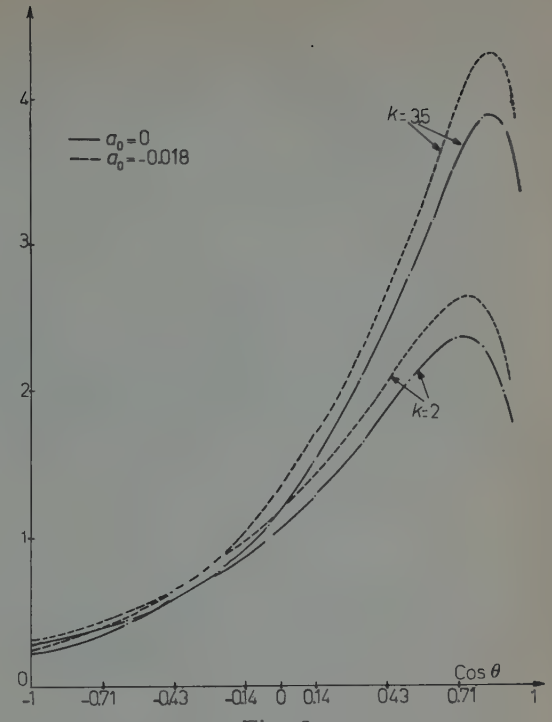

Fig. 3.

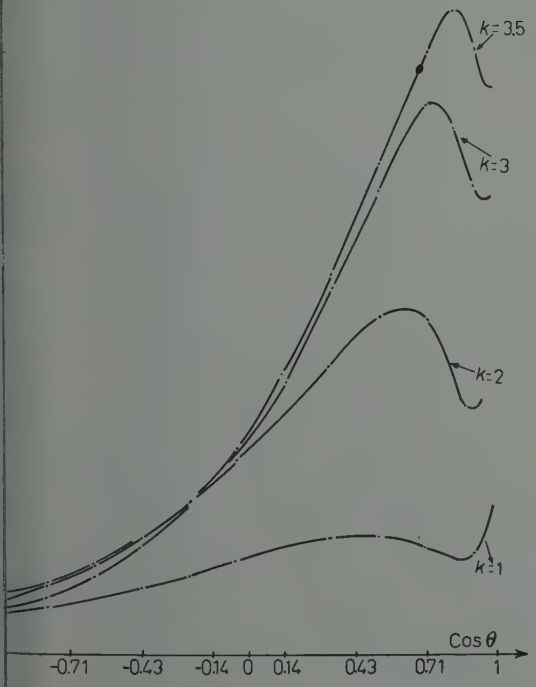

Fig. 4.

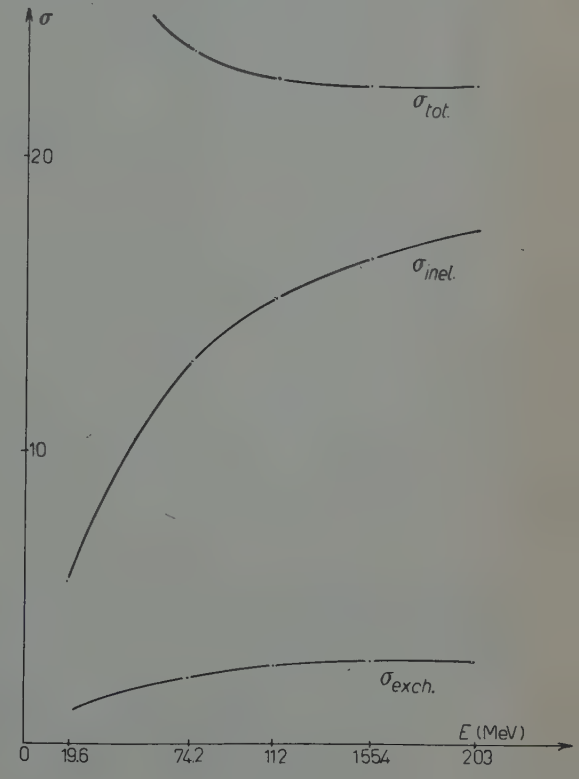

Fig. 5.

3833

3·2. *Inelastic differential cross-section* (Fig. 4). – The most striking feature of these curves is the presence of a maximum and of a minimum in the angular distribution. The interpretation seems to be the following: let us forget foo the moment the Coulomb effects; in the forward direction, collisions with zerr momentum transfer are permitted by kinematics but forbidden by orthogonality of the initial and final states. A detailed study of the correlation between p and q shows that in the forward direction, the transfer can be very small even if the c.m. energy of the nucleons is relatively large. This explains the presence of a maximum. If we add Coulomb effects we should expect a dip between this maximum and the infinite peak in the forward direction due to dissociation of the deuteron by a pure Coulomb excitation. This dip should not be interpreted as due to an interference.

On the other hand we find in the backward direction the same phenomena as in the exchange scattering.

The dependence of the cross-section on A_0 is extremely small. This is already clear on the cross-section on free nucleons:

$$\sigma_{(\text{free})} = 4\pi \left[|A_1|^2 + \left| \frac{A_1 + A_0}{2} \right|^2 \right].$$

3·3. *Total cross-sections* (Fig. 5). – We keep the same cut-off angle as in I ($\cos\theta \leqslant 90°$). It turns out that the total cross-sections are little affected by the final interaction of the two nucleons, provided the comparison with the free final state results is properly made. The new exchange cross-section must be compared with the old exchange cross-section, but one should compare the old « inelastic » cross-section with the sum of the elastic and the new inelastic cross-sections. The exchange cross-section at 200 MeV still differs from the high energy limit corresponding to a collision on a *free* neutron. The inelastic cross-section starts from zero at zero energy, due to orthogonality of the initial and

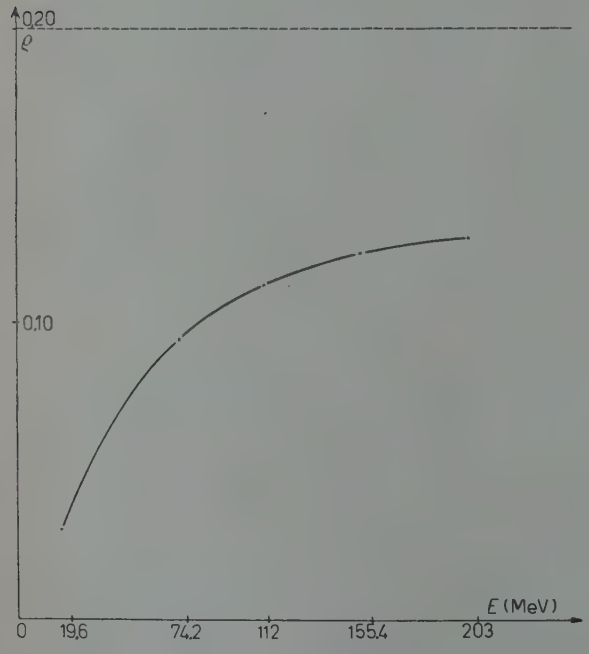

Fig. 6.

final states; it reaches the high energy limit faster than the exchange cross-section.

The ratio of the total cross-sections

$$\varrho = \frac{\sigma(K^+ \to K^0)}{\sigma(K^+ \to K^+)},$$

seems to be the most suitable quantity that permits to determine A_0. It happens that this is also easier to measure than angular distributions. Fig. 6 gives a plot of ϱ for $A_0 = 0$; at the maximum energy considered (200 MeV) the ratio of the actual ϱ value to the asymptotic values is .77.

4. – Concluding remarks.

As already indicated in the introduction, we have made for simplicity some assumptions which are only valid for a limited range of energies of the incident K^+-meson.

The most questionable one concerns the $I = 0$ elementary amplitude. It must be understood that the present calculation is an estimate of the effects of the nuclear forces, as well in the deuteron as in the final state, on the K^+-deuteron scattering. It shows that it is possible to deduce, from the experimental data, the cross-sections corresponding to scattering of a K^+-meson on a free neutron, and, if we restrict ourselves to total cross-sections, this connection remain valid when more complicated elementary amplitudes are assumed.

The neglect of the deuteron quadrupole moment has probably not too serious effects on the total inelastic cross-section. The validity of the impulse approximation does not seem too much questionable in the present case, as was already discussed. We must notice, however that if *coherent* effects are conveniently taken into account, screening effects such as those considered by GLAUBER ([11]) are disregarded. This means in particular that our treatment is not suitable for the very high energy case (above 500 MeV). On the other hand one may have of course some doubt on the validity of the impulse approximation below 50 MeV; but in this region, the results are probably very sensitive to the 4 MeV $K^0 - K^+$ mass difference.

Another question arises: this work uses the traditional approach to the determination of the interaction of a particle with another particle contained in a complex target. In principle it is possible to apply to this problem the

---

([11]) R. J. GLAUBER and P. C. MARTIN: *Phys. Rev.*, **109**, 1329 (1958).

3635

new extrapolation technique of CHEW and LOW ([12]). Is this feasible? We feel that this is far beyond the present experimental possibilities for various reasons:

a) The extrapolation method needs very high statistics, such experiments are very difficult when one uses π-meson beams. The present case is much worse.

b) We are essentially interested in situations where the « spectator » particle is a proton, *i.e.* we must look at proton recoils with an energy which must be of the order of magnitude of the absolute value of the deuteron binding energy (this is specific to a deuteron target). It happens that this is extremely difficult, much more than in the case of a neutron recoil where time of flight measurements are possible ([13]).

The measurements we suggest—especially those of total cross-sections—are probably the less difficult ones, although the measured apparent exchange cross-section, will be one half the computed cross-section (identification of the event by the decay of K^0 meson).

* * *

The numerical computations were performed by courtesy of the IBM-France Company, through their European Research Fund and we are especially indebted to Mr. SIMON for his help in programming.

We thank Dr. Y. YAMAGUCHI for several very valuable discussions. One of us (A.M.) wishes to thank Professor FIERZ and Professor BAKKER for the hospitality of C.E.R.N.

APPENDIX

The two form factors $F(p, q)$ and $G(p, q)$ are given by the following expressions:

$$F(p, q) = \tfrac{2}{3} \sum_{J=0}^{\infty} (2J+1) \sum_{L=J-1}^{L=J+1} |H(p, q; J, L)|^2 ,$$

$$G(p, q) = \tfrac{2}{3} \sum_{J=0}^{\infty} (2J+1) \sum_{L=J-1}^{L=J+1} (-1)^L |H(p, q; J, L)|^2 ,$$

([12]) G. F. CHEW and F. E. LOW: *Phys. Rev.*, **113**, 1640 (1959).
([13]) P. MARIN: private communication.

where $H(p, q; J, L)$ is a function depending on the nuclear phase shifts. By convention, we adopt the simplified notation: δ_J^L for the phase shift and according to the result of Rohrlich and Eisenstein ([14]) we have

$$\delta_J^\alpha \Rightarrow \delta_J^{J-1}, \qquad \delta_J^\gamma \Rightarrow \delta_J^{J+1}, \qquad \delta_J^\beta \Rightarrow \delta_J^J,$$

δ_J^α, δ_J^β, δ_J^γ are the real phase shifts corresponding to eigenvectors of the hamiltonian H including tensor forces that mix the $L = J + 1$ and $L = J - 1$ states. (We must remark that the true phase shifts $\delta_J^{J\pm1}$ are complex). We obtain:

$$|H(p, q; J, L)|^2 = [\cos \delta_J^L B_L(p, q) + \sin \delta_J^L C_L(p, q)]^2 .$$

The two functions B_L and C_L are Bessel transforms of the deuteron wave function

$$B_L(p, q) = \int_0^\infty j_L\left(\frac{pr}{2}\right) j_L\left(\frac{qr}{2}\right) \psi_D(r) r^2 \, dr ,$$

$$C_L(p, q) = \int_0^\infty (1 - \exp[-Zr])^{L+1} n_L\left(\frac{pr}{2}\right) j_L\left(\frac{qr}{2}\right) \psi_D(r) r^2 \, dr .$$

The explicit expression for $B_L(p, q)$ is given in terms of the Legendre functions of second type

$$B_L(p, q) = \frac{2}{pq}\left[Q_L\left(\frac{\beta^2 + (p^2 + q^2)/4}{pq/2}\right) - Q_L\left(\frac{\alpha^2 + (p^2 + q^2)/4}{pq/4}\right)\right] .$$

If we neglect the nuclear phase shifts δ_J^L, we obtain, after summation over L, the form factors F and G given in I. For the function $C_L(p, q)$, we use recurrence formulae between Legendre polynomials.

It is interesting to write the factors F and G in a form in which explicitly appear the free form factors $F^{(0)}$ and $G^{(0)}$

$$F(p, q) = \tfrac{2}{3} \sum_J (2J + 1) \sum_L \{|H(p, q; J, L)|^2 - B_L^2(p, q)\} + F^{(0)}(p, q) ,$$

$$G(p, q) = \tfrac{2}{3} \sum_J (2J + 1) \sum_L (-1)^L \{|H(p, q; J, L)|^2 - B_L^2(p, q)\} + G^{(0)}(p, q) .$$

([14]) F. Rohrlich and J. Eisenstein: *Phys. Rev.*, **75**, 705 (1949); M. Gourdin: *Journ. Phys. Rad.*, **17**, 988 (1956); **18**, 85 (1957).

The expressions for $F^{(0)}(p, q)$ and $G^{(0)}(p, q)$ are given in I and the summation over J and L is only reduced to non-zero phase shift states; *i.e.* to S, P, D, F, triplet states

$$|H(p, q; J, L)|^2 - B_L^2(p, q) = \sin^2 \delta_J^L [C_I^2(p, q) - B_L^2(p, q)] + \sin 2\delta_J^L B_L(p, q) C_L(p, q) .$$

RIASSUNTO (*)

L'importanza della diffusione K^+-deuterio nello studio dell'interazione K^+-nucleone ci ha indotto a migliorare un calcolo precedente. Qui teniamo conto dell'interazione dei nucleoni nello stato finale quando il deuterio è dissociato nella collisione. Sono mantenute le altre approssimazioni fatte in precedenza: approssimazione dell'impulso, costanza delle ampiezze di diffusione elementari. Le sezioni efficaci totali sono modificate relativamente poco. Le sezioni efficaci differenziali al contrario sono molto sensibili all'interazione nello stato finale. I calcoli numerici sono stati eseguiti sulla calcolatrice elettronica IBM 704. Diamo le distribuzioni angolari e le sezioni efficaci totali di diffusione. Queste ultime sembrano, come il rapporto fra diffusione con scambio e diffusione senza scambio di carica, il mezzo più semplice per avere informazioni sull'ampiezza di diffusione nello stato di spin isotopico $I = 0$ del sistema mesone K^+-nucleone.

(*) *Traduzione a cura della Redazione.*

3638

IL NUOVO CIMENTO Vol. XIV, N. 4 16 Novembre 1959

Vapour Pressure of Isotopic Liquids (*).

I. – A, N_2, O_2 Below Boiling-point.

G. Boato, G. Scoles and M. E. Vallauri

Istituto di Fisica dell'Università - Genova
Istituto Nazionale di Fisica Nucleare - Sezione di Genova

(ricevuto il 30 Luglio 1959)

Summary. — A static equilibration method was used to measure the single stage separation factor α of isotopic pairs in the vapour liquid equilibrium of A, N_2 and O_2 below boiling-point. Since the corresponding isotopic mixtures are supposed to be ideal, the vapour pressure ratio of the studied isotopic liquids is identical to α. Due to the sensitivity and the precision of the mass spectrometer employed, enriched isotopes needed not be used. No high purity of the gases was necessary since, at least to a certain extent, the adopted method of measurement is insensitive to impurities. The separation factors at the boiling point were found to be the following:

$$^{36}A - {}^{40}A \qquad \alpha = 1.0060 \pm 0.0001,$$
$$^{16}O_2 - {}^{16}O{}^{18}O \qquad \alpha = 1.0050 \pm 0.0001,$$
$$^{14}N_2 - {}^{14}N{}^{15}N \qquad \alpha = 1.0037 \pm 0.0001.$$

The temperature dependence was established in all cases in a relatively narrow range of temperatures. A discussion of the argon results in the light of the quantum theorem of corresponding states is given.

---

1. – Introduction.

The study of thermodynamic, transport and other properties of condensed « simple » systems is proving to be more and more useful for the understanding of the condensed state. The meaning of the word « simple » has been discussed

---

(*) Presented to the Kamerlingh Onnes Conference on Low Temperature Physics, Leiden (June 1958).

at the « Symposium on the condensed state of simple systems » organized in Varenna by the Italian Physical Society during September 1957 (1).

At the Genoa University a program of study on the simple systems with small quantum correction (helium and hydrogens are therefore excluded) has been undertaken recently. Our first object was 1) to understand both on the theoretical and on the experimental side the dependence on mass of some thermodynamic properties and 2) to obtain some additional experimental information on simple liquids.

One of the few properties of such systems where the mass dependence is experimentally easily determined, is the vapour pressure of the liquid.

2. – Experimental method.

Suppose we have a liquid mixture of two isotopic species A and B of the same substance. At constant temperature an isotopic equilibrium will be established between this liquid and the coexisting vapour phase, and a definite enrichment ratio (usually called single stage separation factor)

$$\alpha = \frac{(N_A/N_B)_{vap}}{(N_A/N_B)_{liq}}, \tag{1}$$

will be observed. A is generally assumed to be the lighter isotopic species, B the heavier one.

Since an isotopic mixture (except for H and He) both on theoretical (2,3) and experimental (4-6) basis, is considered to be ideal, the Raoult law is valid and consequently the right hand side of (1) represents the ratio of vapour pressures of the pure isotopic components:

$$\alpha = \frac{p_A}{p_B}, \tag{2}$$

at least as long as the vapour phase behaves like an ideal gas. However, it is of some theoretical and practical interest to check the limit of validity of (2).

---

(1) *Suppl. Nuovo Cimento*, **9**, n. 1 (1958).
(2) I. PRIGOGINE, R. BINGEN and J. JEENER: *Physica*, **20**, 383 (1954).
(3) I. PRIGOGINE and J. JEENER: *Physica*, **20**, 516 (1954).
(4) T. F. JOHNS: *Proc. Phys. Soc.*, **66**, 808 (1953).
(5) T. F. JOHNS: *Proc. of the International Symposium on Isotope Separation* (Amsterdam, 1958), pag. 74.
(6) W. H. KEESOM and J. HAANTJES: *Physica*, **2**, 986 (1935).

3640

On the basis of (1) and (2) an easy (static) determination of the vapour pressure ratio of two isotopic species can be performed, by measuring the isotopic composition of both liquid and vapour phase of a liquid isotopic mixture in equilibrium with its vapour at a given temperature.

The above method has not been very much used to determine p_A/p_B since it was believed that an equilibrium condition would be difficult to reach, due to partial recondensation of the vapour, in analogy with what is happening in ordinary liquid mixtures. Instead, following the pioneer paper of KEESOM and HAANTJES on neon isotopes ([6]), many authors ([4,5,7-9]) have adopted a differential method, consisting in a direct comparison of the vapour pressure of isotopic mixtures of different isotopic composition, using a differential manometer. In this case a test of the ideality of the solution is easily obtained; moreover the measurement can be extended to the solid phase without any remarkable additional difficulty.

We chose the first method due to the following facts:

1) a high purity of the original gases is not required, tank gases being generally satisfactory;

2) no precaution about a strict uniformity of temperature is necessary;

3) enriched isotopic species are not required in most cases, provided a sensitive and precise mass spectrometer is available;

4) finally, no difficulty must arise in measuring single stage fractionation processes if due care is taken in sampling procedure.

The condition under 3) was satisfied by the mass spectrometer we built in Genoa ([10]); the sensitivity of this instrument is 1/2 000 000 and thus one is able to measure a 1% variation of a natural isotopic abundance ratio as low as 1/300, with a standard error of about 1%.

3. – Experimental equipment.

For the measurements below boiling-point, described in this paper, a glass cryostat was designed; such a cryostat was considered a pilot plant for the improved apparatus built for higher temperatures, to be described in a further paper.

([7]) I. KIRSCHENBAUM and H. C. UREY: *Journ. Chem. Phys.*, **10**, 706 (1942).
([8]) W. GROTH, H. IHLE and A. MURRENHOFF: *Zeitf. Naturfor.*, **9***a*, 805 (1954).
([9]) K. CLUSIUS and K. SCHLEICH: *Helv. Chim. Acta*, **41**, 1342 (1959).
([10]) G. BOATO, M. REINHARZ, A. SANNA and M. E. VALLAURI: to be published

3641

The experimental apparatus is schematically shown in Fig. 1, which is self-explanatory.

a) *Measuring cell.* The measuring cell, about 70 cm³ in volume, is made of pyrex glass. The cell is filled for one seventh of its volume with the liquid, by condensation of the gas contained in the twelve liter flask. In such a situation, the vapour phase constitutes only a small fraction of the total weight of the system; hence, as a first approximation, the isotopic composition of the liquid can be taken to be equal to the composition of the gas initially contained in the flask.

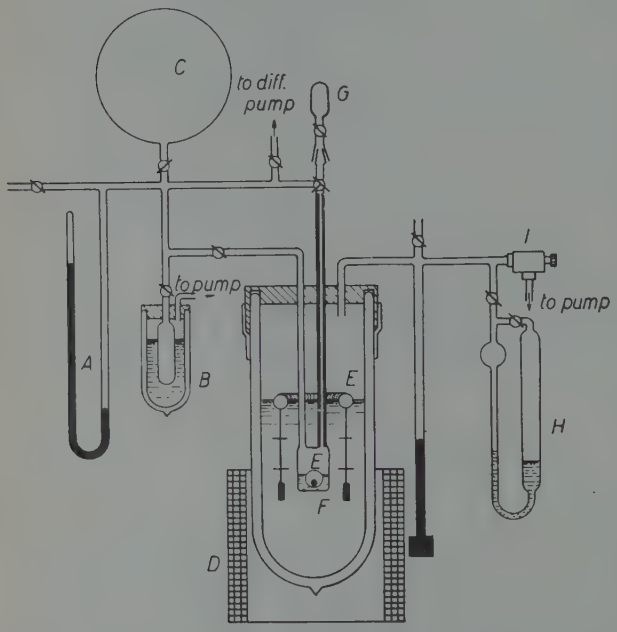

Fig. 1. – Diagram of the apparatus. *A*) Vapour pressure thermometer. *B*) Reduced liquid nitrogen trap. *C*) 12 l gas reservoir. *D*) Coil to apply intermittent magnetic field to stirrers. *E*) Iron core floating stirrers. *F*) Measuring cell. *G*) Gas sampling system. *H*) Oil manometer to control the temperature of the bath. *I*) Fine regulating valve.

On the other hand a representative sample of the vapour can be taken by withdrawing a small amount of it through a fine capillary, in such a way as not to perturb the equilibrium. Since an isotopic analysis may be carried out with an amount of gas as low as 0.5 cm³ NPT, the condition that the sampled volume is small in comparison with the vapour volume is approximately satisfied. The reaching of the isotopic equilibrium is favoured by agitating the liquid with a floating electromagnetic stirrer.

b) *Employed gases.* The filling of the flask is made by letting in the gases directly from the tank. A rough purification of the gases proved sometimes to be useful in reducing the errors of the isotopic analysis. The following gases were used:

Argon 99.5% purity, produced by Società Italiana Ossigeno (SIO)

3642

Oxygen 99% purity , produced by
Società Italiana Ossigeno (SIO)

Nitrogen 99% purity, produced by
Società Italiana Ossigeno (SIO).

A mass spectrometric scanning of the gases was carried out on each occasion to test the purity and individuate the foreign gases. The purity was controlled also by determining the triple point pressure.

c) Filling of the measuring cell. The cell was filled with the liquid either by direct condensation or by condensation of the gas in the trap B and subsequent distillation into the cell itself. All precautions were taken to avoid troublesome isotopic fractionation during the filling. It has to be noted that no fractionation is taking place during a condensation process from the reservoir to a cold trap, provided always the gas-flow through the connecting tube is one-directional and of the viscous type, so that no back diffusion is possible; this point was tested by direct experiments.

The cryogenic bath consisted of liquid oxygen in the cases of argon and oxygen, and liquid nitrogen in the case of nitrogen. The temperature of the bath was lowered by reducing the pressure of the bath by standard technique.

d) Temperature measurement and control. The standard method of mantaining a constant temperature in a cryogenic bath by pumping off the vapour at a given rate through a needle valve, has always the result of producing a temperature gradient inside the bath, the upper part of the bath being the colder. This effect can upset the static equilibrium between vapour and liquid into the cell since recondensation of the vapour can take place in the upper part of the cell. In order to avoid the non-uniformity of the temperature in the bath, the liquid was then vertically stirred by means of a floating device electromagnetically operated. In some experiments the cryostat was embodied in a second dewar vessel filled with liquid oxygen or nitrogen; the stirring of the liquid was not strictly necessary in this case.

The temperature of the cell was determined by measuring the vapour pressure of the liquid employed in the experiment. The thermoregulation of the bath was obtained by keeping constant the above vapour pressure within one mm Hg, operating by hand the needle valve of the bath. Such a strict control of the constancy of temperature was believed to be necessary in order to avoid sudden evaporation or condensation phenomena which could produce a variation of the isotopic equilibrium.

e) Sampling and mass-spectrometric analysis. Having reached a constant temperature of the cell, a lapse of half an hour was allowed to secure isotopic equilibration. Such a time interval was evaluated on the basis of some exper-

3643

imental evidence obtained by upsetting artificially the equilibrium. Then a small amount of vapour was pumped away through the capillary, to clear the sampling line. Finally the sampling was undertaken at 20 minutes time intervals. Thermal diffusion enrichment of the gas along the cryostat inlet and outlet tubings proved to have negligible effects during the time of the experiment.

The isotopic composition of such vapour samples was compared with the composition of the initial gas (representing the liquid composition) by means of the isotope ratio mass spectrometer built in this Institute. As the instrument works in a differential manner, one can read directly the quantity

$$\delta = \frac{R_{\text{sample}} - R_{\text{initial}}}{R_{\text{initial}}}, \tag{3}$$

R being the abundance ratio of the lighter over the heavier isotopic species; the δ thus measured is identical with $\alpha - 1$, α being the separation factor defined by (1).

4. – Results.

The experimental results are shown in Tables I, II and III for the isotopic pairs ^{36}A–^{40}A, $^{14}N_2$–$^{14}N^{15}N$ and $^{16}O_2$–$^{16}O^{18}O$ respectively. For each system two or three temperatures were chosen from the boiling point downwards. The experimental points are plotted in Fig. 2, 3 and 4 together with the data from previous work of other authors. For convenience sake in these figures the δ is plotted versus $1/T$; in fact it is to be noted that to a good approximation,

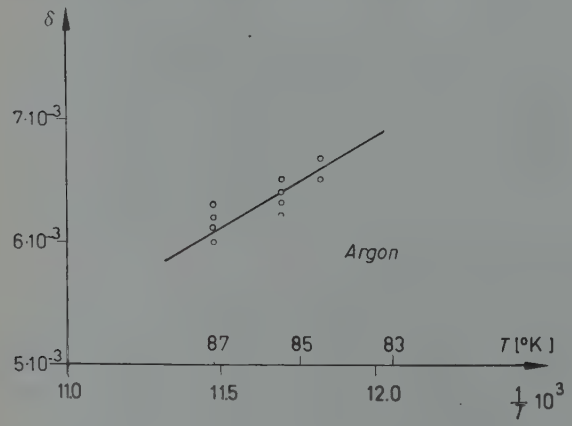

Fig. 2.

$$\delta = \alpha - 1 \cong \ln \alpha, \tag{4}$$

since δ is always smaller than 0.01, and therefore, in the limit of validity of (2)

$$\delta = \ln \frac{p_A}{p_B}. \tag{5}$$

3344

TABLE I. – *Argon results.*

T (°K)	Sample	δ	δ average
83.78 triple point	extrapolated		0.0067 ± 0.0001
84.4	A 25	0.0067	0.0066 ± 0.0001
	A 36	0.0067	
	A 37	0.0065	
85.5	A 21	0.0062	0.0064 ± 0.0001
	A 23	0.0065	
	A 24	0.0063	
	A 34	0.0065	
	A 35	0.0064	
87.0	A 12	0.0060	0.0061 ± 0.0001
	A 13	0.0061	
	A 14	0.0061	
	A 15	0.0063	
	A 16	0.0061	
	A 32	0.0062	
	A 33	0.0060	
87.4 boiling point	extrapolated		0.0060 ± 0.0001

TABLE II. – *Oxygen results.*

T (°K)	Sample	δ	δ average
84.5	O 12	0.0060	0.0061 ± 0.0001
	O 14	0.0061	
89.3	O 2	0.0052	0.0052 ± 0.0001
	O 3	0.0052	
	O 5	0.0055	
	O 15	0.0051	
	O 16	0.0050	
	O 23	0.0052	
	O 24	0.0053	
	O 26	0.0052	
	O 27	0.0052	
90.21	extrapolated		0.0050 ± 0.0001

TABLE III. – *Nitrogen results.*

T (°K)	Sample	δ	δ average
70.6	N 91 N 92 N 93	0.0048 0.0047 0.0049	0.0048 ± 0.0001
73.9	N 94 N 95	0.0041 0.0043	0.0042 ± 0.0001
75.7	N 96 N 97	0.0040 0.0038	0.0039 ± 0.0001
77.2 boiling point	extrapolated		0.0037 ± 0.0001

The plots can then be used for direct comparison with the theory of vapour pressure. Of course since the δ's always come out positive, the lighter isotopic species are always the more volatile.

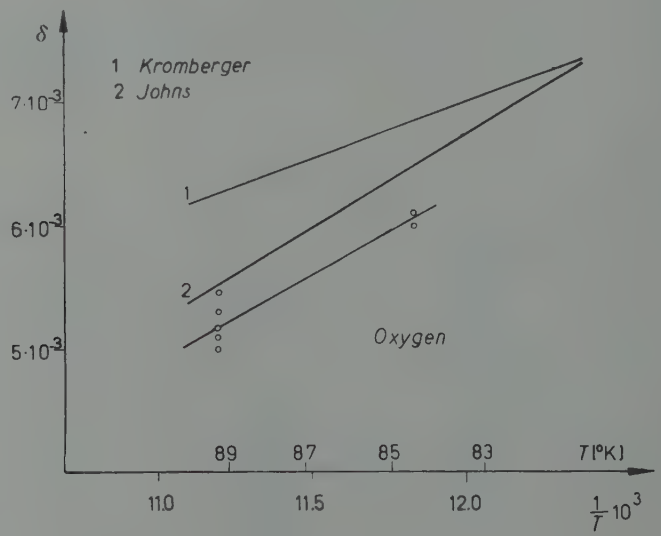

Fig. 3.

The first digit of each sample number refers to the run, the second one is a progressive number in the same run. One will notice that the measurements are well reproducible on different days and that the data at different tempe-

3646

ratures are consistent with each other. The given error is substantially the standard error due to the mass-spectrometrical analysis.

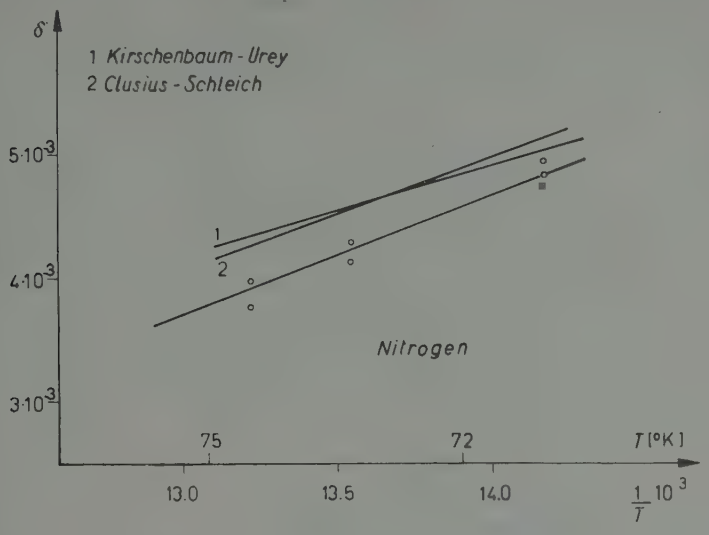

Fig. 4.

5. – Comparison of results with previous measurements.

5·1. *Argon.* – No previous measurements were made of the enrichment factor α for ^{36}A–^{40}A liquid systems with the exception of a rough evaluation of α at boiling point by CLUSIUS and MEYER ([11]) effected by using a small distillation column. The Clusius and Meyer result is not in disagreement with our more precise determination.

5·2. *Oxygen.* – Apart from the less precise measurement by KRONBERGER ([12]) and by THODE and SMITH ([13]), it is interesting to compare our results with the careful work carried out by JOHNS ([5]), who used a manometric differential method. The agreement is good as far as the temperature dependence is concerned but only fair in respect of absolute values; in fact, a systematic difference of about 6% was found. Whether this difference is to be ascribed to experimental errors or to the non applicability of equation (2) has not been possible to determine up to this moment. Further investigation is in progress on this point.

([11]) K. CLUSIUS and H. MEYER: *Helv. Chim. Acta*, **36**, 2045 (1955).
([12]) H. KRONBERGER: cited by T. F. JOHNS ([5]).
([13]) H. G. THODE and S. R. SMITH: N.R.C. Canada Report no. MC-45 (1944).

3847

5·3. *Nitrogen.* – Also in this case a systematic deviation between our data and those determined by using a manometric differential method by KIRSCHENBAUM and UREY (7) and by CLUSIUS and SCHLEICH (9) can be noticed. The difference is about 10% of the total effect and has the same sign as that found in oxygen measurements. The reason for this discrepancy is again not clear.

At this point it can be noted that every effort has been done by us to avoid systematic errors intrinsic with our method of measurement. In the case of nitrogen many runs were done, with different levels of the bath, with or without stirring, with or without the additional external Dewar vessel; all the corrections due to isotopic fractionation in the external connecting tubes and to other causes were evaluated. Some minor sources of errors were found, but no one could justify the gross 10% deviation referred above; the problem is still under study, as for the oxygen case, and further measurements with a new cryostat are under way.

6. – Discussion and comparison with theory.

The isotope separation occuring in the equilibrium between a liquid isotopic mixture and its vapour is a purely quantum effect which gradually disappears with rising temperature. Small quantum effects can be studied theoretically by developing the partition function relative to a pure substance as a series of powers of h^2. This can be done easily in many cases. When very « simple » systems, *i.e.* condensed inert gases, are studied the theory is particularly simple and a correct physical picture can be given introducing the so-called quantum parameter $\Lambda^* = h/\sigma\sqrt{m\varepsilon}$ which is calculated from the knowledge of the molecular parameters ε and σ of the 6-12 Lennard Jones potential (14). Since Λ^* contains a mass factor, the mass dependence of thermodynamic properties can be theoretically investigated if the dependence on Λ^* can be explicitely given.

In Fig. 5 we have plotted in a logarithmic scale the experimental reduced vapour pressures $p^* = p\sigma^3/\varepsilon$ of the liquid inert gases at $T^* = kT/\varepsilon = 0.715$ as a function of Λ^{*2}. We have also plotted the isotopic effect found by us for A and by KEESOM and HAANTJES (6) for Ne at the same reduced temperature. To give these two isotopic effects is equivalent to giving the slope of the $\ln p^* - \Lambda^{*2}$ curve at the A and Ne points. It appears that the vapour pressures alone are in themselves not sufficient to give us a detailed information about the shape of the curve, mainly due to the imperfect knowledge of the

(14) J. DE BOER: *Physica*, **14**, 139 (1948).

quantum parameters; on the contrary, the isotopic effects on A and Ne show us that an approximately linear dependence of $\ln p^*$ on Λ^{*2} is present, as it can be expected from the theory, at least for $\Lambda^* \ll 1$. The knowledge of the isotopic effect of A and Ne allows us then to draw a straight line through the experimental points, its slope being an average between the measured slopes at A and Ne points. The straight line was arbitrarily drawn through the Xe point in Fig. 5.

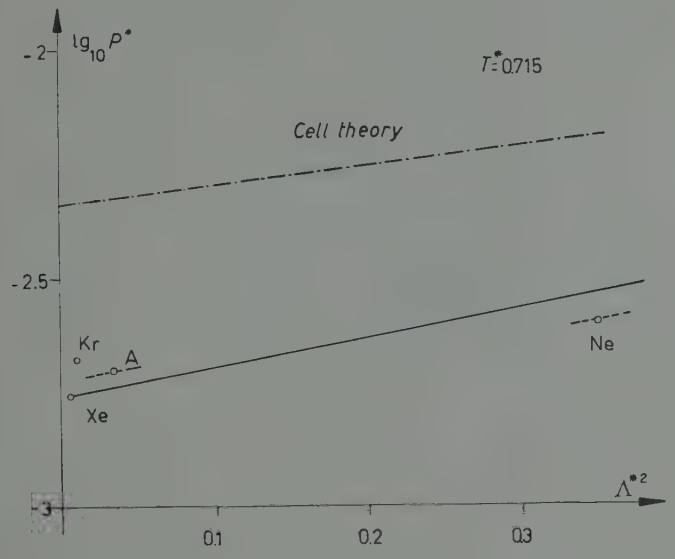

Fig. 5.

This experimental dependence of $\ln p^*$ on Λ^{*2} can be compared with the dependence found on the basis of a simple cell model of the liquid state by DE BOER and LUNBECK ([15]). The cell model is certainly inadequate but is not too bad when near the triple point. The expression of the reduced vapour pressure can be calculated by this model to be

$$(6) \qquad \ln p^* = \frac{\Phi^*}{T^*} + \ln T^* - (\ln {}_0v_f^* + 1) + \Lambda^{*2}\frac{F_1^*}{T^*} + \dots$$

$$\dots + \text{terms containing higher powers of } \Lambda^{*2},$$

where the symbols used are the same as DE BOER and LUNBECK's.

([15]) J. DE BOER and R. J. LUNBECK: *Physica*, **14**, 520 (1948).

The equation (6) gives the approximate linear dependence we are looking for. The slope of the resulting straight line on the $\ln p^* - A^{*2}$ diagram is given by

$$\frac{F_1^*}{T^*} = -\frac{{}_1\gamma_f^*}{{}_0\gamma_f^*},$$

and is calculated to be 0.97 when the co-ordination number inside the liquid is assumed to be 10, a reasonable hypothesis. The calculated curve is plotted in Fig. 5 (decimal logarithms are used); it is seen that while the slope agrees reasonably well with the experimental one, the absolute values of the pressure are far away from the experimental points. This is mostly due to the inadequacy of the cell model as far as the entropy factor is concerned.

A more precise calculation on the basis of the cell model was carried out by Basso and Fieschi [16]; they extended to liquids the anharmonic approximation, introduced with very promising results by Henkel [17] for solids. The values of $\ln p_A/p_B$ calculated by Basso and Fieschi for liquid argon are compared with our experimental results in Table IV. One sees that the agreement is satisfactory (within the limits of validity of the cell model) when the number of the nearest neighbours is again assumed to be 10.

Table IV. – *Theoretical results on argon (by* Basso *and* Fieschi).

	Exp.	$c=8$	$c=10$	$c=12$
$\ln p_{36}/p_{40}$ at 84.2 °K	0.0066	0.0167	0.0070	0.0040
$\ln p_{36}/p_{40}$ at 90.2 °K	(0.0056)	0.0130	0.0061	0.0036
$\Delta \ln (p_{36}/p_{40})/\Delta T$	$-1.7\cdot10^{-4}$	$-6.2\cdot10^{-4}$	$-1.5\cdot10^{-4}$	$-0.7\cdot10^{-4}$

Of course, no theory is at present giving a completely satisfactory physical picture of a liquid and the last comparison is not adding very much to the known situation. However, we feel that a complete study of mass dependence of thermodynamic properties of simple systems can be of some help in searching for a better understanding of the liquid state.

A final comment must be made as far as liquid N_2 and O_2 are concerned. The De Boer picture is only approximate when applied to such systems, since the molecular constituents of the liquid are now diatomic molecules; moreover the vapour pressure is too sensitive to the nature of the molecules. No important consequence can then be derived from a preliminary study as that completed by us on such systems.

---

[16] P. Basso and R. Fieschi: *Suppl. Nuovo Cimento*, **11**, 439 (1959).
[17] J. H. Henkel: *Journ. Chem. Phys.*, **23**, 681 (1955).

3650

* * *

The present work was supported in part by the « Comitato per la Fisica del Consiglio Nazionale delle Ricerche ».

RIASSUNTO

Mediante un metodo statico è stato misurato il fattore di separazione α nell'equilibrio liquido-vapore di alcune coppie di molecole isotopiche a temperature inferiori a quella di ebollizione. Dato che le miscele isotopiche del tipo da noi studiato possono ritenersi ideali, il fattore α si identifica con il rapporto delle tensioni di vapore dei liquidi isotopici puri in considerazione. Non si è fatto uso di isotopi arricchiti, per merito della sensibilità e precisione dello spettrometro impiegato; non si è nemmeno ricorso a gas di elevata purezza, dato che il metodo di misura è relativamente poco sensibile alle impurezze del gas in studio. Al punto di ebollizione dei liquidi studiati, sono stati trovati i seguenti fattori di separazione:

$$^{36}A - {}^{40}A \qquad \alpha = 1.0060 \pm 0.0001,$$
$$^{16}O_2 - {}^{16}O\,{}^{18}O \qquad \alpha = 1.0050 \pm 0.0001,$$
$$^{14}N_2 - {}^{14}N\,{}^{15}N \qquad \alpha = 1.0037 \pm 0.0001.$$

La dipendenza di α dalla temperatura è stata anche determinata in un intervallo di temperatura piuttosto limitato. Per concludere, i risultati ottenuti per l'argon vengono discussi alla luce del teorema quantistico degli stati corrispondenti.

3651

IL NUOVO CIMENTO Vol. XIV, N. 4 16 Novembre 1959

Self Diffusion in Liquid In-Pb Alloys.

A. Paoletti

C.N.R.N., Divisione Studi e Ricerche - Roma

M. Vicentini

Istituto di Fisica dell'Università - Roma

(ricevuto il 30 Luglio 1959)

Summary. — The self diffusion coefficient in the liquid alloys In – 0.5% Pb and In – 1.5% Pb have been measured over a wide range of temperatures, using ^{114}In and RaD as tracers. The results show, within the experimental errors, the independence of the activation energy of the tracer. This fact has been interpreted as an indication of a long range contribution of the atoms to the energy barrier for the diffusion.

1. – Introduction.

The transport properties are of the highest interest in order to improve our knowledge of the liquid state, since thay can provide information to be interpreted on the basis of a microscopic picture of the liquid. The self diffusion in liquid metals has been investigated for few pure elements ([1]).

In the alloys, as yet, only data on the Fe-C and Pb-Bi systems, are available.

In this research we have measured the self diffusion coefficient of Indium and Lead for the alloys In — 0.5 atomic pct Pb and In — 1.5% Pb in the temperature range (522÷817) °K.

([1]) N. H. Nachtrieb: *Second Int. Conf. Geneva*, 1958, A/Conf. 15/P/718.

2. – Experimental.

A detailed report on the apparatus and experimental procedure was given in previous papers ([2,3]).

We just recall that our technique consists in allowing two half rods of radioactive and inert metal to follow a thermal cycle in a mullite capillary. During this cycle the diffusion in liquid phase takes place. The solidified rod is then cut into small segments, and from the penetration curve of the active component, the diffusion coefficient is evaluated.

Here we want to point out that our analysis of the data is very reliable since, on the basis of the penetration curve, we are able to discard the runs where some convection was present. The In–0.5% Pb experiments were performed with capillaries of two different diameters (1.6 mm and 0.8 mm) in order to investigate whether a « wall effect » was present similar to that found in pure Indium self diffusion ([3]).

The metals were (*) of the highest purity; ^{114}In (**) and RaD (**) were used as tracers. Some precaution had to be taken in the analysis of the RaD concentration. RaD (^{210}Pb) decays to ^{210}Bi by the emission of very weak β and γ radiation with a half-life of 22 years. ^{210}Bi decays to ^{210}Po by emitting a 1.17 MeV β-particle with 5.0 days half-life and ^{210}Po decays to stable ^{206}Pb by the emission of 5.3 MeV α-particle and weak γ radiation with a half-life of 140 days. The γ radiation is counted in a Geiger-Müller tube with much less efficiency than β radiation and since the window ($\simeq$30 mg/cm^2) absorbs the α radiation of ^{206}Po and the β radiation from ^{210}Pb, only the ^{210}Bi β radiation will be detected from a mixture of the three isotopes.

In order to be sure that all the activity which is measured, comes from atoms which diffused as Pb, it is then necessary to delay the counting by at least 30 days after sectioning the rods. In this way the activity from atoms which diffused as Bismuth, is practically absent.

3. – Results.

The results of self diffusion of Indium and Lead in the In — 0.5% Pb alloy are given in Table I and II.

(*) From Johnson, Matthey and Co.

(**) Supplied by A.E.R.E., Harwell (England).

([2]) G. Careri, A. Paoletti and F. L. Salvetti: *Nuovo Cimento*, **11**, 399 (1954).

([3]) G. Careri, A. Paoletti and M. Vicentini: *Nuovo Cimento*, **10**, 1088 (1958).

3853

TABLE I. – *Self diffusion in* In – 0.5% Pb (*Tracer* ^{114}In).

Run	T (°C)	$10^3/T$ (°K^{-1})	Time	D 10^5 (cm^2/s)
		$\Phi = 1.60$ mm		
23 *a*	249	1.915	$1^h\ 57^m\ 00^s$	2.76 ± 0.27
23 *b*	249	1.915	$1^h\ 57^m\ 00^s$	2.60 ± 0.12
24 *a*	274	1.828	$3^h\ 53^m\ 00^s$	2.95 ± 0.14
24 *b*	274	1.828	$3^h\ 53^m\ 00^s$	3.03 ± 0.14
25 *a*	394	1.498	$2^h\ 40^m\ 00^s$	4.34 ± 0.17
25 *b*	394	1.498	$2^h\ 40^m\ 00^s$	4.31 ± 0.18
26 *a*	407	1.471	$3^h\ 57^m\ 00^s$	4.33 ± 0.17
26 *b*	407	1.471	$3^h\ 57^m\ 00^s$	4.35 ± 0.17
28 *a*	544	1.224	$2^h\ 57^m\ 30^s$	6.46 ± 0.27
28 *b*	544	1.224	$2^h\ 57^m\ 30^s$	6.43 ± 0.26
		$\Phi = 0.83$ mm		
23 *c*	249	1.915	$1^h\ 57^m\ 00^s$	2.76 ± 0.16
23 *d*	249	1.915	$1^h\ 57^m\ 00^s$	2.68 ± 0.16
24 *c*	274	1.828	$3^h\ 53^m\ 00^s$	2.93 ± 0.14
24 *d*	274	1.828	$3^h\ 53^m\ 00^s$	2.87 ± 0.16
25 *c*	394	1.498	$2^h\ 40^m\ 00^s$	4.28 ± 0.21
25 *d*	394	1.498	$2^h\ 40^m\ 00^s$	4.10 ± 0.18
26 *c*	407	1.471	$3^h\ 57^m\ 00^s$	4.44 ± 0.20
26 *d*	407	1.471	$3^h\ 57^m\ 00^s$	4.63 ± 0.19
27 *c*	335	1.643	$4^h\ 20^m\ 30^s$	3.72 ± 0.17
27 *d*	335	1.643	$4^h\ 20^m\ 30^s$	3.75 ± 0.18
28 *c*	544	1.224	$2^h\ 57^m\ 30^s$	6.10 ± 0.27

3554

TABLE II. – *Self-diffusion in* In – 0.5% Pb (*Tracer* RaD)

Run	T(°C)	$10^3/T$ (°K)	Time	$D\ 10^5$ (cm²/s)
		$\Phi = 1.60$ mm		
95 *a*	487	1.315	$3^h\ 17^m\ 00^s$	4.75 ± 0.23
95 *b*	487	1.315	$3^h\ 17^m\ 00^s$	4.75 ± 0.25
97	299	1.450	$5^h\ 43^m\ 00^s$	3.04 ± 0.13
98 *a*	404	1.478	$4^h\ 52^m\ 00^s$	3.97 ± 0.17
98 *b*	404	1.478	$4^h\ 52^m\ 00^s$	4.15 ± 0.17
106 *a*	388	1.512	$4^h\ 21^m\ 00^s$	3.91 ± 0.15
106 *b*	388	1.512	$4^h\ 21^m\ 00^s$	3.79 ± 0.16
110	349	1.608	$5^h\ 06^m\ 30^s$	3.42 ± 0.14
		$\Phi = 0.83$ mm		
94 *c*	290	1.725	$6^h\ 22^m\ 30^s$	2.73 ± 0.12
95 *c*	487	1.315	$3^h\ 17^m\ 00^s$	4.51 ± 0 18
95 *d*	487	1.315	$3^h\ 17^m\ 00^s$	4.55 ± 0.20
100	252	1.905	$6^h\ 28^m\ 30^s$	2.12 ± 0.10
105	554	1.209	$3^h\ 16^m\ 00^s$	5.29 ± 0.25
106 *c*	388	1.512	$4^h\ 21^m\ 00^s$	3.66 ± 0.16
106 *d*	388	1.512	$4^h\ 21^m\ 00^s$	3.60 ± 0.17
107	218	2.040	$7^h\ 07^m\ 00^s$	1.92 ± 0.10
110	349	1.608	$5^h\ 06^m\ 30^s$	3.11 ± 0.15
127 *c*	335	1.644	$2^h\ 34^m\ 30^s$	3.14 ± 0.19
127 *d*	335	1.644	$2^h\ 34^m\ 30^s$	3.17 ± 0.14

TABLE III. – *Experimental* D_0 *and* Q.

Alloy	Tracer	Φ (mm)	$D_0 10^5$ (cm²/s)	Q (cal/mole)
In – 0.5 % Pb	^{114}In	1.6	26.4 ± 1.8	2 373 ± 83
In – 0.5 % Pb	^{114}In	0.8	26.4 ± 1.8	2 372 ± 83
In – 0.5 % Pb	RaD	1.6	21.0 ± 1.5	2 220 ± 311
In – 0.5 % Pb	RaD	0.8	23.2 ± 2.4	2 435 ± 127
In – 1.5 % Pb	^{113}In	0.8	30.4 ± 2.6	2 550 ± 350

3655

TABLE IV. *Self-diffusion in* In – 1.5% Pb (*Tracer* ^{114}In).

Run	T (°C)	$10^3/T$ (°K)	Time	D 10^5 (cm^2/s)
		Φ = 0.83 mm		
60 *C*	303	1.738	$2^h\ 04^m\ 00^s$	3.27 ± 0.18
60 *D*	303	1.738	$2^h\ 04^m\ 00^s$	3.38 ± 0.15
61 *C*	381	1.530	$2^h\ 34^m\ 30^s$	4.53 ± 0.21
61 *D*	381	1.530	$2^h\ 34^m\ 30^s$	4.28 ± 0.20
62 *C*	400	1.488	$3^h\ 59^m\ 00^s$	4.74 ± 0.22
62 *D*	400	1.488	$3^h\ 59^m\ 00^s$	4.44 ± 0.22
63 *C*	500	1.294	$2^h\ 35^m\ 00^s$	5.95 ± 0.31
63 *D*	500	1.294	$2^h\ 35^m\ 00^s$	5.83 ± 0.28

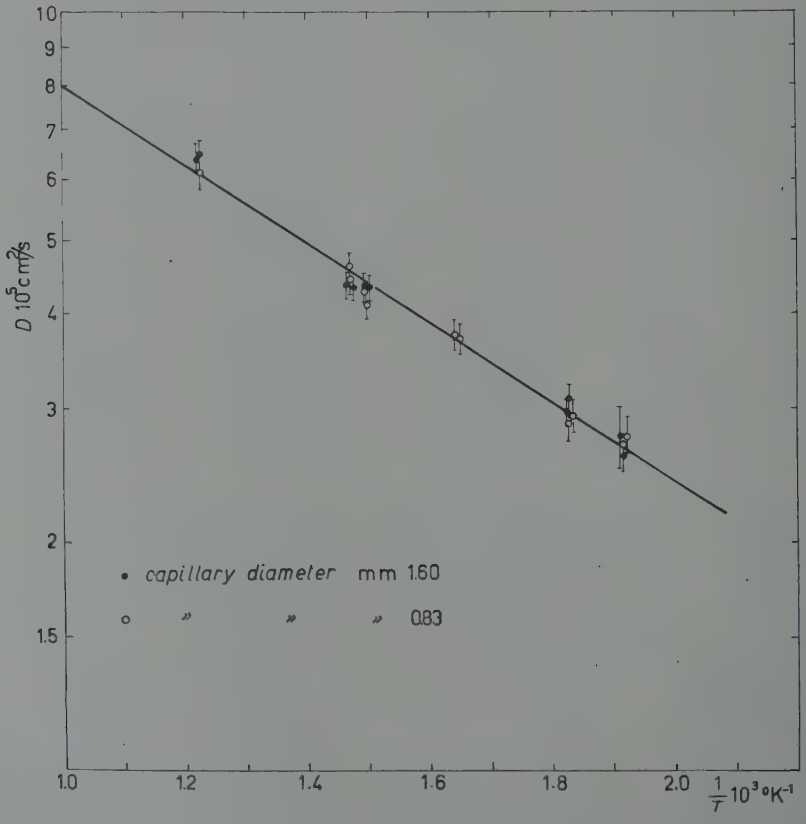

Fig. 1 – Self-diffusion of In in In – 0.5% Pb alloy.

In Fig. 1 and 2, $\ln D$ is plotted as a function of $1/T$ respectively for Indium and Lead: in both cases the Arrhenius equation

$$D = D_0 \exp[-Q/RT]$$

is fairly well verified. The experimental D_0 and Q values are given in Table III.

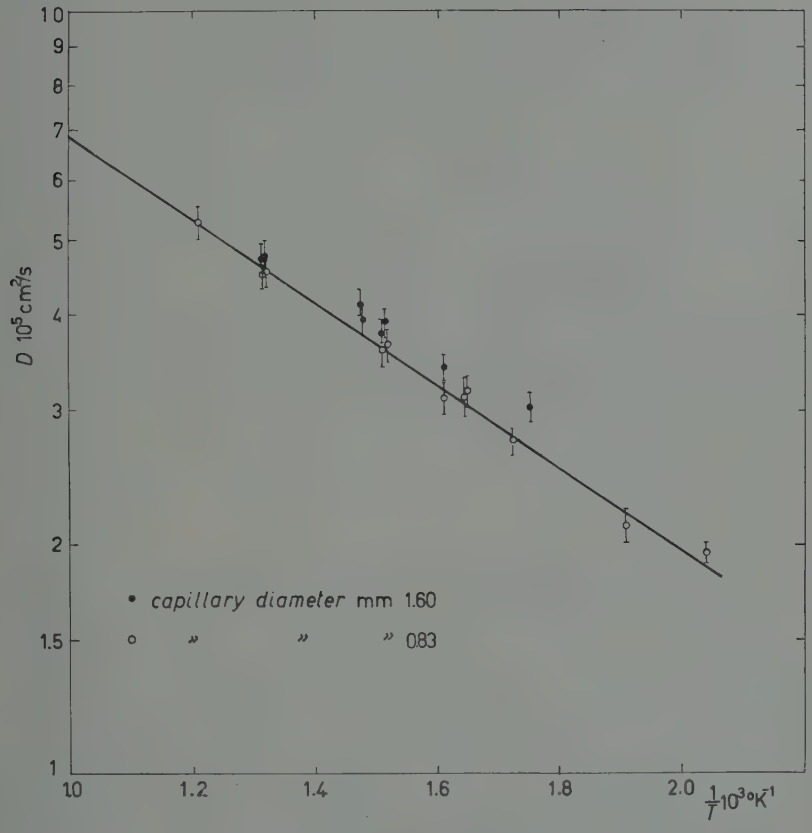

Fig. 2 – Self-diffusion of Lead in In – 0.5% Pb alloy.

The experimental results for the self diffusion of Indium in the alloy In–1.5% Pb are given in Table IV and Fig. 3; also in this case the Arrhenius equation is verified with D_0 and Q values given in Table III.

3657

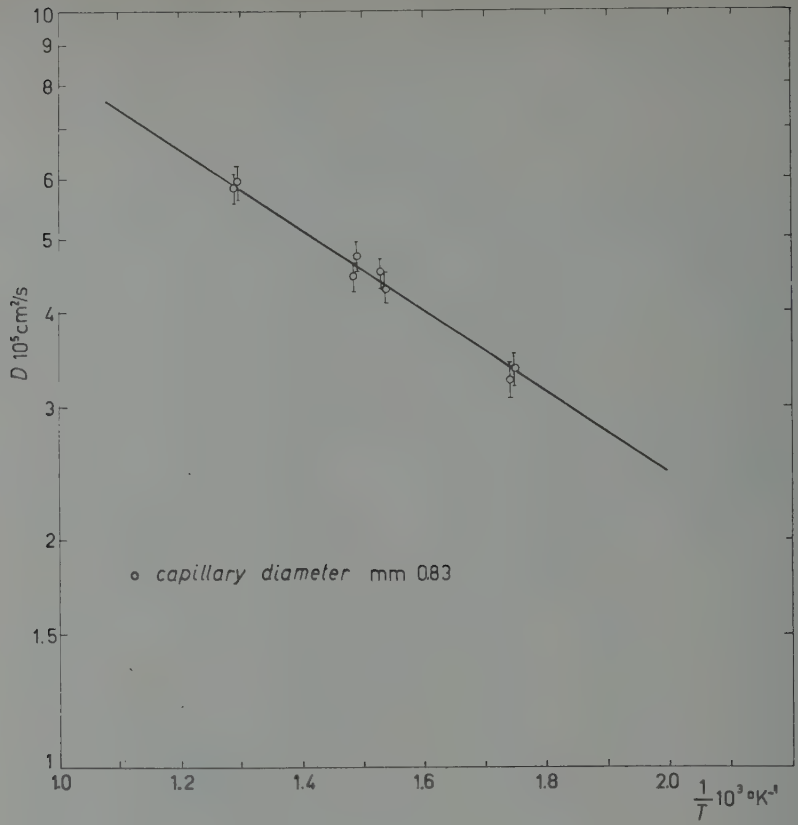

Fig. 3 – Self-diffusion of In in In – 1.5% Pb alloy.

4 – Discussion.

In the In–0.5% Pb diffusion measurements with RaD as tracer, a dependence of the self diffusion coefficient upon the diameter of the mullite capillary has been found. This effect is not so large as was found in pure Indium self diffusion but still detectable. It is anyway useful to emphasize that in these experiments like in pure Indium self diffusion, the « wall effect » doesn't affect within the experimental errors the activation energy value.

By comparing the results obtained for Indium self diffusion, with those for Lead self diffusion in the alloy In–0.5% Pb, we notice in both cases a small change in the diffusity in respect to the pure Indium self diffusion, but the activation energies are equal within the experimental errors, and very close to the activation energy found for pure Indium ([3]). The same behaviour is found in the In–1.5% Pb alloy. In these experiments the diffusivity shows small

8593

deviations from the data for the In–0.5% Pb alloy but the activation energy stays constant.

If we recall that the activation energy for the pure Lead self-diffusion seems to be much higher ([4]), our results give an indication that the energy barrier in a liquid alloy would not be only due to the atoms interested in the diffusion process, but would be determined by a much larger amount of atoms.

The introduction of small impurity concentrations in a liquid metal would then affect only slightly and by the same amount the energy barrier for both the solvent and solute atoms.

It would be interesting at this point, to compare the behaviour of the In-Pb alloy with other alloys in liquid phase. As far we know diffusion coefficients have been measured only for the Fe-C system ([5]) and for Bi and Pb in a Bi-0.255 atomic pct Pb alloy ([6]).

Unfortunately, it is difficult to put any comparison on a definite basis (*).

Other diffusion experiments in liquid phase with different tracers have been performed in liquid Nitrogen ([7]), and in Carbonium tetrachloride with the capillary technique ([8,9]).

In liquid Nitrogen the same activation energy has been found for diffusion of Tritium and Argon and for different concentrations of the tracer in the bath.

In Carbonium tetrachloride, self diffusion coefficients of CCl_4 and the diffusion coefficient of small amounts of I_2 have been measured. Also in this case the experimental activation energies are equal for both tracers.

([4]) S. J. ROTHMAN and L. D. HALL: *Jonrn. of Metals*, **8**, 199 (1956).

([5]) LING YANG, M. T. SIMNAD and G. DERGE: *Journ. of Metals*, **8**, 1577 (1956).

([6]) S. J. ROTHMAN and L. D. HALL: *Journ. of Metals*, **8**, 1580 (1956).

(*) In the experiments on the Fe-C system, the diffusion coefficient of C in Fe-C has not been measured and also the self diffusion coefficient of the pure components are unknown in the liquid phase. For diffusion of Fe in Fe-C, the measurements were taken in the temperature range (1513 ÷ 1673) °K and for 2.5 weight % and 4.6% concentration in C. The activation energy seems to be independent of the concentration but the reproducibility of the experimental results is very poor.

In the Bi-Pb alloy, investigated in the temperature range (554 ÷ 687) °K the activation energy values are very close for diffusing Bi and Pb atoms.

This fact would then support our results, but also in these experiments the data reproducibility is very poor, and it is difficult to say to what extent, our hypothesis of a contribution of a large amount of atoms to the energy barrier in liquid metals diffusion is strenghtened.

([7]) G. CINI-CASTAGNOLI, G. PIZZELLA and F. P. RICCI: *Nuovo Cimento*, **10**, 300 (1958).

([8]) E. W. HAGCOCK, B. J. ALDER and J. H. HILDEBRAND: *Journ. Chem. Phys.*, **21**, 1601 (1953).

([9]) H. WATTS, B. J. ALDER and J. H. HILDEBRAND: *Journ. Chem. Phys.*, **23**, 659 (1955).

3759

It is then important to emphasize that the same behaviour is shown by the activation energy in liquid metals, in simple liquids and in organic liquids.

Also very interesting is the comparison with the diffusion experiments in solid alloys, mainly if one wants to describe the diffusion in liquids with a quasi crystalline model.

Many experiments have been performed for self diffusion of impurities in different solid alloys ([10]). However the most significant results have been obtained for some Ag alloys where, like in our experiments, the self diffusion coefficient for both solute and solvent atoms has been measured ([10-14]).

The qualitative behaviour of diffusing atoms is similar to that in liquid phase, but from a quantitative point of view it must be pointed out that the variation of the diffusivity with the impurity concentration, is usually larger in the solid phase for both solute and solvent atoms.

Attempts to explain this big variation in solids have been made by OVERHAUSER ([15]), LAZARUS ([16]) and REISS ([17]). Besides decorrelation effects which could not explain the whole large amount of the change in D with the impurity concentration, the hypothesis has been made that the presence of solute provides a change in the energy barrier for the motion of the solvent atoms in its immediate vicinity. We want to point out here that this latter hypotesis is difficult to understand since by looking at the dependence of the diffusion coefficients upon the temperature, one realizes that the variation of D with the impurity concentration is not associated to any change in the activation energy which, within the experimental errors, stays constant in the range of impurity concentrations which has been investigated.

HART *et al.* ([18]) on the basis of a « via vacancy » diffusion assume that the diffusivity change with the concentration in their measurements, is due to a variation in the vacancy concentration and/or the atom vacancy exchange frequency. But these parameters, only in the nearest neighbour shell surrounding solute atoms have in the alloys a different value than the corresponding quantities for pure metals. The agreement between theory and experiments was satisfactory in the Ag-Pb and Ag-Tl systems.

([10]) D. LAZARUS: *Tracer Studies of Intermetallic Diffusions*, in *Second Int. Conf. Geneva*, A/Conf. 15/P/834 (1958).

([11]) R. E. HOFFMAN and D. TURNBULL: *Journ. Appl. Phys.*, **23**, 1409 (1952).

([12]) R. E. HOFFMAN, D. TURNBULL and E. W. HART: *Acta Metall.*, **3**, 417 (1955).

([13]) R. E. HOFFMAN: *Acta Metall.*, **6**, 95 (1958).

([14]) N. H. NACHTRIEB, J. PETIT and J. WEIHREMBERG: *Journ. Chem. Phys.*, **26**, 106 (1957).

([15]) A. W. OVERHAUSER: *Phys. Rev.*, **90**, 393 (1953).

([16]) D. LAZARUS: *Phys. Rev.*, **93**, 973 (1954).

([17]) H. REISS: *Phys. Rev.*, **113**, 1445 (1959).

([18]) E. W. HART, R. E. HOFFMAN and D. TURNBULL: *Acta Metall.*, **5**, 74 (1957).

3663

5. – Conclusion.

Our results in liquids, because of the independence of the activation energy from the tracer indicate a long range contribution of the atoms to the energy barrier for the diffusion. From the other side the constancy of the activation energy at different concentrations of the impurity, recalls the results obtained in solid alloys diffusion experiments. In other words our measurements on liquid alloys would confirm the possibility to describe the diffusion in liquid with a quasi crystalline model [19]. The absence of a long range order makes however any quantitative comparison with the solid phase experiments, very difficult.

* * *

Thanks are due to Professor CARERI for suggesting the research and stimulating discussions.

[19] G. CARERI and A. PAOLETTI: *Nuovo Cimento*, **2**, 574 (1955).

RIASSUNTO

Si è misurato il coefficiente di autodiffusione nelle leghe liquide In-0.5% Pb ed In-1.5% Pb, in un ampio intervallo di temperatura e facendo uso di ^{114}In e RaD come traccianti. I risultati mostrano che entro gli errori sperimentali, l'energia di attivazione è indipendente dal tracciante. Ciò è stato interpretato come un'indicazione di un contributo a lungo raggio degli atomi alla barriera d'energia per la diffusione.

IL NUOVO CIMENTO Vol. XIV, N. 4 16 Novembre 1959

Non-Local Effects in Electron-Electron and Electron-Positron Scattering.

G. Furlan and G. Peressutti

Istituto Nazionale di Fisica Nucleare - Sottosezione di Trieste
Istituto di Fisica dell'Università - Trieste

(ricevuto il 2 Agosto 1959)

Summary. — We calculate the effect of a modification of the Coulomb law at small distances, on the cross sections for electron-electron and electron-positron scattering. A detailed analysis shows that the Møller cross section is less sensitive to non-local effects than the Bhabha cross section.

1. – It has been recently pointed out (1) that the high energies now or within a short time possible, enable us to investigate the limits of validity of Q.E.D at small distances by merely electrodynamic processes. The advantage that such methods offer, as compared with the ones generally in use, is that they obviate the use of nucleons or nuclei as sources of an external field. In so doing it is possible to attribute any deviation from a point interaction to a breakdown of Q.E.D., without dealing with questions of nucleon structure.

To this end we have considered two typical electrodynamic processes *i.e.* electron-electron scattering (Møller) and electron-positron scattering (Bhabha). Electron-electron interaction is that which for the lack of valid competitive processes as well as for its characteristic simplicity, should best lend itself to a study of Q.E.D. In fact, as early as 1953 Salecker (2) was studying the Møller cross-section dependence on possible non-local effects. He took the latter into account by modifying photon propagators according to Feyn-

(1) G. Andreassi, P. Budini and I. Reina: *Nuovo Cimento*, **12**, 488 (1959).
(2) H. Salecker: *Zeits. Naturfor.*, **8***a*, 16 (1953).

3662

man's suggestion *i.e.*

$$\frac{1}{q^2} \to \int_0^\infty \left(\frac{1}{q^2} - \frac{1}{q^2 + \lambda^2} \right) G(\lambda)\, \mathrm{d}\lambda ,$$

where G is a quite general structure function.

Subsequently DRELL [3] showed Møller scattering as the ideal process for an analysis at small distances. He emphasized, however, that the small rest mass of the electron made it difficult, but at very high energies, to achieve large momentum transfers.

Putting

$$\frac{1}{q^2} \to \frac{1}{q^2} - \frac{1}{q^2 + \Lambda^2} \; (*) ,$$

it can be seen [3] that a correction less than 10% requires, for Møller scattering, larger energies than 8 GeV with a limit for the validity of Q.E.D. $1/\Lambda \leqslant 0.5$ F.

In fact even such an estimate is unreal. The true difficulty is, besides in the high energies to be used, mainly in the fact that experiments performed on elastic electron-proton scattering seem to indicate that $1/\Lambda < \frac{1}{3} \cdot 10^{-3}$ cm.

Such a limitation for $1/\Lambda$ further increases the energies to be employed in order that electron-electron scattering may allow the lowering of the present limits of validity of Q.E.D.

Nevertheless, as reported by PANOFSKY [4], there are many possibilities, from an experimental viewpoint, of reaching distances even shorter than the present value of the cut-off. According to the methods suggested by the Stanford and Princeton groups, energies from 10 to even 100 GeV in the laboratory system could be reached for Møller scattering. That would allow length measurements up to 0.02 F with a 1% accuracy.

Since we want, however, to confine ourselves, at present, to less pretentious and more immediately feasible projects, we shall point out that a process substantially analogous to the above one, *i.e.* Bhabha scattering, can give more suitable means for an analysis at small distances. Bhabha scattering is no doubt more sensitive than Møller scattering for a possible breakdown of Q.E.D. This greater sensitiveness is dependent on the same structure of electron-positron interaction; the scattering may occur, either directly, or through the

---

[3] S. D. DRELL: *Ann. Phys.*, **4**, 75 (1958).

[4] W. K. H. PANOFSKY: *Ann. Int. Conf. CERN* (Genève, 1958).

(*) This modification of photon propagator is equivalent to a different form of the Coulomb law at small distances according to

$$\frac{1}{r} \to \frac{1}{r} - \frac{\exp[-\Lambda r]}{r} .$$

3663

annihilation and subsequent re-emission of the electron-positron pairs, which effects practically replace the exchange effect in electron-electron scattering. Moreover, the matrix element for the exchange process is, in Møller scattering, practically negligible compared to lhe direct process. On the contrary, in Bhabha scattering, matrix elements for direct and annihilation processes are of the same order: therefore both form factors are important.

Furthermore for the Møller scattering we have a quite special situation: the cross-section is sensitive to possible non-local effects only at very small angles in the laboratory system.

2. – Using the standard techniques we have for the two non-local differential cross-sections in the laboratory system:

Møller:

$$(1)\qquad (\mathrm{d}\sigma)_{NL} = \frac{16 r_0^2 \cos\theta\,\mathrm{d}\Omega}{[2 + (\gamma-1)\sin^2\theta]^2}\,\frac{1}{(\gamma-1)^2}\left\{\frac{A F_1^2}{(1+x)^2} + \frac{B F_2^2}{(1-x)^2} + \frac{2C F_1 F_2}{1-x^2}\right\},$$

with

$$(2)\qquad \begin{cases} A = \frac{1}{2}\{\gamma^2 + 1 + \frac{1}{4}(\gamma-1)^2(1+x^2) - \frac{1}{2}x(\gamma-1)(\gamma+3)\}, \\ B = \frac{1}{2}\{\gamma^2 + 1 + \frac{1}{4}(\gamma-1)^2(1+x^2) + \frac{1}{2}x(\gamma-1)(\gamma+3)\}, \\ C = \frac{1}{2}\gamma(\gamma-2), \\ F_1 = \dfrac{\Lambda^2}{\Lambda^2 + m^2(\gamma-1)(1+x)}, \qquad F_2 = \dfrac{\Lambda^2}{\Lambda^2 + m^2(\gamma-1)(1-x)}, \end{cases}$$

F_1 and F_2 are the cut-off functions which according to Drell modify the propagator of photon, as previously indicated.

Moreover

$$(3)\qquad x = \frac{2 - (\gamma+3)\sin^2\theta}{2 + (\gamma-1)\sin^2\theta}.$$

Here θ represents the angle between the two following directions: direction of incident particle and recoil direction of target particle. For a more effective experimental characterization of θ and its relation to the real scattering angle see Appendix.

Bhabha:

$$(4)\qquad (\mathrm{d}\sigma)_{NL} = \frac{16 r_0^2 \cos\theta\,\mathrm{d}\Omega}{[2 + (\gamma-1)\sin^2\theta]^2} \cdot \left\{\frac{A' G_1^2}{(1-x)^2(\gamma-1)^2} + \frac{B' G_2^2}{4(\gamma+1)^2} + \frac{C' G_1 G_2}{(1-x)(\gamma^2-1)}\right\},$$

$$A' = \tfrac{1}{2}\{\gamma^2 + 1 + \tfrac{1}{4}(\gamma-1)^2(1+x^2) + \tfrac{1}{2}x(\gamma-1)(\gamma+3)\},$$

$$B' = \tfrac{1}{4}x^2(\gamma-1)^2 + \tfrac{1}{4}(\gamma+1)(\gamma+5),$$

$$C' = -\tfrac{1}{2}\{\tfrac{1}{4}x^2(\gamma-1)^2 + \tfrac{1}{2}x(\gamma-1)(\gamma+3) + \tfrac{1}{4}(\gamma+1)(\gamma+5)\}.$$

3664

x is again given by expression (3) but here θ is the actual scattering angle, that is, the angle between the incident positron and the scattered positron.

The form factors G_1 and G_2 are now:

$$(5) \qquad G_1 = \frac{\Lambda^2}{\Lambda^2 + m^2(\gamma - 1)(1 - x)}, \quad G_2 = \frac{\Lambda^2}{\Lambda^2 + 2m^2(\gamma + 1)}.$$

(In calculating form factors use had been made of

$$G(q) = \frac{\Lambda^2}{\Lambda^2 + |q^2|},$$

which prevents G_2 from reaching values greater than unity).

The second form factor is derived from the term which in the electron-positron scattering represents the annihilation of the two particles. It is particularly favourable, because it is independent of x (and of θ) and related only to the energy of the incident positron. As the latter increases G_2 differs considerably from unity and gives rise to a strong non-local effect.

3. – Taking now for $1/\Lambda$ the values 0.3, 0.5 and 0.7 F and for the energies the values 1 GeV and 10 GeV we obtain for $(d\sigma)_{NL}/(d\sigma)_L$ the graphs of Fig. 1, 2 and the values of Table I.

TABLE I.

$(d\sigma)_{NL}/(d\sigma)_L$	$1/\Lambda = 0.3$ F		$1/\Lambda = 0.5$ F	
$\sin\theta$ \ E	1 GeV	10 GeV	1 GeV	10 GeV
0	1	1	1	1
$x = 0$	0.9976	0.9763	0.9959	0.9600
0.1	0.9994	0.9993	0.9989	0.9988
0.2	0.9998	0.9997	0.9997	0.9997
0.3	0.9999	0.9999	0.9998	0.9998
0.4	0.9999	0.9999	0.9999	0.9999
0.5	0.9999	0.9999	0.9999	0.9999
0.6	0.9999	0.9999	0.9999	0.9999
0.7	1	1	0.9999	0.9999
0.8	1	1	1	1
0.9	1	1	1	1
1	1	1	1	1

According to the above considerations, curves relative to $1/\Lambda = 0.5$ F and 0.7 F should have a purely demonstrative value. It is however worth-while noting that for Bhabha scattering at 10 GeV with $1/\Lambda = 0.7$ F, non-local

effects are larger than 20% (*). Just to confine ourselves to the less favourable case, with a cut-off parameter $1/\Lambda = 0.3$ F at 1 GeV there is practically no effect either for electron-positron scattering or for electron-electron scattering. At 10 GeV, for Bhabha scattering this effect is of the order of 5% while it is still practically negligible for Møller scattering ($< 1\%$), but at small θ where we have a $\lesssim 3\%$ effect.

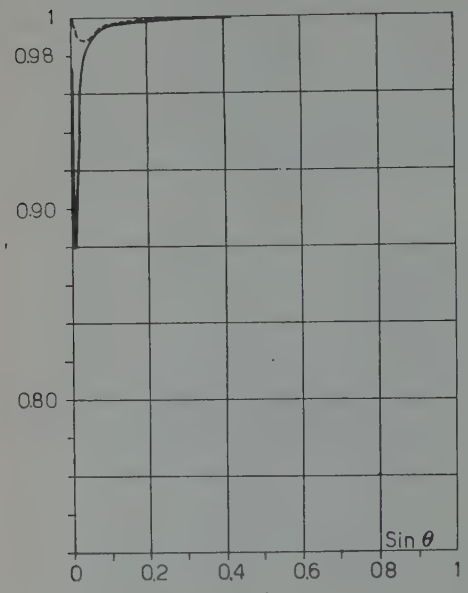

Fig. 1. – Møller scattering. $(d\sigma)_{NL}/(d\sigma)_L$ in L.S. as a function of the angle θ for $E = 1$ GeV (dotted curve) and $E = 10$ GeV (solid curve) and $1/\Lambda = 0.7$ F. Curves relative to the other two values for $1/\Lambda$ are not drawn as they are practically indistinguishable. These values of $(d\sigma)_{NL}/(d\sigma)_L$ are reported in Table I.

This special situation for Møller scattering can easily be explained with a qualitative investigation of the cross-section (1). At $\theta = 0$, $x = 1$ the prevailing term in the brackets is the one by which F_2^2 is multiplied, so that $(d\sigma)_{NL}/(d\sigma)_L = F_2^2|_{x=1} = 1$. At θ such that $x = 0$ $(\sin^2\theta = 2/(\gamma+3))$ we have $F_1 = F_2 = \Lambda^2(\Lambda^2 + m^2(\gamma - 1)) = F'$, therefore $(d\sigma)_{NL}/(d\sigma)_L = F'^2$. For θ values where $\sin^2\theta > 2/(\gamma+3)$, x suddenly turns out to be negative and very near to -1 and this initially causes terms in F_1^2 and $F_1 F_2$ to prevail. As, however, the angle increases (practically for $\sin\theta \geqslant 0.2$) the only really important term is the one in F_1^2 and therefore $(d\sigma)_{NL}/(d\sigma)^L \sim F_1^2$, which is of the order of unity. These considerations emphasize the smallness of non local-effects for Møller scattering even at 10 GeV, but for small θ. This result completes that foreseen by DRELL [3]. DRELL's considerations were in fact confined to the special case that the momentum transfer was the same in direct scattering as well in exchange scattering so that there was a sole form factor to be taken into account. This in our notations occurs only for $x = 0$, *i.e.* when the ratio $(d\sigma)_{NL}/(d\sigma)_L$ presents a maximum non-local effetc. But when $x \neq 0$ the situation is a quite different one: if we take into consideration all values of θ, we can say in general that when the momentum transfer is a maximum

(*) This and other values for $1/\Lambda$ larger than the limit prescribed by electron-proton experiments would be plausible if we admit in the above experiment an interference between the effects of nucleon structure and a breakdown of Q.E.D.

3656

and the corresponding form factor a minimum, the latter multiplies in the cross-section a negligible term with respect to the other terms. Consequently the Møller cross-section is insensitive to a breakdown of Q.E.F. in every case different from the particularly favourable one considered above ($x = 0$).

On the contrary the Bhabha scattering presents a greater effect than the Møller scattering and, owing to a particular compensation of various terms, $(d\sigma)_{NL}/(d\sigma)_L$ is even independent of the angle. A reduction of the limit of validity of Q.E.D. would thus be possible using 10 GeV positrons. Eventual difficulties are not in obtaining 10 GeV positrons but mainly in the dimensions of the Bhabha cross-section at such high energies. Angle measurements from 6° to 30° at 10 GeV would entail the measurement of cross-sections from $1.2 \cdot 10^{-29}$ to $0.2 \cdot 10^{-31}$ cm². The decreased electron-positron cross-section at 10 GeV is mainly due to the occurrence of a valid competitive process, the electron-positron pair annihilation with emission of 2 (or more) γ.

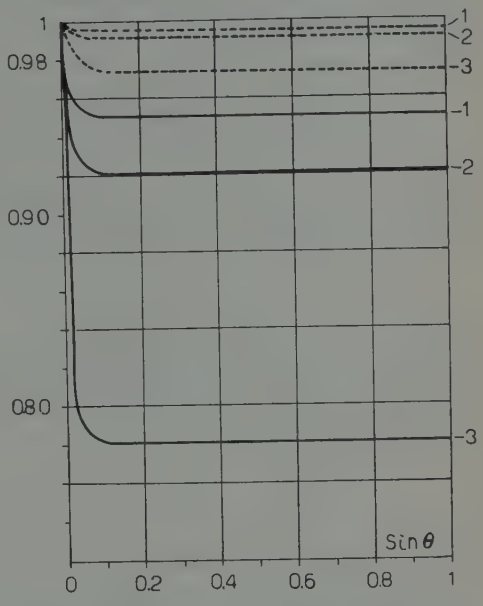

Fig. 2. – Bhabha scattering. $(d\sigma)_{NL}/(d\sigma)_L$ in S.L. as a function of the scattering angle θ for $E = 1$ GeV (dotted curve) and $E = 10$ GeV (solid curve) and $1/\Lambda = 0.3$, 0.5, 0.7 F (curves 1), 2), 3)).

4. – Different modifications of the Coulomb law at small distances have been proposed by CLEMENTEL and VILLI (5) and HOFSTADTER (6) for studying the electron-proton interaction. In this case, in accordance with the usual method, the nucleon charge distribution can be worked out from the given form of the potential. In general we can assume

$$\frac{1}{r} \to \frac{1}{r} - \eta \frac{\exp[-\Lambda r]}{r} - \xi \exp[-\Lambda r],$$

that includes the suggestions of 1) DRELL ($\eta = 1$, $\xi = 0$), 2) CLEMENTEL and VILLI ($\eta > 1$, $\xi = 0$); 3) HOFSTADTER ($\eta = 1$, $\xi = \Lambda/2$).

(5) E. CLEMENTEL and C. VILLI: *Nuovo Cimento*, **4**, 1207 (1956).

(6) R. HOFSTADTER, F. BUMILLER and M. R. YEARIAN: *Rev. Mod. Phys.*, **30**, 482 (1958).

3667

We have used model (1) for former numerical computations. In model (2) the corresponding form of photon propagator is

$$\frac{1}{q^2} \to \frac{1}{q^2} - \frac{\eta}{\Lambda^2 + q^2} = \frac{1}{q^2} \frac{\Lambda^2 + q^2(1-\eta)}{\Lambda^2 + q^2} .$$

Apparently the introduction of the new parameter $\eta > 1$ should further reduce the form factor causing a greater non-local effect. Thus for Bhabha scattering, the most favourable term, corresponding to annihilation, becomes:

$$G_2'(q) = \frac{\Lambda^2 - (\eta - 1)2m^2(\gamma + 1)}{\Lambda^2 + 2m^2(\gamma + 1)} .$$

But the examination of proton-electron data requires a new limitation on Λ. In fact in this case

$$\frac{\sqrt{\eta}}{\Lambda} < \frac{1}{3} \cdot 10^{-13} \text{ cm} ,$$

and therefore the form factor to be compared with the one previously used is actually

$$G_2'(q) = \frac{\eta\Lambda^2 - (\eta - 1)2m^2(\gamma + 1)}{\eta\Lambda^2 + 2m^2(\gamma + 1)} .$$

It can then be easily verified that at 10 GeV with $1/\Lambda = 0.3$ F and for instance $\eta = 1.5$ both G_2 and G_2' have about the same value $\simeq 0.976$.

Quite analogous considerations for model 3) show that

$$\frac{1}{q^2} \to \frac{1}{q^2} \frac{\Lambda^4}{(\Lambda^2 + q^2)^2} ,$$

where, on the other hand:

$$\frac{\sqrt{3}}{\Lambda} < \frac{1}{3} \cdot 10^{-13} \text{ cm} .$$

So we have for the form factor:

$$G_2''(q) = \frac{(3\Lambda^2)^2}{[3\Lambda^2 + 2m^2(\gamma + 1)]^2} ,$$

that for $1/\Lambda = 0.3$ F at 10 GeV is $\simeq 0.98$.

Consequently the use of a modified form of the Coulomb law, other than the more simple one as proposed by DRELL, would not lead to results which allow a distinction to be made between the various models employed. On the

3668

contrary we must realize that, if a Q.E.D. breakdown at high energies is to be found, we get the same situation occurring for electron-proton scattering, where different proton charge distributions fit equally well experimental data. Obviously further introduction of new parameters, by increasing the model flexibility would always allow the description of the experimental situation in a satisfactory way.

5. – An examination of Møller and Bhabha scattering shows that, for the above considerations, the latter process is more convenient than the former. This ensures that the use of high energy positrons can be an effective mean also for an analysis of Q.E.D. at small distances. Obviously the extent of the non-local effect on electron-positron scattering depends critically on the value of the cut-off parameter.

Radiative corrections to the cross-sections can be calculated by standard methods and will not alter the above results. This will be discussed in a subsequent paper.

* * *

We are indebted to Prof. BUDINI for his kind interest and illuminating criticism and to Dr. REINA for her help in calculations.

APPENDIX

Let us consider the collision of two identical particles of momenta $\boldsymbol{p}_1$ and $\boldsymbol{p}_2$, $\boldsymbol{p}_1'$ and $\boldsymbol{p}_2'$ before and after collision respectively. In the laboratory system:

$$\boldsymbol{p}_1 = 0\,, \qquad \theta = \widehat{\boldsymbol{p}_2\boldsymbol{p}_1'}, \qquad \varphi = \widehat{\boldsymbol{p}_2\boldsymbol{p}_2'}\,,$$

as shown in the figure; where φ is by definition the scattering angle and θ is the angle we have used in the text.

They are related by the formula

$$\cos\varphi = \frac{(\gamma+1)\sin\theta}{\sqrt{(\gamma+1)^2\sin^2\theta + 4\cos^2\theta}}\,.$$

Because the incident particle and the target particle are identical it is pratically impossible to distinguish between the two angles. Therefore, if we take into account conservation theorems, we see that the energy of the incident particle after the collision (ε_2') is an increasing (decreasing) function of $\theta(\varphi)$, while the energy of the target particle after the collision (ε_1') is a decreasing function of θ. Energy measurements would give the desired distinction. In a similar way we may relate x to the relative energy transfer during the collision w

$$x = 1 - 2w\,, \qquad w = \frac{\varepsilon_1' - m}{\varepsilon_2 - m}\,,$$

and discuss the cross section as a function of w instead of the angular distribution. This method has been, for instance, used by ASHKIN *et al.* [7] to verify experimentally Møller and Bhabha cross sections at 1 MeV.

It is easily seen that when $x = 0$, $\varepsilon_1' = \varepsilon_2' = (\varepsilon_2 + m)/2$. So, the maximum non-local effect corresponds to a situation where scattered electron and recoil lectron leave the reaction with equal energies.

---

[7] A. ASHKIN, L. A. PAGE and W. M. WOODWARD: *Phys. Rev.*, **94**, 357 (1954).

RIASSUNTO

Si calcola l'effetto di una modificazione della legge di Coulomb alle piccole distanze, sulle sezioni d'urto per scattering di Møller e Bhabha. Un esame dettagliato mostra come la sezione d'urto di Møller sia meno sensibile che non quella di Bhabha a possibili effetti non locali.

3670

IL NUOVO CIMENTO · Vol. XIV, N. 4 · 16 Novembre 1959

Note on the K^--Deuteron Collision.

S. Minami

Department of Physics, Osaka City University - Osaka

(ricevuto il 3 Agosto 1959)

Summary. — The process of $K^- + d \to \mathcal{N} + \mathcal{N} + \bar{K}$ is investigated from the kinematical point of view under the assumption that there exists an excited state Σ^* for the K^--$\mathcal{N}$ system. It is pointed out that the reaction $K^- + d \to n + n + \bar{K}^0$ in the low energy region turns out to be forbidden owing to the Pauli principle in addition to the conservation laws of the total angular momentum and parity. Moreover the parity of Σ^* is discussed on the basis of the character for angular distribution of $\bar{K}$-meson.

Recently Matthews and Salam [1] have suggested the existence of an excited state (isobar) for the K^--$\mathcal{N}$ system (*) in order to explain the experimental fact that the cross-sections for K^--p scattering in the energy region (20 ÷ 60) MeV are much larger than those for K^+-p scattering [4]. And they have thought that the reactions go through the following processes

$$\text{(A)} \qquad K^- + p \to \Sigma^* \to K^- + p \,,$$

$$\text{(B)} \qquad K^- + p \to \Sigma^* \to Y + \pi \,,$$

where Y means Σ or Λ-particle.

---

(1) P. T. Matthews and A. Salam: *Phys. Rev. Lett.*, **2**, 226 (1959).

(*) As for the existence of this Σ^*, some discussions have been done [2,3].

(2) J. D. Jackson and H. W. Wyld jr.: *Phys. Rev. Lett.*, **2**, 355 (1959).

(3) R. H. Dalitz and S. F. Tuan: *Phys. Rev. Lett.*, **2**, 425 (1959).

(4) The report given by M. F. Kaplon at the 1958 *Annual International Conference on High-Energy Physics at CERN*.

According to the experimental results for angular distributions ([4-8]), s-wave interaction seems to play the most important role in K^--p collision at low energy, so it may be said that the spin of Σ^* is $\frac{1}{2}$ and the parity of it is the same as that of $\overline{K}$-meson.

It is the purpose of this paper to examine how the other K-meson reactions are influenced by the existence of the Σ^*. In K^--d collision at low energy there are the following reactions,

(I) $$K^- + d \to Y + \mathcal{N} ,$$

(II) $$K^- + d \to Y + \mathcal{N} + \pi ,$$

(III) $$K^- + d \to \mathcal{N} + \mathcal{N} + \overline{K} ,$$

(III′) $$K^- + d \to d + K^- .$$

Let us consider reactions (III) and (III′). If the Σ^* exists, these reactions ought to go mainly through the following processes,

(IIIa) $$K^- + d \to \Sigma^* + \mathcal{N} \to n + p + K^- ,$$

(IIIb) $$K^- + d \to \Sigma^* + \mathcal{N} \to n + n + \overline{K}^0 \ (^*) .$$

We shall restrict our discussion to an energy region up to about 50 MeV for the incident K^--meson. We may safely suppose, then, that not only Σ^* and $\mathcal{N}$ in the intermediate state but also the two final nucleons will be in an S-state relative to each other. Then the value of the total angular momentum J for the Σ^*-$\mathcal{N}$ system turns out to be 1 or 0. When the orbital angular momentum of K^- relative to deuteron in the initial state is denoted by l', only the states of $l' = 0, 1$ and 2 are allowed by the condition $J = 0$ or 1. But it is not necessary to take into account the state of $l' = 1$ because the parity of the K^--d system must be the same as that of the Σ^*-N system. Thus the state of $J = 0$ can be ruled out from our consideration about the processes (III) and (III′).

Let us consider reaction III(b). The two nucleons in the final state are in a $^1S_0$-state by virtue of the Pauli exclusion principle. If we denote by l the orbital angular momentum of K^0 with respect to the center of mass for

---

([5]) P. Eberhard, A. H. Rosenfeld, F. T. Solmitz, R. D. Tripp and M. B. Watson: *Phys. Rev. Lett.*, **2**, 312 (1959).

([6]) W. Alles, N. N. Biswas, M. Ceccarelli and J. Crussard: *Nuovo Cimento*, **6**, 571 (1957).

([7]) G. Ascoli, R. D. Hill and T. S. Yoon: *Nuovo Cimento*, **9**, 813 (1958).

([8]) R. G. Glasser, N. Seeman and G. A. Snow: *Nuovo Cimento*, **9**, 1085 (1958).

([*]) We assume the parity of $\overline{K}^0$ is the same with that of K^-.

3672

two final nucleons, then the value of l must be equal to 1 in order to satisfy the condition $J=1$. This state of $l=1$, however, is ruled out from our consideration because of the law of conservation of parity.

From the above discussions the following result can be derived. So far as the K^--d collision in the low energy region (up to about 50 MeV) is concerned, reaction (IIIb) turns out to be forbidden. According to the report of CERN Conference (1958) ([9]), one event corresponding to the reaction (IIIb) has been found. But it may probably be difficult to observe this reaction. Now let us discuss reaction (IIIa) which will be easily measured. We denote the R-matrix for the reaction (III) or (III′) by ${}^{2s+1}R_{l'l}(J)$ in the case where the $\bar{K}$-meson is absorbed by the deuteron in the state of orbital angular momentum l' belonging to the total angular momentum J and is emitted in that of orbital angular momentum l with respect to the final two nucleon system which is in the spin state s.

Since there is no contribution from the situation in which the final two nucleons are left in a ${}^1S_0$-state, the angular distribution for K^- in reaction (IIIa) or (III′) is expressed by the following form

$$(1)\quad \frac{d\sigma}{d\Omega} \propto \frac{1}{4k^2}\Big[|{}^3R_{00}(1)|^2+|{}^3R_{20}(1)|^2+|{}^3R_{02}(1)|^2+\frac{3(1+\cos^2\theta)}{4}|{}^3R_{22}(1)|^2+$$

$$+\frac{(3\cos^2\theta-1)}{2}\Big\{\big({}^3R^*_{00}(1)\,{}^3R_{22}(1)+{}^3R^*_{22}(1)\,{}^3R_{00}(1)\big)+$$

$$+\big({}^3R^*_{20}(1)\,{}^3R_{02}(1)+{}^3R^*_{02}(1)\,{}^3R_{20}(1)\big)+\sqrt{\tfrac{1}{2}}\big({}^3R^*_{22}(1)\,{}^3R_{02}(1)+{}^3R^*_{02}(1)\,{}^3R_{22}(1)+$$

$$+\sqrt{\tfrac{1}{2}}\big({}^3R^*_{22}(1)\,{}^3R_{20}(1)+{}^3R^*_{20}(1)\,{}^3R_{22}(1)\big)\Big\}\Big].$$

Thus we can state our conclusions as follows:

If the Σ^* exists,

i) the cross-section for the reaction (IIIb) is much smaller than that for the reaction (IIIa),

ii) the angular distributions of K^- for the latter process have not any large forward-backward asymmetry and have the same form as those for the reaction (III′).

Finally let us discuss the parity of Σ^*. Basing on the experimental results that the angular distributions for both reactions (A) and (B) are isotropic, Σ^* has been regarded as an excited state due to s-wave interaction in the K^--$\mathcal{N}$

([9]) R. D. Tripp: *Annual Intern. Conference on High-Energy Physics at CERN* (1958).

system. However there is another possibility, that is, Σ^* may be regarded as an excited state due to the $p_{\frac{1}{2}}$-state (*). In this case, the reaction (III*b*) goes through the state of $l'=l=1$ belonging to $J=1$. The angular distribution of K^0 with respect to the center of mass in the n-n system becomes as follows

$$\frac{d\sigma(K^- + d \to n + n + \overline{K}^0)}{d\Omega} \propto \frac{1}{4k^2} \cdot \frac{3}{2} \sin^2\theta \, |\, {}^1R_{11}(1) \,|^2 . \tag{2}$$

On the other hand, when the final two nucleons are left in a ${}^3S_1$-state, the state of $l'=l=1$ belonging to $J=0$ or $J=1$ contributes to the reaction, and the angular distributions of K^- are expressed in terms of ${}^{2S+1}R_{l'l}(J)$ as follows

$$\frac{d\sigma}{d\Omega} \propto \frac{1}{4k^2}\left[\frac{3}{4}(1+\cos^2\theta)\,|\,{}^3R_{11}(1)\,|^2 + \frac{1}{3}\,|\,{}^3R_{11}(0)\,|^2\right]. \tag{3}$$

These results will make it possible to solve the problem of the parity of Σ^*. If the experimental results with regard to the angular distribution of $\overline{K}^0$ in the reaction (III*b*) are of the form $\sin^2\theta$, Σ^* will be an excited state due to the $p_{\frac{1}{2}}$-state in the K^--$\mathcal{N}$ system. Since such a measurement as this may practically be difficult, it may be suitable to examine the difference between the shape of the angular distribution for (III*a*) and that for (III′). If the angular distributions of K^- for these reactions (III*a*) and (III′) have the same form, Σ^* can be regarded as an excited state due to the *s*-state for the K^--$\mathcal{N}$ system. While, if there are large differences between the angular distributions of K^- for these reactions, and if the shape of these differences can be expressed by a form of $\sin^2\theta$, then Σ^* can be regarded as an excited state due to the $p_{\frac{1}{2}}$-state for the K^--$\mathcal{N}$ system.

(*) Matthews and Salam have said in their paper [1] that this possibility can be excluded by the discussions about the ratio σ_{ab}/σ_{el} in K^--p collision.

RIASSUNTO (*)

Si esamina dal punto di vista cinematico il processo $K^- + d \to \mathcal{N} + \mathcal{N} + K$, assumendo l'esistenza uno stato eccitato Σ^* del sistema K^--$\mathcal{N}$ Si rileva che la reazione $K^- + d \to n + n + K^0$ nella sezione di bassa energia risulta proibita per il principio di Pauli in aggiunta alle leggi di conservazione del momento angolare totale e della parità. Si discute inoltre la parità del Σ^* sulla base dell'aspetto della distribuzione angolare del mesone K.

(*) *Traduzione a cura della Redazione.*

IL NUOVO CIMENTO Vol. XIV, N. 4 16 Novembre 1959

Some Consequences for Quantum Electrodynamics of an Essential Singularity at $\alpha = 0$ (*).

P. J. Redmond

Physics Department, University of California - Berkeley, Cal. (**)

(ricevuto il 3 Agosto 1959)

Summary. — Many authors have suggested that the functions of relativistic field theories are singular in the region of vanishing coupling constant. Indeed, it is only by virtue of such an assumption that one can hope to reconcile the optimistic attitude that such theories might be mathematically meaningful with the contrary evidence provided by perturbation theory. Once the possibility of such a singularity is allowed many proofs concerning the behavior of field theories become suspect. As an illustration the argument of Gell-Mann and Low concerning the behavior of quantum electrodynamics at small distances is reexamined. Within the context outlined above much weaker restrictions are found than those indicated in the original paper. If an approximation to the photon propagator is calculated by summing a selected infinite set of contributions to the spectral density function, the resulting expression has an essential singularity at $\alpha=0$, it is not of the form predicted by Gell-Mann and Low, but it does satisfy the weaker conditions discussed in this paper.

1. – Introduction.

If the Green's functions of a relativistic field theory have an essential singularity in the region of vanishing coupling constant [1] it is clear that they cannot be represented by their perturbation series expansion. At best such

(*) This work was performed by the author as a Consultant to The RAND Corporation.

(**) Now at University of California at Santa Barbara, Goleta Cal.

(1) F. J. Dyson: *Phys. Rev.*, **85**, 631 (1952); W. Thirring: *Helv. Phys. Acta*, **26**, 33 (1953).

3675

an expansion can be asymptotic. In electrodynamics the perturbation series provides a method for calculating the values of observable quantities which yields results in agreement with experiment. Also, for low order calculations the contributions from successive terms rapidly decrease. On the other hand, in meson theory the early terms in the series are all of the same order of magnitude and it is therefore not possible to reliably estimate the quantitative predictions of the theory. It should be emphasized that if the series is truly asymptotic a knowledge of the entire perturbation series expansion might not provide the necessary information for quantitative predictions.

It is of some interest to note that the above remarks can still be true even if the perturbation series converges, for it could converge to a function which is not a solution of the basic equations of the theory. If this were the case one would find that in trying to verify the solution it would be necessary to perform some operations which could not be justified. However, this is precisely what happens term by term in the perturbation theory expansion. For if an attempt is made to check the equal time commutation relations, the inverse wave function renormalization constant occurs on both sides of the resulting equation, and perturbation theory indicates that the coefficients in its Taylor expansion involve infinities. Of course, the appearance of infinities in a Taylor expansion does not imply that the function or its derivatives are infinite for some non-zero value of its argument, as evidenced by the function α^{-1}. Also the convergence of a Taylor expansion does not imply that the expansion represents the function. As an example of this the Taylor expansion of $\exp[-1/\alpha^2]$ is identically zero.

We can summarize the above remarks by making the following observations: 1) Any quantitative results obtained by a manipulation of the perturbation series must be treated with great caution. In particular, proofs that the theory contains logarithmic poles ([2,3]) or that the renormalization constants are infinite ([4]) should not be accepted too readily. 2) However, such analyses can yield a great deal of information concerning the Taylor expansions for the Green's functions ([5]). 3) There is an infinite set of functions having the same Taylor expansion. Perturbation theory in itself gives no

([2]) L. D. Landau and I. J. Pomerančuk: *Dokl. Akad. Nauk SSSR*, **102**, 489 (1955); J. C. Taylor: *Proc. Roy. Soc. London*, A **234**, 296 (1956).

([3]) If the possibility of an essential singularity for zero coupling constant is accepted the arguments supporting the existence of a logarithmic pole are inconclusive, see P. J. Redmond: *Phys. Rev.*, **112**, 1404 (1958).

([4]) Källén's proof that at least one of the renormalization constants in electrodynamics must be infinite is inconclusive according to S. G. Gasiorowicz, D. R. Yennie and H. Suura: *Phys. Rev. Lett.*, **2**, 513 (1959). This letter contains references to earlier work on this problem.

([5]) A possible exception to this remark is noted later (footnote ([10])).

9473

information indicating which ot these functions is to be preferred. At present the most attractive method for selecting a particular form is to demand that the final result have the correct analytic properties in momentum space. Unfortunately, the general arguments which lead to such criteria are not yet systematically understood.

In the next section we shall briefly outline the argument used by GELL-MANN and LOW to find restrictions on the possible behavior of electrodynamics at small distances (6). Since we only indicate those aspects of the argument which are relevant to our discussion the interested reader is referred to their paper for a more complete presentation. In the final section we exhibit an expression for the photon propagator which has many desirable properties but is not of the form predicted by GML. However, the Taylor expansion of this function is of the form predicted and, as we shall show, the expression is excluded by GML by virtue of an assumption that the theory is regular at $\alpha = 0$.

2. – Quantum electrodynamics at small distances.

The investigation of quantum electrodynamics at small distances initiated by GML is based on a set of functional equations which are obtained by noting that the renormalization program can be carried out in a variety of ways parametrized by two normalization momenta λ and λ'. Although GML appealed to perturbation theory in deriving these equations it was emphasized by BOGOLJUBOV and SHIRKOV (7) that the existence of such a renormalization group follows immediately from the basic structure of the theory.

Following GML we consider the photon propagator and represent it in the form

(GML 4.16) $$D_{FC}(k, e_1^2) = (1/k^2) d_c(k, e_1^2) ,$$

where D_{FC} is the usual renormalized Feynman function and e_1 is the observed charge. They then introduce a function $d(\lambda, k, e_2^2)$ normalized to unity at $k^2 = \lambda^2$ by

(GML 4.20) $$d(\lambda, k, e_2^2) = d_c(k, e_1^2)/d_c(\lambda, e_1^2) ,$$

where the parameter e_2^2 is given by

(GML 4.21) $$e_2^2 = d_c(\lambda, e_1^2) e_1^2 .$$

(6) M. GELL-MANN and F. E. LOW: *Phys. Rev.*, **95**, 1300 (1954). In the following this paper will be referred to as GML.

(7) N. N. BOGOLJUBOV and D. V. SHIRKOV: *Nuovo Cimento*, **3**, 845 (1956).

Because of the general structure of the theory the Taylor expansion in powers of e_1^2 of the quantities $d(\lambda, k, e_2^2)$ and e_2^2, which are defined multiplicatively above, can be evaluated by a subtraction procedure. When the Taylor expansion of $d(\lambda, k, e_1^2)$ is examined it is found that the coefficients remain finite when the mass of the electron (m) is set equal to zero. On the other hand the Taylor expansion of $d_c(k, e_1^2)$ contains terms of the form $e_1^{2n}\{\ln(k^2/m^2)\}^{\varrho}$, $\varrho \leqslant n$. Therefore, the Taylor expansions of the numerator and denominator in (GML 5.20) are singular at $m^2 \to 0$. They thereby conclude that at large momenta these equations take the form

$$\text{(GML 5.4)} \qquad |k^2|, |\lambda^2| \gg m^2 : d\left(\frac{k^2}{\lambda^2}, e_2^2\right) = \frac{d_c(k^2/m^2, e_1^2)}{d_c(\lambda^2/m^2, e_1^2)},$$

$$\text{(GML 5.5)} \qquad e_2^2 = e_1^2 d_c(\lambda^2/m^2, e_1^2).$$

The significance of these equations resides entirely in the dependence on the arguments which is explicitly shown. The derivation of Eq. (GML 5.4) is based on the assumption that the limit $m^2 \to 0$ $d_c(k^2/m^2, e_1^2) = Z_3^{-1}$ is singular ([6]). If the wave function renormalization constant Z_3^{-1} is finite then one can only conclude that the Taylor expansions of the functions involved formally satisfy (GML 5.4). A non-trivial restriction on the Taylor expansion is obtained since it is known that the coefficients in the Taylor expansion are singular.

By analyzing the above equation GML were able to conclude that for $|k^2| \gg m^2$ the photon propagator must have a functional form given by

$$\text{(GML 5.6)} \qquad e_1^2 d_c(k^2/m^2, e_1^2) = F\big((k^2/m^2)\varphi(e_1^2)\big),$$

where F and φ are unknown functions. From this GML were able to show that if the bare charge is finite it is determined by the form of the function F and φ and is therefore a fixed number independent of the value assigned to the observed charge.

The last conclusion is of some interest in that it implies that the observed charge can be calculated if electrodynamics is finite. For, a finite electro-

([6]) That is, if Z_3^{-1} is finite then the equations GML 5.4 and 5.5 become trivial in that the dependence on the momentum variables drops out. Thus $d_c(k^2/m^2, e_1^2)$ would be replaced by Z_3^{-1} in the equation, $d(k, \lambda, e_2^2)$ would approach unity, and the parameter e_2 would be replaced by the base charge. Since the subsequent manipulation of these equations by GML is based on the assumption that the functions involved do vary with momenta their argument breaks down. One then finds that these equations do not impose any quantitative restrictions (other than those indicated above) on the behavior of the functions as a whole although there are formal restrictions on the Taylor expansions.

3678

dynamics is parametrized by bare constants e_B and m_B, everything then being expressed in terms of these parameters. However, because of the dimensions of the quantities involved the expression for e_1 in terms of e_B and m_B cannot depend on m_B. Since GML indicate there is no freedom in choosing e_B then there must also be no freedom to choose e_1. Our reasoning indicated that the argument breaks down at the last step and as a result the theory can exist for at least a range of values of e_1.

3. – An illustrative example.

From first order perturbation theory one obtains the following expression for the photon propagator,

$$d_c(k) = \left\{1 - \frac{\alpha k^2}{3\pi}\int_{4m^2}^{\infty} \frac{\mathrm{d}M^2}{M^2}\,\frac{(1+2m^2/M^2)(1-4m^2/M^2)^{\frac{1}{2}}}{k^2+M^2}\right\}^{-1}. \tag{3.1}$$

The integral on the right hand side is readily evaluated to give

$$d_c(k) = \{1 - (\alpha/3\pi)(B^2 - \tfrac{8}{3} - \tfrac{1}{2}(B^3 - 3B)[(B+1)/(B-1)])\}^{-1}, \tag{3.2}$$

where $B = (1+4m^2/k^2)^{\frac{1}{2}}$. For $|k^2/m^2| \gg 1$ the right hand side can be simplified so that

$$|k^2/m^2| \gg 1: \quad (\alpha/3\pi)\, d_c(k) = (3\pi/\alpha - \ln k^2/m^2 + \tfrac{5}{3})^{-1}. \tag{3.3}$$

In this form it is evident that the denominator vanishes at $k^2 = k_0^2$ where

$$k_0^2/m^2 = \exp[3\pi/\alpha + \tfrac{5}{3})$$

and this exhibits the logarithmic pole in $D_{FC}(k)$ discussed by LANDAU *et al.* [2]. Recently the author [3] suggested a procedure for eliminating this undesirable feature by summing contributions to the special density function, instead of using eq. (3.1) directly. The net effect of such a procedure is simply to subtract away the pole. The residue at the pole can be identified with the wave function renormalization constant Z_3^{-1} and the added term can be shown to have a Taylor expansion zero.

If the right hand side of eq. (3.3) is modified in this way one obtains

$$(\alpha/3\pi)\, d_c(k) \approx (3\pi/\alpha - \ln k^2/m^2 + \tfrac{5}{3})^{-1} + \\ + (1 - \exp[3\pi/\alpha - \ln k^2/m^2 + \tfrac{5}{3}])^{-1}. \tag{3.3'}$$

This expression is clearly a function of the single argument k^2/m^2, $\exp[-3\pi/\alpha]$ and is therefore of the form predicted by GML. The wave function renormalization constant is given by $Z_3^{-1} = \lim_{k^2\to\infty} d_c(k) \approx 3\pi/\alpha$ and one finds that the bare value of the fine structure constant

$$\alpha_B = Z_3^{-1}\alpha = 3\pi \tag{3.4}$$

is independent of α ([9,10]).

We thus have an illustration of the type of behavior predicted by GML. However in obtaining this expression we have made some unnecessary approximations to eq. (3.1.). If we apply the same prescription directly to eq. (3.1) it is necessary to add to the right hand side a term of the form $Z_3^{-1}(k^2 - k_0^2)^{-1}$ where the constants k_0^2 and Z_3^{-1} are determined by locating the pole in the original expression and finding its residue. This leads to the relations

$$B_0 = 1 + (B_0 + 1)\exp[-2(3\pi/\alpha - B_0^2 + \tfrac{8}{3})/(3B_0 - B_0^3)] \tag{3.5}$$

and

$$Z_3 = (\alpha/3\pi)(B_0^2 - 1)\{\tfrac{1}{2}(3 - B_0^2)(B_0^2 - 1)^{-1} - 1 - \\ - (\tfrac{3}{4}B_0)(B_0^2 - 1)\ln[(B_0 + 1)/(B_0 - 1)]\}, \tag{3.6}$$

where $B_0 = (1 + 4m^2/k_0^2)^{\frac{1}{2}}$. When $\alpha = 0$ one can take $B_0 = 1$ ([11]) and it is easy to see that in this region the expressions previously obtained for k_0 and Z_3 are first approximations. By differentiating the right hand side of eq. (3.5) successively with respect to α and then setting $\alpha = 0$, $B_0 = 1$ one finds that the Taylor expansion of B_0 is unity. That is $B_{0T} = 1$. Similarly $Z_{3T} = \alpha/3\pi$. Since the right hand side of eq. (3.6) does not reduce to a simple multiple of

([9]) The above argument is contained in an unpublished manuscript by N. N. Bogoljubov, A. A. Logunov and D. V. Shirkov. As a result they conclude that propagators computed according to the prescription of reference ([3]) are of the form predicted by GML.

([10]) The value obtained for α_B, $\alpha_B = 3\pi$, has no special significance. If the next term in the expansion of the denominator of eq. (3.1) is included it is found that the change in the computed value of this constant is of the same order of magnitude as the original estimate.

([11]) This corresponds to taking the positive square root in the definition $B_0 = (1 + 4m^2/k_0^2)^{\frac{1}{2}}$. If the relationship between α and B_0 is put in the form $\alpha = f(B_0)$, it is found that $f(B_0)$ is an even function of B_0. When the relation is inverted it is permissible to take either the positive or negative branch.

5680

multiple of α our expression for the photon propagator cannot be of the form predicted by GML although its Taylor expansion is [12].

If one examines the system of eqs. (3.5) and (3.6) it is seen that they have a solution for any positive α and that the other quantities of interest lie in the ranges $\alpha_B > 3\pi$, $B_0 > 1$, $1 > Z_3 > 0$, and $k_0^2 > 0$.

[12] It is of some interest to note that the coefficients in the Taylor expansion of Z_3^{-1} as calculated from eq. (3.3′) or eq. (3.6) are all infinite whereas perturbation theory indicates that the constant term is unity. The reason for this apparent discrepancy can be seen by noting that this term is defined in perturbation theory by the double limit $\lim_{k^2\to\infty}\lim_{\alpha\to 0} k^2 D_F(k^2)$. If this limiting process is applied to eq. (3.3′) the perturbation theory value, unity, is obtained. However, the constant term in the Taylor expansion of Z_3^{-1} as obtained by examining the residue of the pole in eq. (3.3′) corresponds to the double limiting process $\lim_{\alpha\to 0}\lim_{k^2\to\infty} k^2 D_{FC}(k^2)$, and this is infinite.

RIASSUNTO (*)

Molti autori hanno suggerito che le funzioni delle teorie relativistiche del campo sono singolari nella regione della costante di accoppiamento tendente a zero. Infatti solo in virtù di questa supposizione si può sperare di riconciliare la tendenza ottimistica secondo cui tali teorie possono essere significative da un punto di vista matematico anche al lume delle riprove contrarie fornite dalla teoria della perturbazione. Una volta ammessa la possibilità di tale singolarità, molte prove relative al comportamento delle teorie del campo diventano sospette. Si riesaminano, a titolo di illustrazione, l'argomentazione di Gell-Mann e Low riguardante il comportamento dell'elettrodinamica quantica a piccole distanze. Nel contesto di cui sopra si trovano restrizioni molto più deboli di quelle indicate nell'articolo originale. Se si calcola un'approssimazione al propagatore fotonico, sommando un infinito gruppo selezionato di contributi alla funzione della densità spettrale, l'espressione risultante ha una singolarità essenziale per $\alpha = 0$, non è della forma predetta da Gell-Mann e Low, ma soddisfa le condizioni più deboli discusse nel presente articolo.

(*) *Traduzione a cura della Redazione.*

3681

IL NUOVO CIMENTO Vol. XIV, N. 4 16 Novembre 1959

Track Distortion in a Liquid Hydrogen Bubble Chamber.

R. Budde, A. Burger, H. Filthuth, Y. Goldschmidt-Clermont, H. M. Mayer, D. R. O. Morrison, Ch. Peyrou and J. Trembley

CERN - Genève

(ricevuto il 10 Agosto 1959)

Summary. — Tracks of 270 MeV pions in a 10 cm hydrogen bubble chamber were measured with the CERN reprojection system (Iep). As a test of track distortion, the curvature of the parabola fitted to the points and the dispersion of these points were calculated. With flash delays of 1 and 2 ms the curvature in the middle region of the chamber was almost the same as that expected from multiple scattering showing that the convection currents which are used in the thermostatisation system, do not produce general distortions in the useful volume of the chamber.

1. – Introduction.

Measurements have been made to determine the mean radius of curvature of tracks formed in a liquid hydrogen bubble chamber, in the absence of a magnetic field.

The chamber used was cylindrical, of 10 cm diameter and 6 cm width with vertical windows. It is expanded by means of a 6 cm diameter piston $3\frac{1}{2}$ cm above the top of the chamber. At the foot of the chamber is a vapour pressure thermometer 2.8 cm long and of 0.8 cm diameter. The tracks used were those of a beam of 270 MeV negative pions from the CERN synchrocyclotron, passing horizontally across the chamber and completely investing it.

The chamber was cooled by means of a pressure regulated bath of liquid hydrogen in thermally contact with the top third of the chamber. The chamber body was made of stainless steel and therefore the liquid was mainly cooled by convection currents so avoiding the formation of a cold layer at the bottom of the chamber (*). This system is such that it can be applied to larger chambers.

(*) The homogeneity of the sensitivity throughout the chamber was checked by measurements of the mean gap length of the beam tracks.

It is of interest to ascertain the effect of these convection currents in causing track distortion.

The chamber expansion started about 8 ms before the passage of the beam and the minimum value of the pressure was reached about $\frac{1}{2}$ ms after the beam. The pressure was almost constant from the time of passage of the beam to the beginning of the recompression about $2\frac{1}{4}$ ms later. The beam lasted a total time of 0.3 ms. The time of the flash above half peak intensity was 20 microseconds.

The distortion of tracks can be expected to depend on the height of the track in the chamber and on the flash delay, *i.e.* the time between the passage of the beam particles and the triggering of the flash. Measurements were made on tracks taken with flash delays of 0.5, 1.0, 2.0 and 2.8 ms. It was found that at 0.5 ms the tracks were too faint for accurate measurements. At each flash delay nine or ten tracks were measured at each of three positions in the chamber, top (mean track length 5.5 cm), middle (mean track length 8.5 cm) and bottom (mean track length 6.5 cm). The tracks went from one side of the illuminated region to the other.

2. – Track measurement.

The tracks were measured with Iep, Instrument for the Evaluation of Photographs. This instrument displays an enlarged image of the film on a screen, where it can be moved with respect to a fixed cross-hair. The observer centres by eye the points to be measured, and their cartesian co-ordinates are recorded on punched tape in digital form. One digit is 2.69 microns.

The co-ordinates of about 15 points per cm were measured along the track except at a flash delay of 0.5 ms when about 10 points per cm were taken. These points were not quite uniformly spaced as the points chosen were individual bubble images (the setting error in positioning the cross-hairs of Iep on a bubble image, at right angles to the track direction, is 1.8 to 2.0 digits. With the film-chamber magnification of 1/5.1 this corresponds to 0.024 to 0.027 mm in the chamber). In the computation using a Mercury computer, a straight line was fitted to the points by a least-squares process using all the measurements. Several checks were used to eliminate measurement and coding errors, for instance, the distance of each point from the straight line was calculated and was printed out as a histogram which allowed a check that some points had not been taken at abnormal distances from the track. The R.M.S. value of the distance of the points from the fitted line was also computed.

A parabola was similarly fitted to the points and the distance of the points from the parabola was calculated and again displayed as a histogram and

3683

the R.M.S. value calculated. The radius of curvature corresponding to this parabola was computed and the R.M.S. error in the sagitta given.

The computer programme also allows the co-ordinates of each point of a track to be fed into a chart plotter. The track is then plotted on to paper with the co-ordinate at right angles to the least squares fitted straight line multiplied by a factor of 50 so that deviations from a straight line may be easily visible.

3. – Reproducibility of measurements.

One series of measurements on 10 tracks at the bottom of the chamber were repeated. The R.M.S. distance of the points from the fitted straight line and from the fitted parabola were 2.0 and 1.7 digits respectively. The R.M.S. of the 10 values of the difference between the two repeated measurements were 0.24 and 0.28 digits. On comparing these values with the Iep setting error of about 2 digits, it is seen that the measurements are reproducible within this setting error. The R.M.S. of the 10 values of the difference between the repeated measurements of the sagittas was 0.011 mm in the chamber which is in satisfactory agreement with the computed R.M.S. error of 0.009 mm in the sagitta measurements, the average value of the sagitta being 0.032 mm.

As a further check one track was measured four times and the magnified track distortions were displayed by means of the chart plotter. It was then seen visually that the main features were reproduced.

4. – Single scatterings.

In two cases the histograms of the distribution of the distances of points from the fitted line and circle were anomalous (some points more than 18 digits from the fitted line). On examining these tracks with the aid of the chart plotter it was seen that they both had single scatterings which appeared as being about 17° on the plot, that is 1/3° on the film. As it was desired to compare the results with those expected from multiple scattering, these tracks were excluded from the statistics. It was calculated that the probability of occurrence of 2 single scatters of more than 1/3° was reasonable.

5. – Sources of track curvature.

A mean curvature of the track may be due to:

a) Multiple scattering of the incident particle.

3084

b) General distortion due to overall movement of the liquid or optical defects, *e.g.* effects of convection currents.

c) Local distortions of the liquid *e.g.* vortices, turbulence.

d) Measurement errors.

The average curvature to be expected from multiple scattering can be calculated, *e.g.* P. M. S. BLACKETT: *Suppl. Nuovo Cimento*, **11**, 264 (1954). For a track of length L (= 8.5 cm), of a particle of momentum p, and velocity v ($=\beta c$), passing through a medium of atomic number Z and with N nuclei per cm^3, the radius of curvature ϱ is given by

$$\frac{1}{\varrho} = \left(\frac{16\pi}{3}\right)^{\frac{1}{2}} \cdot \frac{Z \cdot N^{\frac{1}{2}} \cdot r_e \cdot m_e c^2}{L^{\frac{1}{2}} \cdot p\beta c} \cdot B \,,$$

where for hydrogen Z must be taken as $(Z(Z+1))^{\frac{1}{2}} = 2^{\frac{1}{2}}$

$r_e = 2.8 \cdot 10^{-13}$ cm,

$m_e c^2 = 0.51$ MeV,

$p\beta c = 360$ MeV for a 270 MeV pion

and the density of liquid hydrogen was taken to be 0.059 g/cm^3

$$B = \left(\log_e\left(\frac{\theta_{\text{max.}}}{\theta_{\text{min}}}\right)\right)^{\frac{1}{2}}.$$

where

$$\theta_{\text{m'n.}} = \frac{mcZ^{\frac{1}{3}}}{137p} = 10^{-5} \text{ radians} \,,$$

$\theta_{\text{max.}}$ is difficult to define, but its value is not critical. If the film is projected a single scatter may be visually identified if it is greater than 1/100 radians *i.e.* 0.6°. In this case $\varrho = 25.7$ metres. The limit for chart plotting is about 1/200 radians *i.e.* 0.3° and then $\varrho = 27.1$ metres.

We will take $\varrho = 27$ metres for 8.5 cm long tracks when the corresponding sagitta, s, will be 0.033 mm in the chamber. Due to differences in track lengths at the bottom of the chamber $\varrho = 23.5$ metres and $s = 0.022$ mm while at the top of the chamber $\varrho = 21.5$ m and $s = 0.017$ mm.

The mean curvature to be expected due to the Iep setting error is small compared to that expected from multiple scattering in all cases except for the series at a flash delay of 0.5 ms. Here the tracks were very faint and fewer points per cm track were measured giving a larger R.M.S. distance from the fitted curves. In this case a mean sagitta of the same order as that due to multiple scattering could be expected.

3c85

6. – Results and discussion.

The results are given in the Table and the individual measurements of the sagittas are plotted in the figure. The R.M.S. distances from fitted lines and circles and the average sagittas are expressed in mm in the chamber. Since the distribution of the angle of scattering probabilities is non-Gaussian, the average of the values of the sagittas was taken and the corresponding radius of curvature derived from this. It can be seen that at flash delays of 0.5 and 2.8 ms, the average sagittas and the R.M.S. errors on the sagittas are considerably larger than at intermediate flash delays. The poor values at 0.5 ms are partly due to the difficulty in measuring the faint tracks but in addition there would appear to be some general distortion. The large values of the sagittas at 2.8 ms are expected as recompression had already begun at this time.

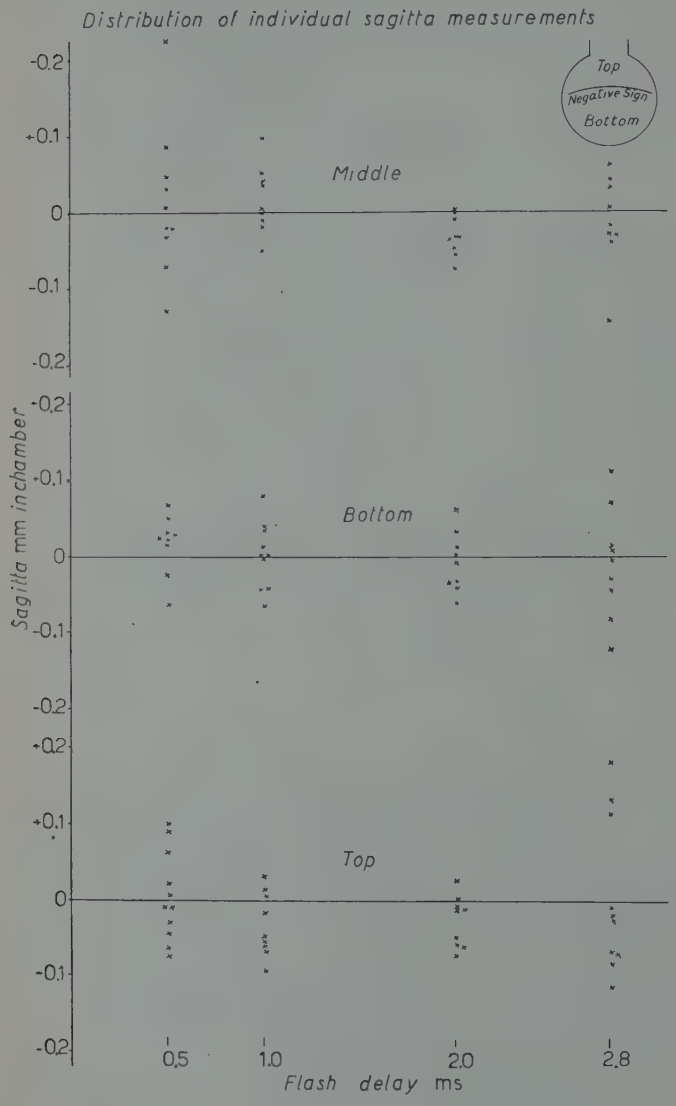

Fig. 1.

An important feature of the figure is that, in general, there are approximately equal numbers of tracks with positive and with negative sagittas

indicating that any systematic distortion in the chamber is small. At a flash delay of 2.0 ms, there tends to be more negative than positive sagittas and this suggests that there may be a small systematic general distortion of the liquid producing a sagitta of about 0.010 to 0.020 mm.

We will now consider tracks taken with flash delays of 1.0 and 2.0 ms.

In the middle of the chamber the sagitta and the distribution of the sagittas are almost the same as those expected from multiple scattering, showing that there is little general distortion.

At the top and bottom of the chamber the spread in values of the sagitta are greater than would be expected from multiple scattering. Visual examination by projection, microscope or chart plotter, show the existence of occasional irregularities in the tracks. These may have amplitudes of up to 0.07 mm in the chamber and extend over 1 to 3 mm. They are rare in the middle tracks and more frequent in the top or bottom tracks. These irregularities can account for those cases where the radii of curvature are less than that expected from multiple scattering. As was shown in the reproducibility tests, these errors are outside the setting errors of Iep. Clearly the effect of these irregularities varies with the length of the track and will be smaller for long tracks.

These local turbulence may be vortices which can move through the liquid. It may be noted that R. Donaldson and R. Watt [1] have calculated that if a vortex is once formed, it takes 13 minutes to decay to half its strength.

The R.M.S. distances from the fitted lines and circles at 1.0 and 2.0 ms, are about equal to the setting error of Iep which shows that the irregularities are not very frequent. This also indicates that the mean displacement of the bubbles from the track direction is less than the setting error, which is about a third to a quarter of the apparent bubble diameter. Hence the scatter of the bubbles about the track direction is less than a quarter of the apparent bubble diameter.

It is of interest to compare these results with those obtained by M. Cresti [2] on the Berkeley 25 cm liquid hydrogen chamber, having horizontal windows and gas expansion (as distinct from the liquid expansion used here), though being an early model this expansion line was of rather small diameter. Whereas in this paper it has been seen that distortion where detectable, is mainly random in sign and probably due to local disturbances, Cresti reported systematic general distortions, greatest near the expansion line of the chamber, and was able to construct a map of the distortions at different points in the chamber and describe their variation with flash delay. Such large scale movements of the liquid were not detected in the present experiment.

---

(1) R. Donaldson and R. Watt: *U.C.R.L. Eng. Note*, 4311-17/M19.

(2) M. Cresti: *U.C.R.L. Eng. Note*, 4312-07/M37 and M37.1.

3687

7. – Conclusions.

1) The smallest sagittas *i.e.* the largest radii of curvature, were obtained at flash delays of 1.0 and 2.0 ms. The larger sagittas found at 2.8 ms may be attributed to recompression of the chamber liquid. The larger sagittas at 0.5 ms may in part be explained by the faintness of the tracks which cause larger R.M.S. distances from the fitted circle, but there may be some distortion as well. It is difficult to understand the causes of such distortions which do not appear at longer flash delays.

2) There may be some systematic general distortion with mainly negative sagittas at a flash delay of 2.0 ms, but the effect was small compared with multiple scattering and the measurement errors. At other flash delays there was no evidence for any systematic general distortion.

3) In the middle region of the chamber at flash delays of 1.0 and 2.0 ms, the tracks have a mean curvature and distribution of curvature close to that expected from multiple scattering. The R.M.S. distance from the fitted line and circle are compatible with the setting error of Iep. It is concluded that within the measurement errors, distortion is not important in this region of the chamber at these flash delays.

4) Near the top of the chamber rather small radii of curvature are observed, of both signs and of widely varying values. It is probable that the low radii of curvature are mainly due to local distortions in the liquid, but there may also be some general distortion. It is not possible to separate these two effects in this small chamber. However, in long tracks in a larger chamber such local distortions should be less important.

5) At the bottom of the chamber similar distortions are observed. In this case, these are probably due to the presence of the relatively large vapour pressure thermometer used in the experimental chamber. It is probable that under normal operating conditions with no thermometer, the distortion would be considerably reduced.

6) The cooling system using convection currents may be employed without introducing appreciable distortions.

3688

8. – Results.

A) *Tracks crossing Middle of chamber.*

Mean track length = 8.5 cm.

From multiple scattering only, { expected mean radius of curvature = 27 m.
expected mean sagitta = 0.033 mm.

Flash delay, ms	0.5	1.0	2.0	2.8
R.M.S. distance from line, mm	0.041	0.029	0.027	0.041
R.M.S. distance from circle, mm	0.032	0.023	0.023	0.038
Average sagitta, mm	0.072	0.035	0.036	0.046
R.M.S. error on individual sagitta, mm	0.014	0.006	0.008	0.013
Radius of curvature, metres	14	26	25	20

B) *Tracks crossing bottom of chamber.*

Mean track length = 6.5 cm.

From multiple scattering only, { expected mean radius of curvature = 23.5 m.
expected mean sagitta = 0.022 mm.

Flash delay, ms	0.5	1.0	2.0	2.8
R.M.S. distance from line, mm	0.037	0.027	0.030	0.044
R.M.S. distance from circle, mm	0.033	0.023	0.026	0.032
Average sagitta, mm	0.038	0.032	0.033	0.055
R.M.S. error on individual sagitta, mm	0.016	0.011	0.009	0.007
Radius of curvature, metres	14	17	16	10

C) *Tracks crossing top of chamber.*

Mean track length = 5.5 cm.

From multiple scattering only, { expected mean radius of curvature = 21.5 m.
expected mean sagitta = 0.017 mm.

Flash delay, ms	0.5	1.0	2.0	2.8
R.M.S. distance from line, mm	0.037	0.033	0.029	0.041
R.M.S. distance from circle, mm	0.033	0.030	0.025	0.033
Average sagitta, mm	0.050	0.041	0.032	0.080
R.M.S. error on individual sagitta, mm	0.021	0.009	0.009	0.009
Radius of curvature, metres	8	9	12	5

Setting error of Iep 0.024 to 0.027 mm.

Notes

(1) All distances are measured in the chamber.
(2) Nine or ten tracks were measured for each flash delay at each position.

3639

* * *

We would like to express our appreciation of many helpful discussions with Dr. C. C. DILWORTH.

We wish to thank Mme F. BOYARD, Mme J. DANJEAN and Mlle G. LAIDERRIER for their careful measurements of the films with Iep.

RIASSUNTO (*)

Si sono misurate col sistema di riproiezione CERN (Iep) tracce di pioni di 270 MeV in una camera a bolle ad idrogeno di 10 cm. Come controllo della distorsione della traccia, si calcolarono la curvatura della parabola, passante per i punti dati, e la dispersione di questi punti. Con intervalli di flash di 1 o 2 ms la curvatura nella zona centrale della camera era quasi uguale a quella che ci si aspettava dallo scattering multiplo, dimostrando che le correnti di convezione usate per ottenere l'effetto termostatico non producono distorsioni generali nel volume utile della camera.

(*) *Traduzione a cura della Redazione.*

3690

IL NUOVO CIMENTO Vol. XIV, N. 4 16 Novembre 1959

Measurement of Longitudinal Polarization of β^- Electrons from ^{204}Tl by Means of Double Coulomb Scattering.

M. Bernardini, P. Brovetto, S. Ferroni and A. Pasquarelli

Istituto Nazionale di Fisica Nucleare - Sezione di Torino

(ricevuto l'11 Agosto 1959)

Summary. — The present work describes a measurement of longitudinal polarization of β^- electrons, emitted by a ^{204}Tl source, performed using the double Coulomb scattering technique. The observed effect is lower (by about 10%) than expected for $-v/c$ polarized electrons. The present results agree, within the errors, with those obtained in a previous work by measuring the circular polarization of the bremsstrahlung γ-rays.

1. – Introduction.

In a previous work [1] we measured the longitudinal polarization of β^- electrons from a ^{204}Tl source. The experiment was performed by means of the well known technique of the Compton scattering on magnetized iron of the polarized bremsstrahlung γ-rays produced by the β^- electrons.

In the present work the polarization of the β^- electrons, from the same ^{204}Tl source, has been measured by means of double Coulomb scattering. The present results are compared with those reported in the paper just mentioned.

2. – Experimental set-up.

It is well known that the electronic longitudinal polarization gives rise to a transversal one after Coulomb scattering [2]. To measure such a transverse polarization we made use of the Mott scattering in a plane normal to

[1] U. Amaldi, M. Bernardini, P. Brovetto and S. Ferroni: *Nuovo Cimento*, **11**, 415 (1959).

[2] M. Bernardini, P. Brovetto and S. Ferroni: *Nuclear Physics*, **8**, 294 (1958).

that of the first one. Our experimental equipment is schematically drawn in Fig. 1. It consists chiefly of an evacuated (about 10^{-3} mm Hg) container in which double scattering takes place. The ^{204}Tl source is supported by

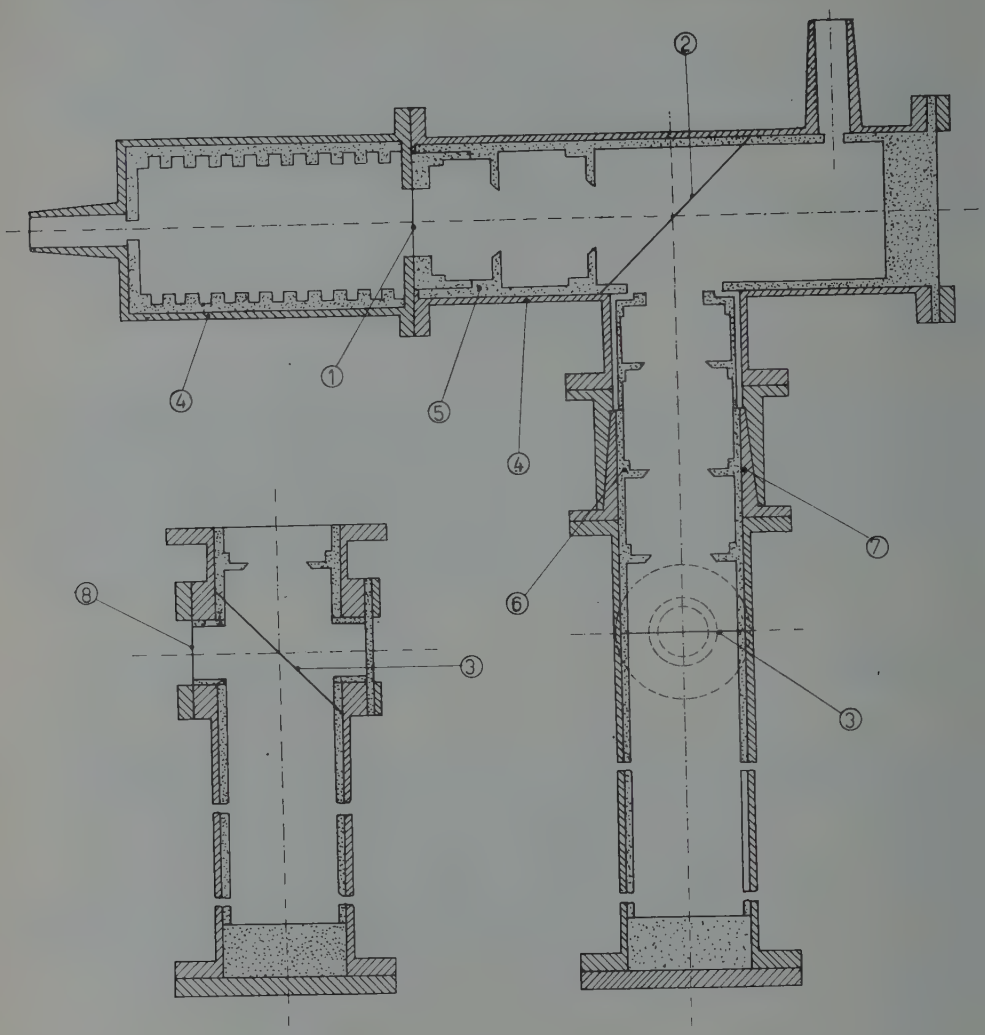

Fig. 1. – Experimental apparatus; 1) source, 2) first scatterer, 3) second scatterer, 4) brass vessel, 5) first set of lucite diaphragms, 6) second set of lucite diaphragms, 7) rotation cone, 8) mica window.

a thin aluminum foil; backscattering is avoided by means of an evacuated « well » behind the source. The electron beam is collimated by a set of lucite diaphragms and strikes the first target. A second set of diaphragms, whose axis in normal to that of the first one, collects on the second scatterer the electrons scattered by the first target.

3692

The electrons going out from the second scatterer are then collimated by a further diaphragm and after passing through a mica window (18.6 mg/cm²) strike an end windowed Geiger tube whose axis is normal to those of both previous diaphragm sets. The counter, together with the second scatterer, could be rotated about the axis of the second diaphragm set without affecting the vacuum. In addition to a conventional shield another thick lead plate was placed in such a way to prevent the bremsstrahlung γ-rays, produced within the source, to strike the Geiger tube. The targets were made from thin gold foils and they made an angle of 45° with the electron beam. They were placed « by transmission » (see Fig. 1) to reduce multiple scattering that would affect the measurements ([3]).

Besides the target could be replaced with other ones of different thickness without changement in the geometry.

The symmetry of our apparatus was checked by measuring the double scattering of electrons using a gold foil as first scatterer (4 mg/cm²) and an aluminum target (4.5 mg/cm²) as second. The result obtained will be given later on.

The pulses of the Geiger counter fed a univibrator and were recorded by a scaler.

3. – Experimental results.

Being N_1 and N_2 the counting rates for the two opposite orientations of the Geiger tubes axis, the azimuthal effect is then defined as:

$$\Delta = 2\,\frac{N_1 - N_2}{N_1 + N_2}\,.$$

To obtain the value of Δ in the case the electrons undergo a single scattering in the second target, we performed a series of measurements using, as second target, foils of different thickness. In such a way, it is possible to extrapolate Δ for a gold foil of zero thickness. In every measurement the same gold foil (4 mg/cm² thick) was used as first scatterer. To take into account the electrons scattered by the lucite wall of the apparatus, measurements have also been done removing either of the gold foils alternatively. We found, by this procedure, that the counting rate without the first gold foil did not differ appreciably from the counter background. By other hand, the counting rate, N_0, obtained with the second scatterer removed, is high enough to appreciably affect the result.

([3]) N. F. Mott and H. S. W. Massey: *The Theory of Atomic Collisions* (Oxford, 1949), p. 84.

In Table I the quantities: N_1, N_2, Δ and Δ_c, that is to say the corrected effect, obtained by taking into account the N_0 counting rate, are given for the various thicknesses of the second gold target. We have:

$$\Delta_c = 2\,\frac{N_1 - N_2}{N_1 + N_2 - 2N_0}\,.$$

TABLE I. – *Experimental results. N_1, N_2, N_0 are expressed in counts for minute.*

Second scatterer thickness mg/cm²	N_1	N_2	Δ	Δ_c
0.29 Au	93.2	99.9	0.069 5 ± 0.006	0.128 5 ± 0.007
0,59 »	122.1	131.8	0.076 8 ± 0.007	0.118 1 ± 0.006
1.63 »	460.4	490.8	0.063 8 ± 0.006	0.070 4 ± 0.010
4.02 »	977.3	1002.8	0.025 7 ± 0.006	0.026 9 ± 0.015
4.5 Al	1378.0	1380.0	0.001 4 ± 0.003 4	0.001 4 ± 0.003 7

$N_0 = 44.4$

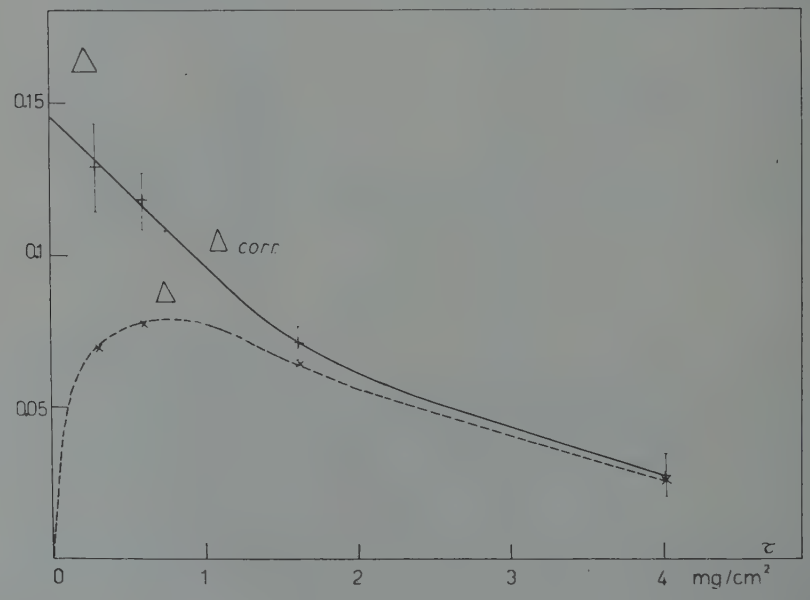

Fig. 2. – The dotted line represents Δ versus τ, the solid one Δ_c.

In the Table I are also included the above mentioned quantities measured when an Al second scatterer is used, and as it can be seen no effect is found, which shows that the experimental setup has sufficiently accurate symmetry.

In Fig. 2 Δ and Δ_c are plotted versus τ, that is the thickness of the second

3694

target. The extrapolated value of A for zero thickness is assumed to give the effect for a single scattering, and turns out to be 0.146.

The spectrum of the electrons outgoing from the first target must be known in order to evaluate correctly the effect on theoretical grounds. This electron

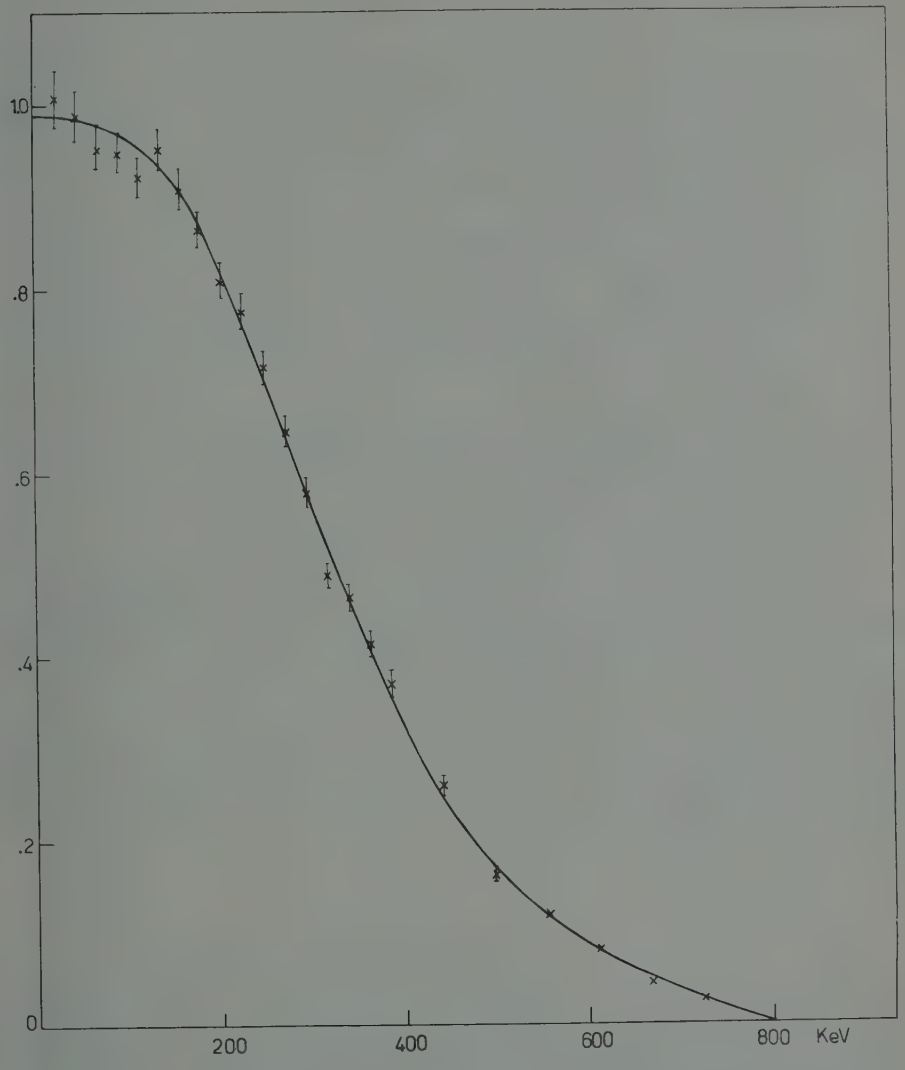

Fig. 3. – Spectrum of the electrons after the first scattering.

spectrum was measured using a CsI(Tl) crystal (1 mm thick) followed by a 6292 Dumont phototube and the pulses, conveniently amplified, were analyzed by a single channel pulse height discriminator. For this measurement the

3C95

second target was replaced by a mica window (8.7 mg/cm²) closely followed by the scintillation detector. In Fig. 3 the result obtained from this measurement is reported.

4. – Discussion.

In the Appendix the effect to be expected in our measurement is calculated for $-v/c$ polarized electrons. The result obtained is $\Delta_{th} = 0.165$. It is about 10% higher than the experimental value. A small difference about the same magnitude was found also in our previous experiment performed by the Compton scattering technique (1).

On the other hand it is to be remarked that a theoretical possibility for this difference was pointed out by B. V. BERESTETSKY and others (4).

It is also to be kept in mind that in the present experiment the electrons undergo a considerable depolarization, due to the finite thickness of the source (about 40 mg/cm²).

The evaluation of Δ_{th} becomes then very complicated because of this fact, as it is shown in the Appendix, and must be considered as only approximate.

In our previous measurement (1) performed on the breamsstrahlung γ-rays, no important depolarization did actually occur because only the γ-rays near the top of the spectrum were detected. In fact, these γ-rays are produced by so high speed electrons ($\beta \simeq 0.9$) that only forward scatterings are present and the polarization undergoes an almost complete precession. Moreover the electrons, can evidently produce the γ-rays after a very short path within the source.

On the other hand, let us point out that the troubles in the evaluation of the depolarization, could be probably avoided by performing a set of measurements with many sources of different thickness and following a suitable method to extrapolate the effect for a source of zero thickness.

APPENDIX

Let us now calculate the effect to be expected in our double scattering.

The number of electrons per unit area and per steradian scattered by the first target and passing through the second set of diaphragms is indicated with $I(\beta)$, this function is obtained from the spectrum of Fig. 3. These electrons have a transversal component of the polarization, $\boldsymbol{P}_{\perp}(\beta)$. The scat-

(1) V. B. BERESTETSKY, B. L. IOFFE, A. P. RUDIK and K. A. TER-MARTIROSYAN: *Nuclear Phys.*, **5**, 464 (1958); *Phys. Rev.*, **111** 522 (1958).

3698

tering cross-section in the second target can be written as:

$$\sigma(\vartheta, \beta, P_\perp) = \sigma_i(\vartheta, \beta) + \sigma_a(\vartheta, \beta)\boldsymbol{P}_\perp \cdot \boldsymbol{n}\,, \tag{A.1}$$

where $\boldsymbol{n}$ is the unit vector normal to the scattering plane,

$$\sigma_i(\vartheta, \beta) = \lambda^2[q^2(1-\beta^2)\operatorname{cosec}^2 \tfrac{1}{2}\vartheta FF^* + \sec^2 \tfrac{1}{2}\vartheta GG^*] \tag{A.2}$$

and

$$\sigma_a(\vartheta, \beta) = 2\lambda^2 q\sqrt{1-\beta^2}\operatorname{cosec} \tfrac{1}{2}\vartheta \csc \tfrac{1}{2}\vartheta \operatorname{Re} FG^*. \tag{A.3}$$

The symbolism used in these two equations is a standard one. The functions $F(\vartheta)$ and $G(\vartheta)$ have been tabulated by SHERMAN (5).

The number of electrons scattered along the path P_1, P_2, P_3 (Fig. 4) is:

$$I(\beta)\,\mathrm{d}\omega_1\,\mathrm{d}S_1\,\frac{Ns\varrho}{\cos\delta_1 A}\,\sigma(\vartheta_{1,2,3}, P_1, \beta)\,, \tag{A.4}$$

where N stands for the Avogadro number, s, ϱ, and A respectively stand for thickness, density and mass number of the second scatterer. We indicate with $\mathrm{d}S_1$, $\mathrm{d}S_2$ and $\mathrm{d}S_3$ the surface elements of the first and second target and of the counter window respectively. By means of the explicit expression of $\mathrm{d}\omega_1$ and $\mathrm{d}\omega_2$, the above relation can be written as:

$$I(\beta)\,\frac{Ns\varrho}{A}\,\frac{\mathrm{d}S_1\,\mathrm{d}S_2}{r_{12}^2}\,\sigma(\vartheta_{1,2,3}, P_\perp, \beta)\,\frac{\mathrm{d}S_3}{r_{23}^2}\cos\delta_2\,. \tag{A.5}$$

As we have $\delta_2 \simeq 0$, we assume $\cos\delta_2 = 1$.

The relation (A.5) has to be integrated; let us note that in our geometry the variation of $\vartheta_{1,2,3}$, is very small when the point P_1 varies. For this reason it is convenient to perform the integration first on P_3 and successively on P_1, P_2, in such a way we are able to apply the mean value theorem for the integral of P_4. In fact the integral on P_3 is almost constant with respect to P_1. The integrated re-

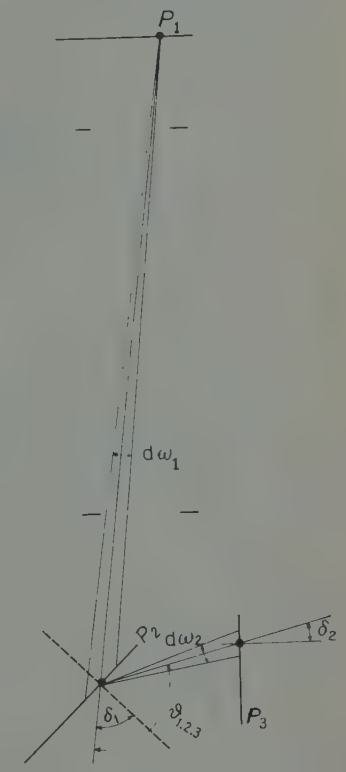

Fig. 4. – Sketch of the experiment.

(5) N. SHERMAN: *Phys. Rev.*, **103**, 1601 (1956).

lation (A.5) becomes:

$$(A.6)\qquad I(\beta)\frac{Ns\varrho}{A}\int_{S_2}\mathrm{d}S_2\int_{S_1(P_2)}\frac{\mathrm{d}S_1}{r_{12}^2}\int_{S_3(P_2)}\frac{r_{23}^2}{\mathrm{d}S_3}\sigma(\vartheta_{1,2,3},P_\perp,\beta)=$$

$$=I(\beta)\frac{Ns\varrho}{A}\int_{S_2}\mathrm{d}S_2\int_{S_3(P_2)}\frac{\mathrm{d}S_3}{r_{23}^2}\sigma(\vartheta_{1,2,3},P_\perp,\beta)\int_{S_1(P_2)}\frac{\mathrm{d}S_1}{r_{12}^2},$$

where $\vartheta_{2,3}$ is a mean value of $\vartheta_{1,2,3}$.

In the eq. (A.4) the integration domain $S_3(P_2)$, for any position of P_2, is always the whole useful surface on the counter. On the contrary $S_1(P_2)$ depends strongly on the position of P_2. In the following, the last integral on S_1 will be indicated with $\omega_1(P_2)$.

By integrating the second member of eq. (A.4) versus β we obtain, for the two orientations of $\boldsymbol{n}$, the electrons scattered in the two opposite directions. We obtain:

$$(A.7)\qquad \Delta_{\mathrm{th}}=2\frac{\displaystyle\int_{\beta_{\min}}^{\beta_{\max}}\mathrm{d}\beta I(\beta)P_\perp(\beta)\int_{S_2}\mathrm{d}S_2\omega_1(P_2)\int_{S_3}\frac{\mathrm{d}S_3}{r_{23}^2}\sigma_a(\vartheta_{2,3},\beta)}{\displaystyle\int_{\beta_{\min}}^{\beta_{\max}}\mathrm{d}\beta I(\beta)\int_{S_2}\mathrm{d}S_2\omega_1(P_2)\int_{S_3}\frac{\mathrm{d}S_3}{r_{23}^2}\sigma_i(\vartheta_{2,3},\beta)}.$$

The value $\beta_{\min}$ represents the velocity of electrons whose range is equal to the mica thickness the electrons must cross to be detected.

In the actual case, the effect is smaller than in an ideal case, in which scattering takes place in an infinitesimal angle around 90°, of about 30%. The transversal polarization, $P_\perp(\beta)$, is proportional to the longitudinal one, $P_\parallel(\beta)$, of the electrons coming out from the source in the normal direction. The proportionality factor depends on the target thickness and on the velocity β; it has been computed by the Montecarlo method for scattering at 90° by G. Adelson-Velsky and others (6). The multiple scattering in the source attenuates the $P_\parallel$ as compared to the polarization P_0 of the electrons emitted from the nucleus. Unfortunately we are able to evaluate this effect only in an approximate way.

The multiple scattering theory was exhaustively developed by G. Molière (7), but it is not sufficient to solve completely our problem. He obtains a function $f(\vartheta,t,\beta)$ that represents the probability that the electrons are deviated by an angle ϑ when they travel through a thickness t. If the electrons' velocity is small ($\beta\simeq 0$) the longitudinal component of the polarization is $P_0\cos\vartheta$. On the contrary, for $\beta\simeq 1$, this component is greater, because, in every single scattering the polarization precesses in the direction of momentum.

---

(6) See: A. I. Alikhanov, G. P. Eliseiev and V. A. Liubimov: *Nuclear Physics*, **7**, 655 (1958).

(7) G. Molière: *Naturforsch.*, **3-a**, 78 (1948).

3698

All which can be done to calculate $P_{\parallel}(\beta)$, is to use the relation:

$$P_{\parallel}(\beta) = \frac{\int_0^d \mathrm{d}t\, n(\beta_i)\, P_0(\overline{\beta}_i) \int_0^{\pi/2} \mathrm{d}\vartheta\, f(\vartheta, t, \overline{\beta}) \sin\vartheta \cos\vartheta}{\int_0^d \mathrm{d}t\, n(\overline{\beta}_i) \int_0^{\pi/2} \mathrm{d}\vartheta\, f(\vartheta, t, \overline{\beta}) \sin\vartheta}, \tag{A.8}$$

which represents a classical approximation, where the precession is not taken into account,

In this equation $n(\beta_i)$ and $P_0(\beta_i)$ are β-decay spectrum and polarization respectively. They are expressed as functions of the initial velocity $\beta_i = \beta_i(t)$ of the electrons emitted from nuclei placed at a depht in the source of thickness d. Obviously β_i is greater than the velocity of emission from the source because of the energy loss by ionization.

The function β_i has been evaluated using the empirical relation of L. Katz [8]. It has to be noted that, for the energies considered in our experiment, we have always $\beta_i < \beta + 0.1$. In Molière's function $f(\vartheta, t, \beta)$ we used a mean value β, equal to $(\beta + \beta_i)/2$. To evaluate the integrals of the eq. (A.8) we took into account, in the Molière function, the exponential and the first two correction terms alone.

In eq. (A.8) we did'nt take into account the electrons emitted in the backward direction, since they can come out forward bound only if they have been multiply scattered both within the layer below and the layer above the emission point.

Obviously this event is very unlikely. Moreover for this reason the integral in eq. (A.8) can be extended only to values of ϑ smaller of $\pi/2$.

This last approximation acts in the opposite sense to that introduced disregarding the precession and therefore partially counterbalances the former.

In such a way, assuming $P_0 = \beta$, we find $P_{\parallel}(0.6) = 0.38$. On the other hand we have evidently $P_{\parallel}(1) = 1$. By means of eq. (A.7) and using a linear approximation for $P_{\parallel}(\beta)$ we find: $\Delta_{\mathrm{th}} = 0.165$.

---

[8] L. Katz and A. J. Penfold: *Rev. Mod. Phys.*, **24**, 28 (1952).

RIASSUNTO

Nel presente lavoro si descrive una misura della polarizzazione longitudinale degli elettroni β, emessi da una sorgente di ^{204}Tl, eseguita mediante la tecnica del doppio scattering coulombiano. L'effetto osservato è più basso (circa il 10%) del valore previsto per elettroni di polarizzazione $-v/c$. I presenti risultati sono in accordo, entro gli errori, con quelli ottenuti in un precedente lavoro misurando la polarizzazione circolare dei γ di bremsstrahlung.

3999

IL NUOVO CIMENTO Vol. XIV, N. 4 16 Novembre 1959

Multiple Meson Production by 9 GeV Protons on Emulsion Nuclei.

E. M. Friedländer

Cosmic Ray Laboratory, Institute of Atomic Physics - Bucharest

(ricevuto il 17 Agosto 1959)

Summary. — 300 meson showers with $n_s \geqslant 4$ produced by 9 GeV protons in an emulsion stack have been analysed as to their multiplicity and angular distributions. It is shown that light and heavy target nuclei can be safely distinguished by the criterion $N_h \leqslant 4$, $N_h \geqslant 7$. The kinematical features of the collisions are consistent with emission of the shower particles from a single mass-center. The c.m.s. angular distribution of the shower particles is proved to be isotropic for all types of collisions. Individual c.m.s. Lorentz factors — γ_c have been estimated for every event. The distribution of γ_c-values agrees well with the predictions of the tunnel model of nucleon-nucleus collisions. The average tunnel lenghts for heavy and light nuclei have been found proportional to the nuclear radii. An excess of very high — γ_c and very low — γ_c events has been tentatively interpreted as due to peripheric collisions with pions in the meson cloud surrounding the colliding nucleons. The fractional energy transfer to pions is found independent of the target nucleus and equal to $\sim 33\%$. One outgoing particle (at least in some cases a pion) is often observed to carry away a large fraction of the available energy.

1. – Introduction.

Soon after the starting of the 9 GeV proton-synchrotron (1), some overall features of the beam proton interactions with nuclei in the photographic emulsion have been investigated. These include average multiplicity of shower

(1) N. P. Bogacev, Van Su Fen, I. M. Gramenitzkij, L. F. Kirillova, R. M. Lebedev, V. B. Liubimov, P. M. Markov, I. P. Merekov, M. I. Podgoretzkij, V. M. Sidorov, K. D. Tolstov and M. G. Safranova: *Atomnaia Energija*, **4**, 281 (1958).

particles, collisions m.f.p. ([1,2]), overall energy transfer to pions ([3]), strange particle production ([4]), secondary stars ([5]), etc. Special care was taken to avoid scanning bias, and thus the « natural mixture » of stars, with its overwhelming majority of low-multiplicity events (including *e.g.* elastic scatters) was used for the analysis.

The present investigation is concerned only with events of relatively high multiplicity of charged shower particles, which can be treated by means of the conventional methods, worked out for research on cosmic-ray jets.

Its main aims were:

a) to check the validity of procedures used in cosmic-ray research for the identification of target nuclei and for the estimation of the c.m.s. velocity, by making use of the monokinetic spectrum of the proton beam;

b) to investigate the mechanism of meson production in proton collisions with heavy and light nuclei, with special regard to the tunnel model of nucleon-nucleus interactions ([6-9]).

c) to obtain information on energy transfer to nucleons and/or mesons of very high energy.

2. – Irradiation, scanning and measurement.

A stack of 100 NIFKI-R emulsions, 10 cm×10 cm×0.04 cm each, was exposed to the internal beam of the Dubna proton synchrotron, circulating at a total proton energy of 9.2 GeV. The total dose was 10^4 proton/cm^2.

To date twenty plates were area scanned (*) for stars produced by beam

---

([2]) N. P. Bogacev, S. A. Buniatov, I. P. Merekov and V. M. Sidorov: *Dokl. Akad. Nauk SSSR*, **121**, 617 (1958).

([3]) G. L. Bayatian, I. M. Gramenitzkij, A. A. Nomofilov, M. I. Podgoretzkij and E. Skrzypczak: *Žurn. Èksp. Theor. Fiz.*, **36**, 690 (1959).

([4]) N. I. Kostanashvili and V. A. Shakhulashvili: *Žurn. Èksp. Theor. Fiz.*, **36**, 1006 (1959).

([5]) G. B. Zdanov, P. K. Markov, V. N. Streltzov, M. I. Tretiakova, Chwen-Pu-In and M. G. Safranova: *Proc. Bucharest Conf. on Cosmic Rays* (1959, under press)

([6]) C. B. A. McCusker and F. C. Roesler: *Nuovo Cimento*, **5**, 1136 (1953).

([7]) E. Friedländer: *St. Cerc. Fiz.* (*Bull. Phys. Inst. Bucharest in Roumanian*), **6**, 63 (1955).

([8]) C. Cocconi: *Phys. Rev*, **93**, 1107 (1954).

([9]) I. L. Rosental and D. D. Cernavskij: *Usp. Fiz. Nauk*, **52**, 185 (1954); *Fortschr. d. Phys.*, **4**, 560 (1956).

(*) A limited scan along the track was also performed, yielding a collision m.f.p. of (35±5) cm in good agreement with previous results ([1]).

protons and containing at least four shower particles (blob density $\leqslant 1.5$ times plateau) in the forward hemisphere in the laboratory system. This selection ensured that we were dealing with genuine multiple production, and also that at least a minimum of statistical information was available for the estimation of the c.m.s. velocity.

In such a scanning, there is an obvious bias against stars with no, or very few black prongs. Furthermore, as the incoming results drew our attention towards interactions with light nuclei, scanning was later on restricted to stars with $N_h \leqslant 4$ (*). Hence, no attempts will be made here to estimate absolute frequencies of stars with different values of N_h.

On each star, the space angles of emission of all shower particles with respect to the incoming proton track were measured. The analysis reported hereafter refers to a sample of 300 meson showers of multiplicity $n_s \geqslant 4$, measured in this way.

3. – Discrimination between heavy and light nuclei.

Ever since the first investigations on cosmic-ray jets, some criteria were sought which would enable one to discriminate between light (C, N, O) and heavy (Br, Ag) target nuclei in the photographic emulsion. Such criteria were usually based on the number of black prongs since from a light emulsion nucleus no more than 8 slow charged particles can be evaporated. On the other hand, after the discussion by HEITLER and TERREAUX ([10]), it is known that meson showers accompanied by a star with no, or very few black prongs can also be produced in a collision with a heavy nucleus; little is still known as to the probability of such events. In the case of cosmic-ray stars the problem is still complicated by the broad energy spectrum of the primaries and their widely varying nature. Hence all criteria advanced so far (say, $N_h \leqslant 6$, or 4, or even 2) were more or less arbitrary and, if too severely applied, had also the disadvantage of cutting down statistics.

The discrimination method used in the present work, which provides also a simultaneous check for the validity of the tunnel model, is based on the following idea:

If the incoming nucleon punches a tunnel through the target nucleus, and mingles with the ejected nucleons in an excited compound state from which mesons are emitted, this process is separated in time from the evaporation of the residual nucleus which occurs much later. Hence the fluctuations in the numbers of emitted mesons and of slow nucleons boiled off from the residual

(*) Bristol notations are used throughout.

([10]) W. HEITLER and C. H. TERREAUX: *Proc. Phys. Soc.*, **66**, 929 (1953).

3709

nucleus should be uncorrelated and the average multiplicity of shower particles $\overline{n}_s$ should be independent of the number N_h of heavy prongs, as long as the target nuclei are of one single kind.

On the other hand the number ν of ejected nucleons depends on the tunnel length which is greater in heavy nuclei ($\sim A^{\frac{1}{3}}$). In turn, the c.m.s. Lorentz factor γ_c is a decreasing function of ν and hence of A:

$$\gamma_c = (\gamma_0 + \nu)(1 + \nu^2 + 2\nu\gamma_0)^{-\frac{1}{2}}, \tag{1}$$

where γ_0 is the total energy of the incoming nucleon (*). For a given γ_0, the total energy available for meson production in the c.m.s.:

$$E^* = (1 + \nu^2 + 2\nu\gamma_0)^{\frac{1}{2}} - (\nu + 1) \tag{2}$$

is thus an increasing function of ν (cf. Fig. 1, curve a, and Fig. 2). Hence, the average multiplicity of meson showers produced in heavy nuclei would thus be expected to be larger than in light nuclei, on account of the higher available

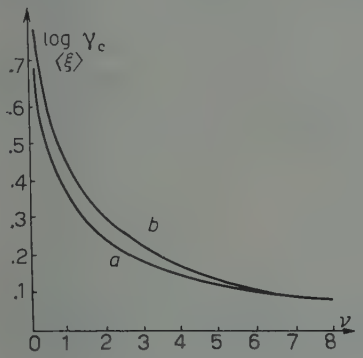

Fig. 1.

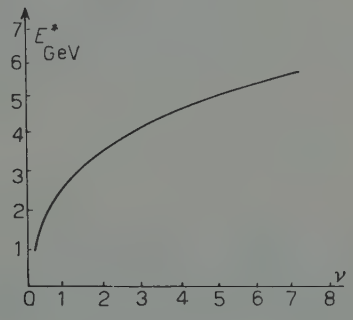

Fig. 2.

energy. Since in the photographic emulsions both species of target nuclei are present, the $\overline{n}_s$ versus N_h plot ought to have a step-like shape, with a transition zone in which light as well as heavy nuclei play comparable roles.

The dependence of n_s on N_h, averaged over suitable N_h intervals is displayed in Fig. 3. The shape of this plot is the predicted one, and leaves little doubt as to the fact that below $N_h = 4$ we are dealing practically only with light nuclei, while above $N_h = 7$ the target is a heavy nucleus. In the present

(*) We use units such that $M = c = 1$, where M is the nucleon mass.

analysis of 9 GeV meson showers, we have excluded all doubtful events ($N_h = 5 \div 6$) and considered only events with $N_h \leqslant 4$ (L-showers) and $N_h \geqslant 7$ (H-showers).

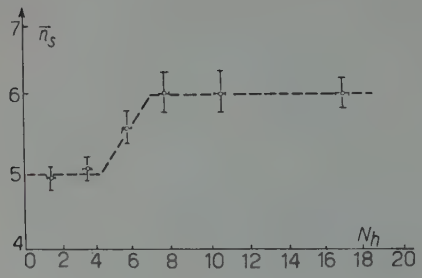

Fig. 3.

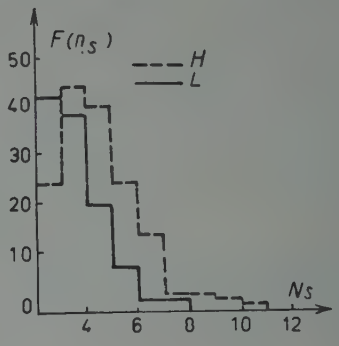

Fig. 4.

The multiplicity distributions for 115 L-showers (*) and 158 H-showers are shown in Fig. 4. The pronounced shift towards higher n_s values on the H-diagram is in good agreement with the higher $\bar{n}_s$ value for $N_h > 7$ as shown by Fig. 3. The average multiplicities (**) are respectively

$$(3) \qquad \begin{cases} (\bar{n}_s)_L = 5.24 \pm 0.14 , \\ (\bar{n}_s)_H = 6.00 \pm 0.30 . \end{cases}$$

The ratio

$$(\bar{n}_s)_H/(\bar{n}_s)_L = 1.15 \pm 0.06$$

is significantly lower than the value one would expect from a plural-type cascade process ([9]) *viz.* $> 2 \div 3$; it is, at least in qualitative agreement with the predictions of the tunnel model ([7,11]), *viz.* $1.2 \div 1.4$ (***).

(*) As stated in Sect. 2, part of the scanning was restricted to L-events only. This accounts for the relatively large number of L events.

(**) Barred symbols will refer to experimental averages, while $\langle\ \rangle$ brackets will be used for expectation values.

([11]) S. Z. Belenkij and L. D. Landau: *Usp. Fiz. Nauk*, **56**, 309 (1955); *Fortschr. d. Phys.*, **3**, 536 (1955).

(***) At extremely high energies, the hydrodynamical theory yields $n_s \sim A^{0.19}$ $(\bar{n}_s)_H/(\bar{n}_s)_L \sim 1.4$ ([11]). At the low energies considered here the approximation $\gamma_c \gg \nu$. made in ([11]) is no longer valid. Using the rigorous expression for the total available energy (Fig. 2) we obtain for this ratio the value ~ 1.2. The good agreement with experiment is rather surprising in view of the crudeness of the thermodynamical approximation at such low energies.

3704

4. – Angular distribution of shower particles.

Another consequence of the tunnel model is that the Lorentz factor γ_c of the c.m.s., should have only one of a set of discrete values according to eq. (1) for integer values of ν, since the primary energy γ_0 is constant. A check of this prediction can be made by means of the so called Castagnoli method ([12]) which, under our conditions has to be formulated as follows:

Define a random variable:

$$x \equiv \lg \operatorname{ctg} \theta \,, \tag{5}$$

where θ is the lab. angle of emission of a shower particle. Consider now the arithmetic mean of x for a given meson shower:

$$\xi \equiv \frac{1}{n_s} \sum_{i=1}^{n_s} x_i \,. \tag{5}$$

The quantity ξ is itself a random variable, whose distribution is connected in an obvious manner with that of x, *i.e.* with the angular distribution in the c.m.s. It has been shown ([12]) that if this latter distribution enjoys mirror symmetry about the aequatorial plane, and if the c.m.s. velocity β' of each particle is practically equal to the velocity β_c of the c.m.s. with respect to the lab. frame, the expectation value of ξ is:

$$\langle \xi \rangle = \lg \gamma_c \,.$$

It has also been shown ([13,14]) that most theories of meson production lead to a gaussian distribution of x about the average ξ, the standard deviation σ of this distribution being a measure of anisotropy (*). Hence, for a given γ_c (*i.e.* in our case for a given ν), ξ will also have a gaussian distribution with a standard deviation:

$$\sigma' = \sigma \cdot n_s^{-\frac{1}{2}} \,. \tag{8}$$

Since in a given nucleus, collisions with different values of ν do occur, one would expect the frequency distribution of ξ to be a superposition of gaussian

---

([12]) C. Castagnoli, G. Cortini, C. Franzinetti, A. Manfredini and D. Moreno: *Nuovo Cimento*, **10**, 1539 (1953).

([13]) L. v. Lindern: *Zeits. Naturfor.*, **11**, 340 (1956); *Nuovo Cimento*, **5**, 491 (1957)

([14]) P. Ciok, J. Coghen, J. Gierula, R. Hołynski, A. Jurak, M. Mięsowicz, J. Saniewska and J. Pernegr: *Nuovo Cimento*, **10**, 741 (1958).

(*) $\sigma = 0.36$ for isotropy; $\sigma > 0.36$ means forward-backward peaking.

curves corresponding to the different ν-values, with peaks lying in the vicinity of the values given by eqs. (7) and (1). The « resolving power » in such a « γ_c-spectrum » is given by σ' which, in turn, depends on the degree of c.m.s. anisotropy, *i.e.* on σ.

The experimentally observed distribution of ξ-values is shown in Fig. 5, separately for H- and for L-events. The arrows show the expectation values of ξ for different ν (*i.e.* for different tunnel lengths) computed by means of eqs. (7) and (1), and corrected for violation of the conditions $\beta' = \beta_c$ according to [15] (see Appendix and also Fig. 1, curve *b*).

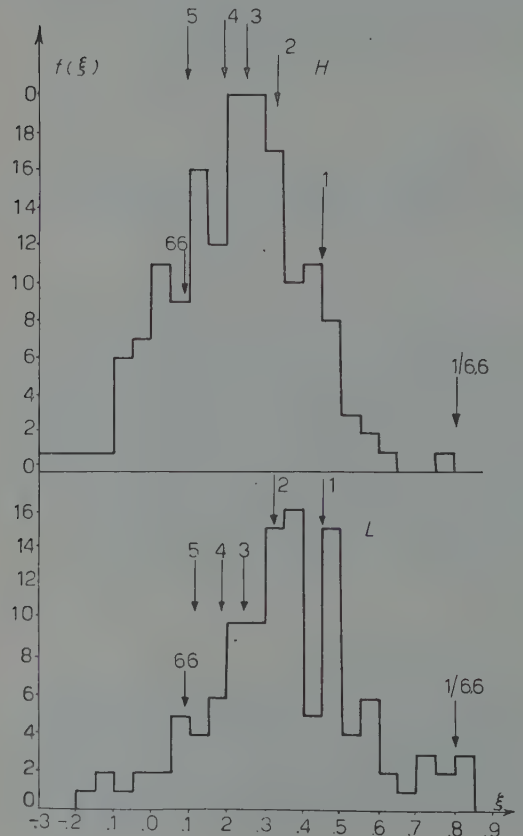

Fig. 5.

The conspicuous shift of the peak on the H-diagram towards higher ν-values, together with the much wider spread of this diagram, as a consequence of the interplay of collisions with widely varying ν-values is again in good qualitative agreement with the tunnel model. The average ξ-values are:

$$(9) \qquad \begin{cases} \bar{\xi}_H = 0\ 214 \pm 0\ 030\ . \\ \bar{\xi}_L = 0.344 \pm 0.024\ . \end{cases}$$

Using curve *b* of Fig. 1, we obtain therefrom:

$$(10) \qquad \begin{cases} \bar{\nu}_H = 3.4 \pm 0.5\ , \\ \bar{\nu}_L = 1.8 \pm 0.2\ . \end{cases}$$

The ratio of these experimentally obtained tunnel lengths is

$$(11) \qquad \bar{\nu}_H/\bar{\nu}_L = 1.89 \pm 0.19\ ,$$

which is to be compared with the ratio of nuclear radii

$$(12) \qquad \frac{\bar{R}_H}{\bar{R}_L} = \left(\frac{\bar{A}_H}{\bar{A}_L}\right)^{\frac{1}{3}} = 1.86\ .$$

[15] E. M. FRIEDLÄNDER: *Nuovo Cimento*, **12**, 483 (1959).

3706

The excellent agreement between the computed (12) and experimental (11) values, not only lends strong support to the tunnel model of jets, but also raises confidence in the usual methods of γ_c-estimation, provided the distribution of transverse momenta ([15]) is properly taken into account. A further argument supporting this conclusion is given by the dependence of $\bar{n}_s$ on ξ shown in Fig. 6-*a*. By means of Figs. 1-*b* and 2, this has been translated into a dependence of $\bar{n}_s$ on the available energy E^* (Fig. 6-*b*). This plot is consistent with a linear increase of $\bar{n}_s$ with E^* (*).

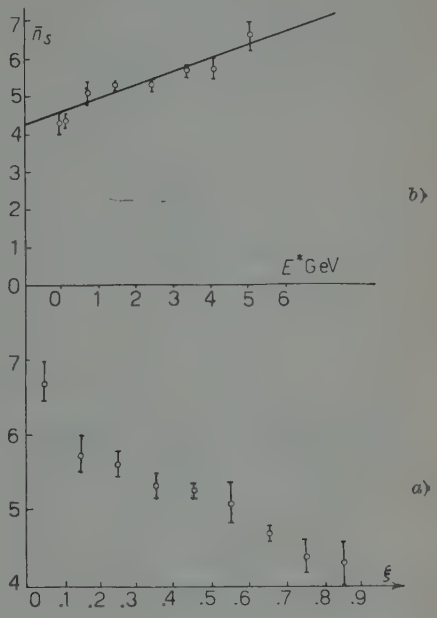

Fig. 6.

Returning to Fig. 5 some interesting features can be observed in the structure of the L-diagram.

First there is the clear-cut separation of events with $\nu = 1$ (nucleon-nucleon collisions) from the rest of the events. (This separation is much less pronounced in the H-diagram where the contribution of nucleon-nucleon collisions is expected to be small).

Then, the tails of the ξ-distribution, both at the high-ξ and low-ξ ends appear to contain more events than would result from the tails of gaussian curves centered about $\nu = 1$ and $\nu = 4$ (the upper limit for L-nuclei). A possible interpretation for these events is that they arise from glancing collisions in which only a « fraction of a nucleon » (*i.e.* $\nu < 1$) is affected. In other words, such collisions, ought to be understood as collisions with a pion in the meson cloud surrounding either the incident nucleon, or a peripheric nucleon of the target nucleus. In the first case, the quantity ν (which is to be understood here as the ratio of the masses of the colliding particles) is equal to 6.6 while in the second case it is 1/6.6. The corresponding expectation values for ξ are marked by arrows in Fig. 5 and the agreement with the observed humps on the histogram is quite encouraging. Nevertheless the statistical weight of this observation is rather poor and further arguments of physical character are needed in order to establish the existence of such glancing nucleon-pion

(*) In any comparison with results of other experiments it should be borne in mind that throughout this paper $\bar{n}_s$ is the average for $n_s \geqslant 4$.

collisions, (which have already been predicted on theoretical grounds for some time ([16-19])).

One such argument might be the observation of different physical characteristics (*e.g.* multiplicity or c.m.s. angular distribution) for showers with very large or very low γ_c-values. Thus in a nucleon-pion collision, the c.m.s. moves fast and only a small amount of energy is available in the c.m.s. for meson production. From Fig. 2 we obtain

$$E^*(\nu = 6.6) \approx 6.6\, E^*(\nu = 1/6.6)\,. \tag{13}$$

Such an effect is apparent in Fig. 6 *a* and *b*.

The L-showers have been split up into three groups denoted symbolically by L^-, L^0 and L^+:

$$L^-\colon\ \xi < 0.2\,; \qquad L^0\colon\ 0.2 \leqslant \xi \leqslant 0.5\,; \qquad L^+\colon\ \xi > 0.5\,. \tag{14}$$

If the interpretation outlined above is true, these three groups are expected to contain mostly:

L^-: pion-nucleon collisions,

L^0: nucleon-tunnel collisions,

L^+: nucleon-pion collisions.

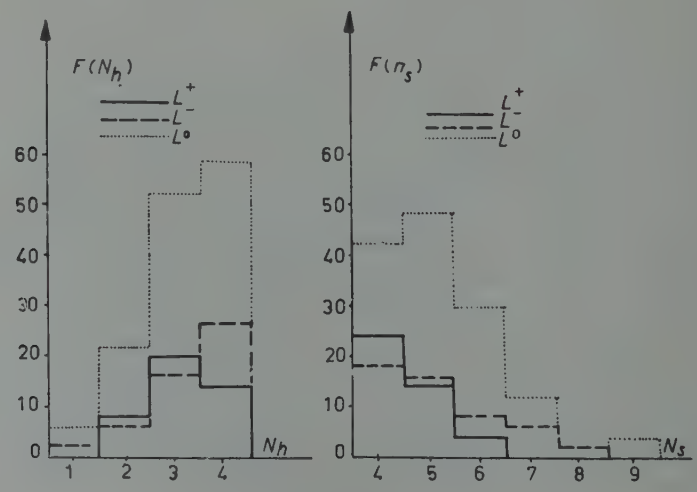

Fig. 7.

([16]) E. L. Feinberg and D. S. Cernavskij: *Dokl. Akad. Nauk SSSR*, **81**, 795 (1951).
([17]) E. M. Friedländer: *Acta Phys. Hung.*, **6**, 237 (1956).
([18]) D. S. Cernavskij: preprint.
([19]) N. M. Duller and W. D. Walker: *Phys. Rev.*, **93**, 215 (1954).

3708

The multiplicity distribution of shower particles n_s and heavy tracks N_h are displayed in Fig. 7. The striking difference between L^+ and L^- and the close resemblance of L^- and L^0 conform well to what one might expect if L^- and L^+ arose from pion-nucleon and nucleon-pion collisions.

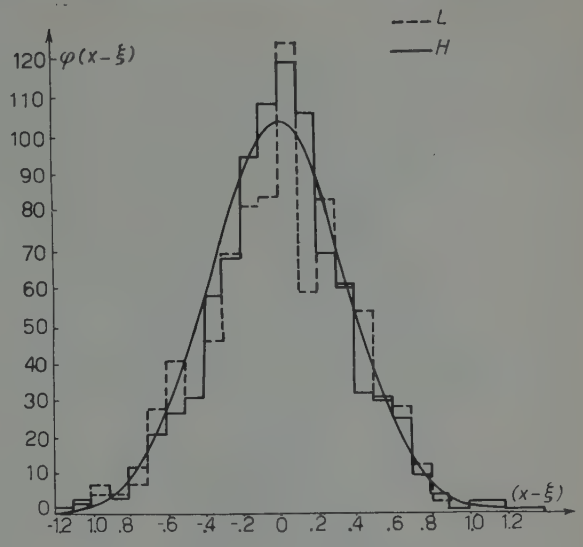

Fig. 8.

Now, one might argue that the large spread of the ξ-histogram is due not so much to a wide spread of the $\langle\xi\rangle$ values (*i.e.* to the contribution of glancing collisions leading to abnormally high or low γ_c-values) but rather to a « natural width » of the « γ_c-lines » corresponding to integer and allowed values of ν only; such a widening of the γ_c-lines could come from a strong anisotropy of the c.m.s. angular distribution such as predicted *e.g.* by the theories of Landau or Heisenberg. In this case the standard deviation σ of the x-distribution, (and consequently also the standard deviation σ' of the ξ distribution for a given γ_c) is much larger than in the case of isotropy. In order to check this argument the differential angular distribution of the quantity $x - \xi$ is plotted in Fig. 8, separately for H- and for L-events. The gaussian curves corresponding to isotropy ($\sigma = 0.36$) are als drawn. It can be seen that any difference between the theoretical curve and experiment, if existing at all, might have at most a tendency to lower the value of σ, not to enlarge it. The same is borne out by the Duller-Walker plots ([19]) shown in Fig. 9. The full lines of slope 2, passing through the origin are the theoretical prediction for isotropy ([19]), and the agreement with the experimental points is obvious. As a

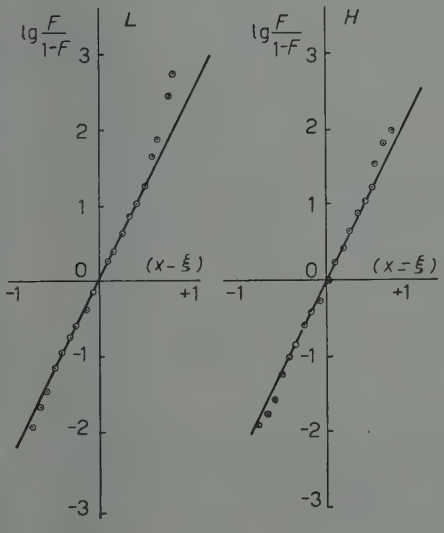

Fig. 9.

3709

ufrther check, isotropy in the c.m.s. was investigated separately for the L^-, L^0 and L^+ groups. The differential angular distributions are given in Fig. 10 and the (integral) Duller-Walker plots in Fig. 11. Pearsons χ^2-test yields satisfactory agreement with isotropy for all three distributions (see Table I).

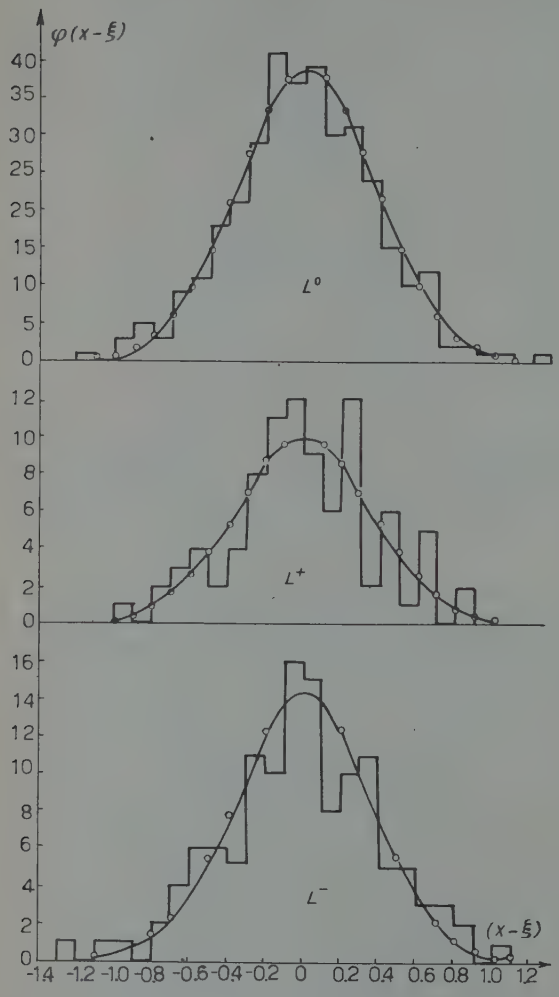

Fig. 10.

Thus, the spread of the ξ-distribution cannot be due to a strong anisotropy of the c.m.s. angular distribution.

The last column of Table I contains the number of tracks used in each group. It is interesting to remark that, contrary to purely statistical expectations, the Pearson probability $\mathscr{P}_{\chi^2}$ decreases with decreasing sample size. This might be an indication for some systematic deviation from isotropy in the L^- and especially in the L^+ group. Such a deviation can indeed be seen on the differential distributions of Fig. 10 which show a systematic drop about $\xi \sim 0.1$. (The same drop appears—albeit very washed out—in the L^0-group too, probably because of some small admixture of L^+ or L^- cases to the L^0- group). If further enlarged statistics will

Table I.

Group	χ^2	Degrees of freedom	P_{χ^2} (%)	Sample size
L^0	7.6	11	75	346
L^-	6.9	8	55	126
L^+	10.7	7	15	90

3710

confirm the existence of such an effect (which, as shown by Table I is at present not statistically significant), it might provide some clue for the understanding of meson-nucleon interactions.

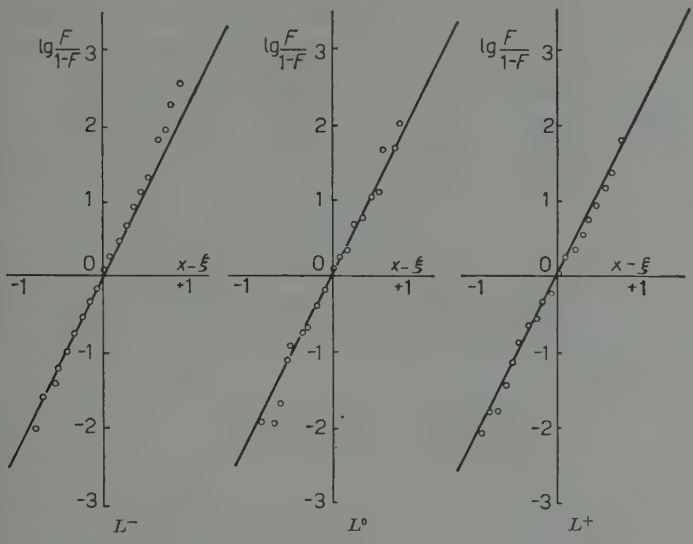

Fig. 11.

5. – Energy transfer.

The problem of energy transfer in meson showers is directly related to the theory of the elementary process. It is a characteristics feature of some theories that they predict the concentration of a large fraction of the incident energy on one or on very few outgoing particles. Direct detection of such an energetically priviledged particle has met until now with considerable difficulties, and only indirect evidence has generally been available such as longitudinal evolution of extensive air-showers ([20]), absorption length of the Cosmic-ray N-component ([21]), etc. Even if in some cases the existence of such a highly energetic secondary seems to be proved, the question still remains open as to the nature of such a particle ([22,23]). This means that it is still unsettled whether the energetic secondary is always a nucleon, or whether it may be some times a pion. A comparative analysis of cosmic ray jets produced by primary

([20]) N. Dobrotin: *Proc. Budapest Conf. on Cosmic Rays* (1956).
([21]) G. T. Zacepin: *Žurn. Èksp. Theor. Fiz.*, **19**, 1104 (1949).
([22]) N. Grigorov and N. Murzin: *Izv. Akad. Nauk SSSR, S. Fiz.*, **17**, 21 (1953).
([23]) E. M. Friedländer and E. Ruckenstein: *Žurn. Èksp. Theor. Fiz.*, **35**, 104 (1958).

protons and (secondary) high-energy neutrons ([24]) showed that, on the average, neutrons carry away less than 50% of the primary energy. Similar results were obtained from an analysis of secondary stars produced by the outgoing particles from 9 GeV interactions ([5]).

We have tried to detect the existence of such an energetically preferred particle and to obtain some indication as to its nature by making use of the approximate constancy of transverse momenta ([25,26]) and by a study of forward-backward asymmetry of shower particles in the lab. system.

Denote by q the ratio:

$$q \equiv \frac{p}{p_T} = \operatorname{cosec} \theta \,, \tag{15}$$

where p and p_T are respectively the momentum and transverse momentum of a particle emitted at a lab. angle θ.

If p_T is constant, we have

$$\langle q \rangle = \frac{1}{p_T} \langle p \rangle \,, \tag{16}$$

where the average is taken over a given shower. Now, p_T is known really not to be constant, but to obey a rather narrow distribution (gaussian in $\log p_T$ co-ordinates) about a constant mean. For the following we shall not need a strict constancy of p_T, but only statistical independence of p and p_T, such that

$$\langle q \rangle = \left\langle \frac{1}{p_T} \right\rangle \cdot \langle p \rangle \,. \tag{17}$$

Theoretically such an independence arises from the fact that the transverse momentum component is due mostly to the thermal motion of the created particles ([27]).

On the other hand, measurements on the same proton beam ([3]) have shown that, on the average, a fraction $K \sim 0.30$ of the primary energy γ_0 is transferred to pions. This leaves either $\sim 0.7\gamma_0$ for a single fast nucleon or correspondingly less if this energy is shared among several high-energy secondaries.

([24]) E. M. FRIEDLÄNDER: *Proc. Liblice Conf. Cosmic Rays*; *Proc. Buch. Conf. Cosmic Rays* (1959, under press).

([25]) J. NISHIMURA: quoted by Z. KOBA in *Progr. Theor. Phys.*, **17**, 288 (1957).

([26]) G. B. ZDANOV: *Žurn. Èksp. Teor. Fiz.*, **34**, 856 (1958).

([27]) G. A. MILECIN and L. L. ROSENTHAL: *Suppl. Nuovo Cimento*, **12**, 770 (1958).

3712

Assuming charge symmetry for pions, one may write

$$\langle p \rangle \approx \frac{2}{3} \frac{K\gamma_0}{n_s}, \tag{18}$$

and hence

$$\langle q \rangle \approx \frac{2}{3} \frac{K\gamma_0}{n_s} \left\langle \frac{1}{p_T} \right\rangle . \tag{19}$$

Using the distribution of $\log p_T$ and the numerical values given in ([26]) and ([15]) we obtain

$$\left\langle \frac{1}{p_T} \right\rangle = \frac{0.94}{\mu}, \tag{20}$$

where μ is the pion mass. With this value, and $K \sim 0.3$, eq. (19) becomes

$$n_s \bar{q} = \sum_{i=1}^{n_s} \operatorname{cosec} \theta_i \approx 13 . \tag{21}$$

Owing to the narrow distribution of p_T, most fluctuations in (21) are expected from deviation from charge symmetry. The standard deviation of these fluctuations is $\lesssim 3$.

Assume now that the sum in eq. (21) includes one outgoing nucleon of very high energy. In order to conserve transverse momentum, such a particle ought to move very close to the shower axis ($\theta \ll 1$). Hence inclusion of such a particle into the sum (21) would yield an abnormally large $n_s \bar{q}$-value and also a similarly large $\bar{q}$-value. If this track is eliminated, $n_s \bar{q}$ and $\bar{q}$ should both drop back to normal.

The distribution of $\bar{q}$ is plotted in Fig. 12-*a*, separately for *H*- and for *L*-events. As can be seen, both distributions have long tails towards large $\bar{q}$-values. In all showers in which $\sum$ cosec θ_i exceeded 16 (*i.e.* 13 +one standard deviation), the particle moving at the smallest angle to the shower axis was excluded. The distributions of $\bar{q}$ obtained in this way are shown in Fig. 12-*b*. A comparison of Fig. 12-*a* and Fig. 12-*b* shows quite convincingly that fairly often (in $\sim 40\%$ of the *L*-events and $\sim 30\%$ of the *H*-events) one (*) particle carries away an energy significantly above the average.

Averaging $\bar{q}$ over the histograms in Fig. 12-*b* we obtain

$$\begin{cases} \bar{\bar{q}}_H = 2.28 \pm 0.05 , \\ \bar{\bar{q}}_L = 2.94 \pm 0.06 . \end{cases} \tag{22}$$

(*) Only in 13 cases out of 273 had a second particle to be excluded in order to bring $\sum$ cosec θ_i below 16.

Since $\langle 1/p_T \rangle$ does not depend on the nature of the target nucleus, we expect

$$\frac{\bar{\bar{q}}_H}{\bar{\bar{q}}_L} = \frac{(\overline{n}_s)_L}{(\overline{n}_s)_H} \cdot \frac{\alpha_H}{\alpha_L} \cdot \frac{(\gamma_c E^*)_H}{(\gamma_c E^*)_L}, \tag{23}$$

where α is the fraction of the available c.m.s. energy E^*, going into meson production, and the indices L and H refer respectively to L- and H-events.

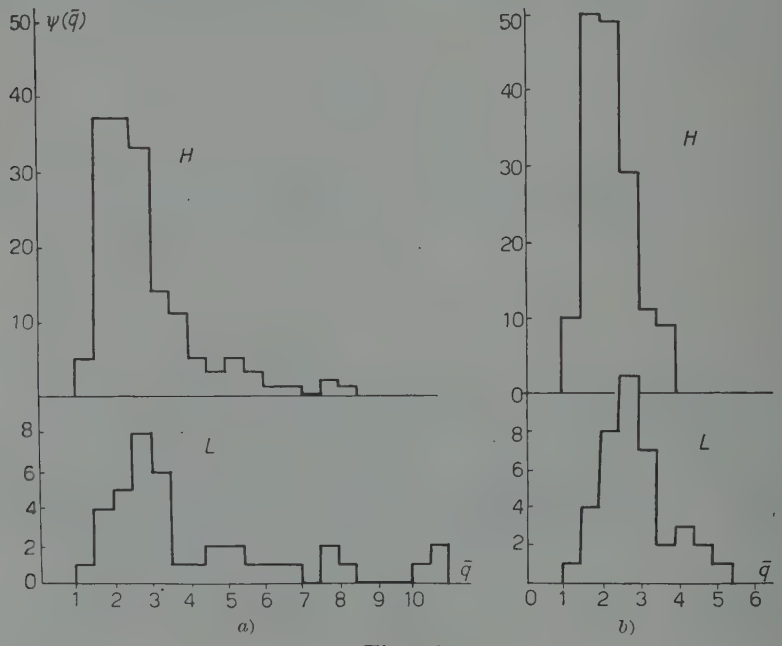

Fig. 12.

Using our experimental $\overline{n}_s$ values we obtain therefrom:

$$\frac{\alpha_H}{\alpha_L} = 1.01 \pm 0.07\,, \tag{24}$$

i.e. the same fraction of the available energy is used up for meson production in light and heavy nuclei. Hence, starting from any of the $\bar{q}$-values one can compute the apparent inelasticity K which is related to α by the equation

$$K\gamma_0 = \alpha E^* \gamma_c\,. \tag{25}$$

We obtain from our experimental values

$$K = (0.33 \pm 0.02) \tag{26}$$

3714

in excellent agreement with results obtained by direct measurement on π^0-produced pairs ([3]).

As to the nature of the high-energy secondary, some information can be obtained by a study of stars containing at least one shower particle in the backward hemisphere in the lab. system (for the sake of brevity, such stars will be called hereafter B-events, and the shower particles emitted backward, B-particles).

This is the case in $(15 \pm 3)\%$ of the L-events and $(29 \pm 4)\%$ of the H-events. Of the total number of shower particles $(3.6 \pm 0.8)\%$ in L-events and $(5.2 \pm 0.7)\%$ in H-events are B-particles. Comparing the relative frequency of B-events and B-particles with the observed shower multiplicities, we see that most B-events contain only one B-particle. The average numbers of B-particles per B-event are respectively (1.25 ± 0.37) for L-events and (1.07 ± 0.18) in H-events.

The increased fraction of B-events among H-events is in good agreement with the predictions of the tunnel model since with increasing ν, γ_c and hence β_c decrease. As is well known, backward emission in the lab. system is possible only if $\beta' > \beta_c$, where β' is the c.m.s. velocity of the B-particle. Now the condition $\beta' > \beta_c$ can be realized in one (or both) of the two following ways:

a) γ_c is very low and although all shower particles have relatively low energies one of them falls by chance in the allowed backward cone of opening θ':

$$\cos\theta' \leqslant -\frac{\beta_c}{\beta'}, \tag{27}$$

or

b) one particle is emitted backwards with high energy $(\gamma' > \gamma_c)$.

In Fig. 13 we have plotted the distribution on ξ-values for B-events in H- and L-showers.

In both diagrams the events appear separated into two groups of high and low γ_c. The low-γ_c B-events can be explained by either of the two mechanisms, but the high-γ_c events (corresponding to $\nu \leqslant 1$) imply necessarily one high-energy B-particle. Indeed, the target nucleons move backwards in the c.m.s. with velocity $\beta_t' = \beta_c$ (per definitionem!). Hence they can never appear in the l-system at angles exceeding $\pi/2$. Suppose now that all pions have in the c.m.s. the same energy $\mu\gamma'$ with

Fig. 13.

$\gamma' > \gamma_c$ so that a fraction $\frac{1}{2}(1 - (\beta_c/\beta'))$ can appear as B-particles (on account of c.m.s. isotropy). Their total energy would exceed $1.5\, n_s \mu \gamma_c \approx 2.8$ GeV in the c.m.s., and ~ 6.5 GeV in the lab. sistem *i.e.* $\sim 72\%$ of the incident energy. This contrasts with the well-established value of $\sim 33\%$. Hence we are forced to admit that, at least in part of the B-events one pion is ejected backwards with an energy considerably exceeding the average. A similar pion would be expected—from symmetry reasons—in the c.m.s. forward cone. In the lab. system such a particle might then carry an appreciable fraction of the total incident energy.

6. – Conclusions.

a) For showers with $n_s \geqslant 4$, light and heavy target nuclei in the photographic emulsion can be safely distinguished by the criterion

$$N_h \leqslant 4 , \qquad N_h \geqslant 7 .$$

b) The average multiplicities of showers with $n_s \geqslant 4$ produced by 9 GeV protons in light and heavy nuclei are respectively:

$$(\overline{n}_s)_L = 5.24 \pm 0.14 ,$$

$$(\overline{n}_s)_H = 6.00 \pm 0.30 .$$

c) The dependence of the average multiplicity on N_h is in good agreement with the tunnel model of meson-producing nuclear collisions.

d) The same conclusion as to the validity of the tunnel model can be drawn from the spectrum of γ_c values. The average tunnel lengths (expressed in numbers of nucleons are respectively):

$$\overline{\nu}_H = 3.4 \pm 0.5 ,$$

$$\overline{\nu}_L = 1.8 \pm 0.2 .$$

These tunnel lengths turn out to be proportional to the corresponding nuclear radii.

e) The angular distribution in the c.m.s. for all types of events cannot be distinguished from an isotropic one. If slight departures from isotropy occur at all, they favour emission in the aequatorial plane. No forward-backward peaking is observed.

f) From *d*) and *e*) there follows that all (or nearly all) shower particles are emitted from a single mass-center. This is in flagrant contradiction with the assumption of an intranuclear cascade ([28]) and proves the validity of the tunnel model.

g) In part of the collisions a particle of sub-nucleonic mass seems to be involved. Reasonable agreement with theoretical predictions is obtained if it is assumed that the collision occurs with a « peripheric » pion in the meson cloud of one of the colliding nucleons.

h) In 35% of the events one charged secondary is emitted with very high energy at a very small angle to the shower axis. In most cases this particle carries an energy comparable with the sum of the energies of all other particles.

i) The fractional energy transfer to pions is the same in heavy and in light nuclei.

j) The fractional energy transfer to pions is $\sim 33\%$ in good agreement with direct energy measurements on π^0-decay products ([3]). The average transverse momentum of the shower particles is $\sim 1.8\,\mu$.

k) If the c.m.s. energy distribution has mirror symmetry about the aequatorial plane, at least some of the high-energy secondaries must be pions.

* * *

The author is very indebted to the Direction of the Joint Institute for Nuclear Research-Dubna, and especially to Professors M. Danysz and Wang-Kan-Chan for the exposed and processed plates, to Prof. I. Ausländer, Mr. S. Alper and Miss M. Spîrchez for useful discussions, to Miss V. Dumitrescu for careful line-scanning and help in the measurements, to Miss M. Gheorghiu and M. Ioniță for help in the computations and to the scanner team, Miss I. Calogheri, E. Hirina, T. Marinescu, A. Spînu and C. Ungureanu for efficient scanning.

Appendix

As has been shown in ([15]) the distribution of transverse momenta ([26]) leads to a $\sim 20\%$ correction of the Castagnoli estimate for γ, if $\gamma_c \gg \gamma'$; in our case this condition is fulfilled practically only for $\nu \leqslant 1$ (*i.e.* for nucleon-nucleon and glancing nucleon pion collisions). For $\nu > 1$ the correction is smaller

([28]) G. Bozoki, E. Fenyves, E. Gombosi and F. Suranyi: *Proc. Bucharest Conf. on Cosmic Rays* (1959, under press).

since γ_c decreases and γ' increases. This can be taken approximately into account by using the curves in Figs. 1 and 2 and the observed multiplicities, in order to compute the average value of γ'/γ_c, and applying a correction to the Castagnoli estimate for γ_c which is proportional to the correction needed in the quantile estimate ([15]). Indeed, similar corrections have been proved to apply to both estimates. So the correction term has been taken equal to

$$\log \frac{1.30}{\{1 + 1.72\,(1 - \langle \gamma'/\gamma_c \rangle^2)\}^{\frac{1}{2}}} .$$

By adding these terms to the corresponding ξ values we obtain curve b of Fig. 1.

RIASSUNTO (*)

Sono stati analizzati, in relazione alla loro molteplicità ed alle loro distribuzioni angolari, 300 sciami mesonici con $n_s \geqslant 4$ prodotti da protoni di 6 GeV in un pacchetto di emulsioni. Si dimostra che i nuclei bersaglio, sia pesanti che leggeri, possono essere distinti in maniera soddisfacente per mezzo del criterio $N_h \leqslant 4$, $N_h \geqslant 7$. Le caratteristiche cinematiche delle collisioni sono coerenti con l'emissione delle particelle dello sciame da parte di un singolo centro di massa. Si prova che la distribuzione angolare del s.c.m. delle particelle dello sciame è isotropica per tutti i tipi di collisioni. Sono stati stimati, per ogni evento, i fattori individuali γ_c di Lorentz del s.c.m. La distribuzione dei valori γ_c è in buon accordo con le previsioni del modello a tunnel sulle collisioni nucleone-nucleo. Si è riscontrato che le lunghezze medie dei tunnel sono proporzionali, sia per i nuclei leggeri che per i nuclei pesanti, ai raggi nucleari. Si è tentato di interpretare un eccesso di eventi $-\gamma_c$, rispettivamente molto alti e molto bassi, come dovuto a collisioni periferiche con pioni della nube mesonica circondante i nucleoni collidenti. Si trova che la frazione di energia trasmessa ai pioni è indipendente dal nucleo bersaglio e che è uguale a $\sim 33\%$. Si osserva sovente che una singola particella emessa (un pione, almeno in alcuni casi) assorbe una frazione notevole dell'energia disponibile.

(*) *Traduzione a cura della Redazione.*

5718

IL NUOVO CIMENTO Vol. XIV, N. 4 16 Novembre 1959

A Soluble Model in Field Theory - I.

E. Kazes

Physics Department, The Pennsylvania State University - University Park, Pa. (*)

(ricevuto il 17 Agosto 1959)

Summary. — The Lee model has been modified by giving the V-particle a more complicated structure, and still leaving the π-θ scattering amplitude exactly soluble. This modification also yields a wider variety of soluble processes. The same limitation that applies to the cut-off size in the Lee model is reproduced in this model. The calculation is performed by using the Hamiltonian formalism as well as dispersion methods.

Introduction.

Soluble field theories have in the past been used as a guide to the structure of realistic field theory problems and also to the properties of decaying particles. In this spirit we have generalized the Lee model by giving the V-particle a great deal more structure without modifying the π or θ particles in the Lee model ([1,2]). In the model presented below mass and wave function renormalization can be performed exactly and, in contrast to the Ruijgrok-Van Hove ([3]) model, vertex renormalization is not required. In this sense our model is more like the Lee model and unlike the Ruijgrok-Van Hove model in that scattering and production amplitudes can be calculated exactly. In this paper it will be assumed that the free and complete Hamiltonians have corresponding stable one particle states. In a subsequent paper unstable particle description within this model will be presented.

(*) Supported in part by the Atomic Energy Commission.

(1) T. D. Lee: *Phys. Rev.*, **98**, 1329 (1954).

(2) G. Källén and W. Pauli: *Dan. Mat. Fys. Medd.*, **30**, no. 7 (1955).

(3) Th. W. Ruijgrok and L. Van Hove: *Physica*, **22**, 880 (1956); Th. W. Ruijgrok: *Physica*, **24**, 185, 205 (1958).

In Section 1 the problem is solved using the Hamiltonian formalism; in Section 2 the same results are obtained using dispersion methods.

1. – The model and its direct solution.

In this Section we shall present the model in its restricted form involving fermions ψ_1, ψ_2, ψ_3, ψ_4 in interaction with bosons φ_2, φ_3, φ_4 such that [4]

$$\psi_2 + \varphi_2 \rightleftarrows \psi_1$$

$$\psi_3 + \varphi_3 \rightleftarrows \psi_1$$

$$\psi_4 + \varphi_4 \rightleftarrows \psi_3$$

are the only possible elementary processes. The generalization to an arbitrary number of such processes will be discussed later. The Lee model is obtained by restricting the number of such processes to one; in that case the ψ_1, ψ_2, φ_2 particles would correspond to the V, $\mathcal{N}$, $\varkappa$ particles respectively. Let

$$H = H_0 + H_I \tag{1.1}$$

and

$$H_0 = m_1\psi_1^+\psi_1 + m_2\psi_2^-\psi_2 + m_3\psi_3^+\psi_3 + m_4\psi_4^+\psi_4 + \sum_{\boldsymbol{k}} \omega_2(k)a_2^+(\boldsymbol{k})a_2(\boldsymbol{k}) + \tag{1.2}$$

$$+ \sum_{\boldsymbol{k}} \omega_3(\boldsymbol{k})a_3^+(\boldsymbol{k})a_3(\boldsymbol{k}) + \sum_{\boldsymbol{k}} \omega_4(k)a_4^+(\boldsymbol{k})a_4(\boldsymbol{k}) .$$

$$H_I = g_2^0\left(\sum_{\boldsymbol{k}} \frac{u(\omega_2)}{\sqrt{2\omega_2 V}}\, a_2(\boldsymbol{k})\psi_1^+\psi_2 + \text{h.c.}\right) + g_3^0\left(\sum_{\boldsymbol{k}} \frac{U(\omega_3)}{\sqrt{2\omega_2 V}}\, a_3(\boldsymbol{k})\psi_1^+\psi_3 + \text{h.c.}\right) + \tag{1.3}$$

$$+ g_4^0\left(\sum_{\boldsymbol{k}} \frac{R(\omega_4)}{\sqrt{2\omega_4 V}}\, a_4(\boldsymbol{k})\psi_3^+\psi_4 + \text{h.c.}\right) - \delta m_1\psi_1^+\psi_1 - \delta m_3\psi_3^+\psi_3 ,$$

with

$$\begin{cases} \omega_2(k) = \sqrt{\mu_2^2 + k^2} , \\ \omega_3(k) = \sqrt{\mu_3^2 + k^2} , \\ \omega_4(k) = \sqrt{\mu_4^2 + k^2} . \end{cases} \tag{1.4}$$

In eq. (1.3) u, U, R are cut-off functions. All the masses that appear in H_0 are observed masses. The field operators will be required to satisfy the fol-

---

[4] Particles and field operators will be denoted by the same symbol.

lowing commutation relations,

$$(1.5)\qquad \begin{cases} \{\psi_i^+, \psi_j\} = \delta_{i,j} \\ \{\psi_i, \psi_j\} = 0 \\ [a_i(\boldsymbol{k}), a_j^+(\boldsymbol{k}')] = \delta_{ij}\delta_{\boldsymbol{k},\boldsymbol{k}'} \\ [a_i(\boldsymbol{k}), a_j(\boldsymbol{k}')] = [a_i(\boldsymbol{k}), \psi_j] = [a_i(\boldsymbol{k}), \psi_j^+] = 0 . \end{cases}$$

The following occupation number operators commute with H

$$(1.6)\qquad \begin{cases} Q_1 = \psi_1^+\psi_1 + \psi_2^+\psi_2 + \psi_3^+\psi_3 + \psi_4^+\psi_4 , \\ Q_2 = \psi_2^+\psi_2 - \sum_{\boldsymbol{k}} a_2^+(\boldsymbol{k})a_2(\boldsymbol{k}) , \\ Q_3 = \psi_3^+\psi_3 + \psi_4^+\psi_4 - \sum_{\boldsymbol{k}} a_3^+(\boldsymbol{k})a_3(\boldsymbol{k}) , \\ Q_4 = \psi_4^+\psi_4 - \sum_{\boldsymbol{k}} a_4(\boldsymbol{k})a_4(\boldsymbol{k}) . \end{cases}$$

The eigenstates of H_0 will be denoted by

$$(1.7)\qquad |n_1, n_2, n_3, n_4;\ n_2', n_3', n_4'\rangle ,$$

where n_1, n_2, n_3, n_4 are the numbers of ψ_1, ψ_2, ψ_3, ψ_4 particles and n_2', n_3', n_4' the numbers of φ_2, φ_3, φ_4 particles respectively. This basis will be used to expand the eigenstates of H. Let $|\psi_1\rangle$ represent the phyiscal ψ_1 particle such that

$$(1.8)\qquad H|\psi_1\rangle = m_1|\psi_1\rangle .$$

Expanding $|\psi_1\rangle$ with the basis (1.7)

$$(1.9)\qquad |\psi_1\rangle = Z_2^{\frac{1}{2}}[|1, 0, 0, 0;\ 0, 0, 0\rangle + \sum_{\boldsymbol{k}'} \Phi_2^{(1)}(\boldsymbol{k}')|0, 1, 0, 0;\ \boldsymbol{k}', 0, 0\rangle + \\ + \sum_{\boldsymbol{k}'} \Phi_3^{(1)}(\boldsymbol{k}')|0, 0, 1, 0;\ 0, 1_{\boldsymbol{k}'}, 0\rangle + \sum_{\boldsymbol{k}',\boldsymbol{k}''} \Phi_4^{(1)}(\boldsymbol{k}', \boldsymbol{k}'')|0, 0, 0, 1;\ 0, 1_{\boldsymbol{k}'}, 1_{\boldsymbol{k}''}\rangle] .$$

Substituting $|\psi_1\rangle$ in eq. (1.8) and using eq. (1.2), (1.3) and (15.) we get

$$(1.10)\qquad \Phi_1^{(1)}(\boldsymbol{k}') = g_2^0 \frac{1}{m_1 - m_2 - \omega_2'} \frac{u(\omega')}{\sqrt{2\omega' V}} ,$$

$$(1.11)\qquad \Phi_3^{(1)}(\boldsymbol{k}')\left[m_1 - m_3 + \delta m_3 - \omega_3' - g_4^{0^2} \sum_{\boldsymbol{k}} \frac{R(\omega_4)}{\sqrt{2\omega_4 V}} \frac{1}{m_1 - (m_4 + \omega_4 + \omega_3')}\right] = g_3^0 \frac{U(\omega_3')}{\sqrt{2\omega' V}} .$$

$$(1.12)\qquad \Phi_4^{(1)}(\boldsymbol{k}', \boldsymbol{k}'') = \frac{g_4^0}{m_1 - (m_4' + \omega_3' + \omega_4'')} \Phi_3^{(1)}(\boldsymbol{k}') \frac{R(\omega_4'')}{\sqrt{2\omega_3' V}} .$$

Normalizing the physical $|\psi_1\rangle$ state to unity and substituting eq. (1.10), (1.11), (1.12) in (1.9) yields

$$\frac{1}{Z_2(1)} = 1 + g_2^{02} \sum_k \frac{u(\omega_2)^2}{2\omega_2 V} \frac{1}{(m_1 - m_2 - \omega_2)^2} + \tag{1.13}$$

$$+ g_3^{02} \sum_k \frac{U(\omega_3)^2}{2\omega_3 V} \frac{1}{L(m_1 - \omega_3)^2 (m_1 - m_3 - \omega_3)^2} \left(1 + g_4^{02} \sum_{k'} \frac{R(\omega_4')^2}{2\omega_4' V} \frac{1}{(m_1 - m_4 - \omega_3 - \omega_4')^2}\right).$$

And the eigenvalue equation for $|1, 0, 0, 0; 0, 0, 0\rangle$ in eq. (1.8) gives

$$\delta m_1 = g_2^{02} \sum_k \frac{u(\omega_2)^2}{2\omega_2 V} \frac{1}{m_1 - m_2 - \omega_2} + \tag{1.14}$$

$$+ g_3^{02} \sum_k \frac{U(\omega_3)^2}{2\omega_3 V} \frac{1}{(m_1 - m_3 - \omega_3) L(m_1 - \omega_3)}.$$

where

$$L(x - \omega_3) = 1 + g_4^{02} \sum_k \frac{R(\omega_4)^2}{2\omega_4 V} \frac{1}{(m_3 - m_4 - \omega_4)(x + i\varepsilon - m_4 - \omega_3 - \omega_4)}. \tag{1.15}$$

The renormalized coupling constant corresponding to g_2^0 is

$$g_2 = Z_2^{\frac{1}{2}}(1)\, g_2^0. \tag{1.16}$$

As in the Lee model if g_2 is fixed and the cut-off goes to infinity the bare coupling constants become imaginary. The wave function and mass renormalization for the physical state of the ψ_3 particle is

$$\frac{1}{Z_2(3)} = 1 + g_4^{02} \sum_k \frac{R(\omega_4)^2}{2\omega_4 V} \frac{1}{(m_3 - m_4 - \omega_4)^2}, \tag{1.17}$$

$$\delta m_3 = g_4^{02} \sum_k \frac{R(\omega_4)^2}{2\omega_4 V} \frac{1}{m_3 - m_4 - \omega_4}, \tag{1.18}$$

and the renormalized coupling constants g_3 and g_4 are given by

$$g_3 = Z_2^{\frac{1}{2}}(1)\, Z_2^{\frac{1}{2}}(3)\, g_3^0, \tag{1.19}$$

$$g_4 = Z_2(3)^{\frac{1}{2}} g_4^0. \tag{1.20}$$

Let $|\psi_2, \varphi_2\rangle$ be the outgoing ψ_2, φ_2 scattering state such that

$$H|\psi_2, \varphi_2\rangle = (m_2 + \omega_2)|\psi_2, \varphi_2\rangle. \tag{1.21}$$

3722

Expanding this state in terms of the eigenstates of H_0

$$(1.22)\qquad |\psi_2, \varphi_2\rangle = \beta\,|1,0,0,0;\,0,0,0\rangle + \sum_{k'} \Phi_2(k')\,|0,1,0,0;\,1_{k'},0,0\rangle + \\ + \sum_{k'} \Phi_3(k')\,|0,0,1,0;\,0,1_{k'},0\rangle + \sum_{k',k''} \Phi_4(k',k'')\,|0,0,0,1;\,0,1_{k'},1_{k''}\rangle ,$$

where

$$(1.23)\qquad \Phi_2(k') = \delta_{k,k'} + \varphi(k') .$$

Substituting eq. (1.23) in (1.22) and using (1.21) yields

$$(1.24)\qquad \beta = \frac{1}{m_2+\omega_2+i\varepsilon-m_1+\delta m_1}\cdot \\ \cdot\left[g_2^0 \sum_{k'} \frac{u(\omega_2')}{\sqrt{2\omega_2' V}}\,\Phi_2(k') + g_3^0 \sum_{k'} \frac{U(\omega_3')}{\sqrt{2\omega_3' V}}\,\Phi_3(k')\right],$$

$$(1.25)\qquad \varphi(k') = \frac{1}{\omega_2+i\varepsilon-\omega_2'}\, g_2^0\, \frac{u(\omega_2')}{\sqrt{2\omega_2' V}}\,\beta ,$$

$$(1.26)\qquad \Phi_3(k') = \frac{1}{m_2+\omega_2+i\varepsilon-(m_3-\delta m_3+\omega_3')}\cdot \\ \cdot\left[g_3^0\, \frac{U(\omega_3')}{\sqrt{2\omega_3' V}}\,\beta + g_4^0 \sum_{k''} \frac{R(\omega_4'')}{\sqrt{2\omega_4'' V}}\,\Phi_4(k',k'')\right],$$

$$(1.27)\qquad \Phi_4(k',k'') = \frac{g_4^0}{m_2+\omega_2+i\varepsilon-(m_4+\omega_3'+\omega_4'')}\,\frac{R(\omega_4'')}{\sqrt{2\omega_4'' V}}\,\Phi_3(k') .$$

Eliminating Φ_4 in eq. (1.26) through (1.27) and using eq. (1.17) yields

$$(1.28)\qquad \Phi_3(k') = \frac{1}{(m_2+\omega_2+i\varepsilon-m_3-\omega_3')L(m_2+\omega_2-\omega_3')}\,\frac{U(\omega_3')}{\sqrt{2\omega_3' V}}\,\beta .$$

Let

$$(1.29)\qquad Z_2(3)\,L(x-\omega_3) = L^R(x-\omega_3) .$$

Using eq. (1.15), (1.17), (1.20) in (1.29)

$$(1.30)\qquad L^R(x-\omega_3) = 1 + g_4^2(\omega_3+m_3-x)\cdot \\ \cdot\sum_{k} \frac{R(\omega_4)^2}{2\omega_4 V}\,\frac{1}{(m_3-m_4-\omega_4)^2\,(x+i\varepsilon-m_4-\omega_4-\omega_3)} .$$

3723

Eliminating Φ_3 from eq. (1.24) and using eq. (1.14), (1.16), (1.19), (1.20) gives

$$(1.31)\quad \beta\Big[m_2+\omega_2-m_1-(m_2+\omega_2-m_1)^2 g_2^2 \sum_{k'} \frac{u(\omega_2')^2}{2\omega_2' V} \frac{1}{(\omega_2+i\varepsilon-\omega_2')(m_1-m_2-\omega_2')^2}+$$

$$+g_3^2 \sum_k \frac{U(\omega_3)^2}{2\omega_3 V}\left(\frac{1}{(m_1-m_3-\omega_3)L^R(m_1-\omega_3)}-\frac{1}{(m_2+\omega_2+i\varepsilon-m_3-\omega_3)L^R(m_2+\omega_2-\omega_3)}\right)-$$

$$-g_3^2(m_2+\omega_2-m_1)\sum_k \frac{U^2(\omega_3)}{2\omega_3 V}\cdot\frac{1}{(m_1-m_3-\omega_3)^2 L^R(m_1-\omega_3)^2}\cdot$$

$$\cdot\left(1+g_4^2(m_1-m_3-\omega_3)\sum_{k'}\frac{R(\omega_4')^2}{2\omega_4' V}\frac{m_3+m_1-\omega_3-2(m_4+\omega_4')}{(m_3-m_4-\omega_4')^2(m_1-m_4-\omega_4'-\omega_3)^2}\right)\Big]=$$

$$=g_2 Z_2^{\frac{1}{2}}(1)\frac{u(\omega_2)}{\sqrt{2\omega_2 V}}.$$

Having obtained β, Φ_2, Φ_3, Φ_4 the transition to various final states is determined. We shall now determine the analytic properties of

$$g_2 Z_2(1)^{\frac{1}{2}}\frac{u(\omega_2)}{\sqrt{2\omega_2 V}}\frac{1}{\beta}\equiv f(\omega_2)\,,$$

after replacing $\omega_2+i\varepsilon$ with z.

Since $L^R(m_2+z-\omega_3)$ is an analytic function in the complex plane outside a cut along the real axis, when $m_3<m_4+\mu_4$, $f(z)$ is also analytic away from the real axis. Note that

$$(1.32)\quad f(\omega+i\varepsilon)-f(\omega-i\varepsilon)=\frac{i}{2\pi}\Big[g_2^2 u(\omega)^2\sqrt{\omega^2-\mu_2^2}\,\theta(\omega-\mu_2)+$$

$$+g_3^2 U(m_2+\omega-m_3)^2\sqrt{(m_2+\omega-m_3)^2-\mu_3^2}\,\theta(m_2+\omega-m_3-\mu_3)+$$

$$+g_3^2 g_4^2\sum_k \frac{U(\omega_3)^2}{2\omega_3 V}\frac{R(m_2+\omega-m_4-\omega_3)^2}{(m_3+\omega_3-m_2-\omega)^2}\cdot\frac{1}{|L^R(m_2+\omega-\omega_3)|^2}\cdot$$

$$\cdot\sqrt{(m_2+\omega-m_4-\omega_3)^2-\mu_4^2}\,\theta(m_2+\omega-m_4-\mu_4-\omega_3)\Big].$$

From eq, (1.31)

$$(1.33)\qquad f(m_1-m_2)=0\,.$$

and

$$(1.34)\qquad \lim_{z\to\infty} f(z)=z\,Z_2(1)\,.$$

3724

From eq. (1.32), (1.33), (1.34) it follows that

$$(1.35)\qquad f(z) = (m_2 + z - m_1)\left[Z_2(1) + \frac{1}{2\pi i}\int_{-\infty}^{+\infty} \mathrm{d}\omega' \frac{f(\omega' + i\varepsilon) - f(\omega' - i\varepsilon)}{(\omega' - z)(m_2 + \omega' - m_1)}\right].$$

We shall now proceed to calculate the scattering amplitude which is

$$g_2^0 \frac{u(\omega_2)}{(2\omega_2 V)^{\frac{1}{2}}}\beta = g_2^2 \frac{u(\omega_2)^2}{2\omega_2 V}\frac{1}{f(\omega_2)},$$

with dispersion methods.

2. – Solution with dispersion relations.

In this Section we shall closely follow the procedure followed by GOLDBERGER and TREIMAN [5] in examining the decay of the V particle. The S-matrix for φ_2, ψ_2 scattering is

$$\langle \psi_2 \varphi_{2\,\mathrm{out}}' | \psi_2 \varphi_{2\,\mathrm{in}} \rangle = \delta_{k,k'} + 2\pi i \frac{u(\omega_2')}{\sqrt{2\omega_2' V}}\,\delta\omega_2,\ \omega_2' \langle \psi_2 | j_2(0) | \psi_2 \varphi_{2\,\mathrm{in}} \rangle ,$$

where

$$(2.1)\qquad j_2(0) = -\,g_2^0 \psi_2^+ \psi_1 .$$

Defining

$$(2.2)\qquad N(\omega_2) = \frac{\sqrt{2\omega_2 V}}{u(\omega_2)} \langle \psi_2 | j_2(0) | \psi_2 \varphi_{2\,\mathrm{in}} \rangle ,$$

it follows that [5]

$$(2.3)\qquad N(\omega_2) = \frac{1}{\pi}\int_{-\infty}^{+\infty} \frac{\mathrm{Im}\, N(\omega_2')}{\omega_2' - \omega_2 - i\varepsilon}\,\mathrm{d}\omega_2' ,$$

where

$$\begin{aligned}(2.4)\qquad \mathrm{Im}\, N(\omega_2) = \pi\Big\{ & |\langle \psi_2 | j_2(0) | \psi_1 \rangle|^2\, \delta(m_1 - m_2 - \omega_2) + \\ & + \sum_{k'} |\langle \psi_2 \varphi_2' | j_2^+(0) | \psi_2 \rangle|^2\, \delta(\omega_2' - \omega_2) + \\ & + \sum_{k'} |\langle \psi_3 \varphi_3' | j_2^+(0) | \psi \rangle|^2\, \delta(m_3 + \omega_3' - m_2 - \omega_2) + \\ & + \sum_{k',k''} |\langle \psi_4 \varphi_3' \varphi_4'' | j_2^+(0) | \psi \rangle|^2\, \delta(m_4 + \omega_3' + \omega_4'' - m_2 - \omega_2)\Big\} .\end{aligned}$$

[5] M. L. GOLDBERGER and S. B. TREIMAN: *Phys. Rev.*, **113**, 1663 (1959).

The sum over a complete set of states above consists of out-states. Note that

$$N(\omega_2) = \frac{\sqrt{2\omega_2 V}}{u(\omega_2)} \langle \psi_2 \varphi'_{2\,\mathrm{out}} | j_2^+(0) | \psi_2 \rangle \,, \tag{2.5}$$

and

$$\frac{\sqrt{2\omega'_3 V}}{U(\omega'_3)} \langle \psi_3 \varphi'^{\,I}_{3\,\mathrm{out}} | j_2^+(0) | \psi_2 \rangle = \frac{\sqrt{2\omega_2 V}}{u(\omega_2)} \langle \psi_3 | j_3(0) | \psi_2 \varphi_{2\,\mathrm{in}} \rangle \,, \tag{2.6}$$

where

$$m_2 + \omega_2 = m_3 + \omega'_3$$

$$j_3(0) = -\, g_3^0 \psi_3^+ \psi_1 \,. \tag{2.7}$$

From eq. (2.1) and (2.2)

$$N(\omega_2) = -\frac{\sqrt{2\omega_2 V}}{u(\omega_2)} g_2^0 \langle \psi_2 | \psi_2^+ | 0 \rangle \langle 0 | \psi_1 | \psi_2 \varphi_{2\,\mathrm{in}} \rangle = -\frac{\sqrt{2\omega_2 V}}{u(\omega_2)} g_2^0 \langle 0 | \psi_1 | \psi_2 \varphi_{2\,\mathrm{in}} \rangle . \tag{2.8}$$

From eq. (2.6)

$$\langle \psi_3 \varphi'_{3\,\mathrm{out}} | j_2^+ | \psi_2 \rangle = -\frac{U(\omega'_3)}{\sqrt{2\omega'_3 V}} \frac{\sqrt{2\omega_2 V}}{u(\omega_2)} \cdot g_3^0 \langle \psi_3 | \psi_3^+ | 0 \rangle \langle 0 | \psi_1 | \psi_2 \varphi_{2\,\mathrm{in}} \rangle = \tag{2.9}$$

$$= \frac{U(\omega'_3)}{\sqrt{2\omega'_3 V}} Z_2(3)^{\frac{1}{2}} \frac{g_3^0}{g_2^0} N(\omega_2) \,.$$

We shall now calculate $\langle \psi_4 \varphi'_3 \varphi''_{4\,\mathrm{out}} | j_2^+ | \psi_2 \rangle$. This can be done by splitting H_I as follows

$$H_I = V' + W \,,$$

$$V' = g_3^0 \left(\sum_{\boldsymbol{k}} \frac{U(\omega_3)}{\sqrt{2\omega_3 V}} a_3^+(\boldsymbol{k}) \psi_3^+ \psi_1 + \mathrm{h.c.} \right),$$

$$W = g_2^0 \left(\sum_{\boldsymbol{k}} \frac{u(\omega_2)}{(2\omega_2 V)^{\frac{1}{2}}} a_2^+(\boldsymbol{k}) \psi_2^+ \psi_1 + \mathrm{h.c.} \right) + g_4^0 \left(\sum_{\boldsymbol{k}} \frac{R(\omega_4)}{\sqrt{2\omega_4 V}} a_4^+(\boldsymbol{k}) \psi_4^+ \psi_1 + \mathrm{h.c.} \right) -$$

$$- \delta m_1 \psi_1^+ \psi_1 - \delta m_3 \psi_3^+ \psi_3 \,.$$

Using the scattering theory for two potentials of GELL-MANN and GOLDBERGER [6] it follows that

$$\langle \psi_4 \varphi'_3 \varphi''_{4\,\mathrm{out}} | j_2^+ | \psi_2 \rangle \frac{u(\omega_2)}{\sqrt{2\omega_2 V}} = -\, g_3^0 \frac{U(\omega'_3)}{\sqrt{2\omega'_3 V}} \langle \psi_4 \varphi''_{4\,\mathrm{out}},\ V' = 0 | \psi_3^+ \psi_1 | \psi_2 \varphi_{2\,\mathrm{in}} \rangle = \tag{2.10}$$

$$= -\, g_3^0 \frac{U(\omega'_3)}{\sqrt{2\omega'_3 V}} \langle \psi_4 \varphi''_{4\,\mathrm{out}},\ V' = 0 | \psi_3^+ | 0 \rangle \langle 0 | \psi_1 | \psi_2 \varphi_{2\,\mathrm{in}} \rangle \,.$$

---

[6] M. GELL-MANN and M. GOLDBERGER: *Phys. Rev.*, **91**, 398 (1953).

where $|\psi_4\varphi''_{4\,\mathrm{out}}, V'=0\rangle$ is an out ψ_4, φ_4 scattering state for $V'=0$. Since the ψ_4, φ_4 scattering is independent of V' it will not be specified further.

From eq. (2.10) and (2.8)

$$\langle \psi_4\varphi'_3\varphi''_{4\,\mathrm{out}} | j_2^+ | \psi_2\rangle = \frac{g_3^0}{g_2^0}\langle \psi_4\varphi''_{4\,\mathrm{out}} | \psi_3^+ | 0\rangle \frac{U(\omega'_3)}{\sqrt{2\omega'_3 V}} N(\omega_2)\,. \tag{2.11}$$

To calculate $\langle \psi_4\psi_{4\,\mathrm{out}} | \psi_3^+ | 0\rangle$ which represents the $\psi_3 \to \psi_4 + \varphi_4$ vertex operator we use the LEHMANN, SYMANZIK, ZIMMERMANN (7) formalism giving

$$\langle \psi_4\varphi_{4\,\mathrm{out}} | \psi_3^+ | 0\rangle \frac{\sqrt{2\omega_4 V}}{R(\omega_4)} \equiv K(\omega_4) = i\int \exp[i\omega_4 t]\langle \psi_4 | [j_4(t), \psi_3^+] | 0\rangle \theta(t)\,\mathrm{d}t\,, \tag{2.12}$$

where

$$j_4(0) = -\, g_4^0 \psi_4^+ \psi_3\,.$$

$K(\omega_4)$ can be used to define a function that is analytic in the upper half complex plane, giving

$$K(\omega_4) = \frac{1}{\pi}\int \frac{\operatorname{Im} K(\omega'_4)}{\omega'_4 - \omega_4 - i\varepsilon}\,\mathrm{d}\omega'_4\,, \tag{2.13}$$

where

$$\operatorname{Im} K(\omega_4) = \pi\big\{\langle \psi_4 | j_4(0) | \psi_3\rangle\langle \psi_3 | \psi_3^+ | 0\rangle\, \delta(\omega_4 + m_4 - m_3) + \sum_{k'} \langle \psi_4 | j_4(0) | \psi_4\varphi'_{4\,\mathrm{out}}\rangle\langle \psi_4\varphi'_{4\,\mathrm{out}} | \psi_3^+ | 0\rangle\, \delta(\omega_4 - \omega'_4)\big\}. \tag{2.14}$$

Since

$$\langle \psi_4 | j_4(0) | \psi_3\rangle = -\, g_4\,,$$

using eq. (2.14) in (2.13) it follows that (5)

$$K(\omega_4) = -\frac{g_4 Z_2(3)^{\frac{1}{2}}}{m_3 - m_4 - \omega_4 - i\varepsilon} + \frac{1}{\pi}\int_{\mu_4}^{\infty} \mathrm{d}\omega'_4\, \frac{\exp[i\delta(\omega'_4)]\sin\delta(\omega'_4)}{\omega'_4 - \omega_4 - i\varepsilon} K(\omega)'_4\,, \tag{2.15}$$

where $\delta(\omega_4)$ is the φ_4, ψ_4 scattering phase shift. Defining $K(z)$ by the substitution $\omega_4 + i\varepsilon \to z$ it follows that

$$K(\omega + i\varepsilon) - K(\omega - i\varepsilon) = -\, 2\pi i g_4 Z_2(3)^{\frac{1}{2}}\, \delta(m_3 - m_4 - \omega) + 2i\exp[i\,\delta(\omega)]\sin\delta(\omega)\, K(\omega + i\varepsilon)\,\theta(\omega - \mu_4) \tag{2.16}$$

(7) H. LEHMANN, K. SYMANZIK and W. ZIMMERMANN: *Nuovo Cimento*, **1**, 205 (1955).

or

$$(2.17)\qquad \begin{cases} K(\omega+i\varepsilon)-K(\omega-i\varepsilon)=-2\pi i g_4 Z_2(3)^{\frac{1}{2}}\,\delta(m_3-m_4-\omega) & \omega<\mu_4\,, \\ K(\omega+i\varepsilon)=K(\omega-i\varepsilon)\exp\left[2i\,\delta(\omega)\right] & \omega>\mu_4\,. \end{cases}$$

The analytic function $K(z)$ satisfying eq. (2.17) and such that $\lim_{z\to\infty} K(z)=0$ is ([8])

$$(2.18)\qquad K(z)=-\frac{g_4 Z_2(3)^{\frac{1}{2}}}{m_3-m_4-z}\,\frac{k(z)}{k(m_3-m_4)}\,,$$

where

$$k(z)=\exp\left[\frac{1}{\pi}\int_{\mu_4}^{\infty}\frac{\delta(\omega)}{\omega-z}\,\mathrm{d}\omega\right].$$

From ref. ([4]) $k(m_3-m_4)=Z_2(3)$, thus

$$(2.19)\qquad k(\omega+i\varepsilon)=\frac{Z_2(3)}{L^R(m_4+\omega)}\,.$$

Using

$$\langle\psi_4|j_2(0)|\psi_1\rangle=-g_2$$

in eq. (2.4) along with (2.9), (2.11), (2.12), (2.18), (2.19) yields

$$\begin{aligned}(2.20)\qquad \operatorname{Im} N(\omega_2)=\pi\Bigg\{ & g_2^2\,\delta(m_1-m_2-\omega_2)+\Bigg[\frac{u(\omega_2)^2}{4\pi^2}\sqrt{\omega_2^2-\mu_2^2}\,\theta(\omega_2-\mu_2)+ \\ & +\frac{g_3^2}{g_2^2}\,\frac{U(m_2+\omega_2-m_3)^2}{4\pi^2}\sqrt{(m_2+\omega_2-\omega_3)^2-\mu_3^2}\,\theta(m_2+\omega_2-m_3)+ \\ & +\frac{1}{4\pi^2}\,\frac{g_3^2}{g_2^2}\,g_4^2\sum_k\frac{U(\omega_3)^2}{2\omega_3 V}\,\frac{R(m_2+\omega_2-m_4-\omega_3)^2}{|L^R(m_2+\omega_2-\omega_3)|^2}\cdot \\ & \cdot\frac{\sqrt{(m_2+\omega_2-m_4-\omega_3)^2-\mu_4^2}\,\theta(m_2+\omega_2-m_4-\mu_4-\omega_3)}{(m_2+\omega_2-m_3-\omega_3)^2}\Bigg]|N(\omega_2)|^2\Bigg\}\,. \end{aligned}$$

Letting

$$(2.21)\qquad h(\omega)=\frac{1}{N(\omega)}\,,$$

it follows that $h(z)$ is an analytic function with a branch cut along the real axis for $\omega>\mu_2$ and a zero at $\omega=m_1-m_2$. As $z\to\infty$, $h(z)\to -z/g_2^{02}$. To

([8]) M. I. Muskhelishvili: *Singular Integral Equations* (Groningen, 1953).

3728

obtain this result it is sufficient to observe that from eq. (2.3)

$$\lim_{z\to\infty} N(z) = -\frac{1}{z}\sum_n \langle \psi_2 | j_2 | n\rangle\langle n | j_2^+ | \psi_2\rangle = -\frac{g_2^{0^2}}{z}\,.$$

Using eq. (2.21) with (2.3) gives

$$h(\omega + i\varepsilon) - h(\omega - i\varepsilon) = \frac{N(\omega - i\varepsilon) - N(\omega + i\varepsilon)}{|N(\omega + i\varepsilon)|^2} = -2i\,\frac{\operatorname{Im} N(\omega + i\varepsilon)}{|N(\omega + i\varepsilon)|^2}\,, \tag{2.22}$$

which is already calculated in (2.20).

Thus

$$h(z) = (m_1 - m_2 - z)\left(\frac{1}{g_2^{0^2}} + \frac{1}{2\pi i}\int_{-\infty}^{\infty} \mathrm{d}\omega'\,\frac{h(\omega' + i\varepsilon) - h(\omega' - i\varepsilon)}{(\omega' - z)(m_1 - m_2 - \omega')}\right). \tag{2.23}$$

Comparing eq. (2.22) and (2.20) with (1.32) it is seen that

$$f(\omega + i\varepsilon) - f(\omega - i\varepsilon) = -g_2^2[h(\omega + i\varepsilon) - h(\omega - i\varepsilon)]\,.$$

Thus the scattering amplitude calculated by dispersion theory equals that calculated directly in Section **1**.

3. – Conclusions.

The generalization of the Lee model described also places an upper bound on the cut-off if the renormalized and unrenormalized coupling constants are to remain real and different from zero. The extent to which this model reproduces the mathematical structure of relativistic field theories is again an open question since it does not involve wave function renormalization for all the particles and produces no vertex renormalization. The former restriction can readily be removed by introducing additional fields that merely give structure to each particle without interacting with the others, and still keep the model soluble. Although in the Ruijgrok-Van Hove model it is not possible to calculate the scattering amplitude exactly, vertex and wave function renormalization can be performed. In that model the cut-off can be made infinite if the renormalized coupling constants are suitably related, and thus is less restrictive than our model. Nevertheless for the purpose of comparing direct and dispersion theoretical solution our model is very convenient. Likewise it lends itself to the study of unstable particle production, which will be given later.

3729

The limitation on the number of fundamental processes can readily be removed by introducing additional processes of the type $\psi_n + \varphi_n \rightleftarrows \psi_{n-1}$: In this case the φ_2, ψ_2 scattering amplitude is still soluble because of the linear and algebraic relation among the amplitude arising from φ_2, ψ_2 interactions.

* * *

I would like to thank Dr. C. H. BLANCHARD for useful remarks during the course of this work.

RIASSUNTO (*)

Si è modificato il modello di Lee dando alla particella V una struttura più complicata e lasciando tuttavia esattamente risolvibile l'ampiezza dello scattering $\mathcal{N}$-θ. Tale modificazione conduce inoltre ad una più ampia varietà di processi risolvibili. Si riproduce in questo modello la stessa limitazione applicata alle dimensioni del taglio nel modello di Lee. Si esegue il calcolo facendo uso del formalismo Hamiltoniano e di metodi di dispersione.

(*) *Traduzione a cura della Redazione.*

3730

IL NUOVO CIMENTO Vol. XIV, N. 4 16 Novembre 1959

Consequences of a Strong π-π Interaction in the Statistical Theory of p-$\bar{p}$ Annihilation.

F. Cerulus

CERN - Geneva

(ricevuto il 21 Agosto 1959)

Summary. — The Fermi statistical model for multiple particle production is applied to the p-$\bar{p}$ annihilation process; calculations are performed for three assumptions on the π-π interaction, *viz.* *a*) a strong resonance in the state $l=1$, $T=1$ with total energy $4m_\pi$; *b*) the same with total energy $3m_\pi$; *c*) no strong interactions. Multiplicities and spectra for 2, 4 and 6-prong stars are computed. The π-π isobar model *a*) agrees well with experiment, taking an interaction volume $\Omega_0 = (\hbar/m_\pi c)^3 \cdot 4\pi/3$. The 2-prong spectrum shows a hump around 760 MeV kinetic energy.

1. – Introduction.

Most of the experiments on p-$\bar{p}$ annihilation [1-4] have been compared with the Fermi theory of multiple production, and it has been found that all measured quantities were in fair agreement with this theory, provided the interaction volume was taken to be 10 Ω_0, where

$$\Omega_0 = \frac{4\pi}{3}\left(\frac{\hbar}{m_\pi c}\right)^3.$$

(1) Antiproton Collaboration Experiment: *Phys. Rev.*, **105**, 1037 (1957).

(2) O. Chamberlain G. Goldhaber, L. Janneau, T. Kalogeropoulos, E. Segrè, R. Silberberg: *Phys. Rev.*, **113**, 1615 (1959).

(3) E. Kalogeropoulos: UCRL 8677.

(4) N. Horwitz, D. Miller, J. Murray and R. Tripp: UCRL 8591.

3731

This is, of course, very unsatisfactory, all the more so because the Fermi-theory gives quite good results in the meson production from p-p collisions, at various energies ([5-7]), with an interaction volume $\Omega = \Omega_0$.

It was therefore proposed ([8,9]) to incorporate into the statistical theory of annihilation a presumed pion-pion resonant state. This improved the result.

We shall show that if one calculates correctly all phase-space integrals, and takes all contributions, to the final state of n_π pions and n_K K-mesons into account, the agreement with experiment is excellent; an important difference with the usual Fermi-theory appears, which seems to be in favour of the isobar-model and could be settled with improved statistics for the 2-prong events.

2. – Outline of calculations.

We take the probability for a certain end state, labelled b, of a p-$\bar{\text{p}}$ annihilation to be proportional to

$$S_b = \Omega_0^{n\pi + n\sigma} \Omega_K^{n_K} \frac{(2l+1)^{n\sigma}}{n_\pi!\, n_\sigma!} (P_b^{(1)} + P_b^{(0)})\, \varrho_{n\pi,\, n\sigma,\, nK}(E, 0)\,,$$

where:

Ω_0 = interaction volume with radius of pion Compton wavelength,

Ω_K = interaction volume with a smaller radius, to be discussed hereafter,

n_π, n_K: numbers of pions and K-mesons in the state b,

n_σ: number of π-π isobars, l their angular momentum,

$P_b^{(1)}$ and $P_b^{(2)}$ give the probability of different charge states in total isospin states 0 and 1. These coefficients are normalized so that the sum over the charge states of the n_π pions, the n_σ π-π isobars and the n_K K-mesons gives the usual statistical factor $W_{\alpha,\beta}$, as defined by YEIVIN-DE SHALIT ([10]) and BARAŠENKOV-BARBAŠEV ([11]),

α: number of isospin $\frac{1}{2}$ particles,

β: number of isospin 1 particles,

([5]) F. CERULUS and R. HAGEDORN: CERN Report 59-3.
([6]) F. CERULUS and R. HAGEDORN: *Meson production at* 6.2 GeV, to be published.
([7]) S. Z. BELENKI *et al.*: *Usp. Fiz. Nauk*, **62** (2), 1 (1957).
([8]) E. EBERLE: *Nuovo Cimento*, **8**, 610 (1958).
([9]) T. GOTÔ: *Nuovo Cimento*, **8**, 625 (1958).
([10]) Y. YEIVIN and A. DE-SHALIT: *Nuovo Cimento*, **1**, 1147 (1955).
([11]) V. S. BARAŠHENKOV and B. M. BARBAŠEV: *Suppl. Nuovo Cimento*, **7**, 19 (1957).

3732

$\varrho_{n_\pi, n_\sigma, n_K}(E; 0)$ is the integral over momentum space:

$$\varrho_{n_\pi, n_\sigma, n_K}(E, p) = \int \ldots \int \mathrm{d}\boldsymbol{q} \ldots \mathrm{d}\boldsymbol{q}_N \, \delta(E - \sum_{i=1}^{N} \sqrt{m_i^2 + q_i^2}) \, \delta(\boldsymbol{p} - \sum_{i=1}^{N} \boldsymbol{q}_i) \, ,$$

with

$$m_1, \ldots, m_{n_\pi} = \mu \qquad = m_\pi \qquad E = \text{total energy},$$

$$m_{n_\pi+1}, \ldots, m_{n_\pi+n_\sigma} \qquad = m_\sigma \, , \qquad p = \text{total momentum},$$

$$m_{n_\pi+n_\sigma+1}, \ldots, m_{n_\pi+n_\sigma+n_K} = m_K \qquad N = n_\pi + n_\sigma + n_K \, .$$

In the following investigation we took the π-π isobar to have $T = 1$, $l = 1$, in accordance with recent speculations on the electromagnetic form factor of the nucleon ([12]). The calculations were done for two masses of the isobar: $m_\sigma = 3\mu$ and $m_\sigma = 4\mu$. According to ref. ([12]) the 4μ isobar should give the best fit.

The $\varrho_{n_\pi, n_\sigma, n_K}(E; 0)$ were computed on the CERN Ferranti « Mercury » computer, by a method described previously ([5]) using a programme written by R. HAGEDORN.

The $P_b^{(0)}$, $P_b^{(1)}$ have been calculated for a large number of end states, and will shortly be published.

The method used ([13]) allows not only the calculation of the multiplicities, but also the spectra of each kind of particle, for each reaction considered.

We shall call then

$$S_{b,j}(\varepsilon_j)\,\mathrm{d}\varepsilon_j = \text{probability that in reaction } b, \text{ particle } j \text{ has a kinetic energy between } \varepsilon_j \text{ and } \varepsilon_j + \mathrm{d}\varepsilon_j .$$

The normalization is such that

$$\int_0^{\varepsilon_j \max} S_{b,j}(\varepsilon_j)\,\mathrm{d}\varepsilon_j = S_b \, .$$

The multiplicities of pions, *e.g.* are computed from the S_b by summing over all reactions yielding the same number of pions, and dividing by the sum over all S_b.

Soon after the annihilation, the isobar decays into two pions, and these pions have quite a different spectrum from directly produced ones. The com-

---

([12]) W. FRAZER and J. FULCO: *Phys. Rev. Lett.*, **2**, 365 (1959).

([13]) F. CERULUS and R. HAGEDORN: *Suppl. Nuovo Cimento*, **9**, 646, 659 (1958).

putation of the decay from the isobar spectrum is part of the programme of the computer.

To compare with experiment, it is useful to compute the spectra of pions produced in two, four and six-prong events. This can by done by selecting those b with 2, 4 or 6 charged pions, and adding the spectra for each reaction. This adding, together with the computation of mean energies and mean particle numbers can again be performed on the computer, following another programme of R. HAGEDORN (*).

3. – Results.

We considered all reactions as taking place from p-$\bar{\text{p}}$ annihilation at rest; *i.e.*, we took

$$E = 2m_N c^2 \quad \text{and} \quad p = 0 .$$

We compared in each case with the results of the Fermi model without isobar, computed by taking $\Omega_\pi = 10\,\Omega_0$.

For Ω_K we took various values, from Ω_0 to $(1/30)\,\Omega_0$. Variation of Ω_K leaves the form of all spectra unchanged, it has only a slight influence on the pion number (except in the no-isobar hypothesis).

The reactions considered were

$$\begin{aligned}
&\mathrm{p} + \bar{\mathrm{p}} \to 2, 3, \ldots, 7 \text{ pions} , \\
&\quad \to \sigma + \pi,\ \sigma + 2\pi,\ \ldots,\ \sigma + 5\pi , \\
&\quad \to 2\sigma,\ 2\sigma + \pi,\ \ldots,\ 2\sigma + 4\pi , \\
&\quad \to 3\sigma,\ 3\sigma + \pi , \\
&\quad \to \mathrm{K} + \overline{\mathrm{K}},\ \mathrm{K} + \overline{\mathrm{K}} + \pi,\ \ldots,\ \mathrm{K} + \overline{\mathrm{K}} + 3\pi , \\
&\quad \to \mathrm{K} + \overline{\mathrm{K}} + \sigma,\ \mathrm{K} + \overline{\mathrm{K}} + \sigma + \pi .
\end{aligned}$$

It is easy to see from a plot of the weights of these reactions that all the others, with higher particle numbers, would contribute almost nothing, because of their vanishing probability.

(*) An extensive description of the two programmes used is available from CERN upon request.

a) *Multiplicities.* – Table I is computed by counting only the prongs in events without K-mesons.

TABLE I. – *Probability in % of events with different charged pion numbers.*

Ω_π:	Ω_0		$2\Omega_0$		$\frac{1}{2}\Omega_0$		no isobar $\Omega_\pi = 10\Omega_0$		
m_σ:	3 μ	4 μ	3 μ	4 μ	3 μ	4 μ	$\Omega_K = \Omega_\pi$	$\Omega_K = \frac{1}{10}\Omega_\pi$	$\Omega_K = \frac{1}{100}\Omega_\pi$
2 prongs	26.7	45.35	21.0	37.9	34.9	54.0	27.5	35.0	35.0
4 prongs	65.0	51.5	69.0	58.2	59.0	42.75	43.7	55.5	56.0
6 prongs	7.5	2.1	9.4	3.1	5.6	1.4	5.7	7.3	7.3

TABLE II. – *Average number of pions.*

Ω_π:	Ω_0		$2\Omega_0$		$\frac{1}{2}\Omega_0$		no isobar $\Omega_\pi = 10\Omega_0$		
m_σ:	3 μ	4 μ	3 μ	4 μ	3 μ	4 μ	$\Omega_K = \Omega_\pi$	$\Lambda_K = \frac{1}{10}\Omega_\pi$	$\Omega_K = \frac{1}{100}\Omega_\pi$
$\overline{n}_{\pi^\pm}$	3.6	3.1	3.75	3.3	3.4	2.9	3.1	3.4	3.4
$\overline{n}_{\pi^0}$	1.7	1.55	1.8	1.6	1.6	1.5	1.35	1.7	1.7
$\overline{n}_\pi$	5.3	4.65	5.6	4.9	5.0	4.4	4.4	5.1	5.1

TABLE III. – *Average number of* K*-mesons per* p-$\overline{\text{p}}$ *annihilation.*

isobar; $\Omega_\pi = \Omega_0$			no isobar; $\Omega_\pi = 10\Omega_0$	
Ω_K/Ω_0 \ $\overline{n}_K$	$m_\sigma = 3$ μ	$m_\sigma = 4$ μ	Ω_K/Ω_0	$\overline{n}_K$
1	(not com-	0.30	10	0.43
0.4	puted)	0.051	4	0.084
0.1	0.0019	0.0034	1	0.0055
0.04	—	0.00052	0.4	0.00088
			0.1	$5.5 \cdot 10^{-5}$

TABLE IV. – *Average energy of prongs* (*rest energy of* 140 MeV *included*) (*in* MeV).

	isobar case; $\Omega_\pi = \Omega_0$		no isobar; $\Omega_\pi = 10\Omega_0$
m_σ	3 μ	4 μ	
0 prongs	640	640	435
2 prongs	430	472	419
4 prongs	335	372	366
6 prongs	294	310	299
average $\pi^\pm$	345	399	371
average π^0	355	410	371

3735

b) *Spectra.* – The spectra of pions from 2, 4 and 6 prong events are displayed in Figs. 1, 2, 3. All the curves are normalized to unit area.

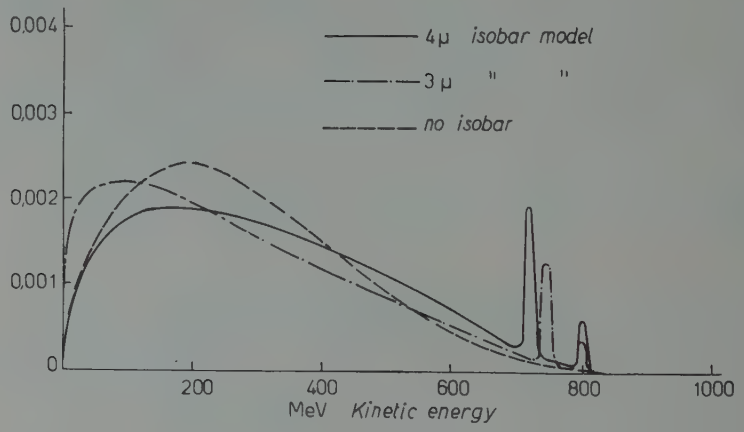

Fig. 1.

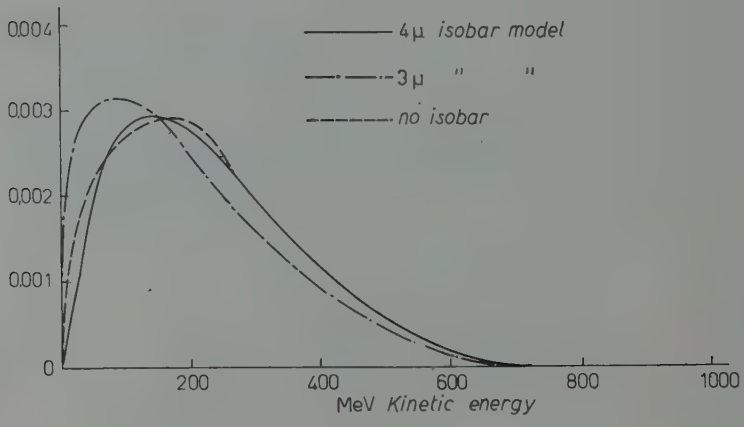

Fig. 2.

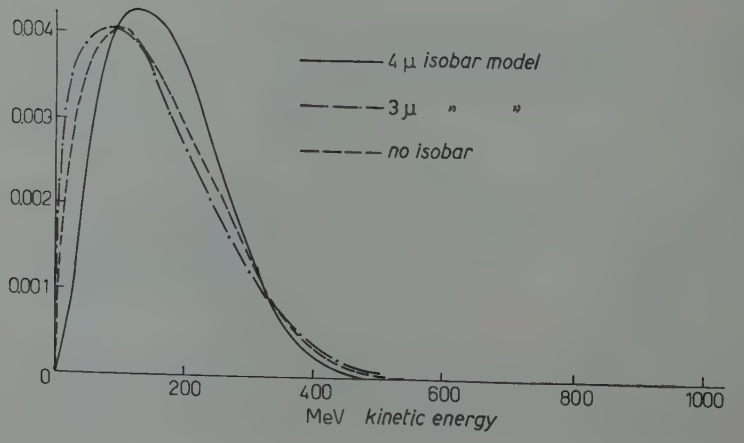

Fig. 3.

3736

4. – Discussion of results.

Comparison with the published experimental data ([3]) shows very good agreement with the isobar model on the whole. Let us consider this in detail:

1) *Multiplicities of pions.* The multiplicities are more sensitive to a variation of the isobar mass than to a variation of the interaction volume If the isobar idea is right, the mass m_σ should be closer to 4μ than to 3μ. This would be in agreement with the average number observed ([14]), and will probably yield the right percentage for the two and four prong events. One should watch out, with better statistics, for the probability of 6 prongs events, which are rather different for the various hypotheses.

The no-isobar model, with small Ω_K, comes fairly close to the experimental numbers too, which is well-known, although with very large statistics the differences might become significant.

2) *Multiplicities of* K-*mesons.* – It has been recognized by various authors that the most straightforward way to correct the too large proportion of K-mesons which statistical theories of meson production tend to give, is to take for K-mesons a smaller interaction volume. There is, in our opinion, no compelling reason to take for it a sphere with the K-Compton wavelength as radius. The smallness of Ω_K is probably only a crude way to express the relative weakness of K-meson interactions, which do not allow statistical equilibrium to be reached during the collision time. If one considers the interaction volume as a substitute for the transition matrix element between the initial p-$\bar{\text{p}}$ state, and the final state b, and if one takes from other theories the conclusion that the K-meson interaction strength is about 1/10 of pion-nucleon interaction strength, then it seems reasonable to look for an Ω_K in the neighbourhood of 1/10 Ω_π.

Applying this idea to meson production in p-p collisions at Bevatron energies, it was found ([6]) that this was indeed the magnitude of Ω_K that gave a.o. a ratio $K/\overline{K}$ compatible with experiment.

We want to emphasize, however, that the details of K-meson production are quite irrelevant for the problem of the validity of a statistical theory of annihilation. It may be that such a theory is unjustified for K-mesons, whereas it is entirely right for the strongly interacting pions, which experimentally make up the bulk of the annihilation products.

([14]) E. Amaldi: private communication.

3737

3) *Spectra and average energies of charged pions in 2, 4 and 6 prong events.* The form of the spectra, and the average energy, are quite insensitive against reasonable variations of Ω_π, and only moderately sensitive against variations of the isobar mass.

Again there is only a small difference on the whole between the spectra from the 4μ isobar model and those from the no-isobar model. Both seem to fit experiments within the limits of statistics.

There is, however, an important feature in the 2 prong spectrum for the isobar model which is entirely absent in the « no-isobar » spectrum *viz.* the peak at the end of the spectrum, around 800 Mc^2 kinetic energy. This is due to the two-body reaction

$$p + \bar{p} \rightarrow \sigma + \pi ,$$

where the directly produced pion has a sharp energy. The width of the bump is—for p-$\bar{p}$ collisions truly from rest—given by the width of the π-π resonance. There is a second, lower bump at a somewhat higher energy, due to

$$p + \bar{p} \rightarrow \pi + \pi .$$

The two together should contain about 5% of all the pions from 2 prong events.

In the bubble chamber data ([3]) there seems indeed to be a bump in the energy histogram at the right place. This might still be a freak of statistics, and further information on this point is very desirable.

There is no way of getting something similar with the no-isobar model, all the more as the two pion annihilation, in that model, has a probability less than 10^{-3}.

If such a bump is found experimentally, it is conclusive evidence for a strong π-π interaction, such as is described by an isobar in a statistical theory.

5. – Conclusion.

As conclusion, we can state that a Fermi-type theory of annihilation, with the assumptions of a π-π interaction and a normal interaction volume can account in detail for all observed facts, using values of the parameters ($\Omega_\pi = \Omega_0$, $\Omega_K \approx \frac{1}{10}\Omega_0$, $m_\sigma = 4\mu$) which are taken from other applications of the Fermi-theory, or from the theory of the electromagnetic form factor of the nucleon. In the 2 prong spectrum the theory predicts a small bump around 780 Mc^2 (kinetic pion energy). Other tests of the isobar model, based on cor-

3738

relations between annihilation products might be devised. This is being investigated.

* * *

The author wishes to thank R. HAGEDORN for the use of his programmes and for numerous discussions and S. FUBINI for discussions on the π-π interaction.

RIASSUNTO (*)

Il modello statistico di Fermi per la produzione di particelle multiple viene applicato al processo di annichilazione p-$\bar{\text{p}}$; i calcoli sono effettuati partendo da tre supposizioni circa la interazione π-π, cioè: *a*) forte risonanza nello stato $l=1$, $T=1$ con energia totale $4m_\pi$; *b*) lo stesso con energia totale $3m_\pi$; *c*) nessuna interazione forte. Si computano le molteplicità e gli spettri di stelle a 2, 4 e 6 rami. Il modello π-π isobaro *a*) si accorda bene agli esperimenti, assunto un volume di interazione $\Omega_0=(\hbar/m_\pi c)^3\cdot 4\pi/3$. Lo spettro delle stelle a 2 rami presenta una gobba verso 760 MeV di energia cinetica.

(*) *Traduzione a cura della Redazione.*

IL NUOVO CIMENTO Vol. XIV, N. 4 16 Novembre 1959

Hyperfragments and Isotopic Spin Selection Rules.

M. S. Swami

Tata Institute of Fundamental Research - Bombay

B. M. Udgaonkar

Atomic Energy Establishment - Trombay

(ricevuto il 21 Agosto 1959)

Summary. — The branching ratios in the decays of hyperfragments have been examined in the light of the selection rule $\Delta T = \frac{1}{2}$, the hyperfragments considered being the doublets $({}^4H_\Lambda, {}^4He_\Lambda)$, $({}^6He_\Lambda, {}^6Li_\Lambda)$, $({}^8Li_\Lambda, {}^8Be_\Lambda)$ and the hypernucleus ${}^7Li_\Lambda$. The experimental information on the doublet $({}^4H_\Lambda, {}^4He_\Lambda)$ is discussed in relation to this selection rules. It is pointed out that a systematic collection of much more data than are available at present is necessary in order to test the validity of the $\Delta T = \frac{1}{2}$ rule in this domain.

1. – Introduction.

The idea of charge independence, as expressed through the conservation of isotopic spin, or the treatment of all states with a given T but different values of T_z on the same footing, has been widely used in the study of strong interactions. It has also been discussed by a number of authors in connection with the branching ratios in the decays of strange particles, where the selection rule $\Delta T = \frac{1}{2}$ was first suggested by Pais and Gell-Mann (1). The experimental

(1) M. Gell-Mann and A. Pais: *Proc. of the Glasgow Conf.*, 1954 (London, 1955); R. Gatto: *Nuovo Cimento*, **3**, 318 (1956); B. d'Espagnat and J. Prentki: *Nuovo Cimento*, **3**, 1045 (1956); C. Iso and M. Kawaguchi: *Progr. Theor. Phys. Japan*, **16**, 177 (1956); M. Kawaguchi and K. Nishijima: *Progr. Theor. Phys. Japan*, **15**, 180 (1956); G. Wentzel: *Phys. Rev.*, **101**, 1215 (1956); M. Kawaguchi: *Phys. Rev.*, **107**, 573 (1957); B. T. Feld: *Nuovo Cimento*, **6**, 650 (1957).

3749

situation (2) seems to be that the rule, in addition to explaining the long lifetime of K^+ relative to that of K_1^0, is capable of explaining the branching ratios in the decays of Λ^0 and $K_{\pi 3}$. The experimental data on $\Sigma^\pm$ decay rates and asymmetries are also not inconsistent with the rule. There, however, seems to be some indication of its violation in the decay-rate of K_2^1 and possibly in the branching ratio of K_1^0 and these may provide evidence of the contribution of $\Delta T = \frac{3}{2}$ to these decays. On the theoretical side, though it is possible to construct a four-fermion decay interaction of the V-A type which selects $\Delta T = \frac{1}{2}$, such an interaction is not consistent with the view-point of FEYNMAN and GELL-MANN (3). These authors consider the four-fermion interaction as a current-current interaction, $J_\mu^* J_\mu$, with only terms involving a charge change $\Delta Q = 1$ being allowed to appear in J_μ. Such a restriction appears necessary in order to forbid certain unobserved decays like $\mu^+ \to e^+ + e^- + e^+$, which would otherwise occur in a scheme of universal Fermi interaction. But it also has for consequence that in the decay of Λ^0, both $\Delta T = \frac{1}{2}$ and $\Delta T = \frac{3}{2}$ contributions come in. In fact, OKUBO *et al.* (4) have pointed out that even in cases like Λ-decay, the agreement with $\Delta T = \frac{1}{2}$ could be fortuitous and that the existence of a substantial contribution of $\Delta T = \frac{3}{2}$ is not ruled out. It therefore seems worth while to look more closely into another domain for the possible application of the $\Delta T = \frac{1}{2}$ rule. We have studied the predictions of this rule for the relative decay-rates of various hyperfragments. The hyperfragment doublet ($^4He_\Lambda$, $^4H_\Lambda$) is of considerable interest from this point of view, and has been considered in some detail. Also considered are the decays of $^7Li_\Lambda$, the doublet ($^8Li_\Lambda$, $^8Be_\Lambda$) and the possible doublet ($^6He_\Lambda$, $^6Li_\Lambda$).

GATTO (1), KAWAGUCHI (1) and ISO and KAWAGUCHI (1) have considered the decay rates of the various branches of $^4H_\Lambda$ and $^4He_\Lambda$ separately, but have not considered the relations involving both $^4H_\Lambda$ and $^4He_\Lambda$. GATTO has given our relation (6*a*), but the other relations given by him are quadratic in the decay rates, and will therefore not remain valid if the final state involves a superposition of several angular momentum states, as it almost certainly does (cf. footnote following equation (2′)). ISO and KAWAGUCHI have given our relations (6*a*, *b*, *c*) which involve only $^4H_\Lambda$, but have not given the relations (3), (4), (5) and (7), which involve both $^4H_\Lambda$ and $^4He_\Lambda$.

The applicability of such isotopic spin considerations to the decays of complex systems like hypernuclei may perhaps be questioned. In fact, one of the purposes of this study was to find to what extent they are applicable

(2) R. H. DALITZ: EFINS-58-113, to be published in *Rev. Mod Phys.*; M. GELL-MANN and A. H. ROSENFELD: *Ann. Rev. Nucl. Sci.*, **7**, 407 (1957).

(3) R. P. FEYNMAN and M. GELL-MANN: *Phys. Rev.*, **109**, 193 (1958); S. OKUBO, R. E. MARSHAK, E. C. G. SUDARSHAN, W. B. TEUTSCH and S. WEINBERG: *Phys. Rev.*, **112**, 665 (1958).

here. In the case of the lighter hyperfragments one is encouraged by the fact that the cores are almost entirely in S-states so that the Λ^0 is bound to the core also in an S-state, and one may therefore treat the hyperfragment as decaying as a whole, which is necessary in order to be able to apply these considerations. Verification of the relations derived in Sections 2·2, 2·3, 2·4 and 2·6.2, which do not depend on the assumption of a selection rule $\Delta T = \frac{1}{2}$, will provide a justification for our procedure. In particular, the ratio

$$\frac{w(^4\mathrm{H}_\Lambda \to {}^4\mathrm{He} + \pi^-)}{w(^4\mathrm{He}_\Lambda \to {}^4\mathrm{He} + \pi^0)} = 2\,,$$

derived in Section 2·2, may be conveniently tested in a liquid helium bubble chamber using the interactions of K^- with helium.

The present data on hyperfragments are too scanty to test our predictions, but it is hoped that sufficiently more data will be available in the near future for this purpose.

2. – Theoretical considerations.

We shall first consider the well-known isotopic spin doublet formed by $^4\mathrm{He}_\Lambda$, $^4\mathrm{H}_\Lambda$, which are known to have very closely lying binding energies, as required by charge-independence of Λ-nucleon forces ([4]). The decays of these two hypernuclei into channels involving the same particles (apart from charge), *viz.* pion, nucleon and (^{3}He, ^{3}H) in the final state can therefore be considered together. Such decays are

$$(1)\qquad \begin{cases} {}^4\mathrm{He}_\Lambda \to {}^3\mathrm{He} + \mathrm{p} + \pi^- \quad (w_1) & {}^4\mathrm{H}_\Lambda \to {}^3\mathrm{H} + \mathrm{n} + \pi^0 \quad (w_5)\,, \\ \quad\to {}^3\mathrm{H} + \mathrm{n} + \pi^+ \quad (w_2) & \quad\to {}^3\mathrm{He} + \mathrm{n} + \pi^- \quad (w_6)\,, \\ \quad\to {}^3\mathrm{He} + \mathrm{n} + \pi^0 \quad (w_3) & \quad\to {}^3\mathrm{H} + \mathrm{p} + \pi^- \quad (w_7)\,. \\ \quad\to {}^3\mathrm{H} + \mathrm{p} + \pi^0 \quad (w_4) & \end{cases}$$

The w's appearing after the reactions are the decay rates corresponding to them. A convenient method for obtaining these various decay rates corresponding to the selection rule $\Delta T = \frac{1}{2}$ is provided by the introduction of Wentzel's spurion, a particle that carries an isotopic spin $\frac{1}{2}$, but no energy or momentum or charge. One imagines that the decaying nucleus absorbs (or emits) a spurion during the decay process. With the spurion included,

([4]) R. H. Dalitz: *Phys. Rev.*, **99**, 1475 (1955); J. T. Jones and J. K. Knipp: *Nuovo Cimento*, **2**, 857 (1955).

3742

one assumes that isotopic spin is conserved during the decay, and one then gets the following expressions for the decay rates (with the selection rule (*) $\Delta T=\frac{1}{2}$).

$$
\left\{
\begin{aligned}
w_1 &= \tfrac{1}{12}|\alpha_1-\sqrt{2}\beta_1+\sqrt{2}\alpha_0|^2,\\
w_2 &= \tfrac{1}{12}|\alpha_1-\sqrt{2}\beta_1-\sqrt{2}\alpha_0|^2,\\
w_3 &= \tfrac{1}{12}|\sqrt{2}\alpha_1+\beta_1-\alpha_0|^2,\\
w_4 &= \tfrac{1}{12}|\sqrt{2}\alpha_1+\beta_1+\alpha_0|^2,\\
w_5 &= \tfrac{1}{6}|\alpha_1-\sqrt{2}\beta_1|^2,\\
w_6 &= \tfrac{3}{4}|\alpha_1|^2,\\
w_7 &= \tfrac{1}{12}|\alpha_1+2\sqrt{2}\beta_1|^2.
\end{aligned}
\right. \tag{2}
$$

Here α_0 is the amplitude for decay into a final state of $T=0$, and α_1 and β_1 are the amplitudes for decay into the two possible groups of final states of $T=1$. We have constructed these as follows: the first set is obtained by first combining the pion and nucleon to form states with $T=\frac{3}{2}$, and then combining these with the (^{4}He, ^{5}H) doublet to give $T=1$; the amplitude α_1 refers to these; the other set is obtained by first combining the pion and nucleon to form states with $T=\frac{1}{2}$, and then combining these with (^{3}He, ^{3}H) to give $T=1$; the amplitude β_1 refers to these.

We have written the expressions for the decay rates as if the amplitudes were characterized only by isotopic spin and not by other quantum numbers like angular momenta. It is easy to see that the introduction of the latter only changes these expressions into

$$
w_1=\sum_\lambda \tfrac{1}{12}|\alpha_{1\lambda}-\sqrt{2}\beta_{1\lambda}+\sqrt{2}\alpha_{0\lambda}|^2 \quad \text{etc.}, \tag{2'}
$$

where λ runs over the other quantum numbers, and that the relations we shall derive below remain unaltered thereby (**). We shall therefore use (2).

We can now write down the relations between the different decay rates that follow from (2). One has

$$
2(w_1+w_2+w_3+w_4)\geqslant w_5+w_6+w_7, \tag{3}
$$

(*) The case, $\Delta T=\frac{3}{2}$ allowed, can be similarly treated by introducing a spurion of isotopic spin $\frac{3}{2}$. We have tried this in order to look for more general relations which must be satisfied even if the $\Delta T=\frac{1}{2}$ rule does not hold. It was, however, found that it is impossible to get any simple relations without introducing some special assumptions.

(**) This, however, is not true of some triangular and other more complicated types of inequalities which can be deduced from (2), and these have not therefore been presented here.

3743

any difference between the left-hand side and the right hand side being due to the presence of $T = 0$ contribution in the final state. One also has

$$w_1 + w_2 = 2(w_3 + w_4 + w_5) - (w_6 + w_7) \,. \tag{4}$$

The rates w_3 and w_5 are, however, not easily observable, since the corresponding final states involve two neutral particles. So instead of (4) one may compare with experiment the weaker relation

$$w_1 + w_2 \geqslant 2w_4 - w_6 - w_7 \,. \tag{4'}$$

Some other simple inequalities are

$$w_1 + w_2 \geqslant w_5 \,, \qquad w_1 + w_5 \geqslant \frac{w_2}{3} \,, \qquad w_2 + w_5 \geqslant \frac{w_1}{3} \,, \tag{5a, b, c}$$

$$w_6 + w_7 \geqslant w_5 \,, \qquad w_5 + w_7 \geqslant \frac{w_6}{3} \,, \qquad w_5 + w_6 \geqslant \frac{w_7}{3} \,, \tag{6a, b, c}$$

$$2(w_3 + w_4) + w_5 \geqslant w_6 + w_7 \,. \tag{7}$$

These again involve decay rates w_3 and w_5, which are not directly observable. They may, however, be useful in putting upper and lower bounds on them.

2·1. – Since most of these relations, except for (4'), are rather difficult to compare with experimental data, we shall proceed to introduce some simplifying assumptions. We shall first make use of the fact that the decay mode

$$^4\mathrm{He}_\Lambda \to {}^3\mathrm{H} + \mathrm{n} + \pi^+$$

has not been observed at all so far, and assume that it is altogether absent; *i.e.* we shall assume that $w_2 = 0$. This implies

$$\alpha_1 = \sqrt{2}\,(\beta_1 + \alpha_0)$$

and it then follows that the following relations must hold amongst the decay rates:

$$w_1 = 2w_5 \,; \qquad w_3 = \tfrac{1}{2} w_7 \,; \qquad w_4 = \tfrac{1}{2} w_6 \,. \tag{8a, b, c}$$

Equations (8) enable us to rewrite the inequalities (6) in the form

$$w_6 + w_7 \geqslant \frac{w_1}{2} \,, \quad \frac{w_1}{2} + w_7 \geqslant \frac{w_6}{3} \,, \quad \frac{w_1}{2} + w_6 \geqslant \frac{w_7}{3} \,. \tag{6'a, b, c}$$

3744

The inequalities (6′) now involve observable quantities only, and can therefore be compared directly with experimental results.

2·1.1. – We shall see in Section 3 that, with the meagre experimental data available so far, there is no strong evidence contradicting the relations obtained above. We may, therefore, try to find the effect of introducing some more assumptions regarding the scattering amplitudes. In particular, let us consider the possibility, suggested by the domination of low energy pion-nucleon phenomena by the $T=\frac{3}{2}$ state, that $\beta_1=0$, *i.e.* the only $T=1$ states that contribute are those where the pion-nucleon system is in the $T=\frac{3}{2}$ state. (We do not now assume $w_2=0$). In this case, it is easy to see that among other relations, one has

$$w_5 : w_6 : w_7 = 2 : 9 : 1 . \tag{9}$$

As discussed in Section 3, experiments appear to be strongly in contradiction with $w_6/w_7=9$, so that the $T=\frac{3}{2}$ state of the pion-nucleon system does not play a dominating role in these decays, if one assumes that $\Delta T=\frac{3}{2}$ is forbidden.

2·1.2. – Having seen that the $T=\frac{3}{2}$ state of the pion-nucleon system is not specially important, and that $\beta_1\neq 0$, we may consider the other extreme possibility that there is a complete degeneracy of the six states with $T=1$, *i.e.* $\alpha_1=\beta_1$ (but $w_2\neq 0$). One then gets

$$\begin{cases} w_5 : w_6 : w_7 = 1 : \dfrac{9(3+2\sqrt{2})}{2} : \dfrac{43+30\sqrt{2}}{2} , \\ w_1 + w_2 + \frac{2}{3}(1+2\sqrt{2})w_6 = 2(w_3+w_4) , \\ w_3 + w_4 \geqslant w_6 , \\ w_1 + w_2 + w_3 + w_4 \geqslant \frac{4}{3} w_6 . \end{cases} \tag{10}$$

2·1.3. – We may finally suppose that $w_2=0$, *i.e.* we consider the case $w_2=0$ and $\alpha_1=\beta_1$. We then see that

$$\begin{aligned} w_1 : w_2 : w_3 : w_4 : w_5 : w_6 : w_7 = \\ = 1 : 0 : \frac{43+30\sqrt{2}}{8} : \frac{9(3+2\sqrt{2})}{8} : \frac{1}{2} : \frac{9(3+2\sqrt{2})}{4} : \frac{43+30\sqrt{2}}{4} . \end{aligned} \tag{11}$$

Some of the relations deduced in Sections 2·1.1–2·1.3 are violated by the present experimental data and some of them quite strongly, as is seen by comparison with relation (22) of Section 3. We have, however, thought it

worthwhile to give them above, in view of the large statistical fluctuations in the present data, which make it rather difficult to rule out any of the possibilities quite definitely.

So much for the various possibilities in the 3-particle pionic decay of $({}^4H_\Lambda, {}^4He_\Lambda)$, with $\Delta T = \frac{3}{2}$ forbidden. We shall now consider some other decays.

2·2. – Let us first consider the two-body mesonic decays of $({}^4H_\Lambda, {}^4He_\Lambda)$. We readily see that

$$\frac{w({}^4He_\Lambda \to {}^4He + \pi^0)}{w({}^4H_\Lambda \to {}^4He + \pi^-)} = \frac{1}{2}. \tag{12}$$

This ratio does not depend on the hypothesis $\Delta T = \frac{1}{2}$, and would provide a valuable check on the applicability of our iso-spin considerations.

2·3. – Let us next consider the following decays:

$$\begin{aligned} {}^4H_\Lambda &\to {}^3H + n \qquad (w_1), \\ {}^4He_\Lambda &\to {}^3He + n \qquad (w_2), \\ &\to {}^3H + p \qquad (w_3). \end{aligned}$$

Here the final state can have $T = 1$ or $T = 0$. Denoting the corresponding amplitudes by α_1 and α_0 respectively, we get

$$\begin{aligned} w_1 &= |\alpha_1|^2, \\ w_2 &= \left|\frac{\alpha_1 + \alpha_0}{2}\right|^2, \\ w_3 &= \frac{|\alpha_1 - \alpha_0|^2}{2}. \end{aligned}$$

From these follow the inequalities

$$w_2 + w_3 \geqslant \frac{w_1}{2}, \tag{13a}$$

$$w_1 + w_3 \geqslant \frac{w_2}{2}, \tag{13b}$$

and

$$w_1 + w_2 \geqslant \frac{w_3}{2}. \tag{13c}$$

3746

2·4. – The hyperfragment doublet ($^6He_\Lambda$, $^6Li_\Lambda$) has not yet been observed with certainty. If it is found to exist, we may look for the decay modes

$$\begin{aligned} {}^6He_\Lambda &\to {}^3H + {}^2H + n \qquad (w_1) \\ {}^6Li_\Lambda &\to {}^3He + {}^2H + n \qquad (w_2) \\ &\to {}^3H + {}^2H + p \qquad (w_3) \end{aligned}$$

and then, just as in Section 2·3, we can expect again the same inequalities (13)

2·5.1. – We now consider the decay of $^7Li_\Lambda$. If, as seems plausible, $^7Li_\Lambda$ has $T = 0$, and if $\Delta T = \frac{3}{2}$ is forbidden, we will expect

$$w_1 = 2w_2 , \tag{14}$$

where w_1 and w_2 refer to the decay rates corresponding to the following decay modes:

$$\begin{aligned} {}^7Li_\Lambda &\to {}^4He + {}^3He + \pi^- \qquad (w_1) , \\ &\to {}^4He + {}^3H + \pi^0 \qquad (w_2) . \end{aligned}$$

2·5.2. – $^7Li_\Lambda$ has also the non-pionic decay modes

$$\begin{aligned} {}^7Li_\Lambda &\to {}^3He + {}^3H + n \qquad (w_1) , \\ &\to {}^3H + {}^3H + p \qquad (w_2) . \end{aligned}$$

Under the selection rule $\Delta T = \frac{1}{2}$, we expect here that

$$2w_1 \geqslant w_2 . \tag{15}$$

If further, we assume that the amplitudes into the two possible sets of final states with $T = \frac{1}{2}$ are equal, we get

$$w_1 = 2w_2 . \tag{16}$$

2·6.1. – We shall finally consider the isotopic spin doublet ($^8Li_\Lambda$, $^8Be_\Lambda$). Considering the following pionic decays

$$\begin{aligned} {}^8Li_\Lambda &\to {}^8Be + \pi^- \quad (w_1) \qquad & {}^8Be_\Lambda &\to {}^8Be + \pi^0 \quad (w_3) \\ &\to {}^8Li + \pi^0 \quad (w_2) & &\to {}^8Li + \pi^+ \quad (w_4) \\ & & &\to {}^8B + \pi^- \quad (w_5) \end{aligned}$$

and assuming that $\Delta T = \frac{3}{2}$ is forbidden, we get

$$w_1 = w_2 \tag{17a}$$

$$w_4 + w_5 = 2w_3 + w_1 \tag{17b}$$

and the inequalities

$$4w_3 + w_5 \geqslant \frac{w_1}{2}\,, \tag{18a}$$

$$4w_3 + w_4 \geqslant \frac{w_5}{2}\,. \tag{18b}$$

2·6.2. – The non-mesonic decays of ($^8\mathrm{Li}_\Lambda$, $^8\mathrm{Be}_\Lambda$)

$$\begin{aligned} {}^8\mathrm{Li}_\Lambda &\to {}^4\mathrm{He} + {}^3\mathrm{H} + \mathrm{n} \qquad (w_1) \\ {}^8\mathrm{Be}_\Lambda &\to {}^4\mathrm{He} + {}^3\mathrm{He} + \mathrm{n} \qquad (w_2) \\ &\to {}^4\mathrm{He} + {}^3\mathrm{H} + \mathrm{p} \qquad (w_3) \end{aligned}$$

will satisfy the inequalities (13) of Section 2·3.

3. – Discussion.

The experimental data available for comparison with these considerations are extremely meagre, and are mainly the following: the Chicago data of W. E. SLATER ( ) and E. M. SILVERSTEIN [6]; the Wisconsin data of SCHNEPS *et al.* [7]; and the world survey data compiled by R. LEVI-SETTI *et al.* [8]. The number of unambiguously identified hyperfragments with $Z \geqslant 3$ is too small to compare with the relations derived in Sections 2·4-2·6. The same is the case with the mesonic and non-mesonic two-body decays of ($^4\mathrm{H}_\Lambda$, $^4\mathrm{He}_\Lambda$) considered in Sections 2·2-2·3. So we shall confine our discussion to the available experimental information on the mesonic three-body decays of the ($^4\mathrm{H}_\Lambda$, $^4\mathrm{He}_\Lambda$) doublet. This information is summarized in Table I below.

It is evident that the numbers of observed decays into different channels are too small to make any really significant comparison with the predicted

[5] W. E. SLATER: *Suppl. Nuovo Cimento*, **10**, 1 (1958).
[6] E. M. SILVERSTEIN: *Suppl. Nuovo Cimento*, **10**, 41 (1958).
[7] J. SCHNEPS, W. F. FRY and M. S. SWAMI: *Phys. Rev.*, **106**, 1062 (1957).
[8] R. LEVI SETTI, W. E. SLATER and V. L. TELEGDI: *Suppl. Nuovo Cimento*, **10**, 68 (1958).

3748

relative decay rates. We can however try to see what are the tentative indications from the present data.

TABLE I.

Source	$^4H_\Lambda$ events	$^4He_\Lambda$ events
World survey data	total 28: 13 ^{4}He π^-; 6 ^{3}He nπ^-; 5 ^{3}H pπ^-; 4 other modes	total 9: 8 ^{3}He pπ^-; 1 ^{2}H ppπ
Chicago data	total 7: 5 ^{4}He π^-; 2 ^{3}H pπ^-	total 8: 7 ^{3}He pπ^-; 1 ^{3}H pπ^0
Wisconsin data	total 2: 1 ^{2}H pnπ^-; 1 ^{3}H pπ^-	total 4: 3 ^{3}He pπ^-; 1 ^{3}H pπ^0

The world survey data compilation gives us

$$\frac{w_6}{w_7} = \frac{w(^4H_\Lambda \to {}^3He + n + \pi^-)}{w(^4H_\Lambda \to {}^3H + p + \pi^-)} = \frac{6}{5} \sim 1 . \tag{19}$$

This ratio is of interest for two reasons. Firstly, the fact that these two decay rates—one of which can be regarded as the decay of a Λ^0 particle outside a ^{3}H core, whereas the other cannot—have comparable decay rates gives us some justification in applying isotopic spin considerations to the hyperfragment as a whole; and secondly, since this ratio is strongly in disagreement with the very large ratio predicted on the basis of the assumptions made in Section 2·1.1, it leads us to conclude that if the selection rule $\Delta T = \frac{1}{2}$ is valid, there is no indication of a strong pion-nucleon interaction in the $T = \frac{3}{2}$ state. Nor is there any indication in favour of the assumption that all the six $T = 1$ states are completely degenerate. (This is similar to the situation in the case of τ-decay). It, therefore, seems that if the selection rule $\Delta T = \frac{1}{2}$ is valid, the only relations one can try to check are those in Sections 2 and 2·1. In the latter, the only assumption made on the decay amplitudes is that $w_2 = 0$. This is based on the experimental observation that no decay of a hydrogen or helium hyperfragment involving a π^+-meson has been observed to-date, even though the number of $^4H_\Lambda$ and $^4He_\Lambda$ hyperfragments listed so far is nearly 100. In fact, a decay involving a π^+-meson seems to be an extremely rare event even amongst the heavier hyperfragments, there being only one

event (9) known to us. Such events would be very easily identifiable, and it appears very improbable that they could have been missed by the various experimental groups.

Another ratio we can get immediately from the Table I is

$$\frac{w_1}{w_4} = \frac{w(^4\mathrm{He}_\Lambda \to {}^3\mathrm{He} + \mathrm{p} + \pi^-)}{w(^4\mathrm{He}_\Lambda \to {}^3\mathrm{H} + \mathrm{p} + \pi_0)} = \frac{10}{2} = 5\,, \tag{20}$$

using the combined Wisconsin and Chicago data.

Before proceeding further to evaluate the other ratios like w_4/w_6, w_1/w_6 etc., we have to normalize the observed numbers of decays of $^4\mathrm{H}_\Lambda$ and $^4\mathrm{He}_\Lambda$ into different channels to the same parent population of $^4\mathrm{H}_\Lambda$ and $^4\mathrm{He}_\Lambda$. For carrying out this normalization, and then estimating these ratios, we shall use only the systematic collection of data of the Chicago and Wisconsin groups. These groups had 9 π^--mesonic decays of $^4\mathrm{H}_\Lambda$ and 10 of $^4\mathrm{He}_\Lambda$. From these numbers it is possible to evaluate the total populations of $^4\mathrm{H}_\Lambda$ and $^4\mathrm{He}_\Lambda$ hyperfragments from which these decays arose, by making use of the experimentally measured values of the ratio R = non-mesonic/mesonic for $^4\mathrm{H}_\Lambda$ and $^4\mathrm{He}_\Lambda$, and further assuming that the experimentally known branching ratio

$$\frac{w(\Lambda^0 \to \mathrm{n} + \pi^0)}{w(\Lambda^0 \to \mathrm{p} + \pi^-)} \approx 0.5\,,$$

for free Λ^0 decay is maintained in the decays of a bound Λ^0 also. This latter assumption may not be strictly true, for this branching ratio can be modified quite strongly by the effect of Pauli's principle, as has been pointed out by Dalitz (10). In view of the fact that the available data are rather scanty, and that there is no experimental determination so far of the departure from the value $\pi^0/\pi^- \approx 0.5$ (which can possibly be measured in a liquid helium bubble chamber using K^- on helium), we shall neglect these effects here, and assume for the present that this ratio has the value 0.5 for $^4\mathrm{H}_\Lambda$ and $^4\mathrm{He}_\Lambda$ decay as in the decay of free Λ^0. The ratio R for hyperfragments of charge one has been measured by both the Chicago and the Wisconsin groups; they obtain a value zero, but the Chicago group places an experimental upper limit of 0.6 on R. Taking this upper limit, the total number of $^4\mathrm{H}_\Lambda$ hyperfragments, which decay either with the emission of a π^- or non-mesonically by its internal conversion, may be estimated to be $(9 \times 1.6 =)\ 14.4$. The total number of $^4\mathrm{H}_\Lambda$ hyperfragments that decay by the emission of a π^0 or non-mesonically by its

(9) J. Schneps: *Phys. Rev.*, **112**, 1335 (1958).
(10) R. H. Dalitz: *Phys. Rev.*, **112**, 605 (1958).

3750

internal conversion may then be estimated to be $(14.4 \times 0.5 =) 7.2$, thus making a total of 21.6 for the parent population of $^4H_\Lambda$. As regards $^4He_\Lambda$, we have the experimental value $R = 1.8$ obtained by the Chicago, Wisconsin and Northwestern University (11) groups. Using this ratio, the total $^4He_\Lambda$ population (*) can be estimated, in an exactly similar manner, to be 42. The number of $^4He_\Lambda$ fragments is thus $42/21.6 \approx 2$ times the number of $^4H_\Lambda$ fragments. The individual $^4H_\Lambda$ events have therefore to be multiplied by 2 before comparing with any of the $^4He_\Lambda$ events for getting relative decay rates. Thus we get

$$\frac{w_7}{w_4} = \frac{w(^4H_\Lambda \to {}^3H + p + \pi^-)}{w(^4He_\Lambda \to {}^3H + p + \pi^0)} = \frac{3 \cdot 2}{2} = 3 . \tag{21}$$

Combining (19), (20), (21), we get

$$w_1 : w_4 : w_6 : w_7 = 5 : 1 : 3 : 3 . \tag{22}$$

These « experimental » estimates may be compared with equation (8*c*) of Section 2·1 where one expects $w_4 = \frac{1}{2} w_6$. There is thus an indication of a contradiction. We cannot, however, insist on this, in view of the poor statistics. The large amount of statistical fluctuation in the sample is brought out by the fact that $N_7 = 3$, $N_6 = 0$ in the Wisconsin-Chicago sample whereas $N_7 \approx N_6$ in the world survey data compilation.

We may remark that while the experimental investigations on hyperfragments so far have been directed towards problems like the determination of binding energies and non-mesonic/mesonic ratios, no attempt seems to have been made to evaluate the different branching ratios of the types considered by us. It will be seen from our analysis that such a study can yield very fruitful information, provided sufficient data are available. For example, in the case of the ($^4H_\Lambda$, $^4He_\Lambda$) doublet, since easily verifiable relations (*viz.* 6′ and 8) arise only on the assumption of $w_2 = 0$, it is very desirable to know to what extent this mode is forbidden. It is also necessary to look very carefully for decays which involve a π^0. We have only two cases of $^4He_\Lambda \to {}^3H + p + \pi^0$

---

(11) P. E. Schlein: to be published in *Phys. Rev. Lett.*

(*) It may be remarked that this number is a lower limit, since the actual value of R may be considerably higher than the value 1.8 assumed here. In fact, from the asymmetry coefficient (12) in Λ^0-decay, $\alpha = 0.85^{+0.15}_{-0.30}$ one can calculate the relative contributions of *s*- and *p*-waves in Λ^0-decay, and use these to get a value (11) of $4.8^{+.2}_{-1.9}$ for the non-mesonic/mesonic ratio. What needs noting is the fact that a higher value for this ratio tends to increase the small discrepancy discussed later.

(12) E. Boldt, H. S. Bridge, D. O. Caldwell and Yash Pal: *Phys. Rev. Lett.*, **1**, 256 (1958).

from the systematic studies of the Wisconsin and Chicago groups. Now that the binding energies of the hyperfragments have been fairly well established, they could be used to identify such decays. It is to be hoped that more experimental information on these points will be available in the near future.

* * *

We wish to thank Professor M. G. K. MENON for his helpful comments.

RIASSUNTO (*)

Alla luce della regola di selezione $\Delta T = \frac{1}{2}$, si esaminaano i rapporti di « branching » nei decadimenti di iperframmenti essendo ($^4He_\Lambda$, $^4He_\Lambda$), ($^6He_\Lambda$, $^6Li_\Lambda$), ($^8Li_\Lambda$, $^8Be_\Lambda$) i doppietti e $^7Li_\Lambda$ l'ipernucleo. In relazione a tali regole di selezione si discutono i dati sperimentali sul doppietto ($^4H_\Lambda$, $^4He_\Lambda$). Si fa rilevare che è necessaria una raccolta sistematica di un numero di dati di gran lunga maggiore di quello disponibile attualmente allo scopo di saggiare la validità della regola $\Delta T = \frac{1}{2}$ in tale dominio.

(*) *Traduzione a cura della Redazione.*

7752

IL NUOVO CIMENTO Vol. XIV, N. 4 16 Novembre 1959

Equations of Motion for Renormalized Fields.

F. L. Scarf (*)

CERN - Geneva

(ricevuto il 26 Agosto 1959)

Summary. — Solutions to conventional equations of motion are generally well-defined only in the « wrong » Hilbert space with all antiparticle states filled. The meaningful quantity which can be renormalized is a Wick product of some functional of the physical particle operators. When the field theory has infinite wave function renormalization, there is no direct connection between the two representations for the field operators. An example is given for which the two forms have different space-time developments.

1. – Introduction.

Several problems are encountered in any attempt to determine equations of motion for renormalized field quantities. It has been noted that $(\psi^R)^2$ or $(\psi^{*R})^2$ $(\psi^R = Z^{-\frac{1}{2}}\psi)$ must be of order Z^{-1} since $\psi^*\psi$ is fixed by the commutation relations to be of order unity. Whenever Z^{-1} is infinite, the equations of motion will therefore contain undefined operator products if everything is expressed in terms of renormalized fields. Some authors have proposed that this effect may be treated by averaging over small time intervals ([1,2]), and by using special limiting procedures to define the products ([2,3]).

(*) U. S. National Science Foundation Fellow on leave from the University of Washington, Seattle, Washington.

([1]) W. Heisenberg: *Nucl. Phys.*, **4**, 532 (1957).

([2]) R. Haag and G. Luzzatto: *Nuovo Cimento*, **13**, 415 (1959).

([3]) J. G. Valatin: *Proc. Roy. Soc.*, A **226**, 254 (1954).

3753

In this note we wish to point out another, quite distinct, difficulty which is usually present when Z vanishes. In these cases, the solutions to the non-renormalized equations of motion for spinor fields are undefined in the Hilbert space containing the true vacuum state. Well-defined bare particle fields must be Wick-ordered products of the phyiscal particle operators. When $Z=0$, these ordered expressions do not necessarily obey the « renormalized » equations derived from the original equations of motion. This is indeed found to be true for the Thirring model where the ordered quantity satisfies a non-local integral equation. No such difficulties arise for the neutral scalar meson theory with fixed source, although they do appear in the Lee model and should be present for realistic theories.

2. – The ordering problem.

Consider a system of k spinor fields with an interaction which is hermitian, local and covariant. The invariant Lagrangian, $L(\bar{\psi}_i, \psi_i, \lambda_i)$, $i = 1 \ldots k$, leads to the equation of motion

$$(i\gamma^\mu \partial_\mu + m_i)\psi_i + f_i(\bar{\psi}_j, \psi_j, \lambda_j) = 0 \,, \tag{1}$$

and its hermitian conjugate. The Lagrangian also admits the constants of motion $P_\nu(\bar{\psi}_i, \psi_i, \lambda_i)$ and $N_i = \int \mathrm{d}^3x\, j_i^{(0)}(\bar{\psi}_i, \psi_i, \lambda_i)$. If any of the m_i are zero, the corresponding pseudo-currents are conserved, and symmetry properties of the Lagrangian under isotopic rotations may lead to additional constants of motion.

The problem is solved by defining physical particle fields, φ_i, $\bar{\varphi}_i$, such that $(i\gamma^\mu \partial_\mu + M_i)\varphi_i = 0$ (M_i may not equal m_i) and

$$P_\nu(\bar{\psi}_i, \psi_i, \lambda_i) = P_\nu^{(0)}(\bar{\varphi}_i, \varphi_i) + \text{const.} \,, \tag{2}$$

where $P^{(0)}$ means all $\lambda_i = 0$. A particular solution of eq. (1) is then written as

$$\psi_i = \varphi_i g_i(\lambda_j, \bar{\varphi}_j, \varphi_j, x_\mu) \tag{3}$$

so that $\psi_i \to \psi_i^{\mathrm{in}} = \varphi_i$ as $t \to -\infty$. Finally, free field anti-commutation relations are imposed on the φ operators. The state vectors are eigenstates of P_ν and any of the other constants of motion whose operator representatives commute with P_ν. The entire discussion may also be carried out with the modified Lagrangian $L' = :L: = L + \text{const.}$ This leads to $P'_\nu = :P_\nu:$, etc., but it yields the same equation of motion for ψ_i, and the same functional solution, g.

3754

When φ_i is decomposed as

$$(4) \qquad \varphi_i = (2\pi)^{-\frac{3}{2}} \int \mathrm{d}^3\boldsymbol{p} (M_i/\omega_i)^{\frac{1}{2}} (u(\boldsymbol{p}) a_i(\boldsymbol{p}) \exp[ipx] + v(\boldsymbol{p}) b_i^*(\boldsymbol{p}) \exp[-ipx]) ,$$

a Hilbert space is defined by $a_i|0) = b_i^*|0) = 0$. Then, since the P_ν (or P'_ν) are polynomials in $(\bar{\varphi}_i F \varphi_i)$, and since $\varphi_i|0) = 0$ possible eigenstates of P are $|\alpha, \beta) = (a_i^*)^\alpha (b_i)^\beta |0)$. In this Hilbert space N_i and eq. (3) are well-defined for any function g_i which can be expanded in powers of $\bar{\varphi}$, φ. Thus, a complete solution may be obtained in this representation and the equations of motion have direct meaning with reference to the space-time development of ψ.

However, this Hilbert space is not the correct one since its « vacuum » has all anti-particle states filled and the energy is not positive definite. The correct Hilbert space has $a|0\rangle = b|0\rangle = 0$; the two are connected by $|0\rangle = T|0) = \prod_{n,i} b_i(P_n)|0)$, where we have tentatively assumed that a cut-off is present so that there are a finite number of degrees of freedom. In this Hilbert space the *same* operators P_ν or P'_ν are diagonal and well-defined, and their eigenstates are $|\alpha, \beta\rangle = (a_i^*)^\alpha (b_i^*)^\beta |0\rangle$.

We must now investigate to what extent eqs. (1), (3) are well-defined in the true Hilbert space. This question may easily be answered if a cut-off exists. Then T is unitary and well-defined, $\psi|0\rangle = \psi T|0)$, and ψ may be commuted with T to evaluate the expression. However, it is impossible to obtain an exact solution with a finite cut-off and one cannot determine how $\psi|0\rangle$ behaves in the limit $k_{\max} \to \infty$. Relativistic theories always contain an infinite number of degrees of freedom so that T does not exist. Under these circumstances, one must *define* the function

$$(5) \qquad \tilde{\psi}_i = z^{\frac{1}{2}} \varphi_i : G_i(\bar{\varphi}_j, \varphi_j, \lambda_j, x_\mu) : ,$$

by requiring *a*) that $\tilde{\psi}_i^R = \tilde{\psi}_i Z^{-\frac{1}{2}} \to \varphi_i$ as $t \to -\infty$. *b*) $\langle 1|\tilde{\psi}_i|0\rangle \approx \langle 1|\psi_i|0\rangle$, t finite. *c*) $\tilde{\psi}_i$ satisfies the same commutation relations as does ψ_i. Then $\tilde{\psi}_i^R$ is well-defined in the true Hilbert space (*i.e.*, it has finite matrix elements) and it is *the* renormalized Heisenberg operator for the bare particle field.

If $Z^{\frac{1}{2}}$ turns out to be finite, $\tilde{\psi}_i$ is presumably obtained from ψ_i by regrouping terms, adding constants, etc. In general, however, $Z^{\frac{1}{2}}$ vanishes. For these cases $\tilde{\psi}_i$ does not necessarily have the same space-time dependence as does ψ_i. In particular, the renormalized, ordered operator satisfies

$$(6) \qquad (i\gamma^\mu \partial_\mu + M_i)\tilde{\psi}_i^R = \varphi_i : (i\gamma^\mu \partial_\mu + M_i) G_i : ,$$

while the « renormalized », unordered operator obeys $(i\gamma^\mu\partial_\mu+m_i)\psi_i^R+Z^{-\frac{1}{2}}f=0$, $\psi_i^R=\psi_i Z^{-\frac{1}{2}}$. Since $\tilde{\psi}_i^R$ and ψ_i^R are connected only by having the same commutation relations and asymptotic values, there is no reason to believe that these equations describe the same entity. In fact, there is no meaning to the operation of renormalizing ψ, and we assert that only eq. (6) may be regarded as the equation of motion for the renormalized operator. Similar considerations generally apply when L contains coupled fermion and boson fields.

3. – Some specific examples.

Let us first examine the two-dimensional Thirring model [4] for which the equation of motion is $i\gamma^\mu\partial_\mu\psi+2\lambda(\bar{\psi}\psi)\psi=0$. In the standard representation one of the components satisfies $\partial\psi_1/\partial u=i\lambda:\psi_2^*\psi_2:\psi_1$ $[u=t+x,\ v=t-x]$; we have also let $\psi_1\to\psi_1\exp[icu\,\delta(0)])$ and the solution is $\psi_1(x,t)=\varphi_1(v)\cdot$ $\cdot\exp[i\lambda]\int_{-\infty}^{u}:\varphi_2^*\varphi_2:\mathrm{d}u'$. Glaser has shown [5] that the commutation relations $\varphi_2(u')\psi_1(u,v)=\psi_1(u,v)\varphi_2(u')\exp[i\lambda\theta(u-u')]$ can be used to recast ψ_1 in the well-defined ordered form, $\tilde{\psi}_1=\varphi_1 Z^{\frac{1}{2}}:\exp[Q]:$, or

$$(7)\qquad \tilde{\psi}_1=Z^{\frac{1}{2}}\varphi_1(v):\exp\left[\frac{\exp[i\lambda]-1}{2\pi i}\cdot\right.$$
$$\left.\cdot\int\mathrm{d}p\,\mathrm{d}q\left(\frac{p_+}{q_-}\right)^{\lambda'/2\pi}\frac{\exp[i(q-p)u]}{p_+-q_-}\,C_2^*(p)\,C_2(q)\right]:,$$

where $C_2(q)=\theta(-q)a(q)+\theta(q)b^*(-q)$ and $\lambda'=\lambda+2\pi N$ so that $|\lambda'/2\pi|<1$; $(p_\pm)^\lambda$ is real for p real and positive and it has a branch cut from 0 to $+\infty$. In Glaser's paper $Z^{\frac{1}{2}}$ is evaluated by requiring that

$$(8)\qquad \frac{\partial\langle 1|\psi_1|0\rangle}{\partial\lambda}=i\int_{-\infty}^{u}\mathrm{d}u'\langle 1|:\varphi_2^*\varphi_2:\psi_1|0\rangle\,,$$

be valid for $\psi_1\to\tilde{\psi}_1$. Eq. (8) gives the renormalization constant to within a factor independent of λ; since $Z^{\frac{1}{2}}$ must be unity for $\lambda=0$, this factor is unity.

To see that $\tilde{\psi}_1^R=\tilde{\psi}_1 Z^{\frac{1}{2}}$ differs from ψ_1, consider the equation $\partial\tilde{\psi}_1^R/\partial u=$ $=i\lambda:\varphi_2^*\varphi_2:\tilde{\psi}_1^R$. The matrix element $\langle 1|\partial\tilde{\psi}_1^R/\partial u|0\rangle$ is zero since $\langle 1|\tilde{\psi}_1^R|0\rangle=$ $=\langle 1|\varphi_1(v)|0\rangle$, but the other side gives $i\lambda\sin(\lambda/2)\cdot\int_0^\infty\mathrm{d}k\cdot 1\,[\langle 3|'=\langle 1|:\varphi_2^*\varphi_2:$ has

(4) W. E. Thirring: *Ann. Phys.*, **9**, 91 (1958).
(5) V. Glaser: *Nuovo Cimento*, **9**, 1007 (1958).

3756

infinite norm]. One might try to redefine $\tilde{\psi}_1^R \to \tilde{\psi}_1^R \exp[iu \times \infty]$ to eliminate the infinite term but this procedure does not help; the matrix elements between $\langle n|$ and $|m\rangle$ still give different values for the two sides of the equation. In other words $\tilde{\psi}^R$ has a space-time dependence which differs from that of ψ, and the difference cannot be eliminated by a c-number adjustment. If a cut-off exists in k-space, $\langle n| : \varphi_2^* \varphi_2 : \tilde{\psi}^R|0\rangle$ is finite. One may then write $i\lambda : \varphi_2^* \varphi_2 : \tilde{\psi}_1^R = ;R(\varphi_2^*, \varphi_2)\psi_1^R; + S\tilde{\psi}_1^R$ and $\tilde{\psi}_1^R$ can be derived from the equation for ψ_1 (it should be noted that the ordering operation is generally non-local, even if there is a cut-off). In this sense, $\tilde{\psi}_1^R$, which obeys

$$\frac{\partial \tilde{\psi}_1^R}{\partial u} = : \frac{\partial Q}{\partial u} \tilde{\psi}_1^R : , \tag{9}$$

also « satisfies » the original equations of motion, but with a cut-off $Z^{\frac{1}{2}}$ depends on u. In the limit of no cut-off the $\psi \to \tilde{\psi}^R$ connection becomes ill-defined. The quantity $Z^{\frac{1}{2}}$ formally depends on u (eq. (8)), but it is usually regarded as a constant. Each function has meaning in its own Hilbert space, but the original equations of motion are meaningless in the representation with $a|0\rangle = b|0\rangle = 0$.

This result has several immediate consequences. The customary derivation of the Tamm-Dancoff equations ([6]) for many particle amplitudes involves the original equation of motion. For instance, one would have for the Thirring model.

$$\frac{\partial}{\partial u_a} \langle \pi | \psi_1^R(a) \psi_2^R(b) | 0 \rangle = i\lambda \langle \pi | : \varphi_2^*(a) \varphi_2(a) : \psi_1^R(a) \psi_2^R(b) | 0 \rangle , \tag{10}$$

and this can be expanded to obtain an approximate equation for $\langle \pi | \psi_1^R(a) \psi_2^R(b) | 0 \rangle$. However, we find that these amplitudes have no meaning in the true representation. The meaningful amplitude satisfies

$$\frac{\partial}{\partial u_a} \langle \pi | \tilde{\psi}_1^R(a) \tilde{\psi}_2^R(b) | 0 \rangle = \langle \pi | : \frac{\partial Q_2}{\partial u_a} \tilde{\psi}_1^R(a) : \tilde{\psi}_2^R(b) | 0 \rangle , \tag{11}$$

which leads to considerably different results.

There are no difficulties in the neutral scalar meson theory with fixed source ([7]). The content of this model is best explored by examing the inter-

---

([6]) P. T. Matthews and A. Salam: *Proc. Roy. Soc.*, A **221**, 128 (1954).

([7]) T. D. Lee: *Phys. Rev.*, **94**, 1329 (1954).

action representation operator $U(t, -\infty)$,

$$i\frac{\partial U}{\partial t} = HU = \int \mathrm{d}^3x(gB - \delta m)NU\,, \tag{12}$$

where $N = \psi^*\psi = \varphi^*\varphi$, B is the physical boson field operator and δm is the mass renormalization constant. For fixed nucleons, $\partial_\mu N = 0$, $N^2 = N$ and $[N, B] = 0$. Thus, N may be treated as a c-number in eq. (12). The general solution is $U = \exp\left[-i\int_{-\infty}^{\cdot} H\,\mathrm{d}t'\right]$ (time-ordered), which is well defined in the representation with $B^{(+)}|0) = B^{(-)}|0) = 0$. This solution is not meaningful in the true Hilbert space, $B^{(+)}|0\rangle = [B^{(-)}]^*|0\rangle = 0$. However, H of eq. (12) obeys $[H^{(-)}, (H^{(+)})^n] = nc(H^{(+)})^{n-1}$, so that [8]

$$i\frac{\partial U}{\partial t} = ;HU; + f(c)\,U\,. \tag{13}$$

The simple substitution $U = \tilde{U}^R \exp\left[-i\int_{-\infty}^{t} f(c)\,\mathrm{d}t'\right]$ leads to the ordered form, $\tilde{U}^R$, so that U differs from $\tilde{U}^R$ merely by a vanishing c-number factor, and $\tilde{\psi}^R$, $\tilde{B}^R$ obey the original equations of motion after this factor is absorbed.

For the Thirring model $H = \lambda\int \mathrm{d}x : \varphi_1^*\varphi_1\varphi_2^*\varphi_2 :$, and $[H^{(-)}, (H^{(+)})^n]$ is *not* simply related to H. Thus, $\tilde{U}^R$ obeys an equation which is essentially different from the one satisfied by U, even after c-number renormalization. Generally, when H is not a linear function of the field operators, $HU = \alpha; HU; + \sum \beta_i; \varphi_i U; + + \ldots$ where α, β, etc., are non-local functions, and $\tilde{U}^R$ does not satisfy the renormalized equation for U.

4. – Conclusions.

It has been conjectured that renormalized field quantities obey local equations which can be obtained from equations of motion by regrouping terms (to account for mass renormalization, etc.) and factors (to account for coupling constant and wave function renormalization). Since products of renormalized operators are undefined at a sharp time if $Z = 0$, various averaging and limiting processes must accompany the manipulations.

We assert that the equations obtained by these techniques have solutions which are generally ill-defined in the true Hilbert space. For these problems the meaningful renormalized operator is a Wick-ordered product. If $Z = 0$,

---

([8]) L. VAN HOVE: *Physica*, **18**, 145 (1952).

3758

the latter is *not* obtained directly from the original equation of motion or from its « renormalized » form (the neutral scalar meson theory is an exception). It is still necessary to use the averaging and limiting techniques if all quantities in the new equation (*e.g.*, eq. (9)) are to be expressed in terms of renormalized bare particle operators.

* * *

I wish to thank Dr. V. Glaser and Dr. B. Jakšić for several clarifying discussions.

RIASSUNTO (*)

Le soluzioni di equazioni convenzionali del moto sono generalmente ben determinate solo in un « falso » spazio Hilbertiano in cui tutti gli stati dell'antiparticella siano riempiti. La grandezza significativa che può essere rinormalizzata è un prodotto di Wick di alcuni funzionali degli operatori della particella fisica. Quando la teoria del campo porta alla rinormalizzazione infinita della funzione d'onda, non vi è alcuna connessione diretta fra le due rappresentazioni degli operatori di campo. Si fornisce un esempio per cui le due forme hanno sviluppi spazio-temporali differenti.

(*) *Traduzione a cura della Redazione.*

IL NUOVO CIMENTO Vol. XIV, N. 4 16 Novembre 1959

A Novel Dispersion Relation for Potential Scattering (*).

A. Klein and B. W. Lee

Department of Physics, University of Pennsylvania - Philadelphia, Pa.

(ricevuto il 28 Agosto 1959)

Summary. — A dispersion relation for potential scattering is found which holds without restriction on momentum transfer. The price paid for this achievement is that the integral in the relation involves a completely non-physical amplitude. Nevertheless it is shown that in combination with the unitarity condition, the Born series, in the event it converges, is completely determined. The transition to the more customary relation is also carried through.

1. – Introduction.

As a consequence of recent work ([1-3]), the analytic properties as a function of energy for fixed momentum transfer of the Schrödinger amplitude for the scattering of a particle by a potential are well-known. In addition an understanding of the properties of the Fredholm series, ([2]), the Born series ([1-3]), and of the partial wave expansions ([3]) have been important by-products of these investigations.

In relation to the previous work, the present note may be viewed as a curiosity. It basically points out the existence (Section **2**) of a dispersion

(*) Supported in part by the U. S. Atomic Energy Commission. Reproduction in whole or in part is permitted for any purpose of the U. S. Government.

([1]) D. Y. Wong: *Phys. Rev.*, **107**, 302 (1957).

([2]) N. N. Khuri: *Phys. Rev.*, **107**, 1148 (1957); N. N. Khuri and S. B. Treiman: *Phys. Rev.*, **109**, 198 (1958).

([3]) C. Zemach and A. Klein: *Nuovo Cimento*, **10**, 1078 (1958); A. Klein and C. Zemach: *Ann. Phys.*, to be published (1959).

c780

relation which differs from the customary one. Though superficially less interesting than the latter because the integral over the absorptive part is completely non-physical, it nevertheless suffices in conjunction with the unitarity condition, to determine the Born series completely in the event that expansion converges.

In Section **3** this claim is substantiated by a computation of the second Born approximation for the Yukawa potential. In this connection it is not completely of academic interest that the new dispersion relations are proved in Section **2** *without restriction on momentum transfer.*

Finally, Section **4** and the Appendix are concerned with the further analysis of these relations, and describe, among other things, a transition to the more customary relations.

2. – Outline of proof.

If we write the Schrödinger equation in the dimensionless version

$$[\nabla^2 + k^2 - \lambda V(\boldsymbol{r})]\,\psi(\boldsymbol{r}) = 0\,, \tag{1}$$

the scattering amplitude takes the form

$$\begin{aligned} f(k,\theta) &= -(4\pi)^{-1}\lambda\int \exp[i\boldsymbol{k}'\cdot\boldsymbol{r}]\,V(\boldsymbol{r})\,\psi(\boldsymbol{r})\,\mathrm{d}^3 r = \\ &= -(4\pi)^{-1}\lambda\int \exp[-i(\boldsymbol{k}'-\boldsymbol{k})\cdot\boldsymbol{r}]\,V(\boldsymbol{r})\,\mathrm{d}^3 r - \\ &\quad -(4\pi)^{-1}\lambda^2\int \exp[-i(\boldsymbol{k}'\cdot\boldsymbol{r}'-\boldsymbol{k}\cdot\boldsymbol{r})]\,V(\boldsymbol{r}')\,G(\boldsymbol{r},\boldsymbol{r}';k)\,V(\boldsymbol{r})\,\mathrm{d}^3 r\,\mathrm{d}^3 r'\,, \end{aligned} \tag{2}$$

where k' is the wave-vector of the scattered particle, and

$$G(\boldsymbol{r}',\boldsymbol{r};k) = \lim_{\eta\to 0}\langle \boldsymbol{r}'|\,[(k+i\eta)^2 - H]^{-1}\,|\boldsymbol{r}\rangle \tag{3}$$

the Green's function or resolvent operator of the full Hamiltonian, $H = -\nabla^2 + \lambda V$, is the solution of the integral equation

$$G(\boldsymbol{r}',\boldsymbol{r};k) = G_0(\boldsymbol{r}',\boldsymbol{r};k) + \lambda\int G_0(\boldsymbol{r}',\boldsymbol{r}'';k)\,V(\boldsymbol{r}'')\,G(\boldsymbol{r}'',\boldsymbol{r};k)\,\mathrm{d}^3 r''\,, \tag{4}$$

with

$$G_0(\boldsymbol{r}',\boldsymbol{r};k) = -\frac{\exp[ik|\boldsymbol{r}'-\boldsymbol{r}|]}{4\pi|\boldsymbol{r}'-\boldsymbol{r}|}\,. \tag{5}$$

In previous studies of the analytic properties of eq. (2) it has been customary to introduce the variables

$$(6)\qquad \begin{cases} \boldsymbol{\pi} = |\boldsymbol{\pi}|\hat{\boldsymbol{n}} = \tfrac{1}{2}(\boldsymbol{k}+\boldsymbol{k}')\,, & \boldsymbol{\Delta} = \boldsymbol{k}'-\boldsymbol{k}\,, \\ \boldsymbol{\pi}\cdot\boldsymbol{\Delta} = 0\,, & \pi^2 = k^2 - \tfrac{1}{4}\Delta^2\,, \end{cases}$$

and study the amplitude as a function of k for fixed $\hat{\boldsymbol{n}}$ and $\boldsymbol{\Delta}$. We shall instead carry out our investigation with the aid of the variables

$$(7)\qquad \boldsymbol{k} = k\hat{\boldsymbol{e}}\,, \qquad \boldsymbol{\Delta} = \boldsymbol{k}'-\boldsymbol{k}\,,$$

though we shall subsequently adjoin to our results those for the more usual choice. In terms of the variables of eq. (7), we may rewrite (2) in the form

$$(8)\qquad f(k,\theta) = F(k, |\boldsymbol{\Delta}|, \hat{e}\cdot\hat{\Delta}) = -(4\pi)^{-1}\int \exp[-i\boldsymbol{\Delta}\cdot\boldsymbol{n}]\,V(\boldsymbol{r})\varphi(\boldsymbol{r};k,\lambda)\,\mathrm{d}^3r =$$

$$= \mu(\Delta) - (4\pi)^{-1}\lambda^2\int \exp[-i\boldsymbol{\Delta}\cdot\boldsymbol{r}]\,V(\boldsymbol{r})\exp[ik\hat{\boldsymbol{e}}\cdot(\boldsymbol{r}'-\boldsymbol{r})]\,G(\boldsymbol{r},\boldsymbol{r}';k)\,V(\boldsymbol{r}')\,\mathrm{d}^3r\,\mathrm{d}^3r'\,,$$

where

$$(9)\qquad \varphi(\boldsymbol{r};k,\lambda) = \exp[-i\boldsymbol{k}\cdot\boldsymbol{r}]\,\psi(\boldsymbol{r};k,\lambda)\,,$$

and

$$(10)\qquad \mu(\Delta) = -(4\pi)^{-1}\lambda\int \exp[-i\boldsymbol{\Delta}\cdot\boldsymbol{r}]\,V(\boldsymbol{r})\,\mathrm{d}^3r\,.$$

For the remainder of this paper we shall primarily study F as a function of k for fixed Δ and $\hat{e}\cdot\hat{\Delta}$. Since in fact $\hat{e}\cdot\hat{\Delta} = -\Delta/2k$ this choice is novel in that it keeps fixed some of the normal k dependence. In terms of eq. (8) this choice devolves upon the study of the function $\varphi(\boldsymbol{r};k,\lambda)$ in the first instance and upon the examination of $\exp[ik\hat{\boldsymbol{e}}\cdot(\boldsymbol{r}'-\boldsymbol{r})]\,G(\boldsymbol{r},\boldsymbol{r}';k)$ for the second form.

We may note for future use that it follows from (8) that

$$(11)\qquad F^*(k,\Delta,\hat{e}\cdot\hat{\Delta}) = F(-k,\Delta,-\hat{e}\cdot\hat{\Delta})\,.$$

To achieve the special dispersion relation toward which we are aiming, we find it necessary to impose only the following conditions on the spherically symmetric potential:

$$(\mathrm{A})\qquad \int |V(\boldsymbol{r})|\,\mathrm{d}^3r \leqslant L < \infty\,,$$

3762

and

$$\text{(B)} \qquad \max(\boldsymbol{r}') \frac{1}{4\pi} \int \frac{|V(\boldsymbol{r})|}{|\boldsymbol{r}-\boldsymbol{r}'|} \, \mathrm{d}^3 r \leqslant M < \infty ,$$

where Max $(\boldsymbol{r}')$ means maximum with respect to the variation of $\boldsymbol{r}'$. The conditions (A) and (B) turn out to be sufficient for the proof of dispersion relations for the function F. To go over to the more usual relations, we shall then require in addition that the potential fall off at least exponentially,

$$\text{(C)} \qquad \int \exp[\alpha r] |V(\boldsymbol{r})| \, \mathrm{d}^3 r \leqslant N < \infty , \qquad \alpha > 0 .$$

For the sake of clarity and completeness we also restate the fundamental theorem upon which rests the proof of the dispersion relations [4]. Consider the integral

$$\text{(12)} \qquad F(\zeta) = \int_A I(\zeta, x) \, \mathrm{d}x ,$$

where $I(\zeta, x)$ is analytic in ζ in a region $\Gamma(\zeta)$ with boundary curve $B(\zeta)$. Then $F(\zeta)$ is an analytic function of ζ if $\int I(\zeta, x) \, \mathrm{d}x$ converges uniformly with respect to ζ. A sufficient condition for the latter is that

$$\text{(13)} \qquad |I(\zeta, x)| < \Psi(x) \qquad \text{on} \qquad B(\zeta) ,$$

and

$$\text{(14)} \qquad \int_A \Psi(x) \, \mathrm{d}x < \infty .$$

In application $\Gamma(\zeta)$ will comprise the upper half of the $\zeta = k + i\eta$ plane and $B(\zeta)$ the real axis and the infinite semi-circle which bounds this region.

For the remainder of this section we shall outline our proof of the new dispersion relations, omitting many of the details which have been given in previous papers on other aspects of this problem. We follow a program suggested by the above theorem, but we pursue this program in two stages. We first employ the reasoning of the theorem to establish the analytic properties of the wave function $\varphi(\boldsymbol{r}; k, \lambda)$ defined by eq. (9). Consequently we apply the same reasoning again to the scattering amplitude in the first form given in eq. (8).

---

[4] This theorem is an adaptation of those found in E. C. TITCHMARSH: *The Theory of Functions* (London, 1939), p. 99.

According to the latter equation, $\varphi(\boldsymbol{r}; k, \lambda)$ may be expressed as

$$\varphi(\boldsymbol{r}; k, \lambda) = 1 + \lambda \int \exp[-ik\hat{\boldsymbol{e}}\cdot(\boldsymbol{r}-\boldsymbol{r}')] G(\boldsymbol{r}, \boldsymbol{r}'; k) V(\boldsymbol{r}')\, \mathrm{d}^3 r' . \tag{15}$$

Now the integrand of (15) has well-known analytic properties ([5]). For real λ, to which we confine ourselves, $G(\boldsymbol{r}, \boldsymbol{r}'; k)$ as the resolvent of a self-adjoint operator, is for almost all $\boldsymbol{r}$, $\boldsymbol{r}'$ analytic in ζ^2 everywhere except on the spectrum of the Hamiltonian $H = -\nabla^2 + \lambda V$. In the UH (upper half) ζ plane the only singularities arise from bound states and are confined to the imaginary axis. Under condition (B), it has further been shown ([6]) that the number of such points $\zeta^2 = -\varkappa_i^2$, $i = 1, 2, \ldots, N$ is finite.

Let us write

$$G(\boldsymbol{r}, \boldsymbol{r}'; \zeta) = G^B(\boldsymbol{r}, \boldsymbol{r}'; \zeta) + G^S(\boldsymbol{r}, \boldsymbol{r}'; \zeta) , \tag{16}$$

where, employing the bilinear formula for G,

$$G^B(\boldsymbol{r}, \boldsymbol{r}'; \zeta) = \sum_{i=1}^{N} \frac{\psi_i(\boldsymbol{r})\psi_i(\boldsymbol{r}')}{\zeta^2 + \varkappa_i^2} , \tag{17}$$

is the contribution to G arising from bound states, the wave-functions for these states, $\psi_i(\boldsymbol{r})$, having been chosen real. The isolation of G^B from G removes its only part with singularities for $\eta > 0$. We are thus led to study the function

$$\Phi(\boldsymbol{r}; \zeta\hat{\boldsymbol{e}}, \lambda) = \varphi(\boldsymbol{r}; \zeta\hat{\boldsymbol{e}}, \lambda) - \sum_{j=1}^{N} \frac{\varrho_j(\boldsymbol{r}; i\varkappa_j\hat{\boldsymbol{e}}, \lambda)}{\zeta^2 + \varkappa_j^2} , \tag{18}$$

where

$$\varrho_j(\boldsymbol{r}; \zeta\hat{\boldsymbol{e}}, \lambda) = \lambda \int \psi_i(\boldsymbol{r})\psi_i(\boldsymbol{r}') \exp[-i\zeta\hat{\boldsymbol{e}}\cdot(\boldsymbol{r}-\boldsymbol{r}')] V(\boldsymbol{r}')\, \mathrm{d}^3 r , \tag{19}$$

and $\varrho_j(\boldsymbol{r}; i\varkappa_j\hat{\boldsymbol{e}}, \lambda)$ is real. The exponential decay of the function $\psi_j(\boldsymbol{r})$ in conjunction with condition (A) guarantees that (18) exists at the point $\zeta = i\varkappa_i$, which is all we require.

We may now attempt to apply the reasoning of the theorem to the function Φ since it satisfies the necessary prerequisites. In studying the behavior on the boundary, however, we may equally well revert to the original func-

---

([5]) These have been summarized and suitably referenced by E. GERJUOY: *Phys. Rev.*, **109**, 1806 (1958).

([6]) V. BARGMANN: *Proc. Natl. Acad. Sci. U. S.*, **38**, 961 (1952).

3764

tion φ, in view of the regular behavior of the second term of (18) on the real axis and its disappearance at infinity. Moreover since $G(\boldsymbol{r}, \boldsymbol{r}'; k)$ is a continuous, bounded function of k on the finite k axis ([5]), we take for granted that eqs. (13) and (14) can be satisfied on that part of the boundary. It remains therefore to examine the behavior of $\varphi(\boldsymbol{r}; \zeta\hat{\boldsymbol{e}}, \lambda)$ as $|\zeta| \to \infty, \eta \geqslant 0$. In our previous studies ([3]) we have essentially shown that φ is uniformly bounded as $|\zeta| \to \infty$, indeed that $\varphi \to 1$, its first Born approximation. It follows that for a potential of arbitrary strength, but satisfying conditions (A) and (B), $\varphi(\boldsymbol{r}, \zeta\hat{\boldsymbol{e}}, \lambda)$ is a meromorphic function of ζ in the UH plane, continuous and uniformly bounded on the real axis and at infinity, with at worst a finite number of simple poles exhibited in (18).

The analytic properties of the scattering amplitude now follow immediately from the first version of eq. (8). In particular we consider the function

$$\mathscr{F}(\zeta, \Delta, \hat{e}\cdot\hat{\Delta}) = F(\zeta, \Delta, \hat{e}\cdot\hat{\Delta}) - \sum_{j=1}^{N} \frac{\mathscr{R}_j(i\varkappa_j, \Delta, \hat{e}\cdot\hat{\Delta})}{\zeta^2 + \varkappa_j^2}, \tag{20}$$

with

$$\mathscr{R}_j(\zeta, \Delta, \hat{e}\cdot\hat{\Delta}) = -\frac{\lambda^2}{4\pi}\int \exp[-i\boldsymbol{\Delta}\cdot\boldsymbol{r}]V(\boldsymbol{r})\,\psi_j(\boldsymbol{r})\psi_j(\boldsymbol{r})\cdot \cdot\psi_j(\boldsymbol{r}')\exp[-i\zeta\hat{e}\cdot(\boldsymbol{r}-\boldsymbol{r}')]V(\boldsymbol{r}')\,\mathrm{d}^3r\,\mathrm{d}^3r', \tag{21}$$

and $\mathscr{R}_j(i\varkappa_j, \Delta, \hat{e}\cdot\hat{\Delta})$ real. We conclude that $\mathscr{F}$ is, for fixed Δ, $\hat{e}\cdot\hat{\Delta}$, an analytic function of ζ in the UH plane, is bounded and continuous on the real axis, and approaches $\mu(\Delta)$, its Born approximation, uniformly as $|\zeta| \to \infty$. The latter properties obtain as well for the function F.

Upon application of Cauchy's theorem, we thus find

$$\mathscr{F}(\zeta, \Delta, \hat{e}\cdot\hat{\Delta}) = \mu(\Delta) + \sum_{j=1}^{N} \frac{\mathscr{R}_j(i\varkappa_j, \Delta, \hat{e}\cdot\hat{\Delta})}{\zeta^2 + \varkappa_j^2} + \frac{1}{2\pi i}\int_{-\infty}^{\infty} \mathrm{d}k' \frac{[\mathscr{F}(k', \Delta, \hat{e}\cdot\hat{\Delta}) - \mu(\hat{\Delta})]}{k' - \zeta}. \tag{22}$$

Letting $\zeta \to k$, the physical value associated with Δ and $\hat{e}\cdot\hat{\Delta}$, and taking the real part of both sides, we find

$$\mathrm{Re}\,F(k, \Delta, \hat{e}\cdot\hat{\Delta}) = \mu(\Delta) + \sum_{j=1}^{N} \frac{\mathscr{R}_j(i\varkappa_j, \Delta, \hat{e}\cdot\hat{\Delta})}{k^2 + \varkappa_j^2} + \frac{P}{\pi}\int_0^{\infty} \mathrm{d}k' \left\{\frac{\mathrm{Im}\,F(k', \Delta, \hat{e}\cdot\hat{\Delta})}{k' - k} + \frac{\mathrm{Im}\,F(k', \Delta, -\hat{e}\cdot\hat{\Delta})}{k' + k}\right\}, \tag{23}$$

where we have also utilized the symmetry condition eq. (11).

3. – Determination of the Born series.

The result of the previous section, eq. (23) is on the face of it a disturbingly useless relation. The apparent difficulty arises because the scattering amplitude is in reality a function of only two independent scalars, for example, k and Δ. Moreover each may be varied widely, and as long as we maintain the condition $\Delta < 2k$, we continue to enjoy a possible physical situation. We have chosen, however, to study the amplitude as a function of three variables. For given Δ and $\hat{e}\cdot\hat{\Delta}$, there is a unique k which is physically compatible with these. This means that the function appearing under the integral sign in (24) is completely non-physical. This is the price we have paid in order to obtain a relation valid without the requirement of exponential decay of the potential. To show that this price is not excessive we now indicate that our new relation serves at least as well as the usual one for the determination of the Born series.

For this application we suppose that there are no bound states. Then, as has been pointed out innumerable times (7), the dispersion relations used in conjunction with a unitarity condition can serve to determine the Born series for the scattering amplitude, given the potential. The unitarity condition in question which normally reads

$$\text{Im}\, f(k,\theta) = \frac{k}{4\pi}\int f^*(\boldsymbol{k}'\,|\,\boldsymbol{k}'')f(\boldsymbol{k}''\,|\,\boldsymbol{k})\,\mathrm{d}\Omega'', \tag{24}$$

may be rewritten for our purposes as

$$\text{Im}\, F(k,\Delta,\hat{e}\cdot\hat{\Delta}) = \frac{k}{4\pi}\int F^*(\boldsymbol{\Delta}+k\hat{\boldsymbol{e}}\,|\,\boldsymbol{k}'')F(\boldsymbol{k}''\,|\,k\hat{e})\,\mathrm{d}\Omega''. \tag{25}$$

if attention is paid to the precise definition of the function F. Given $\mu(\Delta)$, eqs. (23) and (25) together *should serve to determine the Born series for any potential satisfying conditions A and B alone.* As we have remarked these conditions are, in fact, weaker than those required in the proof of the more customary relations, since no restriction on momentumt transfer is involved.

We shall illustrate these remarks by consideration of a now standard example, *i.e.*, by using eqs. (23) and (25) to compute the second Born approximation for the Yukawa potential,

$$V(r) = \frac{\exp[-\mu r]}{\mu r}. \tag{26}$$

(7) See reference (1), for example.

From eq. (10), we have for the first Born approximation

$$F^{(1)} = \mu(\Delta) = -[\mu(\mu^2 + \Delta^2)]^{-1} . \tag{27}$$

Equation (25) is then written as

$$\begin{aligned} \operatorname{Im} F^{(2)}(k, \Delta, \hat{e}\cdot\hat{\Delta}) &= \frac{k}{4\pi\mu^2}\int \mathrm{d}\Omega'' \frac{1}{[\mu^2 + (\boldsymbol{\Delta} + k\hat{\boldsymbol{e}} - \boldsymbol{k}'')^2][\mu^2 + (\boldsymbol{k}'' - k\hat{\boldsymbol{e}})^2]} = \\ &= \frac{k}{4\pi\mu^2}\int \mathrm{d}\Omega'' \int_0^1 \frac{\mathrm{d}x}{\{x[\mu^2 + (\boldsymbol{\Delta} + k\hat{\boldsymbol{e}} - \boldsymbol{k}'')^2] + (1-x)[\mu^2 + (\boldsymbol{k}'' - k\hat{\boldsymbol{e}})^2]\}} = \\ &= \frac{k}{4\pi\mu^2}\int_0^1 \mathrm{d}x \int \frac{\mathrm{d}\Omega''}{\{[\mu^2 + 2k^2 + x(\Delta^2 + 2k\hat{\boldsymbol{\Delta}}\cdot\hat{\boldsymbol{e}})] - 2\boldsymbol{k}''\cdot(\boldsymbol{\Delta}x + k\hat{\boldsymbol{e}})\}} , \end{aligned} \tag{28}$$

or after performing the angular integration,

$$\operatorname{Im} F^{(2)}(k, \Delta, e\cdot\hat{\Delta}) = \frac{k}{\mu^2}\int_0^1 \frac{\mathrm{d}x}{\alpha(x)k^2 + 2\beta(x)k + \gamma(x)} , \tag{29}$$

where

$$\begin{cases} \alpha(x) = 4\mu^2 + 4x\Delta^2 - 4x^2[\Delta^2 - (\hat{\Delta}\cdot\hat{e})^2] , \\ \beta(x) = \boldsymbol{\Delta}\cdot\hat{\boldsymbol{e}}(2x\mu^2 + 2x^2\Delta^2) , \\ \gamma(x) = \mu^4 + 2x\mu^2\Delta^2 + x^2\Delta^4 = (\mu^2 + x\Delta^2)^2 . \end{cases} \tag{30}$$

It is important to notice that

$$\beta^2 - \alpha\gamma = -4[\mu^2 + x\Delta^2(1-x)][\mu^2 + x\Delta^2] < 0 , \qquad 0 \leqslant x \leqslant 1. \tag{31}$$

In performing the integral

$$\operatorname{Re} F^{(2)}(k, \Delta, \hat{e}\cdot\hat{\Delta}) = \frac{P}{\pi}\int_{-\infty}^{\infty} \mathrm{d}k' \frac{1}{k' - k} \operatorname{Im} F^{(2)}(k', \Delta, \hat{e}\cdot\hat{\Delta}), \tag{32}$$

we conveniently interchange the k' and x integrations. For the former integral we find

$$\begin{aligned} P\int_{-\infty}^{\infty} \frac{\mathrm{d}k'}{k' - k}\left[\frac{k'}{\alpha(x)k'^2 + 2\beta(x)k' + \gamma(x)}\right] = \\ = \frac{\pi}{[\alpha(x)k^2 + 2\beta(x)k + \gamma(x)]}\left\{\frac{\beta(x)k + \gamma(x)}{[\alpha(x)\gamma(x) + \beta^2(x)]^{\frac{1}{2}}}\right\} . \end{aligned} \tag{33}$$

3767

Inserting the values from eq. (30), we then find

$$\text{(34)} \qquad \operatorname{Re} F^{(2)}(k, \Delta, \hat{e}\cdot\hat{\Delta}) = \operatorname{Re} f^{(2)}(k, \theta) = \\ = \frac{1}{2}\int_0^1 \mathrm{d}x \frac{1}{[16(x-x^2)k^4 \sin^2(\theta/2) + 4k^2\mu^2 + \mu^4][(x-x^2)4k^2 \sin^2(\theta/2) + \mu^2]^{\frac{1}{2}}} .$$

Since the integral over k' has been performed, we have, in (34), been able to insist that k, Δ, $\hat{e}\cdot\hat{\Delta}$, all refer to the physical point k, θ. The integration (34) is elementary and yields

$$\text{(35)} \qquad \operatorname{Re} f^{(2)}(k, \theta) = \frac{1}{\mu^2\Delta[\mu^2 + 4k^2(\mu^2 + \Delta^2/4)]^{\frac{1}{2}}} \operatorname{tg}^{-1}\left\{\frac{\frac{1}{2}\mu\Delta}{[\mu^2 + 4k^2(\mu^2 + \Delta^2/4)]^{\frac{1}{2}}}\right\},$$

the correct result [1]. With the same provisos, the imaginary part of the amplitude can be evaluated from (29), with the result [1]

$$\text{(36)} \qquad \operatorname{Im} f^{(2)}(k, \theta) = \frac{1}{2\mu^2\{4k^2 \sin^2(\theta/2)[\mu^4 + 4k^2(\mu^2 + k^2 \sin^2(\theta/2))]\}^{\frac{1}{2}}} \cdot \\ \cdot \log \frac{[\mu^4 + 4k^2(\mu^2 + k^2 \sin^2(\theta/2))]^{\frac{1}{2}} + 2k^2 \sin(\theta/2)}{[\mu^4 + 4k^2(\mu^2 + k^2 \sin^2(\theta/2))]^{\frac{1}{2}} - 2k^2 \sin(\theta/2)} .$$

4. – Deduction of the usual dispersion relation; analytical continuation into the unphysical region.

The remainder of this paper will be concerned with a deduction of the customary dispersion relations from eq. (23). As the initial step in carrying out this program we shall develop an expansion for $F(k', \Delta, \hat{e}\cdot\hat{\Delta})$ in powers of Δ, where k' *need not* be at the physical value corresponding to Δ and $\hat{e}\cdot\hat{\Delta}$. First expanding the exponential in eq. (8), we write

$$\text{(37)} \qquad F(k', \Delta, \hat{e}\cdot\hat{\Delta}) = \sum_{n=0}^{\infty} \Delta^n H_n(k', \hat{e}\cdot\hat{\Delta}) ,$$

where

$$\text{(38)} \qquad H_n(k', \hat{e}\cdot\hat{\Delta}) = -\frac{\lambda}{4\pi}\frac{(-i)^n}{n!}\int (\hat{\Delta}\cdot\hat{r})^n r^n V(\boldsymbol{r})\varphi(\boldsymbol{r}; k'\hat{e}, \lambda)\,\mathrm{d}^3r .$$

Since φ is uniformly bounded for all r, k', λ, $|\varphi| < M'$ we have

$$\text{(39)} \qquad |H_n| \leqslant \frac{\lambda}{4\pi}\frac{M'}{n!}\int r^n |V(\boldsymbol{r})|\,\mathrm{d}^3r .$$

3768

Thus

$$(40)\qquad |F(k', \Delta, \hat{e}\cdot\hat{\Delta})| \leqslant \frac{\lambda M'}{4\pi} \sum_{n=0}^{\infty} \frac{1}{n!} \int (\Delta r)^n V(\boldsymbol{r})\, \mathrm{d}^3 r = \\ = \frac{\lambda M'}{4\pi} \int \exp[\Delta r] |V(\boldsymbol{r})|\, \mathrm{d}^3 r \leqslant \frac{\lambda}{4\pi} M' N ,$$

if we require condition (C) and $\Delta < \alpha$. The convergence of (30) is thus absolute and uniform with respect to k', and $\hat{e}\cdot\hat{\Delta}$, for k' real and $\hat{e}\cdot\hat{\Delta}$ the cosine of a real angle.

We next exhibit the $H_n(k', \hat{e}\cdot\hat{\Delta})$ as finite polynomials in Δ. For this purpose we introduce into Eq. (38) the representation

$$(41)\qquad (\hat{\Delta}\cdot\hat{r})^n = \sum_{l=n,\, n-2,\ldots} a_{n,l} \left(\frac{4\pi}{2l+1}\right)^{\frac{1}{2}} Y_{l0}(\hat{\Delta}\cdot\hat{r}) ,$$

with known values of $a_{n,l}$ [8], for the power function and the well known addition theorem

$$(42)\qquad Y_{l0}(\hat{\Delta}\cdot\hat{r}) = \left(\frac{4\pi}{2l+1}\right)^{\frac{1}{2}} \sum_{m=-l}^{l} Y_{lm}(\hat{e}\cdot\hat{\Delta})\, Y^*_{lm}(\hat{e}\cdot\hat{\Delta}) ,$$

and readily find an expression of the form

$$(43)\qquad H_n(k', \hat{e}\cdot\hat{\Delta}) = \sum_{l=n,\, n-2,\ldots} \frac{2^l (l!)^2}{(2l)!} P_l(\hat{e}\cdot\hat{\Delta}) S_{n,l}(k') .$$

Here P_l is the ordinary Legendre polynomial,

$$(44)\qquad S_{n,l}(k') = -\lambda \frac{a_{n,l}}{n!} \frac{(2l)!}{2^l (l!)^2} (-1)^{n-l} \cdot \int_0^{\infty} \mathrm{d}r\, r^{n+2} V(r) \omega_l(k'r) ,$$

and $\omega_l(k'r)$ is defined by the equation

$$(45)\qquad i^l [4\pi(2l+1)]^{\frac{1}{2}} \omega_l(k'r) = \int Y^*_{l0}(\hat{e}\cdot\hat{r})\, \varphi(\boldsymbol{r}; k\hat{e})\, \mathrm{d}\Omega .$$

As the final step in the present sequence we introduce into (43) the explicit polynomial expression for $P_l(\hat{e}\cdot\hat{\Delta})$,

$$(46)\qquad P_l(x) = \frac{(2l)!}{2^l (l!)^2} \left\{ x^l - \frac{l(l-1)}{2(2l-1)} x^{l-2} + \ldots \right\} = \frac{(2l)!}{2^l (l!)^2} \sum_{m=l,\, l-2,\ldots} (-2)^m b_{l,m} x^m ,$$

---

[8] E. W. Hobson: *Spherical and Ellipsoidal Harmonics* (New York, 1955), p. 44.

the factor $(-2)^m$ having been inserted for convenience, and recall that $\hat{e}\cdot\hat{\Delta} = -(\Delta/2k)$. We find that

$$(47)\qquad H_n(k', \hat{e}\cdot\hat{\Delta}) = h_n(k', k, \Delta) = \sum_{l=n,\,n-2\,\ldots} \sum_{m=l,\,l-2,\,\ldots} \left(\frac{\Delta}{k}\right)^m b_{l,m} S_{n,l}(k') =$$

$$= \sum_{m=n,\,n-2,\,\ldots} \left(\frac{\Delta}{k}\right)^m \sum_{l=m,\,m+2\,\ldots}^{n} b_{l,m} S_{n,l}(k') = \sum_{m=n,\,n-2\,\ldots} \left(\frac{\Delta}{k}\right)^m T_{n,m}(k')\,,$$

the last form of eq. (47) defining the functions $T_{n,m}(k')$.

We now introduce eq. (47) into eq. (37) and carry out the following substitution on the summation indices:

$$(48)\qquad m + n = 2p\,, \qquad n - m = 2q\,.$$

We find the result

$$(49)\qquad F(k', \Delta, \hat{e}\cdot\hat{\Delta}) = \sum_{p=0}^{\infty} F_{2p}\Delta^{2p}\,,$$

where

$$(50)\qquad F_{2p}(k', k) = \sum_{q=0}^{p} k^{-p+q} T_{p+q,\,p-q}(k)'\,.$$

It is necessary to observe that the transition from (37) to (49) has involved some rearrangement of infinite series which requires further justification. This question is studied in the Appendix where conditions for the convergence of (49) are established.

The analysis carried out thus far in this section can also be applied step by step to the dispersion relation (23). For the sake of simplicity we now omit the bound state contributions. We also note the expansion

$$(51)\qquad \mu(\Delta) = \sum_{n=0,2,\,\ldots} \mu_n \Delta^n$$

valid for $|\Delta| < \alpha$. From the uniform convergence of (37) with respect to k', we then conclude the dispersion relations

$$(52)\qquad \mathrm{Re}\, H_n(k, \hat{e}\cdot\hat{\Delta}) = \mu_n \delta(n, \text{even}) +$$

$$+ \frac{P}{\pi}\int_0^{\infty} \mathrm{d}k' \left\{ \frac{\mathrm{Im}\, H_n(k', \hat{e}\cdot\hat{\Delta})}{k' - k} + (-1)^n \frac{\mathrm{Im}\, H_n(k', -\hat{e}\cdot\hat{\Delta})}{k' + k} \right\}.$$

From eqs. (43) and (52) we then infer that the $S_{n,l}$ satisfy the relations

$$\text{Re } S_{n,l}(k) = \mu_n \delta_{l0} + \frac{P}{\pi}\int_0^\infty \mathrm{d}k' \, \frac{2k' \, \text{Im } S_{n,l}(k')}{k'^2 - k^2}\,, \qquad (n, \text{ even}), \tag{53}$$

$$= \frac{2k}{\pi} P\int_0^\infty \mathrm{d}k' \, \frac{\text{Im } S_{n,l}(k')}{k'^2 - k^2}\,. \qquad (n, \text{ odd}). \tag{54}$$

From eq. (47) it also follows that the $T_{n,m}(k)$ obey relations precisely analogous to those for the $S_{n,l}(k)$ with δ_{m0} replacing δ_{l0} in eq. (53). We may terminate the present sequence of observations by noting that the application of (43) to (46) and (47) leads to relations for $F_{2p}(k', k)$.

It is unfortunately true and will become apparent below that all the relations enunciated in the previous paragraph are purely of academic interest, since they do not involve elements of physical interest. We first encounter such elements if we set $k' = k$ in eq. (50). Thus the quantities

$$F_{2p}(k, k) = f_p(k) \tag{55}$$

which occur in the expansion

$$f(k, \Delta) = \sum_{p=0}^{\infty} f_p(k) \, \Delta^{2p} \tag{56}$$

may be expressed in terms of the phase shifts by comparing (56) with the usual formula

$$f(k, \Delta) = \sum_l \left(\frac{\exp[2i\delta_l] - 1}{2ik}\right)(2l + 1) P_l(\cos\theta)\,. \tag{57}$$

By means of the formula

$$P_l(\cos\theta) = F(n+1, -n;\ 1;\ \Delta^2/4k^2)\,, \tag{58}$$

where F is *here* the hypergeometric function, we infer directly that

$$f_p(k) = \sum_{l=p}^{\infty}\left(\frac{\exp[2i\delta_l] - 1}{2ik^{2p+1}}\right)(-1)^p \, \frac{(2l+1)}{2^{2p}} \, \frac{(l+p)!}{(l-p)!(p!)^2}\,. \tag{59}$$

A dispersion relation for $f_p(k)$ follows readily from those already given if we add but a single observation to our previous considerations, ([5]), namely

that $T_{n,m}(k)/k^n$ is finite at $k = 0$. This may be concluded from the definition eq. (47) of $T_{n,m}(k)$ in terms of the $S_{n,l}(k)$ and from the fact that the dependence of the latter on k, eq. (44), follows from that of $\omega_l(kr)$, which behaves like a regular radial wave function of angular momentum l near $k = 0$. From eqs. (47), (53), and (54), we can then derive the dispersion relation

$$\text{(60)} \qquad \mathrm{Re}\,[T_{n,m}(k)/k^m] = \mu_n \delta_{m,0} + \frac{P}{\pi}\int_0^\infty \mathrm{d}k' \, \frac{2k'}{k'^2 - k^2}\, \mathrm{Im}\,[T_{n,m}(k')/k'^m] \,.$$

From eq. (50), we deduce further that

$$\text{(61)} \qquad \mathrm{Re}\, f_p(k) = \mu_p + \frac{P}{\pi}\int_0^\infty \mathrm{d}k' \, \frac{2k'\, \mathrm{Im}\, f_p(k')}{k'^2 - k^2} \,, \qquad p = 0, 1, 2, \ldots \,.$$

Equations (61) constitute an infinite set of dispersion relations involving the successive derivatives of the scattering amplitudes in the forward direction valid under conditions (A), (B), and (C) of Section **2**. On the other hand, if instead of condition (C), only a finite number of moments of the potential exist, for example, the moments up to and including order $2p$, only the first p relations of (61) obtain. It should also be remarked that eqs. (61) do not presuppose the convergence of (49) or (56).

To deduce from (61) the customary dispersion relations, however, requires knowledge of the convergence of these series, in particular (56). In the Appendix, we show that (56) converges in the physical region, as long as $k > \frac{1}{2}\Delta$ uniformly in k for $\Delta < [\sqrt{2} - 1]\alpha$. (In actuality the condition $\Delta < 2\alpha$ has been obtained in previous works [3]). This permits us, to write tor this range of Δ,

$$\text{(62)} \qquad \mathrm{Re}\, f(k, \Delta) = \mu(\Delta) + \frac{P}{\pi}\int_{\Delta/2}^\infty \mathrm{d}k' \, \frac{2k'\, \mathrm{Im}\, f(k', \Delta)}{k'^2 - k^2} + \\ + \frac{P}{\pi}\sum_{p=0}^\infty \Delta^{2p}\left\{\int_0^{\Delta/2} \mathrm{d}k' \, \frac{2k'\, \mathrm{Im}\, f_p(k')}{k'^2 - k^2}\right\} .$$

which constitutes the customary dispersion relation, but in a form which exhibits explicitly a valid continuation of $f(k, \Delta)$ into the non-physical region $k < \Delta/2$.

3772

APPENDIX

To justify the terminal considerations of Sect. **4**, we must establish the convergence of the serie (49). This can be most effectively done ab initio [3]. Here, however, we wish to study the transition from eq. (37) to eq. (49).

To estimate the convergence of (49), we require bounds on the $F_{2p}(k'k)$. We set ourselves the task of obtaining these by first obtaining bounds on the $T_{n,m}(k')$ of eq. (50). These, in turn are found by reverting to eq. (47), which we write as

$$H_n(k', \hat{e}\cdot\hat{\Delta}) = \sum_{m=n,\ n-2,\ \ldots} c_{n,m}\Delta^m , \tag{A.1}$$

with

$$c_{n,m} = T_{n,m}(k')/k^m . \tag{A.2}$$

What we require then from (A.1) are bounds on the $c_{n,m}$ given only eq. (39),

$$|H_n| \leqslant \frac{\lambda}{4\pi}\frac{M'}{n!}\int r^n |V(\boldsymbol{r})|\,\mathrm{d}^3 r = \frac{\lambda}{4\pi}\frac{M'}{n!}\langle r^n\rangle . \tag{A.3}$$

For the sake of algebraic simplicity we choose

$$\langle r^n\rangle = 4\pi\,\frac{n!}{\alpha^{n+1}}, \tag{A.4}$$

corresponding to a potential $V\sim \exp[-\alpha r]/r^2$. Though this doesn't quite satisfy condition (B), the argument is not essentially changed for either Yukawa or exponential potentials, only the subsequent algebra becoming somewhat more involved.

We now develop an argument which, in its essentials, is the same as one employed by BREMMERMAN, OEHME and TAYLOR [9]. The function

$$G_n(Z) = H_n(k', \hat{e}\cdot\hat{\Delta})|_{\Delta=Z}[Z + i(4k^2 - Z^2)^{\frac{1}{2}}]^{-n} \equiv \tag{A.5}$$
$$\equiv h_n(k', k, Z)[Z + i(4k^2 - Z^2)^{\frac{1}{2}}]^{-n},$$

is analytic everywhere except for the cut $-2k \leqslant Z < 2k$. We can therefore write by the maximum modulus theorem

$$|G_n(Z)| \leqslant \max_{|Z|\leq 2k}|G_n(Z)| \leqslant C_n/(2k)^n , \tag{A.6}$$

[9] H. J. BREMMERMAN, R. OEHME and J. G. TAYLOR: *Phys. Rev.*, **109**, 2178 (1958).

where

$$c_n = \lambda M'/d^{n+1}\,, \tag{A.7}$$

from (A.3) and (A.4).

From Cauchy's formula, we write, in view of (A.1)

$$|c_{n.m}| \leqslant \frac{1}{2\pi}\left|\int_{|Z|=R} \frac{G_n(Z)[Z + i(4k^2 - Z^2)^{\frac{1}{2}}]^n}{Z^{m+1}}\,\mathrm{d}Z\right| \leqslant \frac{c_n}{(2k)^n R^m}[R + (R^2 + 4k^2)^{\frac{1}{2}}]^n. \tag{A.8}$$

Remembering (A.2), we can now obtain a bound for $F_{2p}(k', k)$, Eq. (52). We have

$$\begin{aligned} |F_{2p}(k', k)| &\leqslant \sum_{q=0}^{p} |c_{p+q,\,p-q}| = \\ &= \frac{\lambda M'}{\alpha^{p+1}} \frac{[R + (R^2 + 4k^2)^{\frac{1}{2}}]^p}{(2kR)^p} \sum_{q=0}^{p} \frac{R^q}{(2\alpha k)^q}[R + (R^2 + 4k^2)^{\frac{1}{2}}]^q = \\ &= \frac{\lambda M'[R + (R^2 + 4k^2)^{\frac{1}{2}}]^p}{\alpha^{p+1}(2kR)^p} \frac{1 - \left\{\dfrac{R[R + (R^2 + 4k^2)^{\frac{1}{2}}]}{2\alpha k}\right\}^p}{1 - \left\{\dfrac{R[R + (R^2 + 4k^2)^{\frac{1}{2}}]}{2\alpha k}\right\}}. \end{aligned} \tag{A.9}$$

With this result, the ratio test applied to (49) yields the condition

$$\lim_{p\to\infty} \frac{\Delta^2[R + (R^2 + 4k^2)^{\frac{1}{2}}]}{2\alpha k R} \frac{1 - \left\{\dfrac{R[R + (R^2 + 4k^2)^{\frac{1}{2}}]}{2\alpha k}\right\}^p}{1 - \left\{\dfrac{R[R + (R^2 + 4k^2)^{\frac{1}{2}}]}{2\alpha k}\right\}^{p-1}} < 1\,. \tag{A.10}$$

If

$$R[R + (R^2 + 4k^2)^{\frac{1}{2}}] \leqslant 2\alpha k\,, \tag{A.11}$$

we then have

$$\Delta^2 < \frac{2\alpha k R}{[R + (R^2 + 4k^2)^{\frac{1}{2}}]} < R^2\,. \tag{A.12}$$

If the inequality (A.11) reverses, we find similarly

$$\Delta^2 < \frac{4\alpha^2 k^2}{[R + (R + 4k^2)^{\frac{1}{2}}]^2}\,. \tag{A.13}$$

The optimum condition obtains for the equality sign in (A.11), whence we then find that

$$R^2 = \alpha/[1 + (\alpha/k)]\,, \tag{A.14}$$

3774

or

$$\Delta^2 < \alpha^2/[1+(\alpha/k)] \,. \tag{A.15}$$

Under this condition the convergence of (49) is uniform with respect to k'. Now setting $k' = k$, we obtain a condition for the convergence of (56). As long as $k > \frac{1}{2}\Delta$ (the physical region), (56) will then converge uniformly with respect to k if

$$\Delta^2 < \frac{\alpha^2}{1+2(\alpha/\Delta)} \,, \tag{A.16}$$

or solving (A.16)

$$\Delta < (\sqrt{2} \geqslant 1)\alpha \,, \tag{A.17}$$

as stated in Sect. **6**.

RIASSUNTO (*)

Si trova per lo scattering del potenziale una relazione di dispersione che è valida senza imporre alcuna restrizione al trasferimento dell'impulso. Benchè l'integrale che figura nella relazione si estenda su un'ampiezza completamente non fisica, si dimostra che, in combinazione con la condizione di unitarietà, la serie di Born, se convergente, è determinata in maniera completa. Si esegue anche il passaggio alla relazione più usuale.

(*) *Traduzione a cura della Redazione.*

3775

IL NUOVO CIMENTO Vol. XIV, N. 4 16 Novembre 1959

Transverse Polarization in Allowed β Transitions.

R. H. Good jr. (*) and M. E. Rose

Oak Ridge National Laboratory - Oak Ridge, Tenn.

(ricevuto il 2 Settembre 1959)

Summary. — In an allowed β-transition, in which the recoil direction is observed in coincidence with the β-particle, it is possible under appropriate circumstances to produce completely polarized electrons. For pure Fermi transitions no additional conditions need be imposed. For Gamow-Teller transitions it is also necessary that the nucleus be oriented and, if the alignment is zero, the nuclear polarization must have the maximum possible value consistent with this condition, namely $\frac{2}{3}$. Also, in a Gamow-Teller transition from a completely polarized nucleus to a nucleus with one lower spin-value, the electron polarization is complete even without observation of the recoil. In general, the polarization of the β-particle is at least partly transverse. The conditions for purely transverse polarization are investigated. For Fermi transitions, where the transverse polarization would have unit value, this can be accomplished at any energy but the effect can be observed, in principle, only for monoenergetic electrons. In practice the energy band can be rather broad without seriously changing the nature of the polarization. For transitions with an appreciable Gamow-Teller contribution and no nuclear polarization, the β-particle polarization is not only incomplete but can be made purely transverse only at undesirably low energies. It is possible, however, to produce appreciable transverse polarization at higher energies even when the longitudinal polarization is not small. In an Appendix a discussion is given of the appropriate form of the electron-positron polarization operator.

1. – Introduction.

It is customary to think of the polarization of β-particles in allowed transitions as being almost entirely longitudinal, especially for interactions which are time reversal invariant. Even if time reversal invariance is valid, as pre-

(*) On leave from Iowa State University, summer 1959.

3776

sent experimental data indicate, and small Coulomb corrections are neglected, there does exist a possibility of obtaining large transverse polarization in an allowed transition provided the neutrino, or recoil, is observed in coincidence with the β-particle. Of course, when the neutrino is not observed and the nucleus is unoriented, the result is as usual, a polarization $\pm v/c$ along the direction of the β momentum.

It is to be emphasized that the bare statement of this fact is not new although the fact that the transverse polarization can be even *complete*, under circumstances to be described below, has perhaps not been generally realized. The existence of some transverse polarization when the neutrino unit vector $\hat{\boldsymbol{q}} = \boldsymbol{q}/q$ and $\boldsymbol{p}$ are simultaneously measured is obvious from a physical point of view. Moreover, the standard literature [1] contains many of the necessary formulae to investigate this effect. However, the fact is that a number of aspects of this question have received little or no discussion heretofore.

The first and most obvious point of discussion concerns the circumstances under which large transverse polarization is to be expected. The second concerns the interpretation. Even here most of the machinery for the interpretation is at least implicit in the literature [2]. In connection with the interpretation we wish to emphasize that eigenstates of the β-particle exist for which the polarization is exactly unity (*) and that for certain transitions the β-interaction with a two-component neutrino creates particles into these states. The fact that these states may be states of transverse polarization is then merely a matter of choosing the experimental conditions appropriately.

The main conclusions to which we arrive in the following are then based on the assumptions of allowed transitions and a two-component neutrino theory with a $V - \lambda A$ β-interaction. We first assume that the recoil direction is observed. In addition, the small Coulomb effects of order $\frac{1}{2}\alpha^2 Z^2$ are neglected. Our conclusions are:

a) The polarization (for both electrons and positrons) can always be made transverse but it is only in the case of a pure Fermi (**) transition that this polarization will be large under practical circumstances.

---

(1) J. C. Jackson, S. B. Treiman and H. W. Wyld jr.: *Phys. Rev.*, **106**, 517 (1957); *Nucl. Phys.*, **4**, 206 (1957); M. E. Ebel and G. Feldman: *Nucl. Phys.*, **4**, 213 (1957).

(2) H. A. Tolhoek: *Rev. Mod. Phys.*, **28**, 277 (1956).

(*) Of course, experimental limitations of finite energy and angular resolution will result in less than 100% polarization. Henceforth it will be understood that when reference to complete polarization is made we refer to ideal experimental conditions.

(**) This means, in addition to $0^{\pm} \to 0^{\pm}$ transitions, those in which the Gamow-Teller matrix element is small, whatever the reason. Thus, ^{35}A is the most interesting case.

b) In a pure Gamow-Teller transition the electron is never emitted with complete polarization unless the emitting nucleus is oriented (polarized, say). If the nucleus is unoriented the polarization is appreciable only if the β-energy is not low but then it is almost completely longitudinal. The polarization can be made purely transverse only at very low energies ($W < 1.06$, *i.e.*, kinetic energies less than about 30 keV) and the magnitude of this polarization is always less than $\frac{1}{9}$. Without the condition for purely transverse polarization the transverse component is at most $\frac{1}{3}$ and decreases with energy roughly like $1/W$.

c) If the initial state is polarized in a pure Gamow-Teller transition it is possible to obtain complete polarization of the β-particles and it is also possible to make this completely transverse. For this purpose it is not necessary that the initial nucleus be completely polarized. However, it is assumed that no nuclear alignment occurs ([3]) and under these circumstances the required nuclear polarization must have the maximum possible value.

d) In a mixed ($F-GT$) transition with no nuclear orientation the polarization is always less than unity and one obtains pure transverse polarization again only at low energies. The energy below which the polarization can be made entirely transverse depends on the ratio

$$y = \lambda^2 \frac{|M_{GT}|^2}{|M_F|^2}, \tag{1}$$

where $\lambda = -C_A/C_V \approx 1.2$. In fact, if a is the electron-neutrino correlation coefficient (*), then $W \leqslant (1-a^2)^{-\frac{1}{2}}$ is required. If the electron-neutrino angle is chosen to give a maximum transverse component of polarization, the magnitude of this decreases (roughly like $1/W$) from a maximum value of $|a|$ at $W=1$.

e) If we do not use a two component neutrino theory all the polarizations are multiplied by the customary factor; for instance, for Fermi transitions by $2CC'/[C^2+C'^2]$ in the usual notation ([1]). Therefore, the observation of the effects discussed here is, in the usual sense, a test for the validity of the two-component theory. Alternatively, it is possible in mixed transitions to obtain information on the matrix element ratio y. The quantity y enters in just the same way as it does in the correlation parameter a and so the same information is obtained as in a standard recoil experiment, which is hardly surprising.

([3]) M. E. ROSE and J. M. JAUCH: *Phys. Rev.*, **84**, 1155 (1951).

(*) That is, the probability per unit energy and solid angle range, for emission of leptons with momenta $\boldsymbol{p}$ and $\boldsymbol{q}$ is proportional to $1+a\hat{\boldsymbol{q}}\cdot\boldsymbol{p}/W$.

3778

If we relax the assumption that the neutrino direction is observed, then the electron polarization is still complete in a Gamow-Teller transition provided the initial nuclear polarization is also complete and the nuclear spin decreases by 1.

What is surprising, perhaps, is the conclusion just mentioned above. It would appear plausible that the completely polarized β-particle arises only because no averaging over physical observables is done. Thus, in the Fermi transitions, where polarization can be complete, the neutrino spin is not averaged because there is only one spin state. The nuclear matrix element is independent of any averaging process. On the other hand, when the neutrino directions *are* averaged, the polarization is less than unity except in the trivial case of very energetic electrons. In the Gamow-Teller case the averaging implied by non-oriented nuclei does indeed reduce the β-polarization to values less than unity. Nevertheless the conjecture that pure states must be measured in order to get complete polarization must be modified in view of the results cited.

2. – Discussion of the polarization of the β-particle.

2·1. *Fermi transitions.* – We consider a β-transition in which the electron (positron) has momentum $\boldsymbol{p}$ and the antineutrino (neutrino) has momentum $\boldsymbol{q}$ and helicity $+1$ (-1). In addition, we consider electrons completely polarized in the direction of the unit vector $\hat{\boldsymbol{s}}$, see Appendix. The transition rate, per unit range of energy and solid angle, for the process described has the general form

$$I(\hat{\boldsymbol{s}}) = \frac{1}{2} I_0 \left(1 + \frac{\boldsymbol{p}\cdot\hat{\boldsymbol{q}}}{W}\right)(1 - \hat{\boldsymbol{s}}\cdot\boldsymbol{r}) , \tag{2}$$

where I_0 is the spectral distribution and W is the total electron energy. The units throughout are such that the electron mass m and c are both unity. For the pure Fermi transitions $\boldsymbol{r}$ is given by

$$\boldsymbol{r} = \pm \frac{\hat{\boldsymbol{q}} + \boldsymbol{p} + (W-1)\hat{\boldsymbol{p}}\cdot\hat{\boldsymbol{q}}\hat{\boldsymbol{p}}}{W + \boldsymbol{p}\cdot\hat{\boldsymbol{q}}} . \tag{3}$$

Throughout we adopt the convention that the upper sign applies for electron emission and the lower sign for positron emission.

The degree of polarization along $\hat{\boldsymbol{s}}$ is then

$$P_s = \boldsymbol{P}\cdot\hat{\boldsymbol{s}} = \frac{I(\hat{\boldsymbol{s}}) - I(-\hat{\boldsymbol{s}})}{I(\hat{\boldsymbol{s}}) + I(-\hat{\boldsymbol{s}})} = -\boldsymbol{r}\cdot\hat{\boldsymbol{s}} . \tag{4a}$$

Since this applies for any direction of $\hat{\boldsymbol{s}}$ the (average) polarization vector is

$$\boldsymbol{P} = -\boldsymbol{r} . \tag{4b}$$

3779

Only when $\boldsymbol{r}$ is a unit vector will the electrons emerge in a *pure* state with $\hat{\boldsymbol{s}} = -\boldsymbol{r} = \boldsymbol{P}$. This is actually the case for the $\boldsymbol{r}$ given by eq. (3). Therefore, in the Fermi transitions with the neutrino observed, the interesting result emerges that no transitions occur to the eigenstate (*) with $\hat{\boldsymbol{s}} = \boldsymbol{r}$ and all transitions occur in the state with $\hat{\boldsymbol{s}} = -\boldsymbol{r}$.

An alternative interpretation of eq. (2) is obtained by replacing $\hat{\boldsymbol{s}}$ by the two-by-two Pauli matrices $\boldsymbol{\sigma}$. Then I is the density matrix and the transition probability is the trace of I, equal to $I_0(1 + \boldsymbol{p}\cdot\hat{\boldsymbol{q}}/W)$, and the polarization vector $\boldsymbol{P}$ is

$$\boldsymbol{P} = \frac{\mathrm{Tr}\,\boldsymbol{\sigma} I}{\mathrm{Tr}\, I} = -\boldsymbol{r}\,, \tag{4c}$$

as before.

To make the polarization purely transverse we impose the condition $\boldsymbol{r}\cdot\boldsymbol{p} = 0$ to obtain

$$\hat{\boldsymbol{p}}\cdot\hat{\boldsymbol{q}} = -p/W\,. \tag{5}$$

In terms of the recoil momentum

$$\boldsymbol{R} = -(\boldsymbol{p} + \boldsymbol{q})$$

this is equivalent to

$$\begin{cases} \hat{\boldsymbol{p}}\cdot\hat{\boldsymbol{R}} = -p(W-q)/WR\,, \\ R = (p^2 + q^2 - 2p^2q/W)^{\frac{1}{2}}\,. \end{cases} \tag{6}$$

The direction of the polarization is given by

$$\hat{\boldsymbol{r}}\cdot\hat{\boldsymbol{R}} = \mp\, q/RW\,. \tag{6a}$$

The total intensity, per unit energy range, is then I_0/W^2 which is proportional to $pq^2F(Z, W)/W$, where F is the usual Fermi function. If ^{35}A is regarded as a pure Fermi transition one obtains the following results: I_0/W^2 has a fairly broad maximum near $W = 1.8$ and $\hat{\boldsymbol{p}}\cdot\hat{\boldsymbol{R}}$ has a very broad maximum of 0.88 at $W = 3.1$ and has the value 0.81 at $W = 1.8$. The flatness of the $\hat{\boldsymbol{p}}\cdot\hat{\boldsymbol{R}}$ maximum implies that for given solid angles of the detectors the

(*) We refer to the eigenstates of the polarization operator $\boldsymbol{O}^{\mp}\cdot\hat{\boldsymbol{s}}$ where

$$\boldsymbol{O}^{\mp} = \pm\boldsymbol{\sigma}\cdot\hat{\boldsymbol{p}}\hat{\boldsymbol{p}} + \hat{\boldsymbol{p}}\times(\beta\boldsymbol{\sigma}\times\hat{\boldsymbol{p}})\,,$$

which is the generalization of the spin operator, see Appendix. For $\hat{\boldsymbol{s}}$ parallel to $\boldsymbol{p}$ we find $\boldsymbol{O}^{\mp}\cdot\hat{\boldsymbol{s}}$ = helicity operator.

3780

energy band which has to be selected from the spectrum may be quite wide ($\Delta W \sim 2.5$ around the maximum).

2·2. *Gamow-Teller transitions.* – We first consider the β-transition without averaging over the nuclear substates. Then

$$I = \frac{1}{2} I_0 \left(B - \frac{\boldsymbol{p}\cdot\boldsymbol{A}}{W} \right) (1 - \hat{\boldsymbol{s}}\cdot\boldsymbol{r}) , \tag{7}$$

where now

$$-\boldsymbol{r} = \pm \frac{\boldsymbol{A} - B\boldsymbol{p} + (W-1)\hat{\boldsymbol{p}}\cdot\boldsymbol{A}\,\hat{\boldsymbol{p}}}{WB - \boldsymbol{p}\cdot\boldsymbol{A}} , \tag{8}$$

and

$$\boldsymbol{A} = \pm i\boldsymbol{M}\times\boldsymbol{M}^* + \boldsymbol{M}\cdot\boldsymbol{M}^*\hat{\boldsymbol{q}} - \hat{\boldsymbol{q}}\cdot\boldsymbol{M}\boldsymbol{M}^* - \hat{\boldsymbol{q}}\cdot\boldsymbol{M}^*\boldsymbol{M} , \tag{8a}$$

$$B = \boldsymbol{M}\cdot\boldsymbol{M}^* \pm i\hat{\boldsymbol{q}}\cdot\boldsymbol{M}\times\boldsymbol{M}^* \geqslant 0 , \tag{8b}$$

$$\boldsymbol{M} = (f|\boldsymbol{\sigma}|i) . \tag{8c}$$

In (8*c*) the nuclear matrix element refers to an arbitrary pair of nuclear substates. Obviously $\boldsymbol{A}$ and B are real.

It is of interest to note that $\boldsymbol{r}$ is a unit vector if and only if $A = B$. For perfectly oriented initial and final states, so that $\boldsymbol{M}$ and $\boldsymbol{M}^*$ are statistically independent vectors, this condition is indeed fulfilled. Since it would be very difficult to perform a recoil experiment in which the nuclei are completely oriented and the β-polarization analyzed, we inquire as to whether the condition is still fulfilled for unoriented nuclei.

For unoriented nuclei

$$\langle i\boldsymbol{M}\times\boldsymbol{M}^*\rangle = 0 \; ; \quad \langle|\boldsymbol{M}|\rangle^2 = |M_{GT}|^2 , \quad \langle\hat{\boldsymbol{q}}\cdot\boldsymbol{M}\boldsymbol{M}^*\rangle = \tfrac{1}{3}\hat{\boldsymbol{q}}\,|M_{GT}|^2 , \tag{9}$$

where the angular brackets refer to the average over the ensemble of nuclear states. Then

$$-\boldsymbol{r} = \pm \frac{\frac{1}{3}\hat{\boldsymbol{q}} - \boldsymbol{p} + \frac{1}{3}(W-1)\hat{\boldsymbol{p}}\cdot\hat{\boldsymbol{q}}\,\hat{\boldsymbol{p}}}{W - \frac{1}{3}\boldsymbol{p}\cdot\hat{\boldsymbol{q}}} . \tag{10}$$

Clearly,

$$r^2 = 1 - \frac{\frac{8}{9}}{(W - \frac{1}{3}\boldsymbol{p}\cdot\hat{\boldsymbol{q}})^2} \neq 1 , \tag{11}$$

except for the trivial case of high energy.

Although the β-emission to a pure state does not occur, the polarization

can be made entirely transverse. The condition for this is

$$\hat{\boldsymbol{p}}\cdot\hat{\boldsymbol{q}} = \frac{3p}{W}\,. \tag{12}$$

In order that this be fulfilled it is necessary that $p^2 \leqslant \frac{1}{8}$ and $W \leqslant \frac{3}{2}\sqrt{2} = 1.06$. This corresponds to such a low energy that the case of pure transverse polarization is of doubtful interest.

Alternatively, without attempting to make the polarization transverse, one may attempt to maximize this component. The magnitude of this component

$$r_\perp = |\boldsymbol{r}\times\hat{\boldsymbol{p}}| = \frac{1}{3}\frac{[1-(\hat{\boldsymbol{p}}\cdot\hat{\boldsymbol{q}})^2]^{\frac{1}{2}}}{W-\frac{1}{3}\boldsymbol{p}\cdot\hat{\boldsymbol{q}}}\,, \tag{13}$$

is a maximum for

$$\hat{\boldsymbol{p}}\cdot\hat{\boldsymbol{q}} = \frac{p}{3W}\,, \tag{13a}$$

and

$$(r_\perp)_{\max} = (9W^2 - p^2)^{-\frac{1}{2}}\,. \tag{13b}$$

This is largest for $W=1$ where $(r_\perp)_{\max}$ is $\frac{1}{3}$ but for larger W the magnitude of the transverse polarization decreases fairly rapidly.

In view of these results it is of interest to investigate the case of a polarized emitter. For simplicity we assume zero alignment ([3]). We define a vector $\boldsymbol{N}$, which is proportional to the nuclear polarization, by

$$\langle i\,\boldsymbol{M}\times\boldsymbol{M}^*\rangle = \boldsymbol{N}\langle\boldsymbol{M}\cdot\boldsymbol{M}^*\rangle\,; \qquad N\leqslant 1\,. \tag{14}$$

As long as the initial nucleus is not aligned we still have

$$\mathrm{Re}\,\langle\hat{\boldsymbol{q}}\cdot\boldsymbol{M}\boldsymbol{M}^*\rangle = \tfrac{1}{3}\hat{\boldsymbol{q}}\langle\boldsymbol{M}\cdot\boldsymbol{M}^*\rangle$$

and $\langle\boldsymbol{M}\cdot\boldsymbol{M}^*\rangle = |M_{GT}|^2$ in any case. We shall require that $\langle|\boldsymbol{A}|\rangle = \langle B\rangle$ so that $\boldsymbol{r}$ will be a unit vector. Introducing

$$\boldsymbol{N}\cdot\hat{\boldsymbol{q}} = N\cos\varphi$$

we find the condition

$$N = \frac{2}{3\sin^2\varphi}[\pm\cos\varphi + (1+\sin^2\varphi)^{\frac{1}{2}}], \tag{15a}$$

or

$$\cos\varphi = \pm\frac{1}{N}\left[-\frac{2}{3} + \left(N^2 - \frac{4}{9}\right)^{\frac{1}{2}}\right]. \tag{15b}$$

3782

From (15a) or (15b) it is seen that $N \geqslant \frac{2}{3}$ is necessary: for electrons this occurs for $\varphi = \pi$ and for positrons at $\varphi = 0$. In terms of the nuclear polarization $\langle \boldsymbol{J} \rangle / J$ we have

$$N = \lambda_1(J, J') \langle \boldsymbol{J} \rangle / J \,, \tag{16}$$

where the transition is from nuclear spin J to J' and

$$\lambda_1 = 1 \,, \qquad J = J' + 1 \,, \tag{16a}$$

$$\lambda_1 = (J+1)^{-1} \,, \qquad J = J' \,, \tag{16b}$$

$$\lambda_1 = -J/(J+1) \,, \qquad J = J' - 1 \,. \tag{16c}$$

It would appear from these results that it is possible to get complete β-polarization with the nucleus less than completely polarized. This is actually true. Moreover one might be tempted to say that if the nuclear polarization $|\langle \boldsymbol{J} \rangle / J| > \frac{2}{3}\lambda_1$ the magnitude of the polarization vector $\boldsymbol{r}$ would be greater than unity. However, it is not difficult to see, under the assumption that no nuclear alignment is present, that the above inequality is impossible and that the required nuclear polarization is the maximum possible under the stated conditions. The proof is as follows.

We consider a description of the ensemble of nuclear states by a diagonal density matrix. The elements of this matrix p_m $(-J \leqslant m \leqslant J)$ are the relative populations of the initial substates. Then

$$\sum_m p_m = 1 \tag{17a}$$

and

$$\eta_2 = \frac{1}{J(2J-1)} \sum_m [3m^2 - J(J+1)] p_m = 0 \,, \tag{17b}$$

and we determine the maximum value of

$$\eta_1 = \frac{1}{J} \sum_m m p_m \,, \tag{17c}$$

under the restrictions (17a) and (17b). It is clear that

$$\eta_1 = \frac{2 + \eta_2}{3} - \sum_m \frac{(J-m)(J-m-1)}{J(2J-1)} p_m \,, \tag{18}$$

is an identity. Since all the terms in the sum are positive or zero it is clear

that

$$\eta_1 \leqslant \frac{2+\eta_2}{3}. \tag{18a}$$

The equality sign can be realized only if all p_m ($m \leqslant J-2$) can be set equal to zero. For $\eta_2 = 0$ this requires that

$$3(J-1)^2 - J(J+1) = (2J-1)(J-3) \leqslant 0$$

or $J \leqslant 3$. The case $J = \frac{1}{2}$, for which $\eta_2 = 0$ automatically, is discussed separately. From (16) and (16a)–(16c) it is seen that (with $J > \frac{1}{2}$),

$$N_{\max} = \lambda_1(\eta_1)_{\max} \leqslant \tfrac{2}{3} \tag{19}$$

and the equality (necessary for $r = 1$) can be achieved only if $J = J' + 1$. For $J = \frac{1}{2}$ the result $(\eta_1)_{\max} = 1$ is obvious but $J = J' + 1$ is impossible. Indeed (19) is again fulfilled and the equality applies for $J = J'$ only.

Our condition for a pure state is therefore seen to require the maximum nuclear polarization consistent with no alignment. The condition is further: parallel directions of $\hat{\boldsymbol{q}}$ and $\boldsymbol{N}$ in the positron emission and antiparallel directions of $\hat{\boldsymbol{q}}$ and $\boldsymbol{N}$ in the electron emission.

It is also simple to analyze the case of the emitting states (axially) aligned but not polarized. In this case

$$\frac{\langle \boldsymbol{A} \rangle}{\langle B \rangle} = \frac{1}{3}\hat{\boldsymbol{q}} - \lambda_2\eta_2(\hat{\boldsymbol{q}} - 3\hat{\boldsymbol{q}}\cdot\hat{\boldsymbol{k}}\,\hat{\boldsymbol{k}}),$$

where $\hat{\boldsymbol{k}}$ is a unit vector along the axis of alignment ($\hat{\boldsymbol{k}}$ and $-\hat{\boldsymbol{k}}$ are physically equivalent) and

$$\lambda_2 = \tfrac{1}{3}, \qquad J = J' + 1,$$

$$\lambda_2 = -\frac{2J-1}{3(J+1)}, \qquad J = J',$$

$$\lambda_2 = \frac{J(2J-1)}{3(J+1)(2J+3)}, \qquad J = J' - 1.$$

Then complete β-polarization ($|\langle \boldsymbol{A} \rangle| = \langle B \rangle$, $r = 1$) results either for $\lambda_2\eta_2 = -\frac{2}{3}$ or for

$$0 \leqslant \frac{4}{9\lambda_2\eta_2} - \frac{1}{3} \leqslant 1.$$

It follows that for $\eta_2 > 0$ one obtains $r = 1$ only for $J = J' + 1$, ($J \geqslant 1$) and

$\eta_2 = 1$ is necessary. In addition $\hat{\boldsymbol{q}} \cdot \hat{\boldsymbol{k}} = \pm 1$. For $\eta_2 < 0$ the necessary and sufficient conditions for $r = 1$ are:

$$\eta_2 = (\eta_2)_{\min} = -\frac{J+1}{2J-1}, \qquad J = J', \ \hat{\boldsymbol{q}} \cdot \hat{\boldsymbol{k}} = \pm 1,$$

and J must be integer; or

$$\eta_2 = (\eta_2)_{\min} = -2, \qquad J = 1, \qquad J' = 0$$

and $\hat{\boldsymbol{q}} \cdot \hat{\boldsymbol{k}}$ is arbitrary. It is seen that the emitting state must be populated in only one non-equivalent sublevel: $|m| = J$ for $\eta_2 = 1$ and $m = 0$ for $\eta_2 = (\eta_2)_{\min}$. The restriction to $J = 1 \to J' = 0$ is understood in that the final as well as the initial nuclear state is pure. Since $\Delta m = 0$ no direction of $\hat{\boldsymbol{q}}$ is singled out. In the other cases the sign of $\hat{\boldsymbol{q}} \cdot \hat{\boldsymbol{k}}$ is correlated with the sign of Δm. The restriction to $J = J' + 1$ when $\eta_2 = 1$ is understood because then in the final state only $|m'| = J'$ is populated. In the case $\eta_2 < 0$ the result $J = J'$ can be understood in that only $m' = \pm 1$ can be populated and these two substates are equivalent in terms of nuclear alignment.

The condition for complete transverse polarization with $\eta_2 = 0$ is, ($\langle \boldsymbol{A} \rangle = -\frac{1}{3}\hat{\boldsymbol{q}}$ for both electron and positron emission),

$$\hat{\boldsymbol{p}} \cdot \hat{\boldsymbol{q}} = -p/W,$$

just as in the pure Fermi transition, see eq. (5). Therefore eq. (6) also applies here.

One may ask also what polarization effects will result from the decay of a completely polarized nucleus when the neutrino momentum is not observed. An average over neutrino direction is carried out in (8) and $\boldsymbol{N}$ is written as $\lambda_1 \hat{\boldsymbol{k}}$, where $\hat{\boldsymbol{k}}$ is the direction of nuclear polarization. Then $\boldsymbol{A}/B$ has the value $\pm \lambda_1 \hat{\boldsymbol{k}}$ and the electron polarization formula reduces to

$$-\boldsymbol{r} = \pm \frac{\pm \lambda_1 \hat{\boldsymbol{k}} - \boldsymbol{p} \pm \lambda_1 (W-1) \hat{\boldsymbol{p}} \cdot \hat{\boldsymbol{k}} \hat{\boldsymbol{p}}}{W \mp \lambda_1 \boldsymbol{p} \cdot \hat{\boldsymbol{k}}}. \tag{20}$$

The condition that the polarization be transverse is

$$\hat{\boldsymbol{k}} \cdot \hat{\boldsymbol{p}} = \pm \frac{p}{\lambda_1 W}.$$

When $J = J' + 1$, λ_1 is 1 and the electron polarization is complete. This is an especially interesting result because it does not involve a recoil effect. Even if the nucleus is not completely polarized it is still true that one can get appreciable transverse electron polarization. However the nucleus can in prin-

3785

ciple be completely polarized and it is difficult to give a physical explanation of the complete electron polarization which ensues even though a pure observation has not been made.

2·3. *Mixed transitions.* – In this Section we give the results for unoriented nuclei. The polarization depends on y, see eq. (1), and the only parameter which enters is

$$a = \frac{1 - y/3}{1 + y}, \tag{21}$$

where a is the coefficient of p/W in the electron-neutrino correlation. In terms of this parameter

$$\boldsymbol{r} = \pm \frac{\boldsymbol{p} + a\hat{\boldsymbol{q}} + a(W-1)\,\hat{\boldsymbol{p}}\cdot\hat{\boldsymbol{q}}\,\hat{\boldsymbol{p}}}{W + a\boldsymbol{p}\cdot\hat{\boldsymbol{q}}}. \tag{22}$$

Except for $a = 1$ (pure Fermi transitions) the magnitude of the polarization vector is smaller than unity,

$$1 - r^2 = \frac{1 - a^2}{(W + a\boldsymbol{p}\cdot\hat{\boldsymbol{q}})^2}.$$

Of course, $-\frac{1}{3} \leqslant a \leqslant 1$.

The condition for transverse polarization ($\boldsymbol{r}\cdot\boldsymbol{p} = 0$) gives

$$\hat{\boldsymbol{p}}\cdot\hat{\boldsymbol{q}} = -\frac{p}{aW}. \tag{23}$$

For a given y or a this means that

$$p/W \leqslant a \qquad \text{or} \qquad W \leqslant (1 - a^2)^{-\frac{1}{2}}. \tag{23a}$$

As an example, if we take a to be 0.70 we find $W \leqslant 1.40$ (kinetic energy not larger than 205 keV). Consequently, as a general rule, pure transverse polarization can be obtained only for rather low energies unless the Gamow-Teller matrix element is very small.

Abandoning the requirement of pure transverse polarization, we find in general that the magnitude of the transverse polarization is given by

$$r_\perp^2 = r^2 - (\boldsymbol{r}\cdot\hat{\boldsymbol{p}})^2 = \frac{a^2[1 - (\hat{\boldsymbol{p}}\cdot\hat{\boldsymbol{q}})^2]}{(W + a\boldsymbol{p}\cdot\hat{\boldsymbol{q}})^2}. \tag{24}$$

The choice of electron-neutrino angle corresponding to

$$\hat{\boldsymbol{p}}\cdot\hat{\boldsymbol{q}} = -\frac{ap}{W}, \tag{25}$$

3786

which is always possible, maximizes $r_\perp$. The resulting optimum value is

$$(r_\perp)_{\max} = |a|(W^2 - a^2p^2)^{-\frac{1}{2}} . \tag{26}$$

The total polarization is now given by

$$r^2 = 1 - W^2 \frac{(1-a^2)}{a^4} (r_\perp)^4_{\max} . \tag{26a}$$

For $a = 0.70$ and $W = 2$, for example, we obtain $(r_\perp)_{\max} = 0.37$. The total polarization would be 0.91 and the longitudinal component 0.83. The direction of $\boldsymbol{r}_\perp$ is given by

$$-\boldsymbol{r}\times\hat{\boldsymbol{p}} = \mp \frac{a\boldsymbol{q}\times\boldsymbol{p}}{W + a\boldsymbol{p}\cdot\hat{\boldsymbol{q}}} = \mp \frac{aW\,\hat{\boldsymbol{q}}\times\hat{\boldsymbol{p}}}{W^2 - a^2p^2} = \pm \frac{aW\boldsymbol{R}\times\hat{\boldsymbol{p}}/\boldsymbol{q}}{W^2 - a^2p^2} , \tag{27}$$

where the last equalities apply for the maximum transverse polarization.

Appendix

Electron-positron polarization operator.

As a matter of notation, the Dirac equation is written in the form

$$H\Psi = (-i\boldsymbol{\alpha}\cdot\nabla + \beta)\Psi = i\partial\Psi/\partial t , \tag{A.1}$$

where

$$\boldsymbol{\alpha} = \begin{pmatrix} 0 & \boldsymbol{\sigma} \\ \boldsymbol{\sigma} & 0 \end{pmatrix}, \qquad \beta = \begin{pmatrix} 1 & 0 \\ 0 & -1 \end{pmatrix}.$$

The plane wave solutions are

$$\Psi = \psi \exp[i(\pm\boldsymbol{p}\cdot\boldsymbol{x} \mp Wt) , \tag{A.2}$$

where

$$H\psi = (\pm\boldsymbol{\alpha}\cdot\boldsymbol{p} + \beta)\psi = \pm W\psi , \tag{A.3}$$

and $\boldsymbol{p}$ and $W = (p^2+1)^{\frac{1}{2}}$ are the physical momentum and energy of the particle. As an alternative to the hole theory, we interpret the solutions of eq. (A.3) with lower signs as positron wave functions so that the operators for energy, momentum, and angular momentum are

$$\pm H, \qquad \mp i\nabla, \qquad \text{and} \qquad \pm(-i\boldsymbol{x}\times\nabla + \tfrac{1}{2}\boldsymbol{\sigma}) .$$

3787

The *polarization operator* is defined to be

$$\boldsymbol{O}^{\mp} = \pm \boldsymbol{\sigma}\cdot\hat{\boldsymbol{p}}\,\hat{\boldsymbol{p}} + \hat{\boldsymbol{p}}\times(\beta\boldsymbol{\sigma}\times\hat{\boldsymbol{p}})\,. \tag{A.4}$$

We recall that the upper sign refers to electron, the lower to positron. The operator $\boldsymbol{O}^{\pm}\cdot\hat{\boldsymbol{s}}$ provides a generalization of the helicity operator to arbitrary direction $\hat{\boldsymbol{s}}$. In the non-relativistic limit β is effectively ± 1 and $\boldsymbol{O}^{\mp}$ reduces simply to $\pm\boldsymbol{\sigma}$. If one introduces a right-handed orthogonal set of unit vectors $\hat{\boldsymbol{e}}_1 = \hat{\boldsymbol{p}}, \hat{\boldsymbol{e}}_2, \hat{\boldsymbol{e}}_3$ then it is seen that the algebra of the components $\boldsymbol{O}_i^{\mp} = \boldsymbol{O}^{\mp}\cdot\hat{\boldsymbol{e}}_i$ is similar to that of the Pauli matrices:

$$\boldsymbol{O}_i^{\mp}\boldsymbol{O}_j^{\mp} = \delta_{ij} \pm i\varepsilon_{ijk}\boldsymbol{O}_k^{\mp}\,. \tag{A.5}$$

Although, as is easily verified, $\boldsymbol{O}^{\mp}$ commutes with H, one cannot simultaneously diagonalize $\boldsymbol{O}^{\mp}$ and H because the different components of $\boldsymbol{O}^{\mp}$ do not commute with each other. However, for an arbitrary direction $\hat{\boldsymbol{s}}$, one can find functions which are simultaneously eigenfunctions of H and $\boldsymbol{O}^{\mp}\cdot\hat{\boldsymbol{s}}$. Since

$$(\boldsymbol{O}^{\mp}\cdot\hat{\boldsymbol{s}})^2 = 1\,,$$

the eigenvalues of $\boldsymbol{O}^{\mp}\cdot\boldsymbol{s}$ are ± 1. Explicit formulas for the functions satisfying

$$\pm H\psi^{\mp}(\hat{\boldsymbol{s}}) = W\psi^{\mp}(\hat{\boldsymbol{s}})\,,$$
$$\boldsymbol{O}^{\mp}\cdot\hat{\boldsymbol{s}}\psi^{\mp}(\hat{\boldsymbol{s}}) = \psi^{\mp}(\hat{\boldsymbol{s}})\,,$$

are as follows:

$$\psi^{-}(\hat{\boldsymbol{s}}) = \cos\tfrac{1}{2}\theta\,\exp[-\tfrac{1}{2}i\varphi]u_{+} + \sin\tfrac{1}{2}\theta\,\exp[-\tfrac{1}{2}i\varphi]u_{-} \tag{A.6}$$

$$\psi^{+}(\hat{\boldsymbol{s}}) = \cos\tfrac{1}{2}\theta\,\exp[\tfrac{1}{2}i\varphi]v_{-} - \sin\tfrac{1}{2}\theta\,\exp[-\tfrac{1}{2}i\varphi]v_{+}\,, \tag{A.7}$$

where θ and φ are the polar and azimuth angles of $\hat{\boldsymbol{s}}$. The functions $u_{\pm}$ and $v_{\pm}$ are

$$u_{\pm} = [2W(W+1)]^{-\frac{1}{2}}\begin{pmatrix}(W+1) & \chi_{\pm}\\ \boldsymbol{\sigma}\cdot\boldsymbol{p} & \chi_{\pm}\end{pmatrix}, \tag{A.8}$$

$$v_{\pm} = [2W(W+1)]^{-\frac{1}{2}}\begin{pmatrix}\boldsymbol{\sigma}\cdot\boldsymbol{p} & \chi_{\pm}\\ (W+1) & \chi_{\pm}\end{pmatrix}, \tag{A.9}$$

where

$$\chi_{+} = \begin{pmatrix}1\\0\end{pmatrix}, \qquad \chi_{-} = \begin{pmatrix}0\\1\end{pmatrix}.$$

These functions $u_{\pm}$ and $v_{\pm}$ are the « spin up » and « spin down » functions very frequently used in Dirac theory; it is seen that they are eigenfunctions of $\boldsymbol{O}^{\mp}\cdot\hat{\boldsymbol{s}}$ with $\hat{\boldsymbol{s}}$ in the $\pm z$ direction. To obtain a complete set of solutions to the Dirac equation one uses $\psi^{\mp}(\hat{\boldsymbol{s}})$ and $\psi^{\mp}(-\hat{\boldsymbol{s}})$, for it is clear that

$$\pm H\psi^{\mp}(-\hat{\boldsymbol{s}}) = W\psi^{\mp}(-\hat{\boldsymbol{s}})\,,$$
$$\boldsymbol{O}^{\mp}\cdot\hat{\boldsymbol{s}}\psi^{\mp}(-\hat{\boldsymbol{s}}) = -\psi^{\mp}(-\hat{\boldsymbol{s}})\,.$$

3788

Another pertinent property of these eigenfunctions is that the expected value of $\boldsymbol{O}^{\mp}$ in state $\psi^{\mp}(\boldsymbol{s})$ is $\hat{\boldsymbol{s}}$:

$$\psi^{\mp *}\boldsymbol{O}^{\mp}\psi^{\mp} = \hat{\boldsymbol{s}} .$$

If a particle is in one of the eigenstates $\psi^{\mp}(\hat{\boldsymbol{s}})$, one can say that it is polarized in the $\hat{\boldsymbol{s}}$ direction.

The operator $\boldsymbol{O}^{\mp}\cdot\hat{\boldsymbol{s}}$ is related to the covariant spin operator [4] $i\gamma_5\gamma_\mu n_\mu$ (greek letters run from 1 to 4 and x_4 is it). Here n_μ is a Lorentz four-vector with components $(\hat{\boldsymbol{s}}, 0)$ in the rest system of the particle and the matrices are given by

$$\gamma_i = -i\beta\alpha_i , \qquad \gamma_4 = \beta .$$

The four-vector n_μ satisfies the equations

$$n_\mu n_\mu = 1 ,$$
$$n_\mu p_\mu = 0 ,$$

and in the laboratory system its components are

$$\boldsymbol{n} = \hat{\boldsymbol{s}} + (W-1)\,\hat{\boldsymbol{s}}\cdot\boldsymbol{p}\,\hat{\boldsymbol{p}} ,$$
$$n_4 = i\boldsymbol{p}\cdot\hat{\boldsymbol{s}} .$$

The difference between the two operators is

$$\boldsymbol{O}^{\mp}\cdot\hat{\boldsymbol{s}} - i\gamma_5\gamma_\mu n_\mu = \pm\,\hat{\boldsymbol{s}}\cdot\hat{\boldsymbol{p}}\boldsymbol{\sigma}\cdot\hat{\boldsymbol{p}}\beta(\pm\boldsymbol{\alpha}\cdot\boldsymbol{p} + \beta \mp W) .$$

As long as electron states and positron states are considered separately, the quantity on the right is zero and the operators $\boldsymbol{O}^{\mp}\cdot\hat{\boldsymbol{s}}$ and $i\gamma_5\gamma_\mu n_\mu$ are equivalent.

The eigenfunctions $\psi^{\mp}(\hat{\boldsymbol{s}})$ are used to construct a projection operator

$$D^{\mp}_{\sigma\varrho} = \psi^{\mp}_{\sigma}(\hat{\boldsymbol{s}})\psi^{\mp}_{\varrho}(\hat{\boldsymbol{s}}) , \tag{A.10}$$

and this enters in the calculation of the β-transition probability according to

$$I \sim \mathrm{Tr}\, D^{\mp}\omega\Lambda(\nu)\omega^* ,$$

where

$$\Lambda(\nu) = \tfrac{1}{2}(1 + \boldsymbol{\alpha}\cdot\hat{\boldsymbol{q}}) ,$$

is the neutrino projection operator and the general form of the operator ω is

$$\omega = \gamma_4\gamma_\mu(1+\gamma_5)(f\,|\,\gamma_4\gamma_\mu(1+\lambda\gamma_5)\,|\,i) .$$

[4] L. Michel and A. S. Wightman: *Phys. Rev.*, **98**, 1190 (1955). See also ref. [2].

It is evident that

$$D^{\mp} = \Lambda^{\mp}(\beta)\tfrac{1}{2}(1 + \boldsymbol{O}^{\mp}\cdot\hat{\boldsymbol{s}}) , \tag{A.11}$$

where

$$\Lambda^{\mp}(\beta) = \frac{1}{2W}(W + \boldsymbol{\alpha}\cdot\boldsymbol{p} \pm \beta) ,$$

is the energy projection operator for electrons (—) and positrons (+).

RIASSUNTO (*)

In una transizione β permessa, nella quale si osservi la direzione di rinculo in coincidenza con la particella β, è possibile produrre, sotto appropriate condizioni, elettroni completamente polarizzati. Per le transizioni pure di Fermi non è necessario che sia imposta alcuna condizione supplementare. È altresì necessario, per le transizioni di Gamow-Teller, che il nucleo sia orientato e, qualora l'allineamento sia zero, che la polarizzazione nucleare debba avere il massimo valore possibile compatibile con tale condizione, cioè $\frac{2}{3}$. Inoltre, in una transizione di Gamow-Teller da un nucleo completamente polarizzato ad un nucleo con un valore di spin inferiore, la polarizzazione degli elettroni risulta completa, anche senza osservazione del rinculo. In generale la polarizzazione della particella β è, almeno parzialmente, trasversa. Si investigano le condizioni per una polarizzazione puramente trasversa. Per le transizioni di Fermi, per le quali la polarizzazione trasversa avrebbe valore unitario, si può farlo ad ogni energia; tuttavia, come regola generale, tale effetto può essere osservato solo per elettroni monoenergetici. In pratica la banda di energia può essere piuttosto larga senza mutare seriamente la natura della polarizzazione. Per transizioni con un apprezzabile contributo di Gamow-Teller e senza alcuna polarizzazione nucleare, la polarizzazione della particella β è non solo incompleta, ma può essere resa puramente trasversa solo ad energie indesiderabilmente basse. È possibile tuttavia produrre una apprezzabile polarizzazione trasversa ad energie più elevate anche quando la polarizzazione longitudinale non è debole. Si discute in un'Appendice la forma più peculiare dell'operatore di polarizzazione elettrone-positone.

(*) *Traduzione a cura della Redazione.*

3790

IL NUOVO CIMENTO Vol. XIV, N. 4 16 Novembre 1959

The $\pi^- - \pi^0$ Mass Difference.

P. Hillman (*), W. C. Middelkoop, T. Yamagata (*)
and E. Zavattini

CERN - Geneva

(ricevuto il 3 Settembre 1959)

Summary. — We have measured the time of flight of the neutron resulting from the reaction at rest $\pi^- + p \to \pi^0 + n$. We obtain from this a value for the $\pi^- - \pi^0$ mass difference of (9.01 ± 0.08) electron masses.

1. – Method and apparatus.

Using techniques developed in preparing an experiment on the inverse photoproduction reaction $\pi^- + p \to \gamma + n$ (in flight), we have determined the difference between the masses of the π^- and π^0 mesons by measuring the time of flight of the neutron resulting from the reaction at rest

$$\pi^- + p \to \pi^0 + n \,. \tag{1}$$

The 65 MeV pion beam originated in a beryllium target bombarded by 600 MeV protons inside the CERN Synchro-cyclotron and was focused into a spot about 10 cm in diameter with an intensity of about $2 \cdot 10^4$ pions per second. The pions were slowed down in carbon and about $5 \cdot 10^3$ pions per second stopped in a liquid hydrogen target, which was a vertical cylinder 12.5 cm in diameter. The mean free path of the neutrons in liquid hydrogen is only 3.46 cm, and in the final runs we used a collimator covering 8 cm of the target to reduce background produced in the hydrogen. The geometry in shown in Fig. 1.

(*) Ford Foundation Fellow.

3791

The 0.4 MeV ($\beta = 0.03$) neutrons were detected in a plastic scintillator 18 cm in diameter and 2.5 cm thick, viewed by one 5 inch RCA 7046 photomultiplier through a plexiglass light guide. The centre of the scintillator was

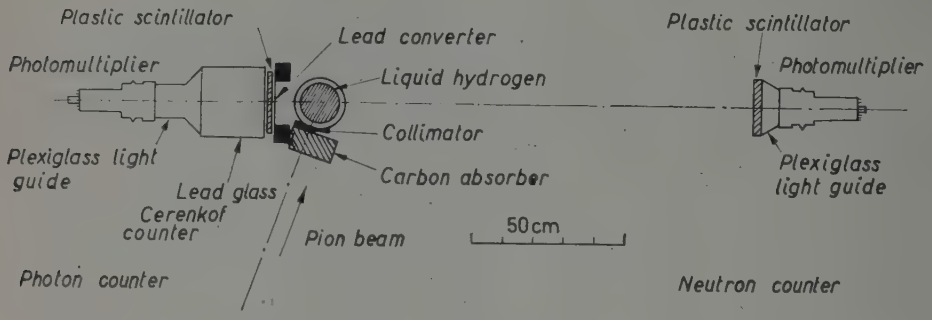

Fig. 1. – The experimental geometry.

142.8 cm from the centre of the target. Those photons going in roughly the opposite direction were converted in a 5 mm thick lead sheet 15 cm in diameter, 14 cm from the centre of the target, and detected by coincidences between a 1 cm thick plastic scintillator S and a 21 cm thick lead-glass Čerenkov counter 23 cm in diameter. This counter was also viewed by one 7046 photomultiplier through a plexiglass light guide. This arrangement practically eliminates counting of photons not originating in the liquid hydrogen. In addition, the S pulse is better for timing purposes than the Čerenkov pulse, which has a more variable shape and size. The neutron counter was shielded with (from inside out) 5 cm lead, (5÷10) cm borax, and about 80 cm heavy concrete, and the Čerenkov counter with 5 cm of lead and some concrete.

The times of flight were measured by photographing on single sweeps of an Edgerton Type 2236 travelling-wave oscilloscope the appropriately delayed anode pulses from the scintillator S, the Čerenkov counter, and the neutron counter. The 80 ns cm^{-1} sweep was triggered by a triple coincidence circuit with S-Čerenkov and S-neutron resolution times of 20 and 60 ns respectively (1 ns $\equiv 10^{-9}$ s). The traces were photographed with a one-to-one image-to-object ratio, and the trace thickness of the film was about 0.1 mm. A stabilized 300 MHz sine-wave was also photographed intermittently to calibrate the sweep speed and linearity. The pictures were projected onto a screen, and the distances measured between the S and neutron pulses, using the points of intersection of the linear extrapolation of the steepest rise with the base line. For the Čerenkov pulses only the amplitudes were measured, and the rare cases in which the pulses were obviously not properly time-correlated with the S pulses were discarded. The heights of the neutron pulses were also measured.

3792

The neutron counter pulse-height corresponding to a given energy-loss in the plastic scintillator was determined by measuring the spectrum from a ^{22}Na source, whose upper limit should correspond to an electron energy of about 1.1 MeV (Compton recoil limit). The electronic bias was then set 25 times lower than this point; taking into account the saturation effect ([1]), this should correspond to biasing against protons below about 0.2 MeV. To find a reasonable Čerenkov counter bias, the delays were set so that the second γ from the π^0-decay be recorded in coincidence in the neutron counter, which has enough γ-sensitivity to give quite a high counting rate. The Čerenkov bias was then set just below the peak in the differential bias curve.

2. – Procedure.

The number of stopping pions was maximized by maximizing the S-Čerenkov coincidence rate against beam position and absorber thickness. Four runs were then made.

a) The delay lengths were adjusted as above so that coincidences between the photons from π^0-decays were recorded. We then used as our time zero the position of the observed γ-γ peak minus the calculated photon flight time, 4.7 ns. This automatically takes into account all electronic delays. (Total counting rate about 1 s^{-1}). The 9 MeV ($\beta = 0.14$) neutron from the competing reaction

$$\pi^- + p \to \gamma + n \qquad (2)$$

also appears on the same film with a delay of about 30 ns with respect to the γ peak.

b) Delays of 30 ns were then inserted into the S and Čerenkov channels, so that the neutron from reaction (2) gave a peak at the same place on the oscilloscope sweep as the γ peak in run *a*). For these two runs the neutron pulse had to be attenuated to give a pulse of reasonable size on the oscilloscope. (Counting rate about 25 min^{-1}.)

c) Next the 30 ns delays were replaced by 150 ns delays, with which the coincidence resolution time comfortably bracketed the expected time of flight of the low energy (π^0) neutrons. (Total counting rate about 5 min^{-1}; a run was also made at reduced beam, 1 min^{-1}.)

([1]) D. Kraus, K. Lande, E. Leboy and W. Selove: NYO 8547, August 1958 (unpublished).

3793

d) Finally, the 150 ns delays were removed and a 60 ns delay placed in the neutron channel. In this situation no real coincidences could occur, so that this gave the spectrum of random coincidences. The purpose of this run was to look for any effects of the radio-frequency structure of the beam. (Counting rate about 5 min^{-1}.)

The use of delay cables to keep the relative positions of the pulses on the oscilloscope screen roughly fixed permits the use of a much faster sweep and makes the time measurements simple and accurate, but the delay lengths must then be carefully measured. This is done for each cable by short-circuiting one end and applying a high-frequency sine-wave to the other end. The frequency f is then varied until a minimum in the voltage at the open end is obtained. There is then an integral number n of half-cycles of the standing-wave in the cable and the desired delay time in the cable is $L/v=n/2f$. This was done for several frequencies near the frequency corresponding to the rise times of the photomultiplier pulses; since no appreciable variation was found, the result is unambiguous. The Rohde and Schwarz type SMLM.BN 4105 Power Signal Generator was calibrated against harmonics from a 50 MHz crystal-controlled Tektronix type 180-S1 Time-Mark Generator.

3. – Corrections and errors.

A definite time-dependence of the pulses on the photomultiplier output amplitude was found in the experimental analysis. Besides the expected distortion for saturated pulses, small pulses were found on the average to occur later than large pulses, the effect increasing rapidly to about three nanoseconds for very small pulses, fifty times below saturation. We ascribe the effect tentatively to the increased probability, when there are only a few photoelectrons produced in the photomultiplier, that most of them should come from those regions of the photocathode corresponding to larger transit time or from the tail of the scintillator light decay curve. From runs *a*) and *b*) the quantitative dependence was established and all data were corrected for this effect.

Our interpretation of the photomultiplier effect is given some support by our finding that with a variable light source and 2 inch photomultiplier (RCA 6810A) with a central 1 cm^2 aperture, no time-amplitude dependence was found greater than one nanosecond. Also, pulse-generator measurements showed that to ± 0.3 ns the pulse position was not a function of the variable attenuator, or of the pulse height in the amplifier, in the oscilloscope, or on the film (« reading error »). The quoted accuracy of the time-amplitude law includes this uncertainty.

3794

The pulse-generator measurements showed that the decrease in the amplifier gain used as part of the neutron pulse attenuation in run *a*) produced an apparent speed-up of the pulse by (0.15 ± 0.3) ns, and a correction was made for this effect.

The only other major correction was for drift in the oscilloscope sweep speed, amounting to eight per cent over two days. A small correction was made to the final result of 0.004 MeV for the binding energy of the π^--meson in the Bohr orbit.

Table I lists the non-negligible contributions to the errors on the times of flight for the π^- mass and $\pi^- - \pi^0$ mass difference calculations. Reasonable probability distributions assigned to the (small) systematic errors were folded into the gaussian statistical errors; the final quoted errors are the standard deviations of gaussians approximated to the non-gaussian results.

TABLE I. – *Major errors, in nanoseconds.*

1) Drift and fluctuations of oscilloscope sweep speed .	± 0.3
2) Accuracy of the time-amplitude relation	± 0.5
3) Theoretical peak shapes and fits to experiment . .	± 0.5
4) The possibility that the delay cables were stretched after use and before calibration — for mass difference only	$\begin{cases} +0.0 \\ -0.2 \end{cases}$
5) Amplifier gain-change correction	± 0.3

4. – Results and conclusions.

Fig. 2 shows some of our final time-of-flight spectra in the four cases described at the beginning of Section 2. The only important non-electronic pulse-height selection exercised was the rejection of neutron pulses in cases *c*) and *d*) corresponding to proton recoils of greater than 0.4 MeV. Unfolding the effects of the finite target and counter sizes in the first peak of case *a*) leaves a peak of full width at half height of about 1.5 ns attributable to the total photomultiplier, electronic and film-reading error. This is our basic resolution time.

The pion-beam profile was measured before slowing down or collimation. The expected peak shapes for the neutrons were then calculated taking into account their mean free paths in liquid hydrogen and in plastic scintillator the estimated pion flux distribution after collimation and slowing down, and the above-mentioned resolution time. The effect on the peak of neutrons having lost some energy in scattering in the hydrogen was calculated to be small, though they should give a long flat tail. The arbitrarily normalized results were matched to the experimental points, in case *c*) using only the first eight points of the peak in order to minimize the effects of neutrons scat-

3715

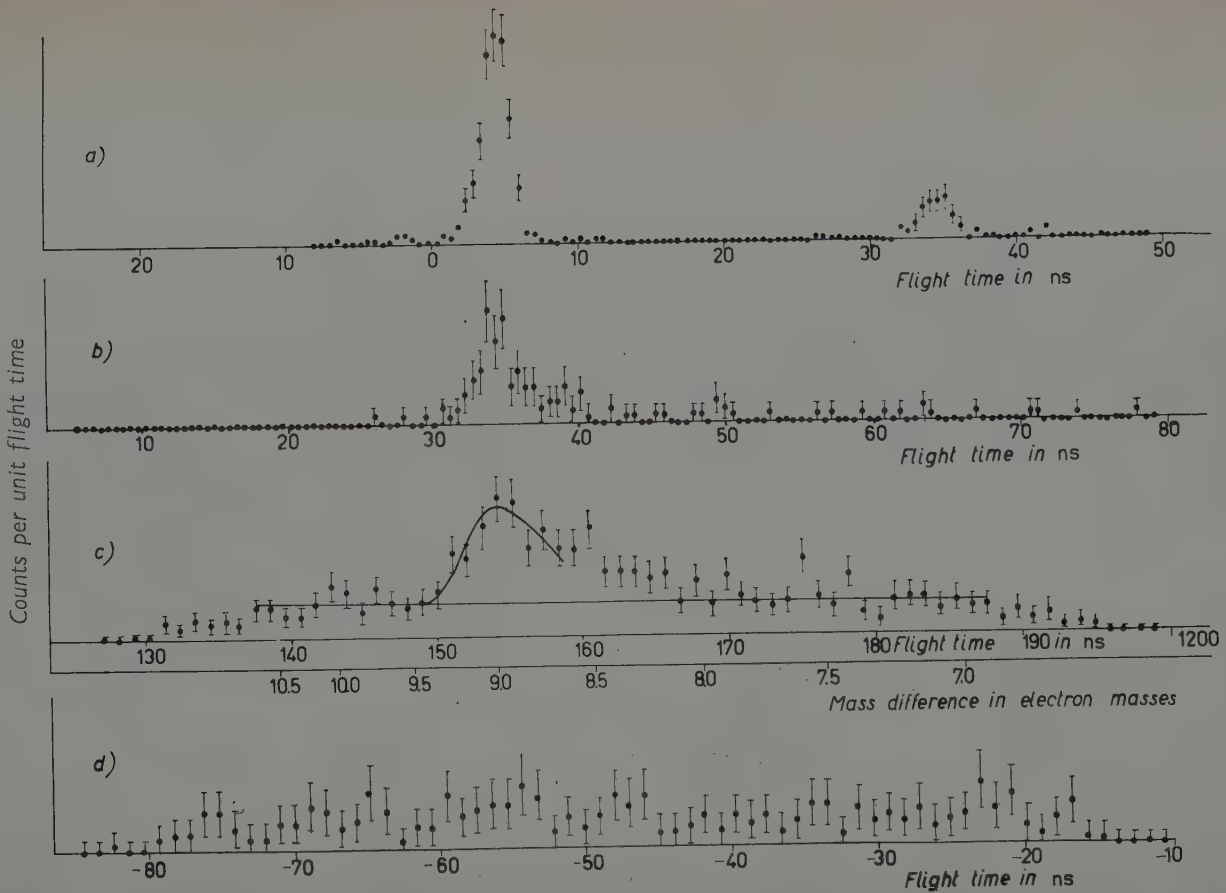

Fig. 2. – The time spectra of pulses in the neutron detector. The zero is derived from the γ-γ peak position in case *a*). The ordinates are arbitrary, except that cases *c*) and *d*) are normalized to the same total incident pion flux. *a*) The photons from π^0 decay and the neutrons from the process $\pi^- + p \to \gamma + n$. *b*) The neutrons from the process $\pi^- + p \to \gamma + n$. *c*) The neutrons from the process $\pi^- + p \to \pi^0 + n$. The straight line is the average background. The theoretical curve, superposed on this line, is least-squares fitted in scale and abscissa to the experimental points. The mass-difference scale corresponds to the peak of the theoretical curve. *d*) Random background.

3796

tered in the hydrogen, shielding materials, and the light guide in the neutron counter. The best fit for case *c*) is shown in Fig. 2 *c*).

The final time-of-flight figures, corresponding to the calculated most-probable flight paths of 140.2 cm for the π^- mass and 138.0 cm for the mass difference, are: for the π^- mass, (34.5 ± 0.6) ns from case *a*) (errors 2) and 5) of Table I not applicable), and (34.1 ± 0.8) ns from the comparison of cases *a*) and *b*) using the measured time-length of the delay cable; and (154.1 ± 0.9) ns for the mass difference.

The final value of the $\pi^- - \pi^0$ mass difference is (9.01 ± 0.08) electron masses. This is to be compared with the results of CHINOWSKY [2] of $(8.8 \pm 0.6)\, m_e$ and of CASSELS [3] of $(8.90 \pm 0.14)\, m_e$ using the angular correlation between the photons from π^0 decay after reaction (1); with those of PANOFSKY [4] of $(10.6 \pm 2.0)\, m_e$ and of MERRISON [5] of $8.8^{+0.4}_{-0.3}$ from the γ-ray energy spectrum from the decays of π^0's from the same reaction; and with that of GETTNER [6] of $(9.6 \pm 0.5)\, m_e$ from a method similar to ours.

From case *a*) and the comparison of *a*) and *b*) respectively we obtain values of the π^- mass of (138.4 ± 2.7) MeV and (140.5 ± 3.7) MeV. The accepted value is (139.63 ± 0.06) MeV [7].

Since the π^0 has a finite lifetime, the uncertainty principle requires that the neutron energy be not perfectly sharp. The sharpness of the rise observed in case *c*) sets a lower limit of about $3 \cdot 10^{-21}$ s on the lifetime, which is below the existing experimental lower limit, established from the proton Compton effect [8], as well as the theoretically expected value [9].

The observed peak in case *c*) is broader than theoretically expected. A rough calculation indicates that this may well be due to π^0 neutrons scattered from the cylindrical iron shield around the photomultiplier and scintillator or from the plexiglass light guide. One might have been tempted to invoke the π^0_0-meson [10] as an alternative explanation had not stronger arguments already

---

[2] W. CHINOWSKY and J. STEINBERGER: *Phys. Rev.*, **93**, 586 (1954).

[3] J. M. CASSELS, D. P. JONES, P. G. MURPHY and P. L. O'NEILL: *Proc. Phys. Soc.* **74**, 92 (1959).

[4] W. K. H. PANOFSKY, R. L. AAMODT and J. HADLEY: *Phys. Rev.*, **81**, 565 (1951).

[5] J. KUEHNER, A. W. MERRISON and S. TORNABENE: to be published in *Proc. Phys. Soc.*

[6] M. GETTNER, L. HOLLOWAY, D. KRAUS, K. LANDÉ, E. LEBOY and W. SELOVE: *Phys. Rev. Lett.*, **2**, 471 (1959).

[7] K. M. CROWE: *Nuovo Cimento*, **5**, 541 (1957).

[8] L. G. HYMAN, R. ELY, D. H. FRISCH and M. A. WAHLIG: *Phys. Rev. Lett.*, **3**, 93 (1959); M. JACOB and J. MATTHEWS: reported by G. BERNARDINI at the *Kiev Conference* (1959).

[9] See M. L. GOLDBERGER and S. B. TREIMAN: *Nuovo Cimento*, **9**, 451 (1958).

[10] Y. YAMAGUCHI: *Progr. Theor. Phys.*, **19**, 622 (1958); A. BALDIN: *Nuovo Cimento*, **8**, 569 (1958).

3797

ruled out this possibility ([11]). A further run is planned for a later date to clear up this point and perhaps to improve the mass difference result.

* * *

We are grateful to Prof. G. BERNARDINI, whose help and encouragement were indispensable; to G. GATTI, who assisted in much of the running and calculations; to D. LAKE for computation; to G. SICHER and B. SMITH for able and willing technical assistance; and to the Gustaf Werner Istitute of Uppsala for the loan of the cryostat.

([11]) M. CINI, R. GATTO, E. L. GOLDWASSER and M. RUDERMAN: *Nuovo Cimento*, **10**. 243 (1958). We note that the broadening of our peak would be attributable to a π_0^0 with a mass only 0.4 m_e higher than the π^0. However, Cini's argument on phase behaviour is independent of the mass.

RIASSUNTO (*)

Abbiamo misurato il tempo di volo del neutrone risultante dalla reazione a riposo $\pi^- + p \to \pi^0 + n$. Ne deriva per la differenza di massa $\pi^- - \pi^0$ il valore di $(9.01 \pm 0.08)\ m_e$.

(*) *Traduzione a cura della Redazione.*

3798

A Possible Experimental Method for the Production and Detection of Heavy Hyperfragments.

R. Levi Setti and W. E. Slater (*)

The Enrico Fermi Institute for Nuclear Studies
The University of Chicago - Chicago, Ill.

(ricevuto il 23 Giugno 1959)

There is considerable theoretical interest in knowing hypernuclear binding energies for species much heavier than those studied in present experiments ($A < 13$) (1). Such knowledge is expected (2) to provide direct information on the depth of the potential well seen by a Λ particle bound in nuclear matter. Hyperfragments of mass greater than that of light elements of emulsion (C, N, and O) have never been detected with certainty. Such hyperfragments, however, might be produced with insufficient energy to yield visible connecting tracks, and thus would not lead to distinguishable two-centered events. In fact, such heavy hyperfragments would probably not be able to penetrate the potential barrier of their parent nuclei.

It would hence appear desirable to devise a process of production in which large energies could be imparted to very heavy nuclear fragments. If one wishes to obtain hyperfragments, this process should also be capable of yielding Λ hyperons. We anticipate that these conditions could both be met in a K^--induced fission process, *e.g.* of uranium nuclei. This involves the assumption that one of the two fission fragments could occasionally « trap » a hyperon. This assumption can only hold if the lifetime of the trapped Λ in nuclear matter (against stimulated decay etc.) is longer than the time required for the fission process to take place. It must be said that an estimate of binding energy B_Λ of very heavy hupernuclei would never be easy, since they are expected to decay non-mesonically with in general multiple neutron emission. A B_Λ estimate for such events could probably only be made on a statistical basis.

We have undertaken a preliminary experiment along these lines. This yielded so far only one example of K^--induced fission. The fact that at least this pro-

(*) Research supported by the U. S. Air Force Office of Scientific Research, Contract no. AF 49(638)-209.

(1) R. Ammar, R. Levi Setti, S. Limentani, P. E. Schlein, W. E. Slater and P. H. Steinberg: *Nuovo Cimento*, to be published.

(2) R. H. Dalitz: *Lectures on the Strong Interaction of Strange Particles*, given at Brookhaven National Laboratory, July 1957.

cess has been observed may justify a future experiment on a larger scale. Fission similarly induced by π^- capture has been reported previously ([3]).

In our preliminary experiment a uranium-loaded stack of 80 600 μm Ilford G-5 2 in. × 4 in. pellicles was exposed to an enriched beam of K^- moderated so as to stop in the stack. The loading procedure was as follows: a purified 10% uranyl nitrate solution was prepared by ether extraction, to remove the β-active daughter products of ^{238}U. This solution was then neutralized with versene ([4]). The stack (with paper sheets between the pellicles) was immersed into it for 8 hours at 5 °C. The sheets were then removed, and the stack and solution were cooled to dry ice temperature when they froze, the freezing point of the solution being — 5 °C. This was done because preliminary tests had shown that very severe fading accompanies a wet exposure of emulsion loaded with this solution, even near 0 °C. It was also found that this fading could be reduced by boiling and saturating with N_2 all liquids in which the pellicles would be immersed. After 57 hours (exposure and travelling time) the stack was thawed out and allowed to soak in distilled water for about an hour to remove most of the loading solution. The pellicles were

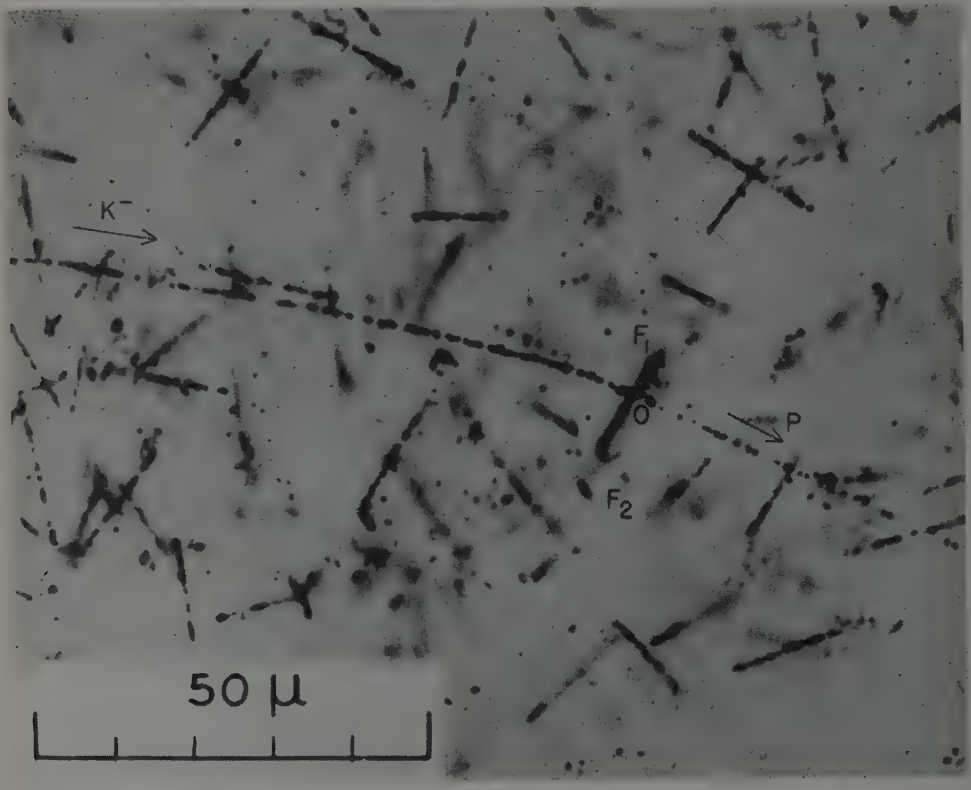

Fig. 1. – A K^--meson, captured at point *O* by a ^{238}U nucleus, gives rise to two fission products F_1 and F_2 at ranges 14.7 and 16.5 respectively and to a proton p of 4.5 mm range.

([3]) N. A. PERFILOV, N. S. IVANOVA, O. C. LOZHIN, V. I. OSTRUMOV and V. P. ŠAMOV: *Proc. of the Conference of the Academy of Sciences of the U.S.S.R. on the Peaceful Uses of Atomic Energy* (July 1, 1955).

([4]) H. G. DE CARVALHO and A. G. DA SILVA: *Notas de Fisica*, **4**, no. 12.

c800

processed free, using standard temperature development techniques. The fixing process was interrupted shortly after clearing when the onset of corrosion was noticed.

The uranium concentration in the pellicles could be determined from the observed density of α-particle tracks. It was found to be $2.8 \cdot 10^{20}$ nuclei/cm^3 or 0.6% of all nucley of the dry emulsion excluding hydrogen. Fig. 1 shows the K^--induced fission event referred to above. As can be seen from Fig. 1, the fission was slightly asymmetric, yielding a probable proton and two heavy particles of unequal mass. Although the direction of the track (K^-) of the initiating particle and the location of the events in the emulsion were those characteristic of K^--induced events in this exposure, we felt that a direct identification of the initiating particle was called for. Since reliable ionization measurements were precluded by the inhomogeneous corrosion we performed constant cell (30 μm) scattering measurements on the initiating track as well as on track p and on a μ-meson found in the same pellicle. Fig. 2 shows a plot of the mean scattering angle *vs.* range, from which it is quite clear that the initiating particle must have been much heavier than a muon. We therefore conclude that it was a K^- and that track p was probably caused by a proton. Further scanning of this stack is in process.

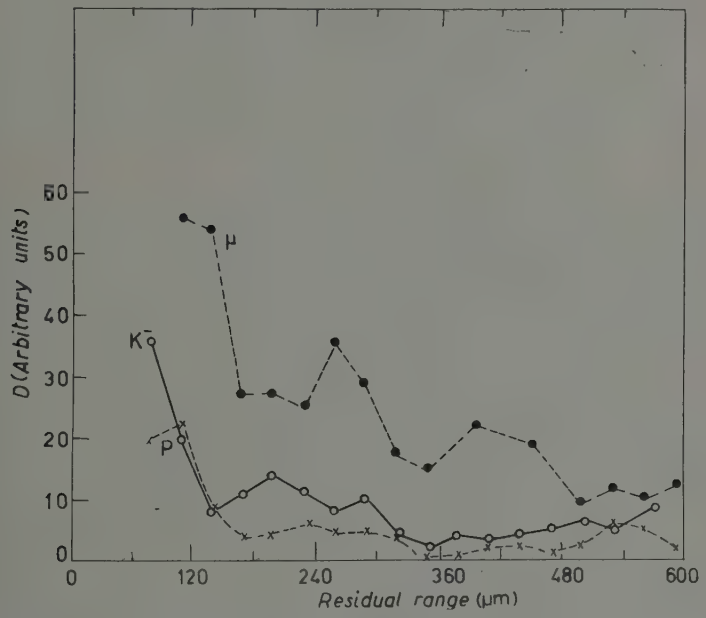

Fig. 2. – Plot of the second differences D versus residual range for a μ-meson, the K^- and track p.

* * *

We are greatly indebted to Professors R. H. Dalitz and V. L. Telegdi for advice and valuable discussions. We are very grateful to Prof. A. Turkevitch for suggestions on the U-loading of the emulsion. We express our thanks to Dr. E. J. Lofgren and the Bevatron staff for making the exposure available to us.

3801

Multiple Scattering of Polarized Particles.

L. Waldmann

Max-Planck-Institut für Chemie (Otto Hahn-Institut) - Mainz

(ricevuto il 10 Settembre 1959)

The multiple elastic scattering of polarized monoenergetic particles on resting scattering centres is governed by the generalized *Boltzmann equation* [1]

$$(1) \qquad \frac{\partial f}{\partial t} + \boldsymbol{v}\,\frac{\partial f}{\partial \boldsymbol{r}} = \frac{n_S v}{k^2}\left[\int a(\boldsymbol{e}, \boldsymbol{e}', \boldsymbol{s})\, f'\, a^{\dagger}(\boldsymbol{e}', \boldsymbol{e}, \boldsymbol{s})\, \mathrm{d}^2 e' - \frac{2\pi}{i}\left(a(\boldsymbol{e}, \boldsymbol{e}, \boldsymbol{s}) f - f a^{\dagger}(\boldsymbol{e}, \boldsymbol{e}, \boldsymbol{s})\right)\right].$$

$f = f(t, \boldsymbol{r}, \boldsymbol{e}, \boldsymbol{s})$ means the half-classical distribution operator of the polarized particles. Apart from the time t, f depends: 1) on the position of the particles $\boldsymbol{r}$ and the direction of their velocity $\boldsymbol{e}$ (unit vector; $\boldsymbol{v} = v\boldsymbol{e}$ velocity itself; k = wave number) as classical variables and 2) on the spin vector $\boldsymbol{s}$ as a quantummechanical variable. The operator f, taken for the velocity direction $\boldsymbol{e}'$, is denoted by f'. The scattering centres, the distance of which shall be large in comparison with $1/k$, are assumed to be statistically dispersed with the number density n_S. If they are spherical, as we suppose from now on, the dimensionless single scattering operator a depends only on the scalars arising from $\boldsymbol{e}, \boldsymbol{e}', \boldsymbol{s}$. Eq. (1) guarantees particle conservation and satisfies the H-theorem [2].

Starting from (1), Mühlschlegel and Koppe [3] have treated the multiple scattering of a beam of nearly parallel, polarized electrons, thus generalizing Molière's small-angle theory [4]. In this note the outlines of a diffusion theory for polarized particles are given, generalizing the work of Bothe [5] and of Bethe, Rose and Smith [6].

In thermal equilibrium f does not depend on $\boldsymbol{e}$ and $\boldsymbol{s}$. States in the neighbourhood can be *expanded in a series of the irreducible tensors*, arising from $\boldsymbol{e}$ and $\boldsymbol{s}$. We shall confine ourselves to particles of spin $\frac{1}{2}$. In this case there are two scalars (one pseudo) and four tensors of every rank $l \geqslant 1$ (two pseudo for every l). The series is broken off at $l = 1$. Then one retains two scalar and four vectorial expansion

---

(1) L. Waldmann: *Zeits. f. Naturfor.*, **12***a*, 660 (1957); **13***a*, 609 (1958).
(2) L. Waldmann: *Handb. d. Phys.*, **12**, 484 (1958).
(3) B. Mühlschlegel and H. Koppe: *Zeits. f. Phys.*, **150**, 474 (1958).
(4) G. Molière, *Zeits. f. Naturfor.*, **3***a*, 78 (1948).
(5) W. Bothe: *Zeits. f. Phys.*, **54**, 161 (1929).
(6) H. A. Bethe, M. E. Rose and L. P. Smith: *Proc. Am. Phil. Soc.*, **78**, 573 (1938).

3802

coefficients, still depending on time and position. They have — with a special normalization — the following physical significance:

$$
\begin{aligned}
&n^{(1)} = (1, f) && \text{density of number;}\\
&n^{(3)} = (2\boldsymbol{es}, f) && \text{density of helicity;}\\
&\boldsymbol{j}^{(1)} = (\boldsymbol{v}, f) && \text{stream of particles;}\\
&\boldsymbol{j}^{(2)} = (\sqrt{2}\boldsymbol{v}\times\boldsymbol{s}, f) && \text{density of « velocity-spin-vector »;}\\
&\boldsymbol{j}^{(3)} = (2\boldsymbol{v}(\boldsymbol{es}), f) && \text{stream of helicity;}\\
&\boldsymbol{j}^{(4)} = (\sqrt{2}(\boldsymbol{v}\times\boldsymbol{s})\times\boldsymbol{e}, f) && \text{density of transversal spin (*).}
\end{aligned}
$$

The abbreviation

$$(\Psi, f) = \mathrm{Tr}\int \Psi f \, \mathrm{d}^2 e \,,$$

is used; Tr means the trace over the spin indices ($2\boldsymbol{s} = \boldsymbol{\sigma}$).

For these expansion coefficients the Boltzmann equation leads to the following system of *diffusion resp. relaxation equations*:

$$
(2a)\qquad
\begin{cases}
\dfrac{\partial n^{(1)}}{\partial t} + \operatorname{div}\boldsymbol{j}^{(1)} = 0\,, \qquad \dfrac{\partial n^{(3)}}{\partial t} + \operatorname{div}\boldsymbol{j}^{(3)} = -\omega_0 n^{(3)}\,,\\[2ex]
\dfrac{\partial \boldsymbol{j}^{(i)}}{\partial t} + \dfrac{v^2}{3}\operatorname{grad} n^{(i)} = -\boldsymbol{g}^{(i)}\,, \qquad (i = 1, 3),\\[2ex]
\dfrac{\partial \boldsymbol{j}^{(2)}}{\partial t} + \dfrac{v}{2}\operatorname{curl}\boldsymbol{j}^{(4)} = -\boldsymbol{g}^{(2)}\,,\\[2ex]
\dfrac{\partial \boldsymbol{j}^{(4)}}{\partial t} - \dfrac{v}{2}\operatorname{curl}\boldsymbol{j}^{(2)} = -\boldsymbol{g}^{(4)}\,.
\end{cases}
$$

Here the $\boldsymbol{g}$'s are linear functions of the $\boldsymbol{j}$'s:

$$(2b)\qquad \boldsymbol{g}^{(i)} = \sum_k \omega_1^{(i,k)}\boldsymbol{j}^{(k)}\,. \qquad (i, k = 1, \ldots, 4)$$

The decay constants ω_0, $\omega_1^{(i,k)}$ are determined by the encounter term of the Boltzmann equation. From the H-theorem it follows that ω_0 is positive and that the matrix $\omega_1^{(i,k)}$ is positive-definite. Until now only spherical symmetry of the scattering centres has been assumed. Invariance of the single scattering operator a against reflection leads to

$$\omega_1^{(i,l)} = 0\,, \qquad \text{for } i = 1, 2,\ k = 3, 4 \text{ or vice versa:}$$

Invariance of a against time reversal leads to

$$\omega_1^{(12)} = -\omega_1^{(21)}, \qquad \omega_1^{(34)} = \omega_1^{(43)}.$$

(*) Apart from a constant factor.

If all these invariances are fulfilled (*e.g.* Mott scattering), a has the well-known form

$$a(\boldsymbol{e}, \boldsymbol{e}', \boldsymbol{s}) = a_0(\chi) + 2ia_1(\chi)\, \boldsymbol{ns}\,,$$

where $\chi = \sphericalangle(\boldsymbol{e}, \boldsymbol{e}')$ is the scattering angle and $\boldsymbol{n} = \boldsymbol{e} \times \boldsymbol{e}'/\sin\chi$ is a unit vector orthogonal to the scattering plane. In this case one has ($\omega = n_S v/k^2$)

$$\omega_0 = \omega \cdot 4\pi \int_0^\pi \left| a_0 \sin\frac{\chi}{2} - a_1 \cos\frac{\chi}{2} \right|^2 \sin\chi \,\mathrm{d}\chi\,,$$

$$\omega_1^{(11)} = \omega \cdot 4\pi \int (|a_0|^2 + |a_1|^2) \sin^2\frac{\chi}{2} \sin\chi \,\mathrm{d}\chi\,,$$

$$\omega_1^{(22)} = \tfrac{1}{2}(\omega_0 + \omega_1^{(11)})\,,$$

$$\omega_1^{(33)} = \omega \cdot 2\pi \int (|a_1|^2 + |a_0 \sin\chi - a_1 \cos\chi|^2) \sin\chi \,\mathrm{d}\chi\,,$$

$$\omega_1^{(44)} = \tfrac{1}{2}\omega_1^{(33)}\,,$$

$$\omega_1^{(12)} = \omega \cdot \sqrt{2}\pi \int i(a_0 a_1^* - a_0^* a_1) \sin^2\chi \,\mathrm{d}\chi\,,$$

$$\omega_1^{(34)} = \omega \cdot \sqrt{2}\pi \int (|a_1|^2 - |a_0 \sin\chi - a_1 \cos\chi|^2) \sin\chi \,\mathrm{d}\chi\,.$$

Thus for Mott scattering the ω's can be calculated from Sherman's tables [7].

The diffusion equations have to be supplemented by a set of boundary conditions. For $n^{(1)}$ and $\boldsymbol{j}^{(1)}$ together one scalar condition can be postulated. The same is true for $n^{(3)}$ and $\boldsymbol{j}^{(3)}$. For $\boldsymbol{j}^{(2)}$ and $\boldsymbol{j}^{(4)}$ together, one can postulate a condition for the tangential component of one vector. The distribution operator of the incoming particles on the surface of the scatterer will be known; the streams or vector densities assigned to these particles are denoted by capital letters ($\boldsymbol{J}^{(i)}$). The unit vector in a surface point, normal to the tangential plane and directed to the vacuum, is denoted by $\boldsymbol{u}$. Then one has as a suitable choice of *boundary conditions* for every surface point

$$\text{(3)} \qquad \begin{cases} \tfrac{1}{2}\boldsymbol{u}\boldsymbol{j}^{(i)} - \tfrac{1}{4}n^{(i)}v = \boldsymbol{u}\boldsymbol{J}^{(i)}\,, \\ (\boldsymbol{j}^{(2)} - \boldsymbol{u}\times\boldsymbol{j}^{(4)})_{\mathrm{tg}} = \tfrac{7}{8}(\boldsymbol{J}^{(2)} - \boldsymbol{u}\times\boldsymbol{J}^{(4)})_{\mathrm{tg}}. \end{cases} \qquad (i = 1, 3)\cdot$$

The tangential boundary condition is chosen symmetrical in $\boldsymbol{j}^{(2,4)}$; this is seen by multiplying vectorially with $\boldsymbol{u}$.

Starting from the diffusion equations (2*a*, *b*) and the boundary conditions (3) one can calculate in a simple way the stationary scattering — transmission and back scattering — of polarized particles by thick foils, with reasonable results. The following cases have been treated: 1) normal incidence of unpolarized electrons; this gives the Mott polarization; 2) normal incidence of longitudinally polarized electrons; this gives an exponential decay of helicity with the depth of penetration; 3) normal incidence of transversally polarized electrons; this gives, respective to the incident beam, a rolling aside of the particles which dies out exponentially with the depth, and an exponential decay of transverse polarization.

---

(7) N. SHERMAN, *Phys. Rev.*, **103**, 1601 (1956).

3804

Alcuni dati sulle interazioni di protoni di alta energia in nuclei leggeri (C, O).

E. Fiorini e S. Ratti

Istituto di Fisica dell'Università - Milano
Istituto Nazionale di Fisica Nucleare - Sezione di Milano

(ricevuto il 30 Ottobre 1959)

Lo studio delle interazioni di protoni di qualche centinaio di MeV con nuclei pesanti è generalmente svolto assumendo un modello di gas di Fermi nello stato fondamentale e considerando l'interazione del protone incidente come una « cascata » di urti singoli protone-nucleone legato (modello di Goldberger [1]). Per studiare la successione delle interazioni singole del protone incidente è stato applicato, con tecniche diverse, il metodo statistico di Montecarlo; i risultati sono in generale in buon accordo con i dati sperimentali [2], almeno per energie abbastanza elevate, tali però che si possa considerare trascurabile la sezione d'urto per la produzione di mesoni.

Non molto si sa invece, nello stesso intervallo di energie, sulle interazioni con nuclei leggeri. Il problema è stato studiato da J. Combe [3] che, assunto valido il modello di gas di Fermi anche per i nuclei leggeri dell'emulsione nucleare (C, O, N), ha esteso ad essi la trattazione col metodo di Montecarlo applicata ai nuclei pesanti. In una prima approssimazione l'unica differenza tra nuclei leggeri e pesanti consisterebbe, secondo J. Combe, in una maggiore trasparenza dei nuclei leggeri.

Alcuni risultati sperimentali ottenuti dallo stesso Combe [4] con emulsioni nucleari (per protoni incidenti di 340 MeV) presentano peraltro un notevole disaccordo coi corrispondenti risultati del metodo di Montecarlo; disaccordo che scompare introducendo l'ipotesi che nei nuclei leggeri l'urto del protone incidente avvenga, nel 30% dei casi, non contro un

(1) R. Serber: *Phys. Rev.*, **72**, 1114 (1947); M. L. Goldberger: *Phys. Rev.*, **74**, 1269 (1948); C. F. Chew e G. C. Wick: *Phys. Rev.*, **85**, 636 (1952).

(2) G. Bernardini, E. T. Booth e S. J. Lindenbaum: *Phys. Rev.*, **82**, 307 (1951); **85**, 826 (1952); **88**, 1017 (1952) e bibliografia ivi contenuta; G. C. Morrison, A. Muirhead e W. G. Rosser: *Phil. Mag.*, **44**, 1326 (1953) e bibliografia ivi contenuta; H. McManus, W. T. Sharp e H. Gellmann: *Phys. Rev.*, **93**, 924 (1954); J. Combe: *Ann. Phys. Paris*, **13**, 468 (1958); N. Metropolis, R. Bivins, M. Storm, A. Turkevich, J. M. Miller and G. Friedlander: *Phys. Rev.*, **110**, 185 (1958). Una buona rassegna è stata recentemente pubblicata da O. R. Frisch: vedi B. G. Harvey: *Progress in Nuclear Physics*, **7**, 90 (London, 1959).

(3) J. Combe: *Suppl. Nuovo Cimento*, **3**, 182 (1956) e bibliografia ivi contenuta.

(4) J. Combe: *Journ. de Phys. et Rad.*, **16**, 445 (1955) e bibliografia ivi contenuta.

nucleone legato, bensì contro una sottostruttura ($^4_2$He, $^3_2$He, $^3_1$H, $^2_1$H) istantaneamente formatasi nell'interno del nucleo stesso ([3,5]). L'ipotesi dell'esistenza di queste sottostrutture istantanee sembra trovare conferma, secondo lo stesso COMBE, anche nei dati di K. STRAUCH e W. F. TITUS ([6]).

Si è ritenuto opportuno utilizzare per un tale studio circa 300 interazioni di protoni nei setti di plexiglas (0.3 cm di spessore) di una camera di Wilson, raccolte nel corso di una precedente esperienza con raggi cosmici. Poichè il dispositivo sperimentale è descritto in un lavoro precedente ([7]), ci limitiamo a ricordare che sotto la camera di Wilson è collocato un grande scintillatore in anticoincidenza; di esso si è dovuto tenere conto nell'elaborazione dei dati (vedi Sez. 2), onde correggere i risultati sperimentali.

In analogia con quanto fatto dal COMBE si sono scartate tutte le interazioni in nuclei di idrogeno. I nostri dati si riferiscono quindi ad interazioni nei nuclei di carbonio e ossigeno del plexiglass.

Affinchè possa considerarsi valido, con buona approssimazione, il modello di Goldberger si sono considerate soltanto le interazioni in cui il protone incidente ha una energia compresa tra 150 e 500 MeV, valutata in base ad una stima della ionizzazione ([7]). L'energia media è di 310 MeV.

I nostri risultati si riferiscono essenzialmente:

1) alla natura e al numero dei secondari veloci di interazione ($E > 30$ MeV);

2) alla distribuzione degli angoli che il secondario forma con il primario nel sistema del laboratorio (*) nelle interazioni con emissione di un solo secondario veloce ionizzante: interazioni di di tipo (p, p'), (p, pn), ecc.;

3) alla distribuzione degli angoli (S.L.) tra i due secondari delle interazioni con due secondari veloci ionizzanti: interazioni di tipo (p, 2p), (p, 2pn).

1. – Nella Tabella I sono confrontati i nostri risultati sperimentali con quelli che altri autori hanno ottenuto sia sperimentalmente sia con il metodo di Montecarlo, circa la percentuale dei vari tipi di interazione con nuclei pesanti e leggeri. Riguardo ai nostri risultati si può osservare, che al variare dell'energia non variano sensibilmente le percentuali dei vari tipi di interazione, ad eccezione della percentuale di interazioni con almeno 3 rami veloci carichi, ovviamente favorite ad energie elevate. Occorre tenere conto, in questo confronto, che J. COMBE ([4]) considera soltanto le interazioni in emulsione accompagnate da rami di evaporazione e quindi non prende in considerazione le deflessioni sotto qualsiasi angolo di protoni non accompagnate da emissione di rami neri.

Dai presenti risultati l'ipotesi dell'esistenza di sottostrutture nei nuclei leggeri risulta confermata; sembra anzi che la percentuale di urti contro sottostrutture istantanee sia superiore al 30%; ciò può essere dovuto al fatto che i nuclei leggeri in considerazione sono soltanto nuclei multipli di particelle α (C ed O).

2. – J. COMBE ha calcolato, col metodo di Montecarlo, la distribuzione degli angoli (S.L.) che il secondario veloce forma

([5]) P. CÜER, A. SAMMAN e J. COMBE: *Compt. Rend.*, **240**, 1527 (1955) e bibliografia ivi contenuta; M. G. K. MENON: *Phil. Mag.*, **41**, 583 (1950); S. TAMOR: *Phys. Rev.*, **77**, 412 (1950).

([6]) K. STRAUCH e W. F. TITUS: *Phys. Rev.*, **95**, 854 (1954); vedi anche H. TYREN e T. A. J. MARIS: *Nucl. Phys.*, **6**, 82 (1958) e bibliografia ivi contenuta.

([7]) M. CONVERSI, G. M. DE MUNARI, A. EGIDI, E. FIORINI, S. RATTI, C. SUCCI, C. RUBBIA e G. TORELLI: *Nuovo Cimento*, **12**, 130 (1959).

(*) Nel seguito indicheremo il sistema del Laboratorio con (S. L.).

TABELLA I.

Autore	Energia del primario (MeV)	Nucleo	Metodo o tecnica impiegati	Percentuale dei vari tipi d'interazione			
				1 ramo ionizzante veloce	nessun ramo ionizzante veloce	2 rami ionizzanti veloci	3 rami ion. veloci
J. COMBE [3]	340	Ag, Br	Montecarlo	53.7±5	37 ±4	9.3±1.5	0
N. METROPOLIS *et al.* [2]	360	Ru (Ag, Br)	Montecarlo	52 ±2.6	27.2±1.9	19.4±1.6	1.6±0.5
G. BERNARDINI *et al.* [2]	300÷400	Ag, Br	Emulsione	54 ±4	35 ±3	9 ±2	1.7±0.7
J. COMBE [4] ($1 \leqslant N_h \leqslant 2$)	340	Ag, Br	Emulsione	52 ±4	25 ±2.5	21 ±2.5	2 ±1
J. COMBE [3]	340	C, N, O	Montecarlo (p-nucleone leg.)	50 ±4	25 ±2.5	24 ±2.5	1 ±1
J. COMBE [3]	340	C, N, O	Montecarlo (30% sottostrutt.)	65 ±4	17.8±2	17 ±2	0.5±1
J. COMBE [4]	340	C, N, O	Emulsione	67 ±4	16.5±2	16.5±2	0
Presente esp.	100÷310	C, O	Camera di Wilson	72.4±5	14.8±2	12.5±2	0.3±1
»	310÷500	C, O	»	68 ±5	13.7±2	16.8±3	1.2±0.6
»	100÷500	C, O	»	70 ±4	14.2±1.5	14.5±2	0.7±0.3

con il primario nell'ipotesi di interazioni ad un solo urto p-nucleone legato; ha mostrato inoltre come la forma di tale distribuzione dipenda sensibilmente non dal numero di urti, ma quasi esclusivamente dalla distribuzione delle quantità di moto dei nucleoni in seno al nucleo.

Nella Fig. 1 sono confrontati i nostri risultati sperimentali con le curve ottenute da J. COMBE col metodo di Montecarlo. Per quanto è stato osservato nella Sezione precedente, J. COMBE non ha potuto confrontare i propri risultati sperimentali con quelli ottenuti col metodo di Montecarlo.

I dati sperimentali della Fig. 1 sono stati corretti con un metodo di approssimazioni successive per tenere conto dell'esistenza dello scintillatore in anticoincidenza. Non si sono considerate le deviazioni inferiori ai 5°, onde eliminare il contributo che la diffusione multipla dà nell'attraversamento dei setti.

La distribuzione angolare sperimentale risulta in accordo con l'ipotesi della esistenza di sottostrutture, in una proporzione probabilmente maggiore di quella prevista da J. COMBE.

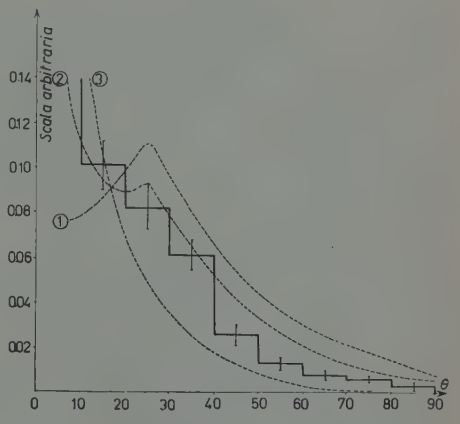

Fig. 1.

1): urto p-nucleone legato (J. COMBE [3]);
2): 70% urti p-nucleone legato, 30% urti p-sottostrutture;
3): urto p-sottostrutture (J. COMBE [3]).

3. – Se si considera l'interazione di un protone con un nucleo e si suppone che questa si possa schematizzare come

un singolo urto p-nucleone legato, le direzioni dei due secondari non sono complanari con la direzione del protone incidente e dalla distribuzione degli angoli (S.L.) tra i due secondari si possono avere alcune informazioni sulla distribuzione delle quantità di moto dei nucleoni in seno al nucleo. In Fig. 2 è

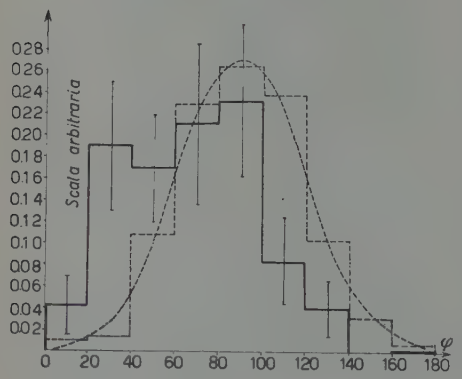

Fig. 2.
--- Metodo di Montecarlo (1 urto), (J. COMBE [5]);
—— risultati sperimentali.
$\varphi<90°$ $(68\mp12)\%$; $\varphi>90°$ $(32\mp8)\%$.

riportata la distribuzione ottenuta dal COMBE in approssimazione non relativistica per gli angoli (S.L.) formati dai due secondari dopo un urto p-nucleone legato, assumendo la distribuzione delle quantità di moto dei nucleoni nel nucleo proposta da J. HEIDMANN [8]: la curva ottenuta è una gaussiana col massimo sui 90° ed una deviazione standard di 28°.

La nostra distribuzione sperimentale dell'angolo (S.L.) tra i due secondari veloci di 47 stelle a tre rami, non risulta simmetrica rispetto ai 90°; gli eventi con angoli minori di 90° sono il $(68\pm12)\%$ Non ci sembra che la bassa statistica sia sufficiente a spiegare questa discrepanza, nè lo sia l'approssimazione non relativistica usata dato che, trattando relativisticamente il problema, il massimo si sposta solo di qualche grado, verso gli angoli piccoli.

Ci sembra invece che una tale discrepanza si possa attribuire ad una troppo drastica assunzione fatta dal COMBE nella trattazione del problema. Le direzioni delle quantità di moto dei nucleoni *urtati* non possono infatti considerarsi distribuite isotropicamente nello spazio, come previsto dal COMBE, perchè la sezione di urto di interazione nucleone-nucleone diminuisce al crescere della velocità relativa del nucleone incidente rispetto al nucleone urtato. La distribuzione nello spazio delle direzioni delle velocità dei nucleoni urtati presenterà di conseguenza una notevole anisotropia, perchè risultano favoriti gli urti con piccola velocità relativa del protone incidente rispetto al nucleone del nucleo, cioè gli urti con piccoli angoli tra le direzioni del nucleone incidente e del nucleone legato, prima dell'urto. D'altra parte sono proprio gli urti con piccola velocità relativa che dànno luogo ad eventi con piccoli angoli (S.L.) tra i due secondari veloci uscenti: tali eventi risultano così favoriti.

Svolgendo un calcolo approssimato della variazione della sezione d'urto in funzione dell'angolo tra i due secondari veloci si è costatato come, correggendo in questo senso i dati del COMBE, si ottenga un buon accordo coi risultati sperimentali.

Uno studio completo del problema col metodo di Montecarlo è attualmente in corso.

* * *

Ci è gradito ringraziare i proff. P. CALDIROLA, G. P. S. OCCHIALINI e G. POLVANI per il loro interessamento ed i nostri colleghi della collaborazione Milano-Pisa [7] per aver messo gentilmente a disposizione tutto il materiale raccolto nella precedente esperienza.

Un particolare ringraziamento intendiamo rivolgere ai colleghi V. AMAR, F. DUIMIO, G. M. PROSPERI ed A. SCOTTI per le utili discussioni ed ai dr. G. BELLINI e M. DI MARCO per l'aiuto prestatoci.

[8] J. HEIDMANN: *Phys. Rev.*, **80**, 171 (1950).

IL NUOVO CIMENTO Vol. XIV, N. 4 16 Novembre 1959

Ferroelectric Properties of a Material made of Titanium Oxide.

L. Nicolini

Istituto di Chimica Industriale ed Applicata, Facoltà di Ingegneria dell'Università - Bologna

(*Nuovo Cimento*, **13**, 257 (1959))

The figures 1 and 3 of this paper have been inadvertently inverted.

Some Remarks on the Calculation of the Polarization Effects - I.

M. Carrassi and G. Passatore

Istituto di Fisica dell'Università - Genova
Istituto Nazionale di Fisica Nucleare - Sezione di Genova

(*Nuovo Cimento*, **13**, 944 (1959))

Unfortunately we have to communicate a mistake which has been done in rewriting the 8 transition amplitudes of formula (13), p. 941:

$H^{1\beta\gamma\delta}$ has to be substituted by $H^{2\beta\gamma\delta}$, and conversely $H^{2\beta\gamma\delta}$ by $H^{1\beta\gamma\delta}$.

This amounts to interchange, in the same order, the values of the amplitudes on the right hand side of the first 4 equations (13) with the ones on the right hand side of the last 4.

3809

LIBRI RICEVUTI E RECENSIONI

W. GALBRAITH – *Extensive Air Showers*. Butterworths Scientific Publications, London, 1958, pagine XVI+211. Prezzo 40 scellini.

Nell'immediato dopoguerra si concentratono sullo studio degli sciami estesi atmosferici gli sforzi di numerosissimi ricercatori di ogni paese. La qualità di osservazioni raccolte in questo periodo risultò considerevolissima e costituisce ancora oggi buona parte delle nostre conoscenze sugli sciami estesi. Successivamente alcuni gruppi di ricercatori continuarono a intraprendere questo tipo di ricerche anche quando lo interesse scientifico dello studio di questi fenomeni venne ridotto, tra l'altro, dall'entrata in funzione di grosse macchine acceleratrici.

In questo libro il Dott. GALBRAITH espone concisamente le nostre attuali conoscenze sugli sciami estesi, inquadrando con elementare trattazione teorica i risultati delle più interessanti osservazioni sperimentali, spesso accompagnati da una chiara illustrazione dei dispositivi impiegati per ottenerli. L'esposizione si può ritenere sufficientemente completa ed aggiornata quando si tenga presente la piccola mole del volume. Non manca ad esempio un capitolo dedicato alla radiazione di Čerenkov prodotta dagli sciami estesi. Anche la biografia consente di rintracciare con facilità i lavori di maggior importanza concernenti ogni aspetto del problema trattato.

Questo volume può quindi risultare assai utile a chi voglia rapidamente aggiornarsi sugli argomenti in esso trattati; inoltre le numerose tabelle di dati e le molte formule presentate in modo chiaro e semplice rendono utile la consultazione di questo libro da parte di coloro che compiono ricerche sperimentali nel campo delle particelle elementari.

A. ALBERIGI

A. MERCIER – *Analytical and Canonical Formalism in Physics*. North-Holland Publishing Company, Amsterdam, 1959, pp. VIII+222. Prezzo 20 guilders.

Questo volume di MERCIER offre una trattazione sistematica e moderna della Meccanica Analitica classica. Due aspetti apparentemente lo differenziano dai numerosi trattati, antichi e recenti, di Meccanica Analitica. Primo, l'accento viene posto sui capitoli e applicazioni la cui conoscenza risulterà utile nelle successive formulazioni quantistiche. Secondo, l'enfasi è posta essenzialmente sul formalismo generale e quasi mai sulle sue particolarizzazioni che sono di più comune interesse.

Dopo una introduzione che permette già di illustrare i principali concetti che saranno usati nel seguito, l'autore descrive il formalismo lagrangiano, partendo deduttivamente dal principio di azione e dal principio di Hamilton, discutendo poi il problema dell'integrazione delle equazioni di Lagrange,

con particolare riguardo all'uso di proprietà di invarianza e corrispondenti integrali primi, ed esaminando in dettaglio la più generale Lagrangiana di secondo grado nelle q, da cui i più importanti sistemi semplici vengono ricavati per successive particolarizzazioni. Lo studio delle Lagrangiane che sono forme quadratiche delle q offre lo spunto per definire i simboli di Christoffel e per presentare le equazioni del moto come equazioni per le geodetiche dello spazio metrico definito con i coefficienti della Lagrangiana. Il capitolo sulla densità di Lagrangiana contiene una discussione dell'invarianza rispetto a trasformazioni proprie di Lorentz, una introduzione algebrica alla teoria degli spinori e una trattazione della teoria classica dei campi secondo il formalismo lagrangiano. Nel capitolo successivo viene svolto il formalismo canonico, con particolare discussione del teorema di Liouville e del problema ergodico. Il formalismo viene quindi applicato alla elettrodinamica nel capitolo successivo. Segue, una discussione generale delle densità di Hamiltoniane, con le relative considerazioni di invarianza ed applicazioni a casi semplici.

La parte più originale del volume va però cercata negli ultimi due capitoli, uno sulle trasformazioni e l'altro sul formalismo canonico con Jacobiano nullo. In questi capitoli l'autore, accanto alla trattazione delle trasformazioni canoniche, sviluppa un formalismo omogeneo, in cui la variabile tempo è considerata anche in meccanica dei punti alla stessa stregua delle altre variabili coordinate e viene introdotta una nuova variabile indipendente per la descrizione del moto. L'autore sviluppa il formalismo deduttivamente a partire da un principio variazionale omogeneo; sviluppa inoltre un formalismo omogeneo per trasformazioni canoniche, e mostra la connessione con il formalismo canonico con Jacobino nullo.

La lettura del volume può senz'altro riuscire utile agli studenti che vogliano approfondire lo studio della meccanica analitica classica e che intendono occuparsi di teorie quantistiche. Non riteniamo che sia adatto per chi invece intenda dedicarsi allo studio di problemi classici, per esempio di dinamica dei sistemi o di meccanica celeste. Si trovano nel volume un centinaio di problemi. Anche questi servono ad illustrare in dettaglio certi aspetti del formalismo, o a rifare dimostrazioni con metodi diversi, e quasi mai ad illustrare particolari esempi fisici. Si tratta quindi di una opera che vuole mantenersi su un piano prevalentemente astratto e certamente potrà risultare utile per consultazione, dato anche il rigore e la nitidezza della esposizione ed il suo tono generale e deduttivo.

R. Gatto

W. Graeub – *Lineare Algebra*. Springer, 1958, pp. XI+219. Prezzo DM 39.

Questa monografia costituisce il 97° volume della serie *Grundlehren der Mathematischen Wissenschaften* della Casa Editrice Springer. L'autore si propone di ottenere una esposizione dell'algebra lineare basata sul concetto algebrico di spazio lineare ed evitando concetti di geometria analitica che di solito formano la base delle trattazioni dell'algebra lineare. Questo programma dà luogo in certi punti a sviluppi originali come per esempio l'introduzione di funzioni multilineari totalmente antisimmetriche allo scopo di ottenere una definizione dell'orientamento in uno spazio lineare indipendentemente dalle coordinate. I primi cinque capitoli della monografia sono dedicati alla discussione generale delle rappresentazioni lineari con particolare accento sulla trattazione simultanea delle rappresentazioni duali. Ven-

3811

gono discussi i determinanti e le loro proprietà e l'algebra tensoriale. I restanti capitoli, meno l'ultimo, sono dedicati agli spazi lineari metrici e contengono la discussione dei problemi ad autovalori, delle forme quadratiche e della loro riduzione agli assi, sempre su basi strettamente algebriche. L'ultimo capitolo riguarda di nuovo spazi lineari senza metrica ed è dedicato al problema della identificazione dei sottospazi invarianti per una data trasformazione lineare, risolto direttamente a partire dalla trasformazione e non attraverso la decomposizione della matrice di trasformazione.

È evidente che un volume di questo tipo può risultare utile al fisico, data la diffusa applicazione di procedimenti di algebra lineare ormai in tutti i rami della fisica. Di particolare interesse ci è parsa la discussione, nel capitolo VIII, di quelle proprietà degli spazi euclidei che restano valide anche in spazi con metrica indefinita. Come è noto lo spazio di Minkowski è un esempio di un tale spazio, e più recentemente l'introduzione di una metrica indefinita nello spazio di Hilbert è stata discussa ai fini di superare talune difficoltà nella quantizzazione di campi d'onda.

In conclusione, pur trattandosi di un volume di matematica e scritto essenzialmente per matematici, riteniamo che la natura dell'argomento e la linea dell'esposizione possano renderlo utile ai fisici.

R. Gatto

PROPRIETÀ LETTERARIA RISERVATA

Direttore responsabile: G. POLVANI Tipografia Compositori - Bologna

Questo Fascicolo è stato licenziato dai torchi il 14-XI-1959

3812